ALGERIAN DEMOCRATIC AND POPULAR REPUBLIC
MINISTRY OF HIGH EDUCATATION AND SCIENTIFIC RESEARCH

UNIVERSITY FRERES MENTOURI CONSTANTINE 1
FACULTY OF SCIENCES EXACTES
PHYSICS DEPARTMENT

Order N°:
Series:

THESIS

PRESENTED FOR LMD DOCTORAT DEGREE REQUIREMENT

SPECIALITY

THIN FILMS PHYSICS

THEME

Cupric Oxide thin films deposition for gas sensor application

---

By

Meryem LAMRI ZEGGAR

Defended on : 22/05/2016

Jury committee:

President :	**N. ATTAF**	**Prof.**	**Univ. frères Mentouri Constantine 1**
Advisor :	**M. S. AIDA**	**Prof.**	**Univ. frères Mentouri Constantine 1**
Examiners :	**Y.S . OCAK**	**Prof.**	**Univ. Dicle Diyar bakir Turkey**
	A.AZIZI	**Prof.**	**Univ. Ferhat Abbes Sétif 1**
	F. KERROUR	**Prof.**	**Univ. frères Mentouri Constantine 1**
	B. BOUDINE	**Prof.**	**Univ. frères Mentouri Constantine1**


بسم الله الرحمن الرحیم

Acknowledgements

__F__irst thanks to __ALLAH__ for his grace and for this help to let me completing my research thesis.

__F__or most, I would like to express my sincere gratitude to my advisor Prof. __Mohammed Saleh Aida__ for the continuous support of my Ph.D study and research, for his patience, motivation, enthusiasm, and immense knowledge. His guidance helped me in all the time of research and writing of this thesis. I could not have imagined having a better advisor and mentor for my Ph.D study. I attribute the level of my PhD degree to his encouragement and effort and without him this thesis, too, would not have been completed or written.

__I__ would like also to thank Prof. __Nadir Attaf__ , who has supported me throughout my thesis with his patience and knowledge whilst allowing me the room to work in my own way. I have been amazingly fortunate to have a second advisor who gave me the freedom to explore on my PhD thesis and at the same time the guidance to recover when my steps faltered.

__I__ address my thanks to Prof __Y. S. Ocak__, Prof __A.Azzizi__ , Prof __F.Kerrour__ and Prof __B.Boudine__ for their acceptance to judge this modest work.

__L__ast but not the least; I would like to thank my family: my parents, for giving birth to me at the first place and supporting me spiritually throughout my life. I cannot forget my sisters, my brothers, my aunt and all my friends.

Meryem Lamri Zeggar

Contents

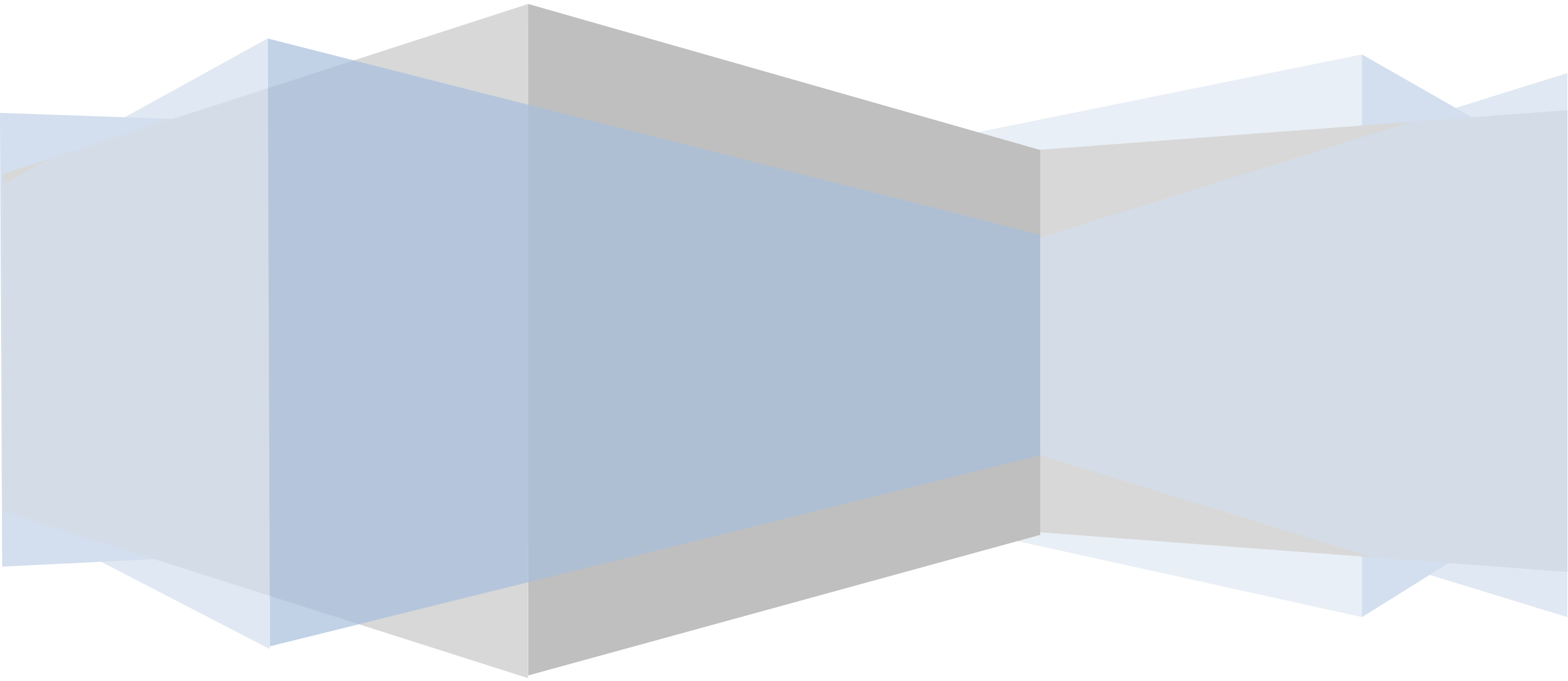

Contents

CHAPTER I

Cupric oxide thin films (CuO) : Review

CHAPTER II

Films deposition and characterization

CHAPTER III

RESULTS AND DISCUSSION

CuO THIN FILMS

CHAPTER IV

APPLICATIONS OF CuO THIN FILMS

Gas and organic vapor sensing

Solar cells

Figures caption

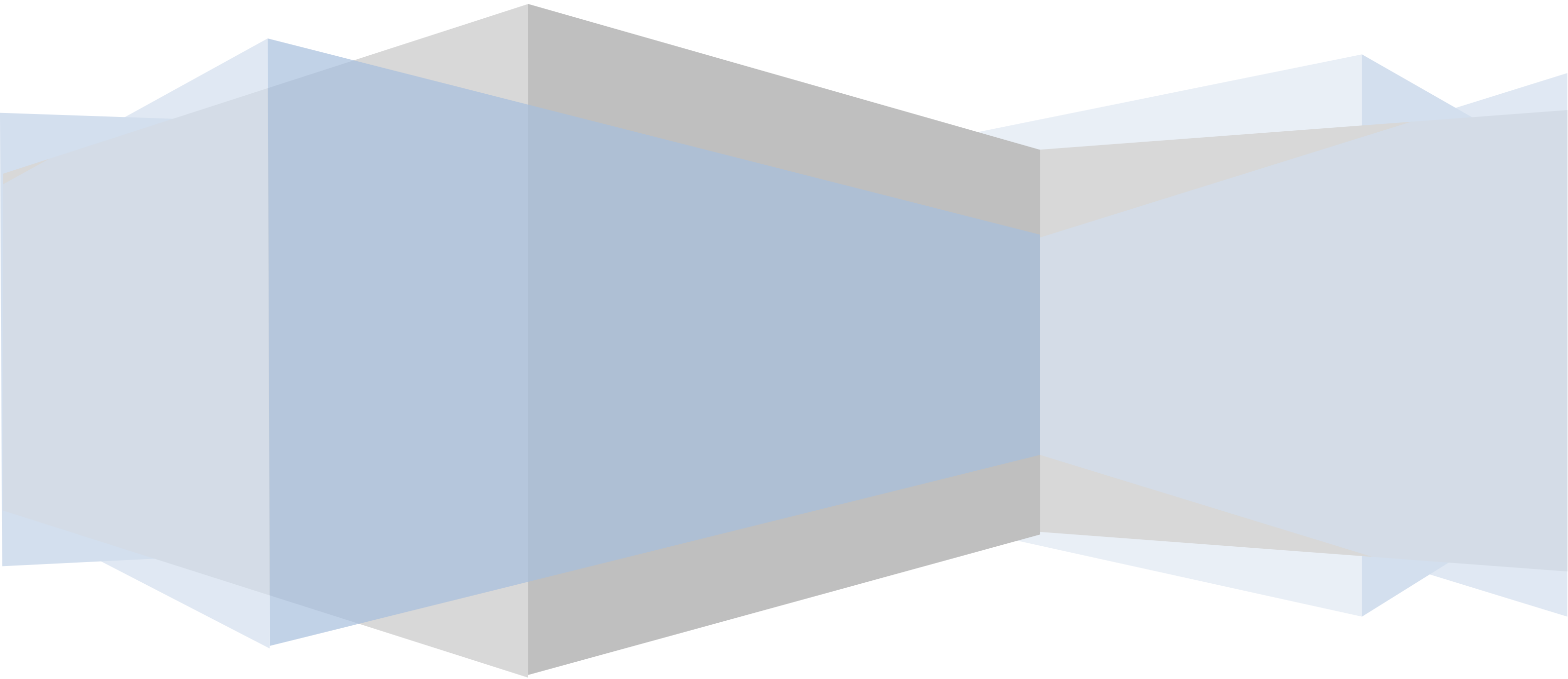

FIGURES CAPTION

INTODUCTION

CHAPTER I

CHAPTER II

CHAPTER III

CHAPTER IV

illumination.

Tables caption

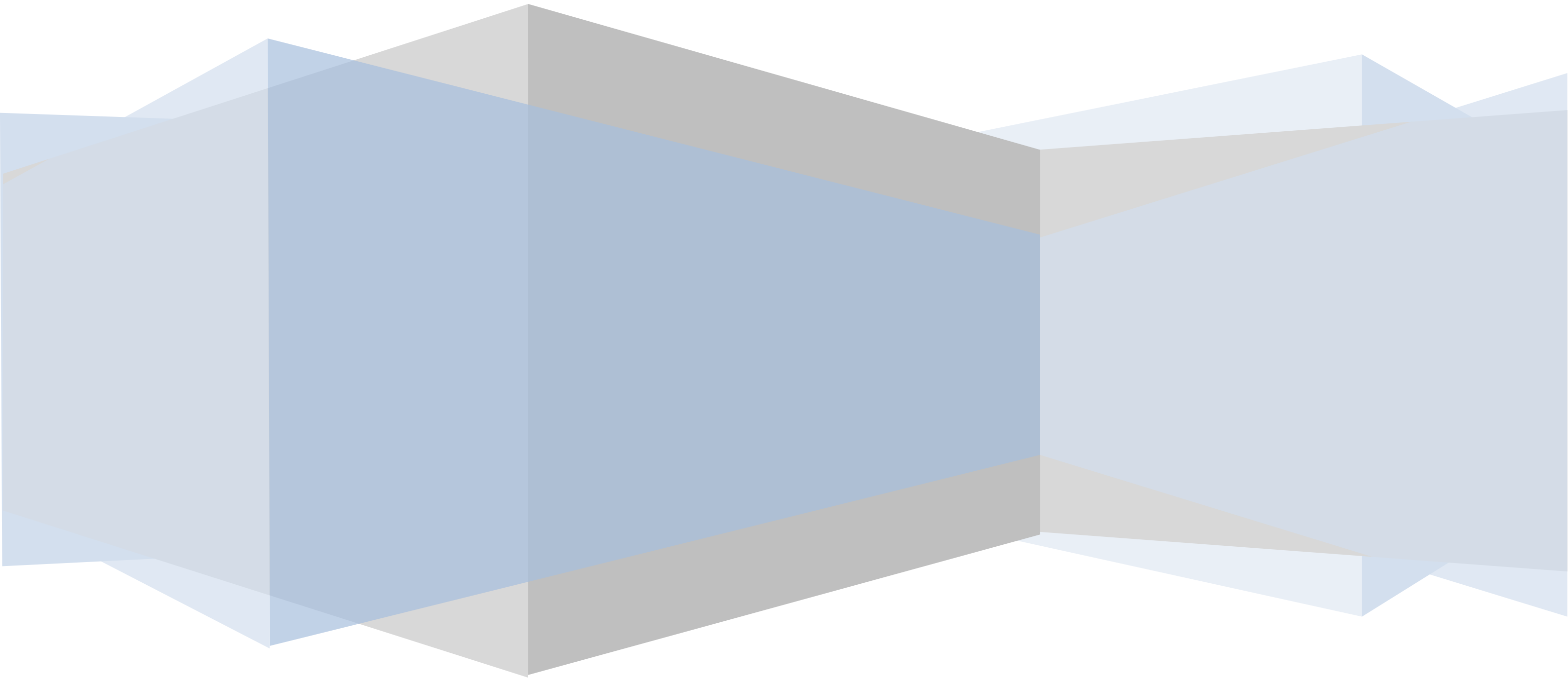

TABLES CAPTION

CHAPTER I

CHAPTER II

CHAPTER III

CHAPTER IV

Introduction

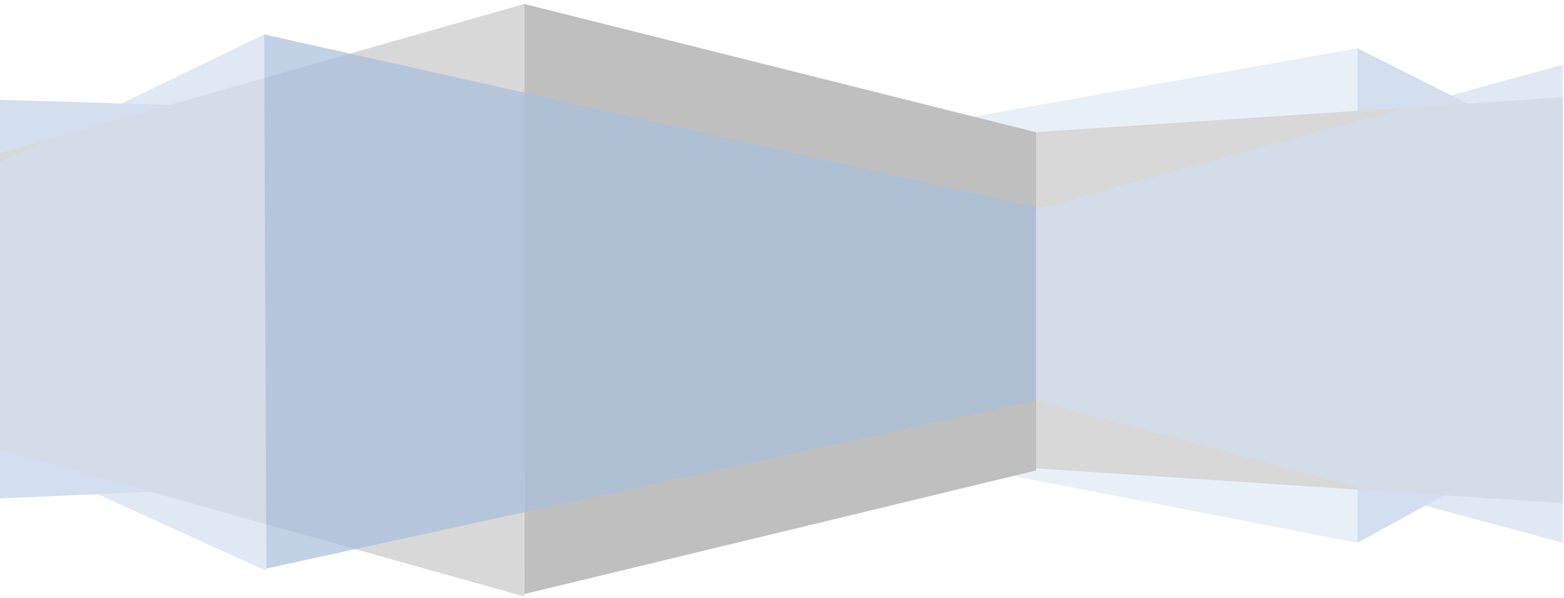

Introduction

Most of the present global energy production is accomplished by burning fossil fuels. However, the limited availability and the environmental issues such as the atmospheric pollution and the greenhouse effect are inherited problems associated with the use of fossil fuels. This forces mankind to search for new, more sustainable and long-term energy solutions to provide the future energy supply. As the demand for more electric power increases and present power plants reach end of-life, the need for generating electricity from alternative sources becomes imperative. Hence, an intensive worldwide research activity is carried nowadays on the research and the development of alternative renewable energies namely: solar energy, wind energy, biomass, geothermal …etc. Conversion of sunlight directly to electricity, commonly called photovoltaic (PV) conversion, is one promising alternative way to produce energy with a clean process respecting the environment.

The first efficient solar cell was developed at Bell lab using a silicon *p-n* junction in 1954. Currently, the efficiency of crystalline silicon based single *p-n* junction device has approached its theoretical limit of 33.7% [1], which however is too expensive for large-scale application. Thin film technologies can reduce the amount of light-absorbing materials needed and have better promise of low cost and flexibility as compared with single crystal silicon cells. CdTe [2], CIGS [3] and amorphous silicon [4] are the three main materials used in thin-film solar cells.

However, the solar energy industry is currently facing the serious technical and cost issues, hindering its development. For example, the purification and production processes of crystalline silicon cause pollution to the environment, and the cost per watt is much higher than conventional energy sources, limiting its large-scale production. Cadmium scale production. Cadmium telluride (CdTe) solar cell contains toxic element Cd, while copper Indium Dieseline (CIS) cell uses rare element indium. For large-scale application, it is necessary to explore other light-absorbing materials that are low-cost, abundant in the earth and environmental friendly. Semiconductor oxides are potential alternatives to the silicon solar cells because they are cheaper to produce, non-toxic and possess high light absorption efficiency. Since the solar spectrum is mainly composed of visible light with wavelength in the range of 380 to 780 nm, only oxides with a band gap smaller than about 3 eV can absorb the visible light. For example, ZnO and TiO2 with band gap around 3.2 eV are well-known transparent oxides, which can absorb the solar light only in the ultraviolet region of the solar spectrum. It is proposed that the semiconductor should possess an optical band gap of 2 eV or below to better utilize the solar energy.

Wadia et al have examined the material extraction cost and annual electricity potential for many semiconductors [5], which are compared with the values of silicon crystal solar cells as shown in figure 1. Semiconductors in the upper-right quadrant possess less cost and larger electricity potential than Si, and thus can be used as alternative solar cell materials. It is noted that both CuO and Cu_2O are among them, which have small band gaps of 1.35 eV [6] and 2.0 eV [7], corresponding to theoretical solar energy conversion efficiency of 31% [8,9] and 20% [10], respectively. These both materials are abundant in the earth and non-toxic.

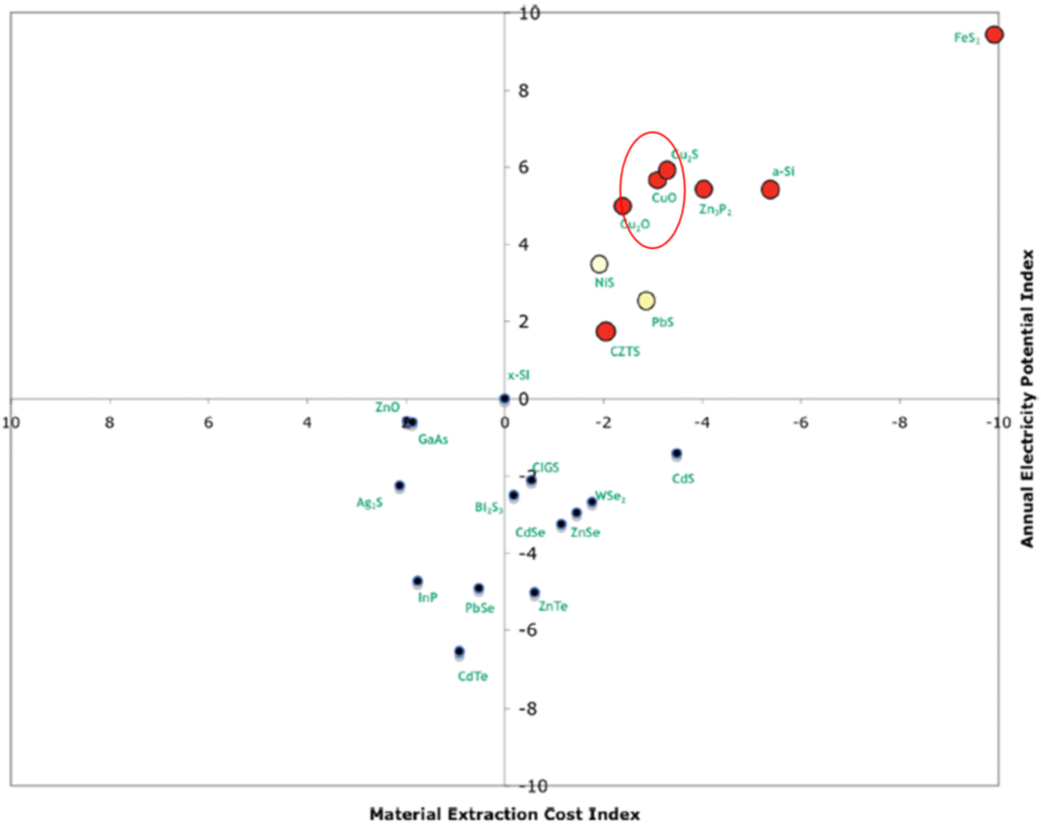

Figure 1 *The naturallogarithm of the values of material extraction cost and annual electricity potential for 23 semiconductors divided by those for crystal Si as from reference. The negative X-and positive Y-values indicates lower cost and higher electricity potential, respectively.*

Copper oxide thin films and nano-materials can be fabricated using various techniques including low-cost chemical process. Compared with Cu_2O, CuO is superior for solar energy harvesting because of its smaller optical band gap. CuO can absorb the whole spectrum of visible light, while Cu_2O can only absorb the part of light with wavelength smaller than 620 nm. Besides, CuO is more stable in air, while Cu_2O can be oxidized into CuO for increased temperatures. In recent years, CuO has received increasing interest due to its promising application for solar energy harvesting. A lot of research and development efforts resulted in conversion efficiency improvements from 10^{-5} % to 3 % for CuO based, small area and laboratory devices. As a result, this material system is being considered nowadays as the basis of PV module technologies for terrestrial power generation. Moreover, these solar cells are very stable, and thus their operational lifetimes are longer.

Due to the industrial Revolution the atmospheric pollution has become particularly serious. Atmospheric pollution is defined as a status containing gases, offensive odors, and particles that are harmful to humans, animals, vegetables, or living environments above the regulation limits in specific regions. Furthermore, due to the recent dramatic growth in population and industrial development, along with an intensified usage of fossil fuels, the natural atmospheric environment has become polluted and is rapidly deteriorating. Yet, since the level of public concern related to living and working in a healthy environment has now increased, the demand for monitoring and controlling the atmospheric environment in the house and workplace has also increased. To prevent or minimize the damage caused by atmospheric pollution, monitoring and controlling systems are needed that can rapidly and reliably detect and quantify pollution sources within the range of the regulating standard values. A lot of recent research and development has been focused on the development of solid-state gas sensors; consequently, their performances have improved dramatically. Over the past 20 years, a great deal of research effort has been directed toward the development of small dimensional gas sensing devices for practical applications ranging from toxic gas detection to manufacturing process monitoring. With the increasing demand for better gas sensors or higher sensitivity and greater selectivity, intense efforts are being made to find more suitable materials with the required surface and bulk properties for use in gas sensors. Among the gaseous species to be detected are nitric oxide (NO), nitrogen dioxide (NO_2), carbon monoxide (CO), carbon dioxide (CO_2), hydrogen sulfide (H_2S), sulfur dioxide (SO_2), ozone (O_3), ammonia (NH_3), and organic gases such as methane (CH_4), propane (C_3H_8), liquid petroleum gas (LPG), and many others.

Sensors are devices that convert physical or chemical quantities into electrical signals that are convenient to be detected. A gas sensor must possess at least two functions: to recognize a particular gas and to transducer the gas recognition into a measurable sensing signal. The gas recognition is carried out through surface chemical processes due to gas–solid interactions. These interactions are resulting form of adsorption, or chemical reactions. The transducer function of a gas sensor is dependent on the sensor material itself. Most gas sensors give an electrical output, measuring the change of resistance or capacitance. Semiconductor gas sensors are solid-state sensors whose sensing component is made up of mostly semiconductor metal oxide. Materials such as tin oxide (SnO_2), zinc oxide (ZnO), titanium oxide (TiO_2) and tungsten oxide (WO_3) have been used by most researchers. The report on a ZnO-based thin film gas sensor by Seiyama et al. in 1962 gave rise to unprecedented development and commercialization of a host of semiconducting metal oxide for the detection of a variety of gases over a wide range of composition. Among this metal oxide, cupric oxide (CuO) have been attract more intention as a sensitive layer for sensing a dangerous, inflammable and toxic gaz. the CuO-based senor thin films have been more successfully employed as sensing devices for the detection and metering of a host of gases such as CO, H_2, H_2O, NH_3, SO_x, NO_x, etc., with varying degree of commercial success. Using this metal oxide has several advantages, such as simplicity in device structure, low cost for fabrication, robustness in practical applications, and adaptability to a wide variety of reductive or oxidative gases.

Several techniques have been used to prepare CuO thin films namely: sputtering [11] , thermal evaporation [12] electrodeposition [13], chemical vapor deposition [14] and sol-gel method [15]. Among these, ultrasonic spray pyrolysis has attracted much attention because it is a simple and cheap technique. Although the fact that CuO thin films deposited with this technique have a good optical proprieties by comparison to the films deposited by the other techniques, they have shown to be the most suitable for solar cells. On other hand, the easy to controller the deposition parameters lead to the controlled of the proprieties suitable for each application. It is well known that films properties regardless the deposition technique is very sensitive to the deposition parameters. The structural, optical and electrical properties of the CuO layer influence drastically the characteristics and the performance of the CuO-based gas sensor and solar cells.

The aim of the present thesis is the investigation of the influence of the deposition parameters on the properties of CuO thin films prepared by ultrasonic spray pyrolysis in order to optimize these parameters to produce a suitable absorber layer for low cost solar cells and gas sensor for sensing organic vapor and different gases. A systematic study of the influence of various parameters related to this technique on film properties will be carried in the present work.

The thesis is organized as following:

- In chapter I: we will present a literature survey on CuO thin films, an insight upon its different properties and applications will be outlined.
- The Chapter II: is dedicated to the experimental details of films deposition and the used their characterization techniques. A review on the different deposition techniques will be presented; more attention will be payee to the techniques used in this thesis.
- In chapter III: the obtained results of the deposited CuO thin films will be reported with a discussion.
- In chapter IV: the realized application of CuO thin films will be represented.

Chapter I

Cupric oxide thin films (CuO): Review

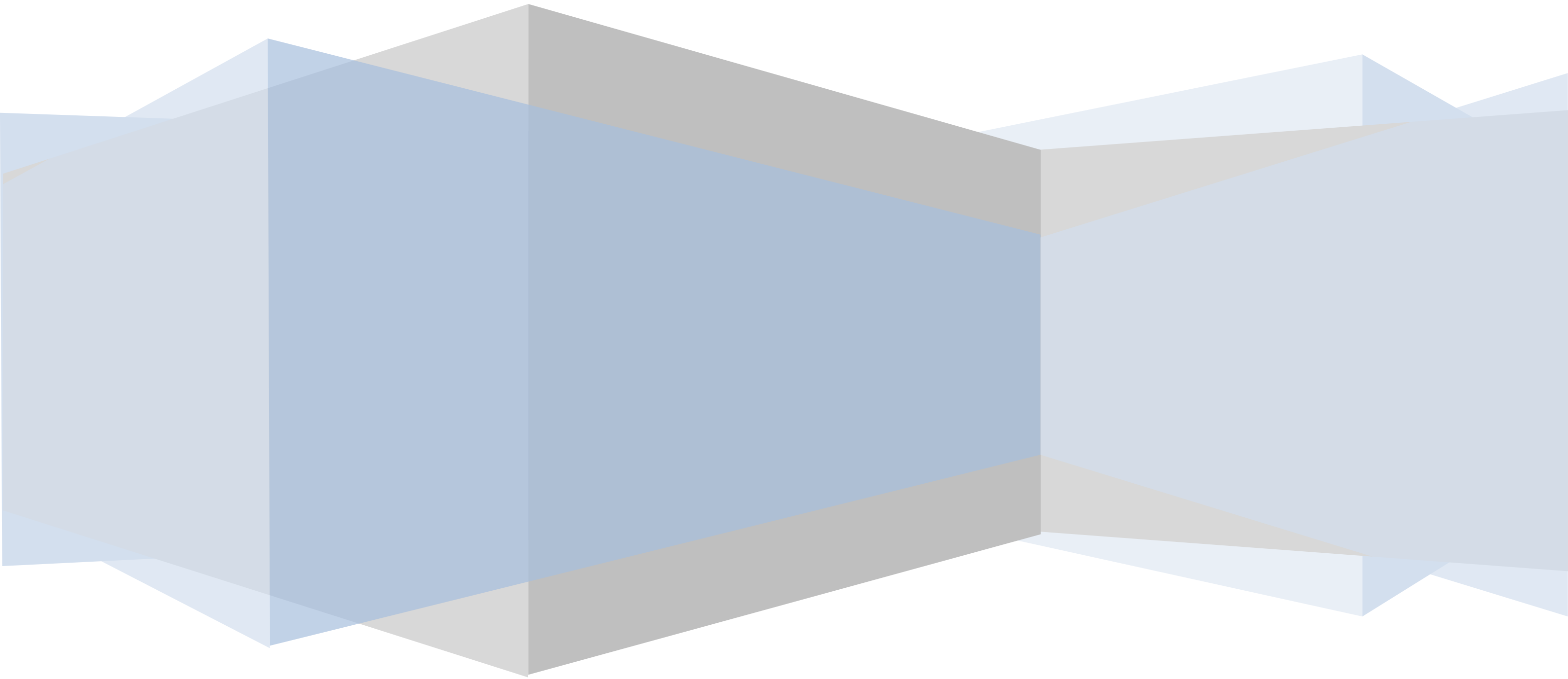

The present chapter is a brief survey on structural, optical and electrical properties of CuO thin films and their most important applications in various technological areas. A review of experimental results obtained by different authors will be presented with a discussion of deposition parameters effect on the different properties of CuO thin films deposited by different techniques.

I.1 Metal oxide thin films

Metal oxides are an important class of materials: from both scientific and technological point of view. They found huge interesting applications in different technological fields. Oxide semiconductors are gaining interest as new materials that may challenge the supremacy of silicon. Metal oxide thin films are known for many years ago due to the industrial interest on their unique properties [16].

The physicochemical properties of metal oxide thin layers are closely related to preparation processes and operating conditions. Indeed, it is possible to obtain thin films having an amorphous or crystalline structure. Thereafter, films structural, electrical and optical properties can be tailored by varying the condition and the deposition process. Control of film properties is therefore key parameters of metal oxide films preparation to be used in wide applications such as: fabrication of microelectronic circuits, sensors, piezoelectric devices, fuel cells, coatings against corrosion, and as catalysts. Some metal oxides, their electronic band gap, and conducting nature are listed in table I.1.

Earlier, research in the field has been devoted to bulk metal oxides before interest in their thin films aspect. These oxides are zinc oxide (ZnO), tin oxide (SnO_2), titan oxide (TiO_2), tungsten oxide (WO_3), cuprous oxide (Cu_2O) and cadmium oxide (CdO). Recently, several metallic oxide thin films have emerged such as vanadium oxide (V_2O_5), nickel oxide (NiO) molybdenum oxide (MoO_2) and cupric oxide (CuO). Among these oxides, cupric oxide (CuO) thin films exhibit an interesting combination of multifunctional proprieties including: optical, semiconducting, magnetic, electronic, and optoelectronic. CuO thin films find many applications in electronic devices such as: gas sensors, solar cells, catalysts and Li batteries.

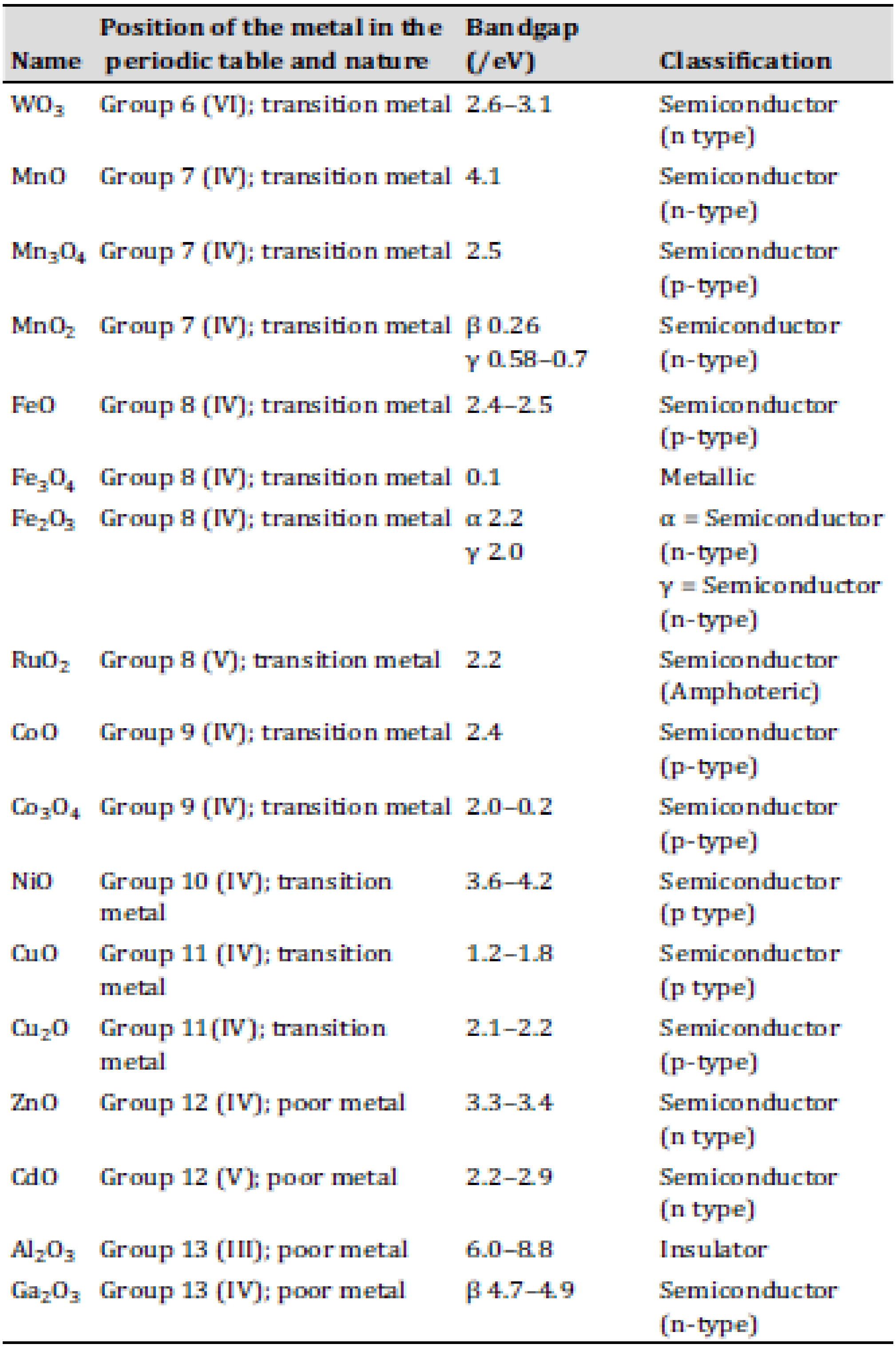

Name	Position of the metal in the periodic table and nature	Bandgap (/eV)	Classification
WO_3	Group 6 (VI); transition metal	2.6–3.1	Semiconductor (n type)
MnO	Group 7 (IV); transition metal	4.1	Semiconductor (n-type)
Mn_3O_4	Group 7 (IV); transition metal	2.5	Semiconductor (p-type)
MnO_2	Group 7 (IV); transition metal	β 0.26 γ 0.58–0.7	Semiconductor (n-type)
FeO	Group 8 (IV); transition metal	2.4–2.5	Semiconductor (p-type)
Fe_3O_4	Group 8 (IV); transition metal	0.1	Metallic
Fe_2O_3	Group 8 (IV); transition metal	α 2.2 γ 2.0	α = Semiconductor (n-type) γ = Semiconductor (n-type)
RuO_2	Group 8 (V); transition metal	2.2	Semiconductor (Amphoteric)
CoO	Group 9 (IV); transition metal	2.4	Semiconductor (p-type)
Co_3O_4	Group 9 (IV); transition metal	2.0–0.2	Semiconductor (p-type)
NiO	Group 10 (IV); transition metal	3.6–4.2	Semiconductor (p type)
CuO	Group 11 (IV); transition metal	1.2–1.8	Semiconductor (p type)
Cu_2O	Group 11(IV); transition metal	2.1–2.2	Semiconductor (p-type)
ZnO	Group 12 (IV); poor metal	3.3–3.4	Semiconductor (n type)
CdO	Group 12 (V); poor metal	2.2–2.9	Semiconductor (n type)
Al_2O_3	Group 13 (III); poor metal	6.0–8.8	Insulator
Ga_2O_3	Group 13 (IV); poor metal	β 4.7–4.9	Semiconductor (n-type)

Table I.1 *Some metal oxides, their position in the periodic table, band gap, and conducting nature [17].*

I.2 Cupric oxide thin films

Copper have two oxidation states +1 and +2, while under special circumstances some compounds of trivalent are also reported. It was shown that this trivalent copper survives not more than few seconds. Consequently, cuprous oxide (Cu_2O) and cupric oxide (CuO) are the two stable forms of copper oxide. However, only cupric oxide (CuO) phase is reported as a gas-sensitive material and exhibits a number of interesting properties.

CuO has attracted particular attention because it is the simplest member of the family of copper compounds and exhibits a range of potentially useful physical properties, such as high temperature superconductivity, electron correlation effects, and spin dynamics.This led to a rapid research expansion in theoretical studies, fabrication, characterization and applications of CuO based devices in the latter half of the 20th century [18].

Cupric oxide can be obtained easily by heating cuprous oxide (Cu_2O) or copper in air at 1273-1373 K nearly, cupric oxide is formed as follows:

$$Cu_2O + \tfrac{1}{2} O_2 \longrightarrow 2CuO$$

$$2Cu + 2\, O_2 \longrightarrow 2CuO$$

But in industrial method it is prepared by heating malachite ore, CuO is produced according the reaction below:

$$CuCO_3.Cu\,(OH)_2 \longrightarrow 2CuO + CO_2 + H_2O + O_2$$

CuO had been studied extensively for a number of decades, with electrical and optical properties reviews, available as early since the 1960’s. The first period of notable growth in CuO research interest occurred in the mid of 1980’s with a series of highly-cited research works [19].CuO thin films have been successfully deposited by several deposition techniques including thermal evaporation [20-21], spray pyrolysis (SP) [22-24], plasma evaporation [25], dc magnetron sputtering [11], elctrodeposition [13], sol-gel [15] .Work in the early part of the 2000s were mainly focused on growth mechanisms and parameters influence. Several review articles dealing with the state-of the-art of CuO have been published with extensive discussion on band structure, thermal, magnetic, optical and electrical properties, doping, growth and devices.

I.2.1 Physical and chemical proprieties of cupric oxide (CuO)

Cupric oxide in mineral form is called “tenorite”. Pure cupric oxide is black solid with a density of 6.32 g/cm^3 and insoluble in water. It is melts above 1134 °C with some loss of oxygen. Table I.2 regroups some physical and chemical properties of cupric oxide.

Cupric oxide (CuO)	
Chemical names	Copper (II) oxide Cupric oxide Copper monoxide Copper oxide (CuO) Oxocopper
Molecular Formula	CuO
Appearance	Black powder
Solubility in water	Insoluble
Molecular Mass	79.55 g/mol
Density	$\rho = 6.32$ g/cm^3
Relative permittivity	12
Melting point	1134°C
Boiling point	2000 °C

Table I.2 *Physical properties of CuO*

I.2.2 Crystal structure of cupric oxide thin films

Cupric oxide has much more complicated tenorite crystal structure. The monoclinic unit cell (space group C_{2h}^{6}) contains four CuO molecules, as shown in figure I.1. The atoms coordination is that each atom has four nearest neighbors of the other kind. For example, in the (110) plan (as depicted in figure I.1), each Cu atom (the big turquoise spheres) is linked to four nearest O atoms at the corner of an almost rectangular parallelogram. While, each O atom (the small red spheres) is coordinated to four Cu atoms in the form of a disorder tetrahedron. Lattice constants and other crystallographic properties are listed in Table I.3.

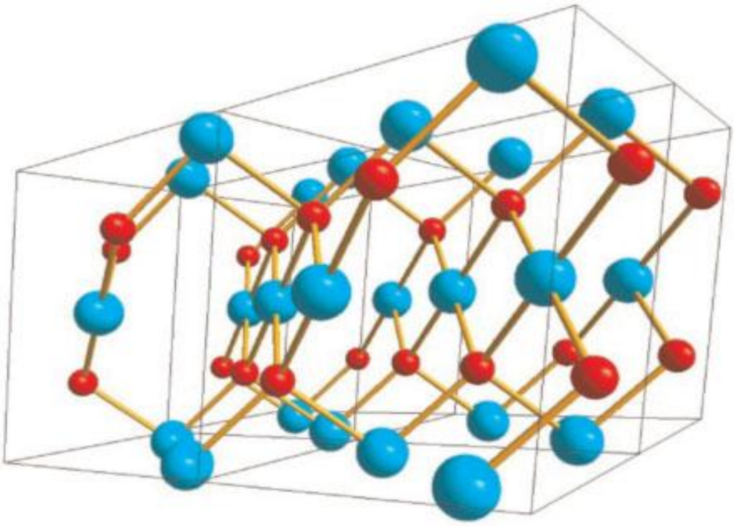

Figure I.1 *Crystal structure of CuO shown by four unit cells.*

Crystallographic properties of CuO	
Space group	C2/c
Unit cell	a = 4.6837 Å b = 3.4226 Å c = 5.1288 Å β = 99.548° α ,γ = 90°
Cell volume	81.08 $Å^3$
Cell content	4 [CuO]
Distances	
Cu-O	1.96Å
Cu-Cu	2.62Å
O-O	2.90Å

Table I.3 *Crystallographic properties of CuO*

I.2.3 Structural properties

It is well argued that thin film growth is strongly related to the deposition conditions and the used method. Indeed, there is a different deposition technique in which the deposition temperature is one of the main parameters that should be controlled to achieve high films quality.

In table I.4 we have compiled effect of substrate, annealing and bath temperatures on the structural properties of CuO thin films deposited by different techniques. From this table, we note that the formation of pure Cu_2O thin films occurs at low temperatures (around 200 °C), while the formation of a pure CuO films requires higher temperature ranged from 300 to 500 °C. However the formation of Cu_4O_3 phase mixed with other CuO compounds are rarely formed. Ooi et al [26] have studied the effect of oxygen percentage on the structural proprieties of cupric oxide (CuO) thin films and they found the presence of the three different phases of copper oxide thin films namely: Cu_2O, Cu_4O_3, and CuO. The apparition of these phases depended strongly to the oxygen percentage. As can be seen, at lower oxygen percentage a pure Cu_2O thin films with cubic structure are deposited with increasing the oxygen percentage a pure CuO thin films with monoclinic structure are elaborated.

The oxidation kinetics depends on many factors such as temperature, oxygen partial pressure, annealing time etc. For CuO thin films elaborated with thermal oxidation, a pure CuO thin film is obtained at higher temperature under oxygen atmosphere however at lower temperature a mixture of the various copper oxides are formed. Ezenwa [30] have deposited CuO thin films by chemical bath deposition, he have found that the annealing temperature effect strongly the structural proprieties of the deposited films. The increasing of annealing temperature from 300 to 400°C leads to the change of phases and structure from a mixture of Cu_2O and CuO phase to formation of pure CuO phase. The same observation is found for the CuO thin films elaborated with sol-gel method [28]. However, no change of phases is observed for the CuO thin films deposited with electrodeposition technique.

Deposition method	Parameter	Present phase	(hkl) plan	Reference
Sol-gel	**Annealing temperature**			[28]
	300 °C	Cu_2O	(200) (110)	
	400 °C	CuO	(111) (002)	
	500 °C	CuO	(111) (002)	
Thermal oxidation	**Temperature**			[12]
	150 °C	Cu_2O, Cu	(111)	
	200 °C	Cu2O	(111) (200)	
	250°C	CuO	(-111) (111)	
Electrodeposition	**Bath temperature**		(-111) (200) (220) (311) (222)	[27]
	45°C	CuO		
	60°C	CuO		
	75°C	CuO		
	90°C	CuO		
Reactive RF sputtering	**Oxygen percentage**			[26]
	10 %	Cu_2O	(111) (200)	
	20 %	Cu_4O_3	(202)	
	30 %	CuO	(-111)	
	40 %	CuO	(-111)	
	50 %	CuO	(-111)	
Chemical bath deposition (CBD)	**Annealing temperature**			[30]
	As-deposited	Cu_2O	(111)(200)(220)	
	300 °C	CuO and Cu_2O	(111)(200)(220)	
	400 °C	CuO	(-111) (200)	

Table I.4 *Crystal growth for CuO thin films elaborated by various deposition techniques.*

The detected (hkl) growth direction along with the preferred orientation extracted from XRD analysis for CuO thin films prepared by spray deposition with different conditions are listed in table I.5. Singh et al [31] have deposited CuO films by ultrasonic spray deposition at differences substrates temperature from 300 to 400°C and show that the CuO films are polycrystalline in nature with presence of two most prominent peaks corresponding to atomic planes (002) and (111), whereas growth along atomic planes (110), (020) and (220) are also observed.

The experimental conditions must be carefully chosen in order to obtain the desired structural properties. For example: some authors agreed that the increase in the substrate temperature improves the films crystallinity and yields to the change from amorphous to polycrystalline structure. In the other hand, Singh et al. [31] has obtained this structural change by varying the deposition time. They have found that CuO thin films deposited for deposition time equal to 10 min are amorphous, with increasing spray time the films becomes polycrystalline with improvement in their crystallinity.

Deposition technique	Parameters studied	(h k l)	The preferred orientation	References
Spray deposition	Substrate temperature **300 – 400** °C	$(\bar{1}11)$ (200) (020) $(\bar{1}13)$ (220) (004)	$(\bar{1}11)$	[32]
	Substrate temperature **300** – **400** °C	(002) (111) (110) (020) (220)	(002)	[31]
	Deposition time **10** min **20** min **30** min	amorphous (002) (111) (110) (002) (111) (020) (220)	(002)	[33]

Table I.5 *Crystal growth and orientation for CuO thin films elaborated by spray deposition.*

Many studies have confirmed the influence of the experimental parameters on the crystallites size, such as: the substrate temperature, deposition time, the nature and concentrations of source solutions, doping and the nature of the substrate. In table I.6 we compiled the values of the crystallites size reported in the literature for CuO thin films deposited by spray deposition technique.

The general reported have found that the crystallites size increases with the substrate temperature or deposition time for CuO films prepared by this technique. For sprayed CuO thin films, Gopalakrishna et al. [32] have reported an increase in crystallites size from 30 to 49 nm by changing the substrate temperatures from 250 to 350 °C. However, Morales et al. [33] have obtained an increase of the crystallites size from 30 to 130 nm with increasing deposition time from 30 to 60 min.

It was emphasized that the film doping may also alter the film structure and the crystallites size. As can be seen from the table I.6 for CuO thin film deposited by spray technique, It was reported that crystallites size decreases from 31 nm for udoped CuO thin films to 27 nm for CuO:Fe doped one with 15% Fe [34] . In addition, Shabu et al. [35] have found that an increases in precursor concentration of the started solution from 0.15 to 0.20 M leads to crystallites size enlargement from 37 to 52 nm.

Deposition technique	Parameters studied	Crystallites size (nm)	Reference
Spray deposition	Substrate temperature **300-400** °C	38-40	[32]
	Substrate temperature **250-350** °C	30-49	[33]
	Fe doped **0-15** %	30-27	[34]
	Deposition time **30-60** min	30-130	[33]
	Precursor concentration **0.15-0.20** M	37-52	[35]

Table I.6 *Values of crystallite size for CuO thin films deposited by spray technique.*

I.2.4 Film morphology

Films surface morphology in is an interesting characteristics that is required for film application as gas sensor or any applications requiring high specific exchange surface or light scattering. CuO thin films morphology is generally examined by SEM (Scanning Electronic Microscopy) and AFM (Atomic Force Microscopy) observation. It is reported that CuO morphology is close related to the deposition technique and conditions.

In figure I.2 we have reported typical SEM images of CuO thin films deposited with diverse techniques. As can be seen, the morphology of CuO thin films is different from deposition technique to another. This diversity in morphology is due to the difference in deposition process involved in each technique.

In PVD techniques (sputtering and pulsed laser deposition) the films formation is achieved through species condensation on the substrate which resulted that the films deposited by this techniques are more homogenous, denser and smoother with good adherence. However, films prepared by CVD techniques (SILAR method) are formed through chemical reaction coming from the solution. CuO films deposited by these techniques are generally uniforms and fewer adherents.

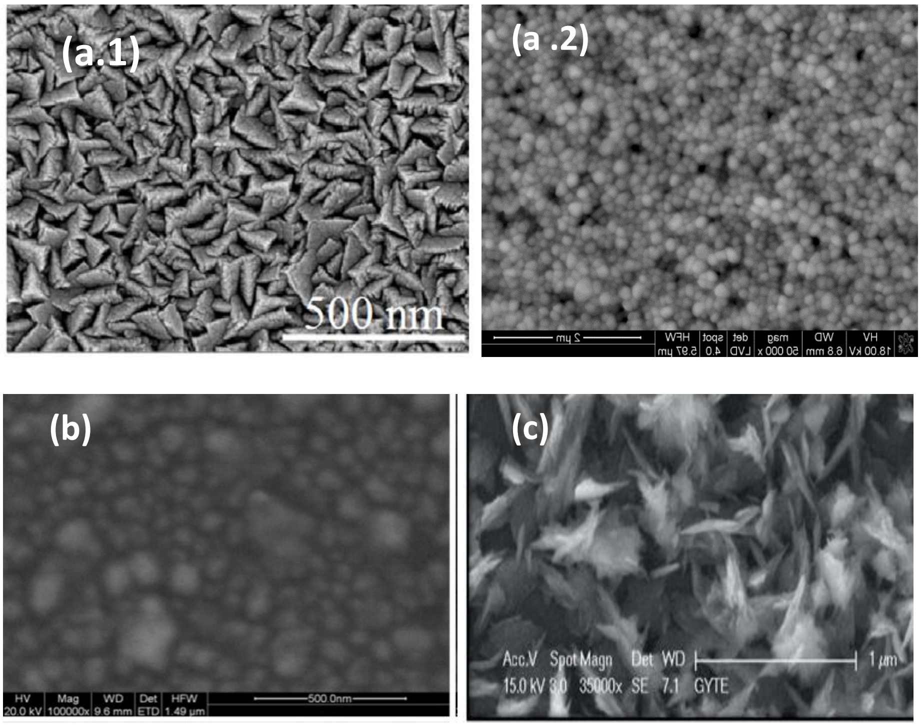

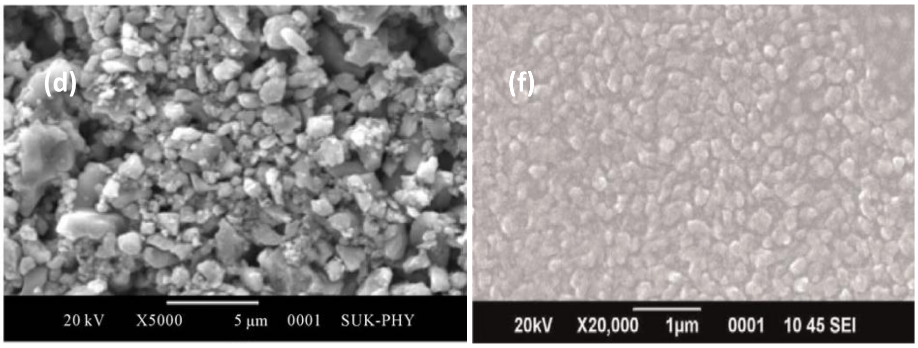

Figure I.2 *SEM images of CuO thin films deposited by (a.1 and 2) sputtering, (b) thermal evaporation, (c) SILAR method, (d) sol-gel method, (f) spray pyrolysis [11-26].*

In figure I.3 we have represented the three dimensional AFM images for CuO thin films deposited with sputtering method at various oxygen percentage and annealing temperature. For CuO thin films prepared by sputtering or thermal evaporation (PVD techniques), the substrate temperature, annealing temperature and oxygen percentage are the most important parameters those affect strongly the film morphology. For example, Ooi et al. [26] have studied the effect of oxygen percentage on CuO thin films growth by reactive radio frequency sputtering, they have found that the films surface roughness decreases from 4.82 nm to 1.78 nm (figure I.3-a) with oxygen percentage increasing in the deposition chamber from 10 to 50 % . In other hand, Guo et al. [36] have reported that the increase in annealing temperature from 500-575 °C the RMS surface roughness increases from 0.8 to 12 nm for CuO thin films deposited by magnetron sputtering (figure I.3-b). As can be seen, the films roughness is also altered by the deposition condition this indicated that the choice of the deposition conditions leads to the control of the morphology of the deposited films by decreasing of increasing the roughness of the films for a particular application such as: photocatalysis and sensing.

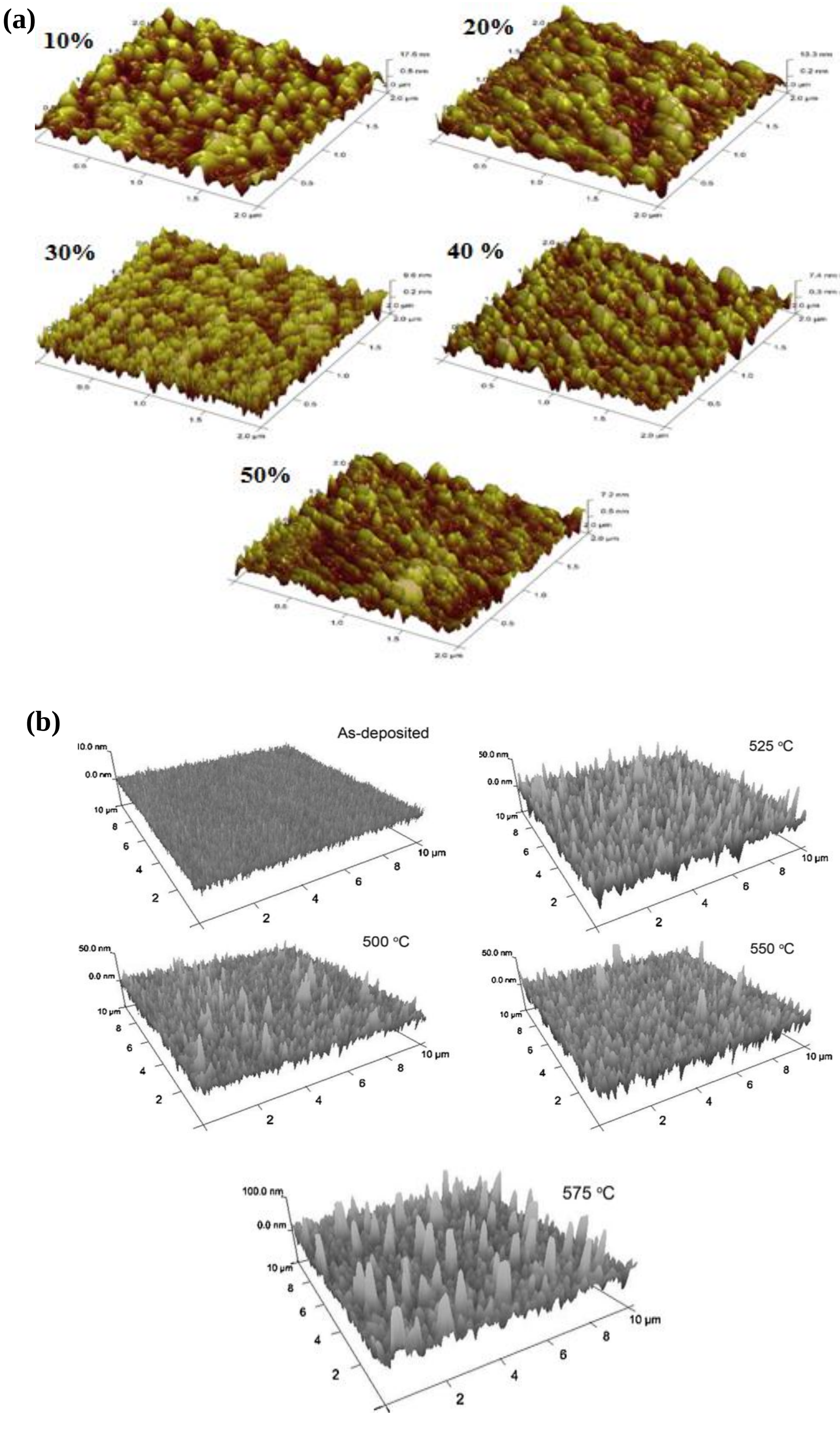

Figure I.3 *Three-dimensional AFM images of CuO thin films grown by sputtering, (a) at various oxygen percentages R (O2), (b) at various annealing temperatures [26-36].*

However, in the case of spray pyrolysis technique, the films morphology can be controlled by several deposition parameters namely: deposition time, substrate temperature, precursor concentration and doping. It is generally argued that substrate temperature is an effective parameter that may controls shape, grains size, surface roughness, porosity and density of voids. For CuO thin films deposited by spray pyrolysis at different substrate temperatures, Gopalakrishna et al [32] and Singh et al [31] have observed an improvement in films surface morphology, they concluded that films become more homogenous and denser with larger grains, with increasing substrate temperature from to 350 and 400°C as shown in figure I.4 illustrating the SEM images of CuO thin films deposited at different substrate. The estimated grain size was also increasing from 255 to 500 nm in the study temperature range.

Atomic Force Microscopy analysis suggested that the deposition time has also an impact on the morphology of CuO thin films deposited by spray technique as shown in figure I.5. For films deposited during 30 minutes, the surface is compact and smooth, showing a granular structure with well-defined grain boundaries. While, film deposited during 60 minutes displays a rather rough and an inhomogeneous surface [33].

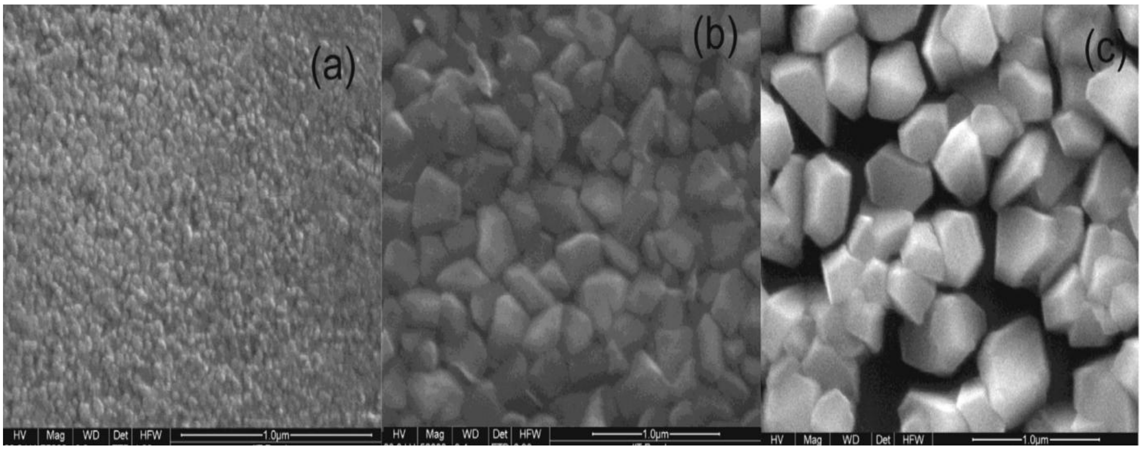

Figure 1.4 *SEM images for CuO thin films deposited by spray pyrolysis for various substrates temperature (a) 300°C, (b) 350°C and (c) 400°C [32].*

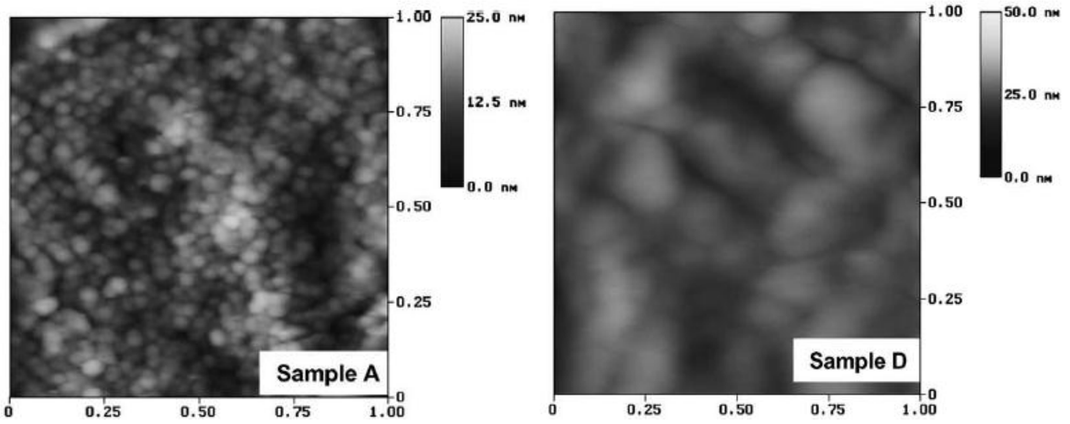

Figure 1.5 *SEM images for CuO thin films deposited by spray pyrolysis for various deposition time (a) 30 min and (d) 60 min [33].*

Nanoscale architectures have attracted strong interests due to their unique properties from large surface-to-volume ratio. Hence, cupric oxide nanostructures offer unique characteristics and advantage for many industrial applications. CuO nanostructures are easy to synthesize via simple chemical methods or oxidation techniques. Several nanostructures of cupric oxide are reported in the literature such as: CuO nanowire, CuO nanorods, CuO nanoribbon, and CuO plates as shown in figure 1.6.

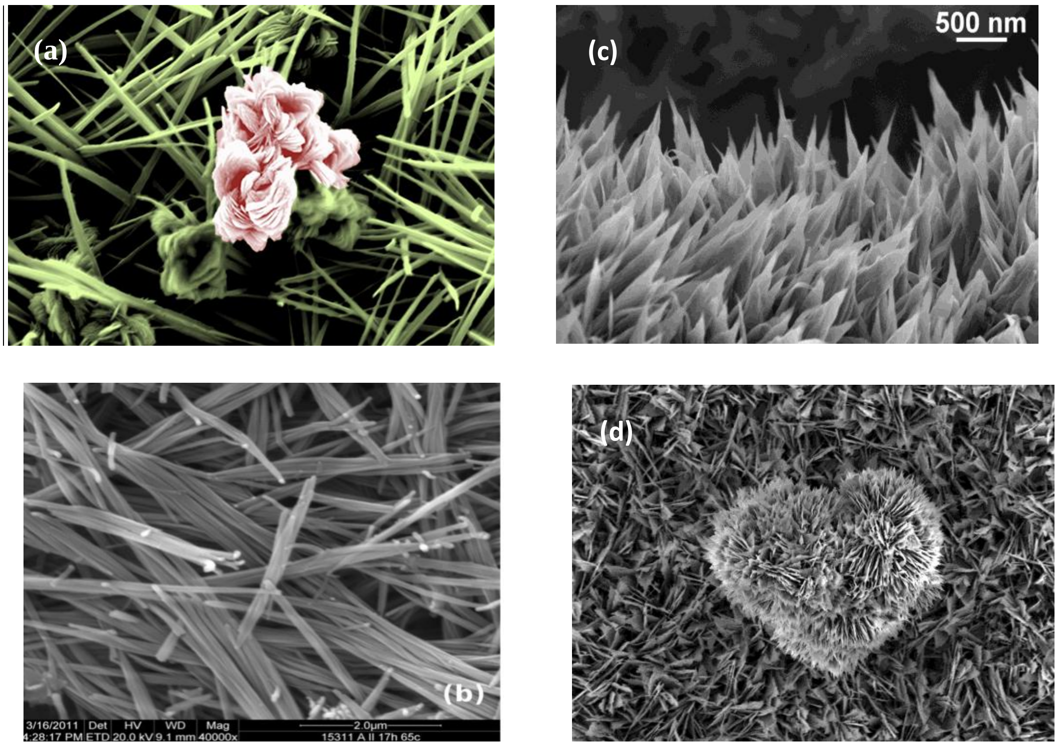

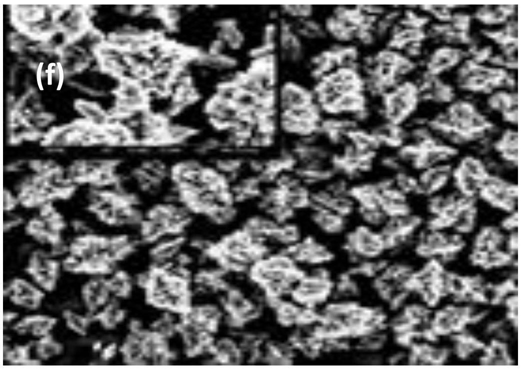

Figure I.6 *CuO nanostructures: (a) nanograss and flowerlike nanostructures,(b) nanorods,(c) scalable,(d) heart shaped, (f) nanoflowe*rs.

I.2.5 Films Composition

CuO thin films composition was generally analyzed by EDX, few composition studies are performed with RBS (Rutherford Back Scattering) and XPS (X-ray photoelectron spectroscopy). It is generally reported that CuO thin films composition varies with deposition techniques and parameters. In contrary, some authors found no changes in the composition with films deposition conditions.

In table I.7 we have illustrated the variation of element composition of CuO thin films deposited by sputtering and spray pyrolysis. The composition of the films depends by the deposition technique used as well as the condition of the elaboration. As can be seen from this table, Ooi et al. [26] have investigated the films elemental composition change with oxygen percentage in deposition chamber during CuO thin films deposited by reactive radio frequency sputtering , they have concluded that Cu amount is reduced with increasing oxygen percentage , whereas O amount is increased . For example film prepared with 10% of oxygen, the Cu:O ratio was 3.38; indicating the formation of Cu-rich cupric oxide films. While for 50% percentage of oxygen, the Cu:O ratio was less than unity.

For sprayed CuO thin films, the effect of substrate temperatures on films composition was investigated by Singh et al [31], they have reported an increase in films oxygen content with increasing substrate temperature. As can be seen the increasing in the substrate temperature leads to the formation of O-rich CuO films. This result are observed in many works, they have found that the increasing in substrate temperature engender the formation of Cu- poor CuO thin films. It can be explained by the volatility of copper.

Deposition technique	Parameters	Element weight (%)	
Reactive radio frequency sputtering	Oxygen percentage (%)	**Cu**	**O**
	10	77	22
	20	52	47
	30	44	50
	40	40	51
	50	37	52
Spray pyrolysis	Substrate temperatures		
	300 °C	43	57
	350°C	42	58
	400 °C	37	63

Table I.7 *Variation of element composition of CuO thin films deposited by sputtering and spray pyrolysis.*

I.2.6 Optical properties

The optical properties are a crucial parameter for thin films dedicated to optoelectronic devices. The importance of CuO optical proprieties originated from it is useful applications as an absorber layer in solar cells. This application requires the fulfillment of a high absorption in the visible range of solar spectrum.

Since the deposition technique and the experimental parameters affects the structural properties, the film surface morphology, the optical properties are also altered by the preparation conditions [8,12, 31]. Regardless the deposition technique, CuO thin films have a transparency ranged from 0 to 80%. In figure I.7 we have reported transmission spectra of CuO thin films deposited by spray pyrolysis, sputtering, SILAR and Sol-gel method. Films elaborated by sputtering technique are characterized by the presence of interference fringe in their transmission spectra, the presence of this fringe are rarely observed in transmission spectra of CuO films. The existence of this interference fringe is a signature of surface smoothness of the deposited films. From the transmission spectra represented in figure I.7, we can notice the absence this fringe for the films prepared by spray technique this indicates that the elaborated films have rough surface by comparison to films deposited by sputtering technique.

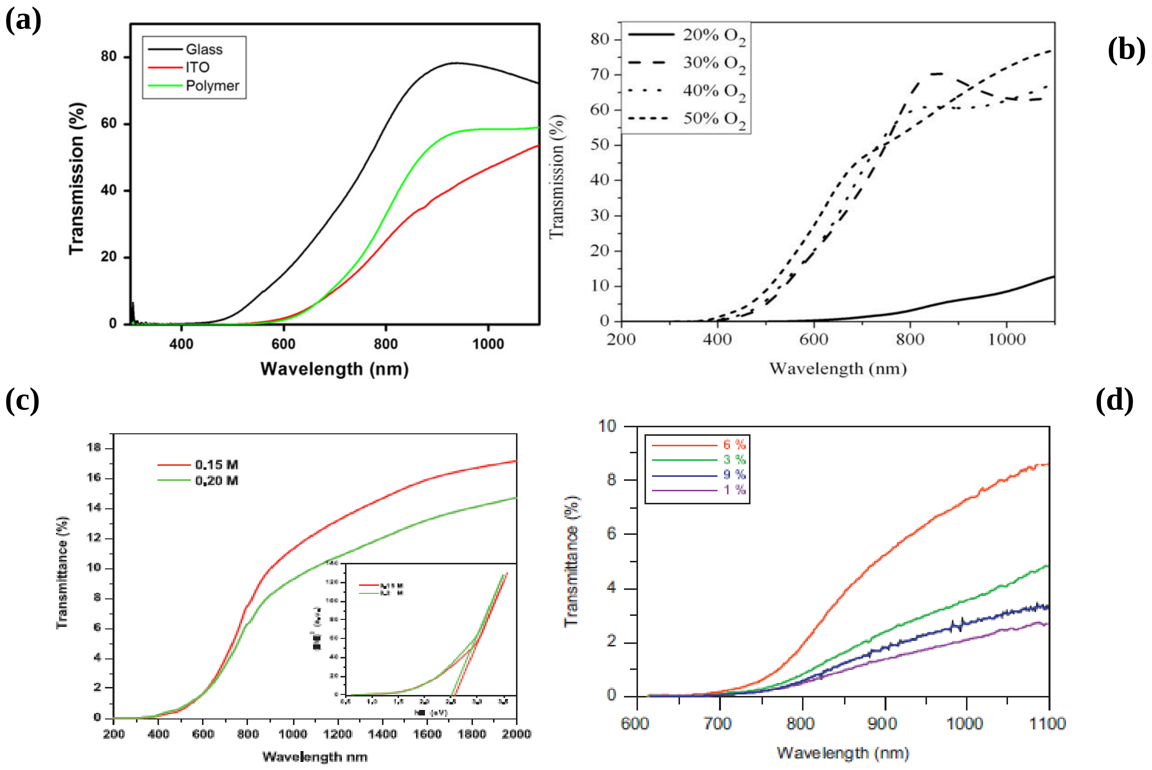

***Figure I.7** Transmittance spectra reported in CuO thin films prepared by different techniques: (a) sol- gel [15], (b) sputtering [11] (c) spray pyrolysis [35], (d) SILAR method [38].*

In figure I.8 we have reported transmission spectra of CuO thin films deposited by spray and SILAR method with different precursor concentration and various doping concentration of Mn, respectively. An increase in transmittance with annealing temperature was recorded by Saravanan et al. [39] in undoped CuO thins films prepared by spray pyrolysis. Gulen et al. [38] have also found an increase in the transmittance of the films with increasing the doping concentrations of Mn for CuO films prepared by SILAR method. They have found the transmittance increases rapidly from 10 to 80 % with the variation of Mn doping concentration from 1 to 5 at %. A decrease in transmittance with various precursor concentrations was observed by Chafi et al. [35] in CuO thin films prepared by spray pyrolysis technique, the decrease in the transmittance of the deposited films is probably due to the increase in the molarity of the solution. But at the same time they noticed an increase in film thickness which may be the main reason of the decrease in transmittance.

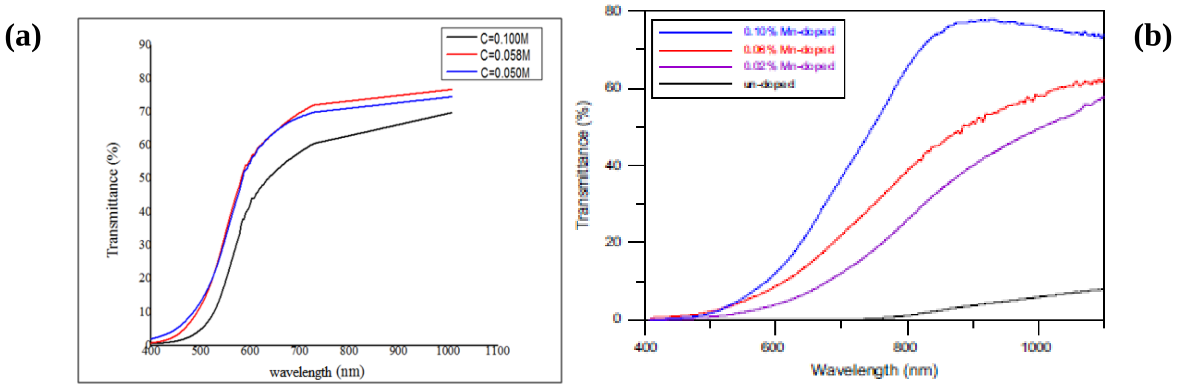

Figure I.8 *Transmittance spectra for CuO thin films deposited by spray pyrolysis technique and SILAR method with different: (a) precursor concentration [39], (b) doping concentration of Mn [38].*

The optical band gap (Eg) is generally deduced from the optical transmittance. Bulk cupric oxides (CuO) have a direct narrow band gap of 1.2 eV. However in CuO thin films the optical band gap can vary in a wide range from 1 to 1.8 eV depending on the deposition techniques and parameters.

Numerous experimental studies emphasized that the band gap variation can be due to various factors such as: grain size, substrates temperature, thickness, doping concentration, lattice strain, structural parameters and disorder. In figure I.9 we have reported the variation of optical band gap for CuO thin films deposited by various deposition techniques and different parameters. The decrease of band gap energy with films was reported by some authors such as Akaltun et al. [40]. They have observed a decrease in films band gap from 2.03 eV to 1.79 eV related to the increase in film thickness from 120 to 310 nm for CuO films prepared by successive ionic layer adsorption and reaction (SILAR) method (figure I.9 (b)).

The dependence of the band gap energy on substrate temperature was recorded by different workers [8, 12, 18, 30]. This dependence is due to the stress in films deposited at low temperatures, which results in films band gap broadening. However, this dependence is also related to variation of other structural parameters such as crystallites size. For spray-deposited CuO thin films on glass substrates, Gopalakrishna et al. [32] reported a decrease in the optical band gap energy from 1.8 to 1.2 eV with increasing substrate temperature from 250-350 °C. They interpreted the optical band gap variation in terms of films morphology and crystallites size variation with substrate temperature (figure I.9 (a.1)). An increase in the optical band gap energy with doping concentration was also observed. For spray-deposited CuO thin films, optical gap increases from its value equal 1.42 eV in un-doped to 2.2 eV in 10 at % Mn-doped CuO thin films [38] (figure I.9 (a.3)). We same behavior is observed for CuO thin films doped with Fe-Cu deposited with spray pyrolysis technique (figure I.9 (d.3)).

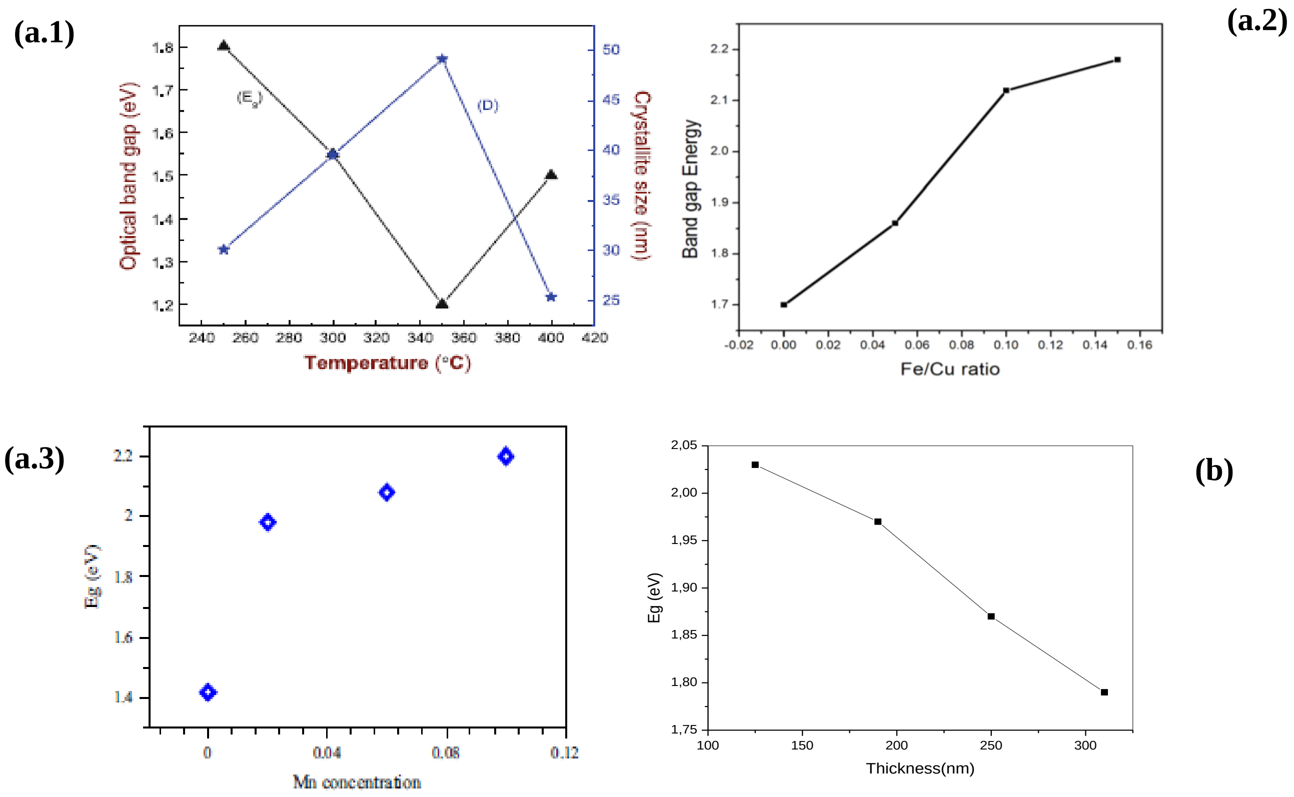

***Figure I.9** Variation of CuO optical band gap with deposition techniques and parameters: (a) spray pyrolys ,(b) SILAR method .*

The refractive index of bulk CuO is equal to 2.63. The later is deduced from the ellipsometric measurements. For CuO thin films, the refractive index changes in the range of 1.5 to 3.5 according to the deposition conditions [27-33]. Which are the same values of the refractive index for the both absorber layer CdTe and CIS. Less attention has been carried to the measurement of the refractive index compared to the other optical quantities for example: optical band gap, transmission and absorption. For CuO thin films deposited by electrodeposition, Dhanasekaran et al [27] have found values of refractive index laying between 2 and 3.5 when the bath temperature is varied from 30 °C to 90 °C. An increase in film thickness leads to the formation of denser films resulting an increase in refractive index as concluded by Akaltun et al. [40] for CuO thin films prepared by SILAR method as shown in figure I.10.

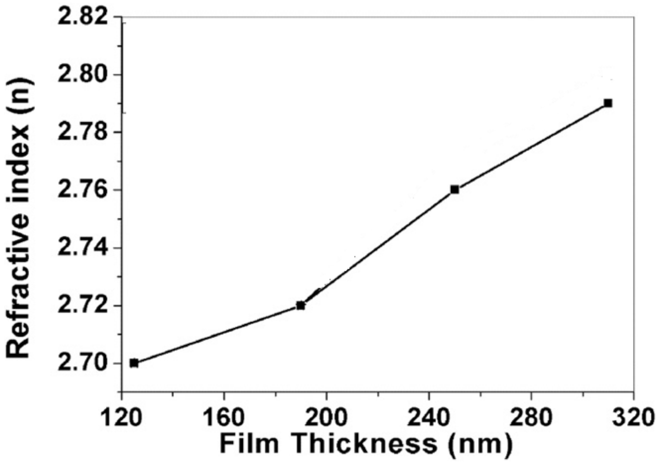

Figure I.10 *Variation of refractive index of CuO thin films elaborate by SILAR method with different thickness*.

The optical band structure and optical transitions are affected by the presence of localized states in the band gap characterized by a band tail. This tail width is commonly known as Urbach tail or disorder in films network (E_{00}). Basically, Urbach energy depends on the static and induced disorder and deposition temperature. Mugwanga et al. [42] have deposited CuO thin films prepared by reactive dc magnetron sputtering and has reported that the values of disorder is in the range 60-192 meV for various oxygen flow rate varied from 5 to 22.5 (Sccm) during films growth . Ravichandran et al [41] have observed a decrease in disorder from 533 to 470 meV for as-deposited CuO thin films by SILAR method and for CuO thin films annealing at 450°C, respectively.

I.2.7 Electric properties

CuO is believed to be intrinsically p-type semiconductor, due to the presence of copper vacancies as acceptors being responsible for the hole conduction. The electrical properties of pure CuO are mostly determined by the dominant intrinsic defects, like copper and/or oxygen vacancies. It is well known that copper vacancies are the most dominant defects in a nonstoichiometric cupric oxide due to the copper volatility [20-22]. Actually, copper vacancies give rise to shallow acceptor levels just above the valence band, which leads to p-type behavior [23].

Several experimental studies have been carried with the goal to investigate the deposition techniques and conditions influence upon CuO thin films electrical proprieties. The reported dark electrical resistivity of CuO thin films is varied from 10 to 10^8 (Ω.cm), depending on the mode of preparation. For the measured free carriers concentration and the hole mobility variation is ranged from 10^{10} to 10^{16} cm^{-3} and 10 to 100 ($cm^2V^{-1}s^{-1}$) ,respectively [43].

Actually any structural changes in thin films alter their electrical properties. These changes include phase change, doping, crystallites size enlargement, grain boundaries and stochiometry deviation .These variations change the number of charge carriers, their mobility and the transport mechanism which directly affect the films resistivity. The influence of deposition parameters on the resistivity is indirectly due to the influence of these parameters on the films stochiometry and the crystallinity structure. The stochiometric films have a larger resistivity. It is likely that the case where low resistivity has been reported can be explained by nonstochiometry. While, it is has been found that the larger the films grains size the lower is the material resistivity.

In the following table I.8 we present a brief review of some experimental results related to electrical properties of CuO thin films deposited with various deposition methods. For CuO thin films prepared by sol-gel method, Dhanasekaran et al. [44] have reported less resistivity equal to 10^2 (Ω.cm) by comparison to other techniques such as thermal oxidation and reactive RF sputtering. The resistivity of sputtered CuO films prepared by Ooi et al. [26] increased with increasing oxygen ratio in the deposition chamber. The lowest resistivity is measured for the deposited CuO film at 10% of oxygen percentage, it was mostly due to the obtained Cu-rich CuO film. While for higher oxygen ratio (50%) the deposited thin films were more resistive due to the obtained O-rich films. This variation is explained in terms of change in the composition of the deposited films and the presence of copper or oxygen vacancies which play an important role in films conductivity.

Moreover, it has been shown that annealing temperature improves films conductivity. The effect of annealing temperature on electrical properties have carried by Saravanan et al. [39], they have found that the resistivity is reduced by one order of magnitude with increasing annealing temperature from 523 to723 K.

Deposition techniques	**Parameters**	**ρ (Ω.cm)**	**Reference**
Reactive RF sputtering	Oxygen percentage (%) **10**	0.001 x 10^3	[26]
	20	0.130 x 10^3	
	30	0.700 x 10^3	
	40	1 x 10^3	
	50	2.500 x 10^3	
Sol- gel	Annealing temperature **400-650** °C	127-371	[44]
Spray pyrolysis	Precursor concentration **0,15** M	1.56 x 10^4	[35]
	0.20 M	2.57 x 10^3	
Thermal oxidation	Annealing temperature **300** °C	2.7 x 10^5	[29]
	400 °C	2 x 10^5	
	500 °C	6.8 x 10^4	
	550 °C	4.8 x 10^4	

Table I.8 *Electrical proprieties of CuO thin films deposited by various deposition method.*

In table I.9 we have reported the electrical properties of CuO thin films deposited by spray pyrolysis for different parameters. Numerous experimental investigations showed that CuO films resistivity decreases with increasing the deposition temperature. For spray-deposited CuO thin films, Gopalakrishna et al. [32] have reported a decrease of the dark resistivity from 10^4 (Ω.cm) to 50 (Ω.cm) and an increase in the carrier concentration (n) by four orders of magnitude from 9 x 10^{11} to 4 x 10^{15} cm^{-3} with increasing the substrate temperature from 250 to 350°C, they explained this behavior by the improvement of films crystalline at higher substrate temperature as concluded from their XRD analysis. It has been also reported that film resistivity increases with precursor concentration as emphasized by Saravanakannan et al. [39]. In contrary, Shabu et al [35] concluded that CuO films resistivity is enhanced with increasing precursor molar concentration.

Deposition technique	Parameters	ρ (Ω.cm)	n (cm^{-3})	µ ()	Ea (eV)	Reference
Spray pyrolysis	Substrates temperature 250 °C	101.5 x 10^{2}	0.91 x 10^{12}	-	0.173	[32]
	300 °C	7.3 x 10^{2}	1.27 x 10^{12}	-	0.152	
	350 °C	0.5 x 10^{2}	3.92 x 10^{12}	-	0.065	
	Annealing temperature 523 K	1.10 x 10^{6}	-	-	-	[25]
	623 K	1.39 x 10^{5}	-	-	-	
	723 K	1.14 x 10^{5}	-	-	-	
	Precursor concentration 0,1 M	0.18 x 10^{4}	4.2 x 10^{14}	2.25 x 10^{3}	-	[39]
	0,15 M	0.69 x 10^{4}	3.6 x 10^{14}	2.16 x 10^{3}	-	
	0,2 M	1.70 x 10^{4}	1.5 x 10^{14}	1.19 x 10^{3}	-	

Table I.9 *electrical properties of CuO thin films deposited by spray pyrolysis for different parameters.*

I.2.8 Electronic and transport properties

Cupric oxide (CuO) is a direct band gap semiconductor with the smallest band gap at the center of Brillouin zone Γ, as depicted in figure I.11-a showing the electronic structure of CuO in the monoclinic structure. The calculation using Density Function Theory (DFT) in located density approximation found a band gap values of 1.251 eV which is in agreement with the experimentally measurements reported at ambient temperature indicating a band gap values in the range 1.2 to 1.9 eV [26]. On the other hand, the band structure calculation by the Local Spin Density Approximation (LSDA) method showed that CuO is a semiconductor with an indirect gap of about 1.0 eV as revealed in figure I.11-b.

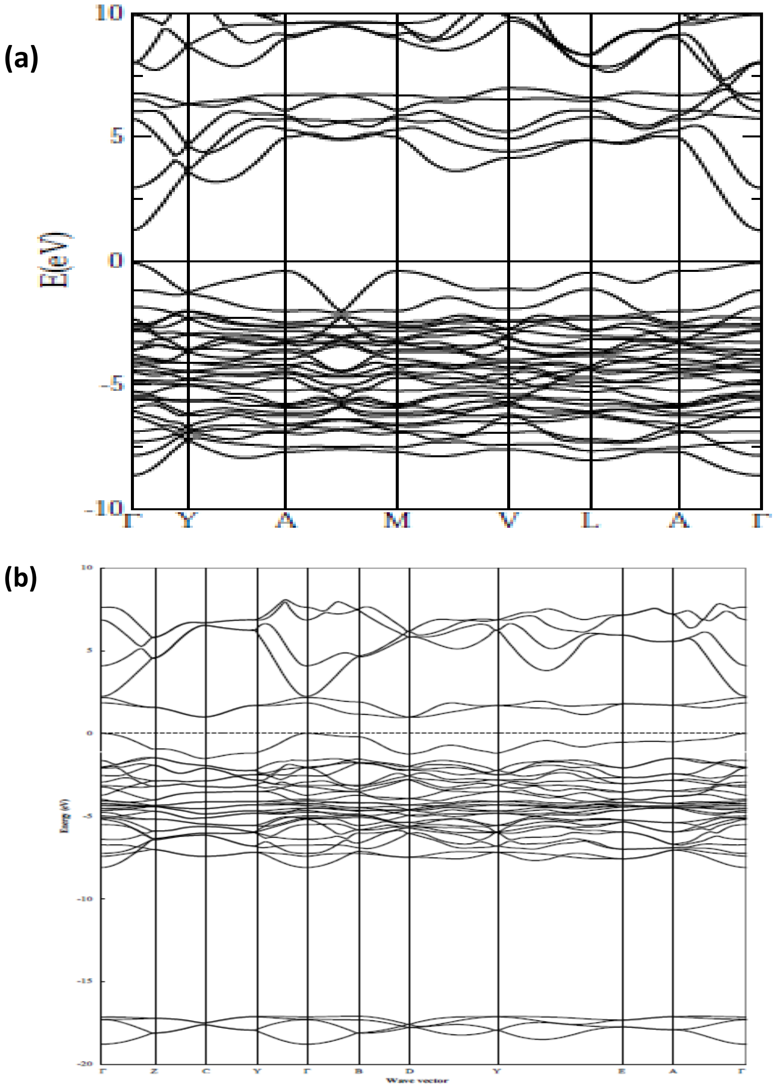

Figure I.11 *Band structure of CuO calculated using (a) the DFT+U method (b) the LSAD+U method. The Fermi level is set at 0 eV.*

Native point defects are intrinsic to semiconductors; they play an important role in semiconductors electronic properties. Wu et al [45] have calculated the structural relaxation and defect levels induced by various native point defects in CuO. The formation energies of these defects are also calculated for three different types of native point defects: vacancies (V_{Cu},V_O), antisite defects (Cu_O, O_{Cu}) and isolated interstitials (Cu_i, O_i). Figure I.12 present the calculated formation energies H_f for different native point defects in CuO as a function of the Fermi level E_F, in O-rich and Cu-rich films. By comparing the formation energies, Cu vacancies (V_{cu}) are the most stable defect in CuO due to its lowest formation energy (less than 1.0 eV), indicating that this defect is very easy to form during CuO thin films growth.

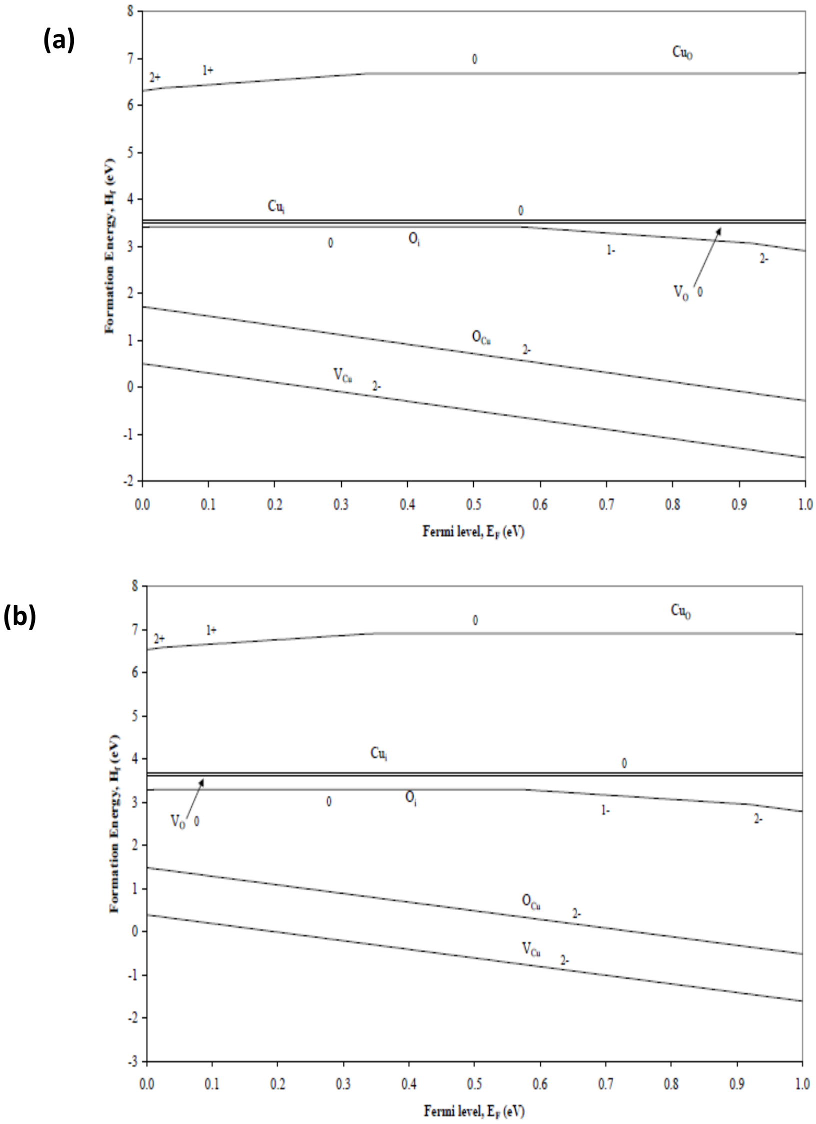

FigureI.12 *Formation energies of native point defects in CuO as a function of the Fermi level E_F (a) in the O-rich environment (b) in the Cu-rich environment.*

I.3 Applications of CuO thin films

CuO is a promising material for various applications due to the abundance of its components in nature, low-cost production, good thermal stability, and electrochemical properties. This combined property enables CuO thin films to be a serious candidate for several applications namely: high-temperature superconductors [8-10], solar cells [8,9], gas sensors [11], magnetic storage media [12], varistors [15] and catalysis [16], antimicrobial activity [33], photoelectrochemical cell [48] and Li batteries [20].

I.3.1 Photoelectrochemical (PEC) cells

Research on photoelectrochemical (PEC) cells, particularly their use in solar energy conversion, has gained importance in the last few decades. PEC cells convert solar energy into storable chemical energy as hydrogen through the photoelectrolysis of water. The photo-electrode in PEC cell, must be chemically stable and should have an optimum band gap (1,4 eV) to efficiently absorb the maximum of solar radiations For this reasons, cupric oxide (CuO) have been investigated as alternative photoelectrodes. Chronological evolution of PEC cells for CuO is regrouped in table I.10. As can be deduced from table, CuO thin films deposition technique and type growth of CuO nanostructute have a strong effect in values of photocurrent. The best photocurrent efficiency is equal to 12 % was found by Kargar et al. [48] for ZnO/CuO heterojunction nanowire.

Years	Method of preparation	J (mA/cm^2)	η_c (%)	Reference
2012	Spray pyrolysis Li doped CuO nanoparticles	1.69	1.3	[46]
2013	Thermal oxidation ZnO/CuO junction nanowire	-	12	[47]
2014	Thermal oxidation CuO nanowires	0.75	-	[48]
2015	Chemical vapor deposition CuO nanoballe films	0.13	-	[49]

***Table I.10** Chronological evolution of photocurrent for CuO-based PEC cells.*

I.3.2 Solar cells

Thin film solar cells are a stack of different layers of various materials. In general, thin film solar cell is composed with transparent conducting oxide (TCO) to draw the current to the outer circuit, buffer layer (n type) to create the junction with the absorber layer (p-type) and metal contact layer as bottom electrode.

Besides, the natural abundance of its constituents, the low fabrication cost, its stability and non-toxic nature, CuO thin film is potential candidate as absorber layer due to its p-type conduction, direct band gap above 1.4 eV that match with the solar spectrum and high absorption coefficient in the visible range . The maximum theoretical conversion efficiency of CuO based solar cells is around 31% [8,9]. Many efforts have been focused to fabricate solar cells using a cupric oxide as a promising active layer using various deposition techniques such as: electrodeposition [13], RF sputtering [20], Sol-gel [17], and plasma evaporation [18].

Some characteristics of based CuO solar cells are listed in table I.11. As can be seen from this table, the CuO based solar cells characteristics are strongly related to the deposition techniques. For example: Kidowaki et al. [50] have prepared Glass/ITO/CuO/ZnO/AL solar cells by electrodeposition technique, they recorded a low conversion efficiency of 1.1×10^{-4} %. However the same solar cells have been elaborated with sputtering, they found that the efficiency is equal to 2×10^{-3} %. The difference in photovoltaic performance of these both solar cells is probably due difference in interfaces formation during the elaboration. The solar cells deposited with electrodeposition technique show a higher defect density at the ZnO/CuO interface, the presence of these defect affect largely the efficiency of the solar cells.

The efficiency of the solar cells is also affected by the type of the window layer used such as: ZnO, Cu_2O, ZnO:Sn and C_{60}. Many studies are focused to improve the solar cell efficiency by controlling the optical and chemical properties of the buffer layer. Efforts are also have being investigated to produce a butter window layer for CuO based solar cells. Omayio et al. [51] have fabricated p-CuO/n-ZnO:Sn heterojunction solar cell using vacuum coater system, they found a conversion solar efficiency equal to 0.232 % They have demonstrated that the ZnO buffer layer doped with Sn improve solar cells efficiency.

The effect of metal contact material on the photovoltaic characteristic of p-CuO/n-Si solar cell fabricated by RF sputtering technique has also reported [52]. They concluded that for CuO-based solar cell, the use of copper (Cu) as front contact achieved conversion efficiency of 0.1 %. However, the use of aluminum (Al) as front contact enhances up the cell efficiency to 1.3 %. Moreover, the use of Cu as intermediate layer between Al contact and CuO layer improve considerably the cell efficiency.

Heterojuction	Voc (mV)	Isc (mA)	FF (%)	η (%)	Reference
CuO/Si **Thin films**	200	0.073	24	9.7 x 10^{-3}	[52]
CuO/ZnO:Sn **Thin films**	480	1.82	0.63	0.232	[51]
CuO/C_{60} **Thin films**	0.24	0.067	0.25	2.3 x 10^{-4}	[53]
CuO/Cu_2O **Thin films**	210	0.310	0.26	0.02	[54]

Table I.11 *PV parameters of different CuO-based solar cells.*

Efficiency of the CuO-based solar cells has been improved significantly over the last four years. The evolution of efficiency the CuO-based solar cells using different deposition techniques is illustrated in figure I.13. In 2010, photovoltaic effects were also observed in Cu_2O/CuO structure with estimated efficiency of 0.02 %. Two years later, Chandrasekaran [54] achieved a conversion efficiency of 0.863% using CuO nanoparticules combined with an organic compound. The best photovoltaic performance has been achieved by Bhaumik et al. [55] for CuO nanostructure thin films deposited by hydrothermally, with conversion efficiency of 2.88 % in 2014. J–V characteristic of this solar cells, in dark and under illumination together with a cross section are reported in figure I.14.

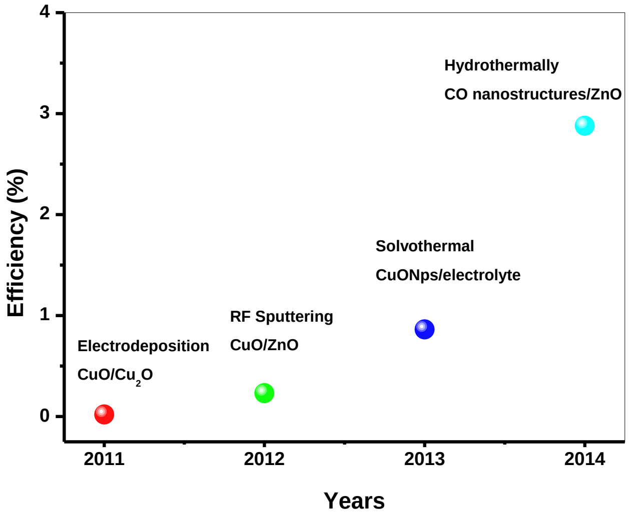

Figure I.13 *Evolution of the efficiency of the based CuO solar cells by years.*

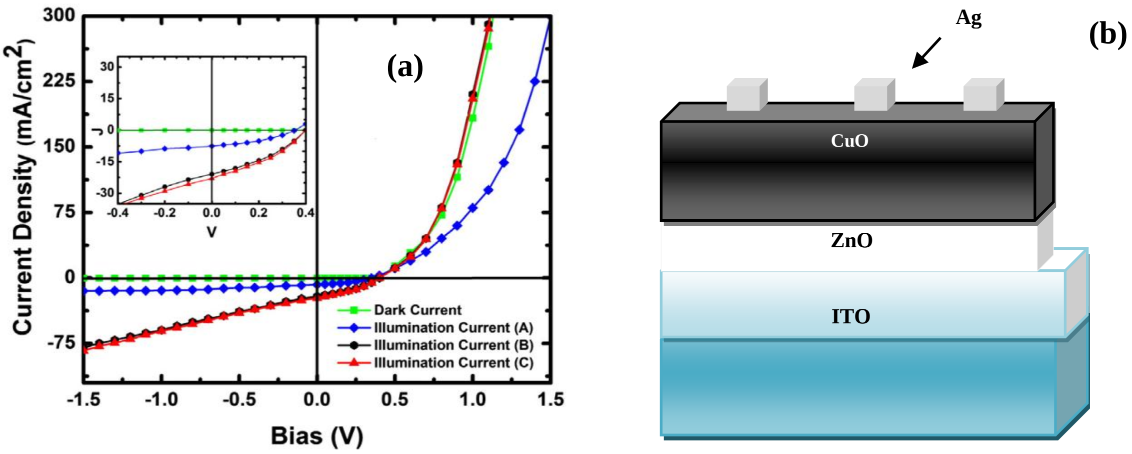

Figure I.14 *(a) J–V characteristic under dark and illumination and (b) cross section of glass/ITO/ZnO/CuO thin film solar cells.*

I.3.3 Gas sensor

Since 1962 it has been known that absorption or desorption of a gas on metal oxide surface may alter its conductivity. This phenomenon has been first demonstrated in zinc oxide (ZnO) thin film layers. Advances in fabrication methods have enabled the production of low-cost gas sensors with improved sensitivity and reliability.

Many metal oxides are suitable for detecting combustible, reducing, or oxidizing gases by conductive measurements. In figure I.15, we represented the mostly used materials metal oxide for gas sensing application. As can be seen, several metal oxides are successfully used as sensitive layer for gas sensors such as : ZnO, In_2O_3, WO_3, TiO_2, MgO, SnO_2, and Mn_2O_3 [3] . However, to date most effort in the fields of metal oxide gas sensor have been devoted to n-type semiconductors, while the sensing properties of p-type metal oxide semiconductors have scarcely been investigated among these cupric oxide (CuO).

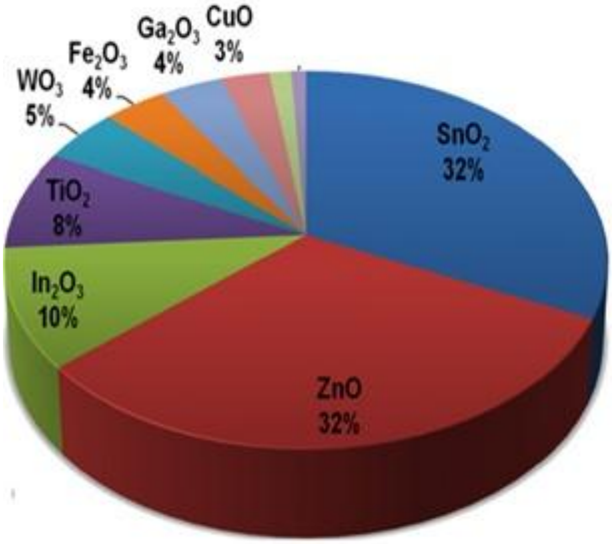

Figure1.15 *Top 10 materials metal oxide used for gas sensor applications in publications since 2002.*

CuO thin films were used for sensing toxic, inflammable and pollutant gas as: NO_2, CO, H_2, CO_2, NH_3 and H_2S [11,12]. Additionally, they have been also tested for organic vapor sensors including: ethanol, methanol and acetone vapor. The performances of CuO-based gas sensor fabricated by various deposition techniques and for various gas, are summarized in table I.12.

Many fabrication methods have been used for CuO-based gas sensors production. Factors that must be considered when selecting the production technique are films purity, surface morphology (highly rough surface increase the specific surface yielding to a higher sensitivity), reliability and reproducibility. An ideal chemical sensor should possess high sensitivity, dynamic range, selectivity and stability; low detection limits; lower operation temperature, response time; and long life cycle.

Sensor and fabrication method	**Gas detection**	**Operation temperature (°C)**	**Sensitivity (%)**	**Response time (s)**
Spray pyrolysis **CuO**	Ethanol 2500 ppm	350	29	247
	Methanol 2500 ppm	400	15	235
	H_2S 100 ppm	200	80	2
RF sputtering **CuO**	NO_2 200 ppm	180	26	6
Sol-gel **CuO**	H_2S 100 ppm	200	24	25
RF sputtering **$CuO-Cu_xFe_{3-x}O_4$**	CO 500 ppm	400	90	1260
PECVD **$SnO_2-CuO-SnO_2$**	H_2 1000 ppm	90	16	-
	Gasoline 1000 ppm	90	28	-
	CO 1000 pmm	90	2	-
Sol-gel **CuO/ZnO**	H_2 3000 ppm	200	60	250

Table I.12 *CuO-based gas sensor performance fabricated by various deposition techniques and for various gas sensing [56-60].*

As one of the important parameters of gas sensors, sensitivity has attracted more attention thereafter; effort has been developed to enhance gas sensors sensitivity. Numerous experimental data showed that CuO-based gas sensor sensitivity is influenced by several factors such as: crystallites size, thickness, chemical composition, microstructure, humidity and surface modification. It has been argued that sensors based on the two components mixed together are more sensitive than the individual components alone. For this reason, more recent works were focused on composite materials, such as SnO_2-ZnO [56], CuO-TiO_2 [57], ZnO-CuO [58]. The combination of metal oxides and other components for example: organic and carbon nanotubes were also investigated.

The composite CuO-$Cu_xFe_{3-x}O_4$ sensors exhibited significantly higher sensitivity for CO gas sensing than other sensors constructed solely from cupric oxide when it is tested under identical experimental conditions [59]. Thin films sensor of SnO_2-CuO-SnO_2 sandwich structure demonstrated higher sensitivity for H_2S at lower work temperature equal to 90°C [60] than the sensor fabricated only with CuO thin films at operation temperature of 200°C. Moreover, the p-n heterojunction between n-ZnO and p-CuO exhibits the best selectivity detection for CO gas in the presence of H_2 gas.

Rydosz et al. [61] have investigated the effect of M-doped CuO-based (M = Ag, Au, Cr, Pd, Pt, Sb, Si) sensors working at various temperatures upon exposure to a very low C_3H_8 concentration. The response of CuO thin films and M:CuO-based nanostructure sensors was measured toward 1 ppm C_3H_8 at 120–380 °C is shown in figure I.16. It is observed that the sensors gas response is greatly influenced by the working temperature due to the temperature-dependent gas adsorption and desorption on the oxide surface. The optimum working temperature was determined at 250 °C for all sensors, except for Ag:CuO-based one, which exhibits a maximum response at 320 °C. The Cr:CuO-based structure, showed the highest sensor response and exhibit a response and recovery time equal to 10 s and 24 s, respectively as represented in figure I.17.

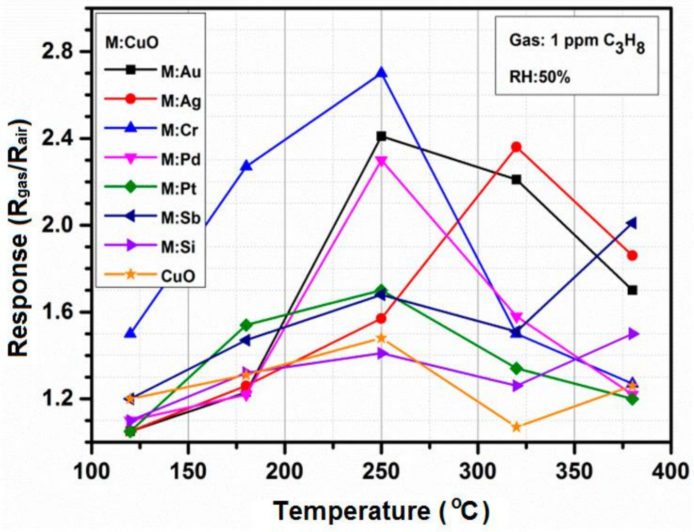

Figure I.16 *Gas response of the CuO- and M:CuO-based sensors (M: Ag, Au, Cr, Pd, Pt, Sb, Si) toward 1 ppm* C_3H_8 *(RH: 50%) as a function of working temperature.*

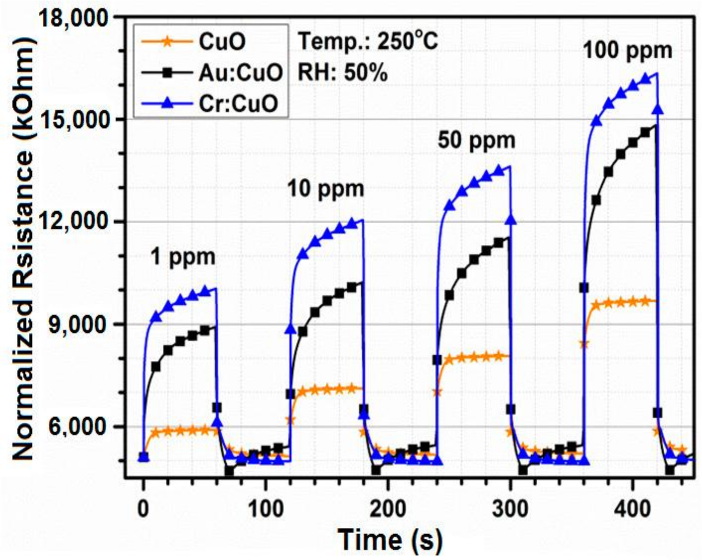

Figure I.17 *Propane curves of the CuO-based, Cr:CuO-based and Au:CuO-based sensor at operation temperature (250 °C) at multiple concentrations.*

I.3.4 Other applications

Cupric oxide (CuO) thin films have been an integral part in constructing high-temperature superconducting materials. CuO-based thin films superconductors have shown superconducting ability above liquid nitrogen temperature. There have been numerous reports and research ongoing to further improve CuO-based high-temperature superconductors**.** CuO thin films have been explored by some researchers with respect to their antimicrobial nature and were found to be quite applicable in this field.

Thermal heat transfer fluid plays a vital role in variety industrial applications. Traditional liquids such as water, oil, and ethylene glycol are inherently poor heat transfer fluids. Therefore an attempt of improving their heat transfer ability or thermal conductivity is a topic of current industrial interest. Nanoparticles have been dispersed in these fluids (nanofluids) and are shown to seriously improve the thermal conductivity of these liquids. Although so far the majority of the nanoparticles that have been used to prepare nanofluids are metallic or polymeric or composite types. Recently using metal oxide nanoparticles has emerged and has proven to be quite successful. Cupric oxide (CuO) has also been quite frequently explored as an option for nanofluids material. It have been reported that 35 % thermal conductivity improved at a temperature of 51 °C of fluid water implemented with 4 vol % of CuO nanoparticles and thermal conductivity increment of ~31% at 5 vol % loading of CuO nanoparticles in water and stabilized with ammonium citrate. Some author reported that 0.1

vol % addition of CuO nanoparticles could improve the thermal conductivity of water up to 46% [10,12].

Rechargeable Li-ion batteries have been a primary component of energy resource for portable computing and telecommunication devices. Researchers for quite some time have been carried for suitable replacements for graphite electrodes. Various reports confirm CuO nanoparticles can be used as anode material in Li-ion batteries with high capacity and excellent retention [39]. They have reported that electrodes made of metal oxide thin films and nanoparticles (MO, where M = Co, Ni, Cu or Fe) demonstrated electrochemical capacities of 700 mAh g^{-1}, with 100% capacity retention for up to 100 cycles and high recharging rates. Li/CuO batteries have been already commercialized. The advantages of this system are a significant volume capacity (4260 Ah / l for CuO alone), a good performance especially at low discharging rate, a very good storage capacity (5% loss of capacity only after 10 years storage at room temperature) and a possible use at high temperatures (up to 150 °C).

Chapter II

Films deposition and Characterization

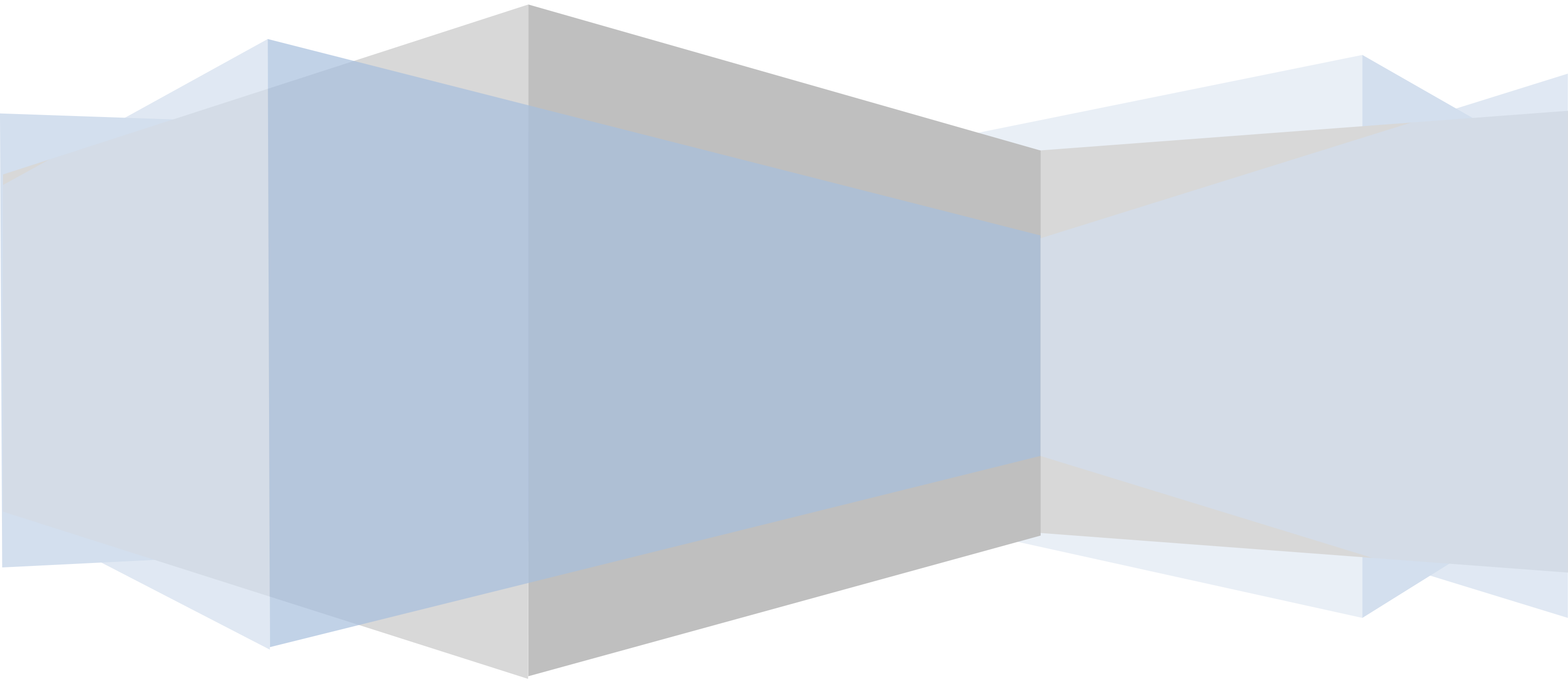

In this chapter we present the experimental details of the carried experiment during the preparation of this thesis. In the beginning an insight on the used deposition technique will be given. The deposition condition of CuO films used in the present study and their characterization will be presented as well as the realized gas sensor and solar cells.

II.1 Thin film deposition

The application of thin films in modern technology is widespread. The methods employed for thin-film deposition can be divided based on the nature of the deposition process. Thin film deposition can be achieved by several techniques regrouped in two categories:

- **PVD** (Physical Vapor Deposition) methods where the films are formed by condensation of incoming species on the substrate. This is the case of solid source. Evaporation, sputtering, ion plating and laser ablation techniques are classified in this category.

- **CVD** (Chemical Vapor Deposition) methods where the films are formed by chemical reaction between incoming species on the substrate. As seen above the techniques using gas and liquid source are listed in this method such as CVD (and varieties PECVD, PACVD, MOCVD, LPCVD), spray, electrodeposition, chemical Bath, dip coating; sol gel …etc .

Indeed there no standard deposition technique that can be used in different situation. Each application requires some specific properties. Deposition techniques are much diversified to answer to the increasing industrial demands. Any deposition technique can be characterized and distinguished by five parameters:

1. Source: solid-liquid or gas.
2. Growth medium: vacuum, air, gas atmosphere or liquid.
3. Introduction method of the coating species in the medium: (premixing, evaporation – sputtering)
4. Nature of coating particles: atoms, ions or molecules
5. Nature of reaction at the surface : condensation or chemical reaction

According to the nature of the deposition method and the source the material to deposit, thin films deposition can be achieved through two or three sequences. For different sources these sequences, as drawn in figures II.1,2 and 3 , in chronological order of deposition are:

II.1.1 Solid Source

- Production of gas species from the source by thermal evaporation or sputtering with energetic species
- Transport of atoms from the source to the substrate. This step needs a relatively high vacuum medium in order to reduce films contamination and produce films with a higher quality. Atoms of a reactive gas can be added in this medium to produce composed films such as oxide, nitride carbide films.
- Species condensation at the substrate.

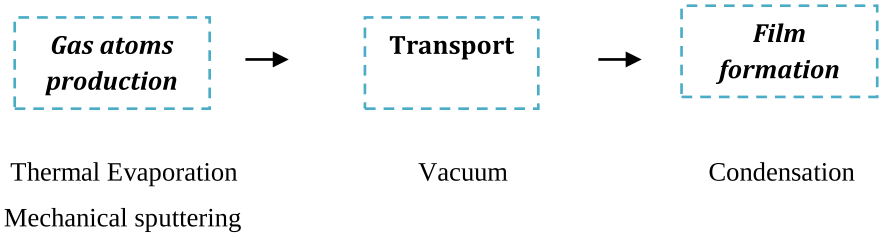

Figure II.1 *Deposition steps for a solid source*

II.1.2 Gas source

In this case, films are formed through these steps.

- Contact between the source and the substrate, carrying the gas into the deposition chamber.
- Gas decomposition to ions and molecules by thermal dissociation or electrical discharge. Reactive gases are added to produce composed alloys. As in the case of solid source, vacuum is needed to avoid films contamination.
- Chemical reactions of various species at the substrate for films formation. Generally, the reaction are initiated or controlled by the substrate temperature.

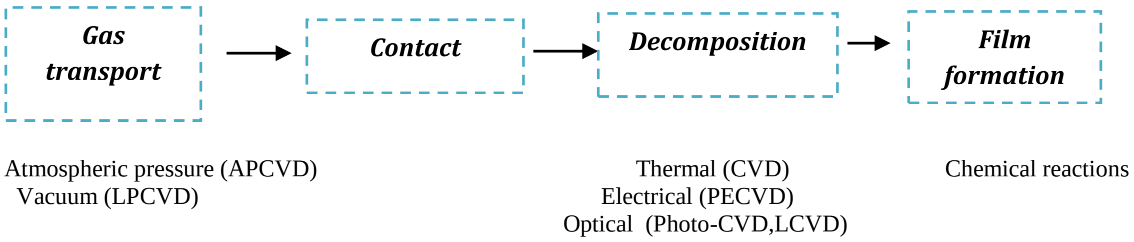

Figure II.2 *Deposition steps for a gas source.*

II.1.3 Liquid Source

The technique using liquid source is based on mainly two steps:

- Liquid contacting with the substrate by direct immersion of the substrate in the liquid or by spraying the solution onto the substrate.
- Films formation by chemical reaction between different species present in the liquid. Substrate temperature plays a key role in this step.

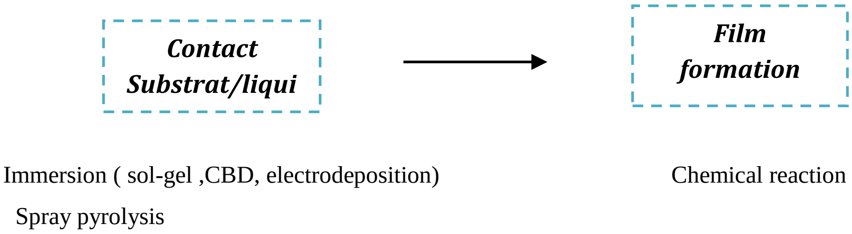

Figure II.3 *Deposition sequences for a liquid source.*

Among the reasons for the growing adoption of CVD methods is the ability to produce a large variety of films and coatings of metals, semiconductors, and compounds in a crystalline or vitreous form, possessing high purity and desirable properties. Furthermore, the capability of controllably creating films of widely varying stoichiometry makes CVD unique among deposition techniques. Other advantages include relatively low cost of the equipment and operating expenses, suitability for both batch and semicontinuous operation, and compatibility with other processing steps. It is beyond the scope of this chapter to present a review of the different techniques in account of the large volume of literature related and devoted to this large and interdisciplinary subject. However, we restrict ourselves to the technique used in this study, namely: spray pyrolysis.

II.2 Spray pyrolysis technique

Spray pyrolysis is a processing technique being considered in research to prepare thin and thick films, ceramic coatings, and powders. Unlike many other film deposition techniques, spray pyrolysis represents a very simple and relatively cost-effective processing method (especially with regard to equipment costs). It offers an extremely easy technique for preparing films of any composition. Spray pyrolysis does not require high-quality substrates or chemicals. The method has been employed for the deposition of dense films, porous films, and for powder production. Even multilayered films can be easily prepared using this versatile technique. Spray pyrolysis has been used for several decades in the glass industry and in solar cell production. Typical spray pyrolysis equipment consists of an atomizer, precursor solution, substrate heater, and temperature controller. The following atomizers are usually used in spray pyrolysis technique: air blast (the liquid is exposed to a stream of air), ultrasonic (ultrasonic frequencies produce the short wavelengths necessary for fine atomization) and electrostatic (the liquid is exposed to a high electric field).

Many studies have been done over about three decades on chemical spray pyrolysis (SP) processing and preparation of thin films, since the pioneering work by Chamberlin and Skarman [62] in 1966 on cadmium sulphide (CdS) films for solar cells. Thereafter, due to the simplicity of the apparatus and good productivity of this technique on a large scale it offered a most attractive way for the formation of thin films of noble metals, metal oxides, spinel oxides, chalcogenides and superconducting compounds. Despite its simplicity, SP has a number of advantages:

1. It offers an extremely easy way to dope films with virtually any element in any proportion by merely adding it in some form to the spray solution.
2. Unlike closed vapor deposition methods, SP does not require high quality targets and/or substrates nor does it require vacuum at any stage, which is a great advantage if the technique is to be scaled up for industrial applications.
3. The deposition rate and the thickness of the films can be easily controlled over a wide range by changing the spray parameters, thus eliminating the major drawbacks of chemical methods such as sol-gel which produces films of limited thickness.
4. Operating at moderate temperatures (100±500 °C), SP can produce films on less robust materials.
5. Unlike high-power methods such as radio frequency magnetron sputtering (RFMS), it does not causes local overheating that can be detrimental for materials to be deposited. There are virtually no restrictions on substrate material, dimension or its surface profile.
6. By changing composition of the spray solution during the spray process, it can be used to make layered films and films having composition gradients throughout the thickness.
7. It is believed that reliable fundamental kinetic data are more likely to be obtained on particularly well characterized film surfaces, provided the films are quiet compact, uniform and that no side effects from the substrate occur. SP offers such an opportunity.

II.3 Thin film formation by spray pyrolysis technique

In the spray deposition process, a precursor solution is pulverized by means of a neutral gas (e.g. nitrogen) so that it arrives at the substrate in the form of very fine droplets. The constituents react to form a chemical compound onto the substrate. The chemical reactants are selected such that the products other than the desired compound are volatile at the temperature of deposition. Figure II.4 shows a typical spraying system. It mainly consists of spray nozzle, precursor solution, substrate heater, temperature controller and air compressor or gas propellant. To measure flow of precursor solution and air, liquid and gas flow meters are used. Vertical and slanted spray deposition arrangements with stationary or linearly moving spray nozzle are frequently used in this technique. To achieve uniform deposition the moving arrangements (either nozzle or substrates or both) have been used. Sometimes the spray assembly is mounted on a moving table and is rastered across the substrates using stepping motors. The properties of the film depend upon the anion to cation ratio, spray rate, substrate temperature, ambient atmosphere, carrier gas, droplet size and also the cooling rate after deposition. The film thickness depends upon the distance between the spray nozzle and substrate temperature, the concentration of the precursor solution and the quantity of the precursor solution sprayed. The film formation depends on the process of droplet landing, reaction and solvent evaporation, which are related to droplet size and momentum. An ideal deposition condition is when the droplet approaches the substrate just as the solvent is completely removed.

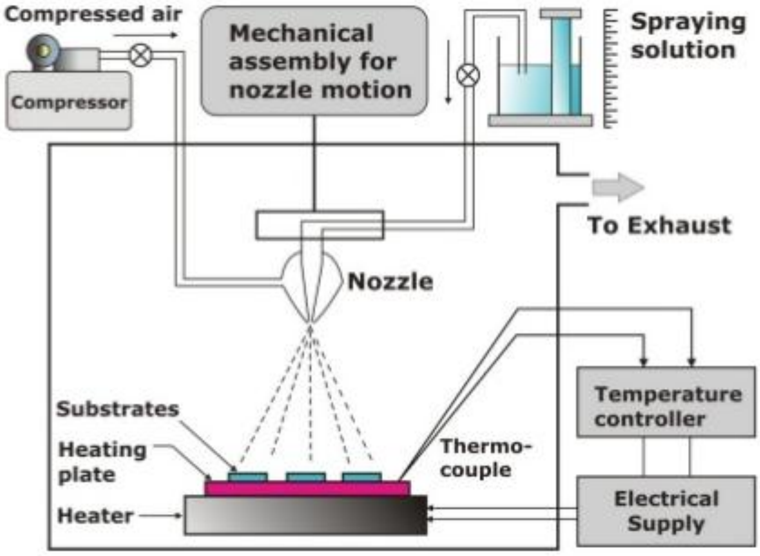

Figure II.4 *Schematic set-up for spray pyrolysis technique.*

Thin films of such metal oxide and metallic spinel oxide materials prepared by SPT have matching properties for wide variety of potential applications [24-26]. Chalcogenide semiconductor compounds of group II-VI and V-VI have applications in precise temperature control of laser diodes, optical recording system, electrochemical devices, strain gauges and thermoelectric devices. These thin films have great technological importance owing to their potential applications in photoelectrochemical cells, solar selective and decorative coatings, optoelectronic devices and thermoelectric coolers [50-55]. Table II.1 presents the deposition conditions for various thin films metal oxide materials prepared by using SP technique during the last decade.

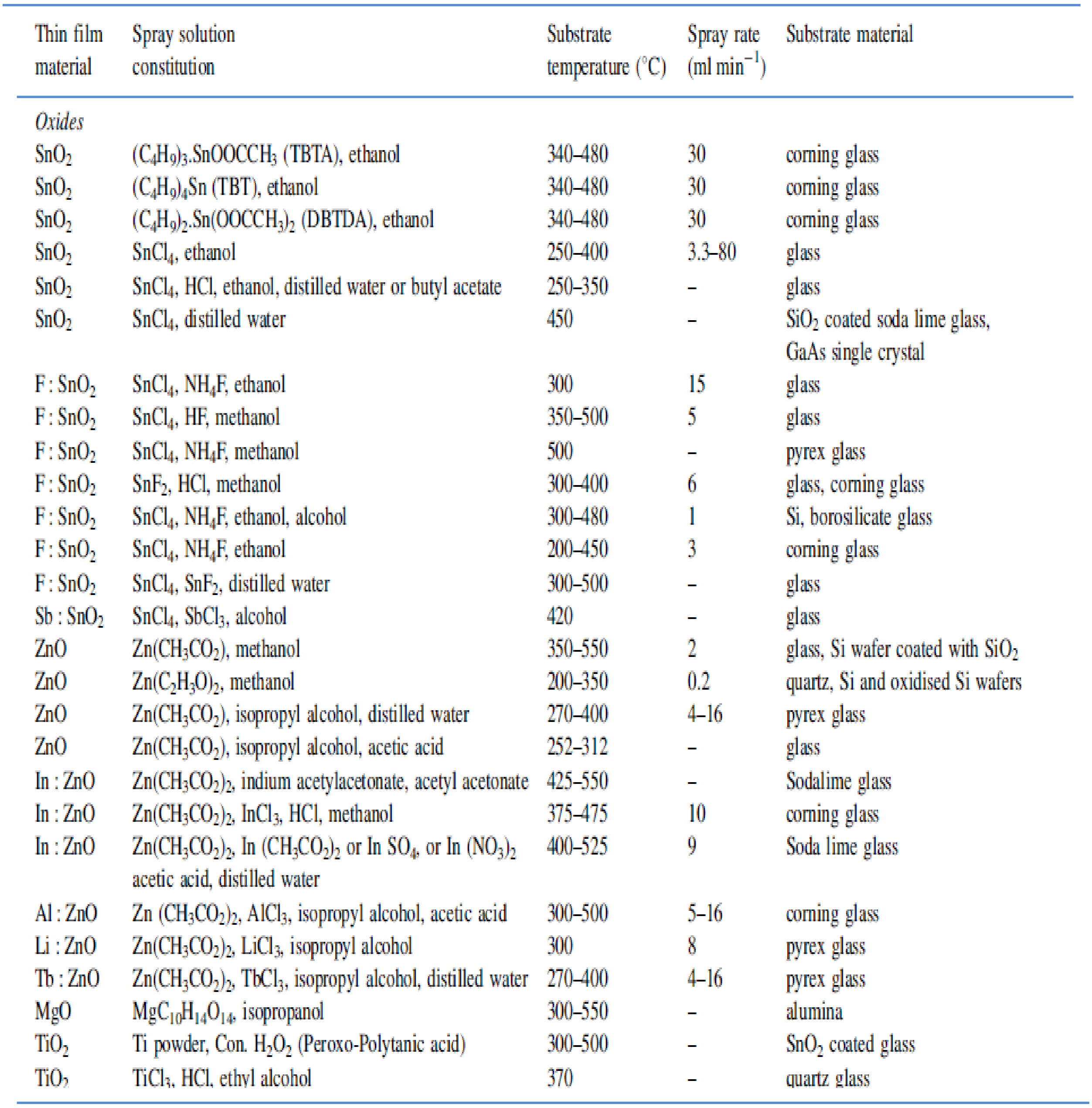

Thin film material	Spray solution constitution	Substrate temperature (°C)	Spray rate (ml min^{-1})	Substrate material
Oxides				
SnO_2	$(C_4H_9)_3.SnOOCCH_3$ (TBTA), ethanol	340–480	30	corning glass
SnO_2	$(C_4H_9)_4Sn$ (TBT), ethanol	340–480	30	corning glass
SnO_2	$(C_4H_9)_2.Sn(OOCCH_3)_2$ (DBTDA), ethanol	340–480	30	corning glass
SnO_2	$SnCl_4$, ethanol	250–400	3.3–80	glass
SnO_2	$SnCl_4$, HCl, ethanol, distilled water or butyl acetate	250–350	–	glass
SnO_2	$SnCl_4$, distilled water	450	–	SiO_2 coated soda lime glass, GaAs single crystal
F : SnO_2	$SnCl_4$, NH_4F, ethanol	300	15	glass
F : SnO_2	$SnCl_4$, HF, methanol	350–500	5	glass
F : SnO_2	$SnCl_4$, NH_4F, methanol	500	–	pyrex glass
F : SnO_2	SnF_2, HCl, methanol	300–400	6	glass, corning glass
F : SnO_2	$SnCl_4$, NH_4F, ethanol, alcohol	300–480	1	Si, borosilicate glass
F : SnO_2	$SnCl_4$, NH_4F, ethanol	200–450	3	corning glass
F : SnO_2	$SnCl_4$, SnF_2, distilled water	300–500	–	glass
Sb : SnO_2	$SnCl_4$, $SbCl_3$, alcohol	420	–	glass
ZnO	$Zn(CH_3CO_2)$, methanol	350–550	2	glass, Si wafer coated with SiO_2
ZnO	$Zn(C_2H_3O)_2$, methanol	200–350	0.2	quartz, Si and oxidised Si wafers
ZnO	$Zn(CH_3CO_2)$, isopropyl alcohol, distilled water	270–400	4–16	pyrex glass
ZnO	$Zn(CH_3CO_2)$, isopropyl alcohol, acetic acid	252–312	–	glass
In : ZnO	$Zn(CH_3CO_2)_2$, indium acetylacetonate, acetyl acetonate	425–550	–	Sodalime glass
In : ZnO	$Zn(CH_3CO_2)_2$, $InCl_3$, HCl, methanol	375–475	10	corning glass
In : ZnO	$Zn(CH_3CO_2)_2$, In $(CH_3CO_2)_2$ or In SO_4, or In $(NO_3)_2$ acetic acid, distilled water	400–525	9	Soda lime glass
Al : ZnO	Zn $(CH_3CO_2)_2$, $AlCl_3$, isopropyl alcohol, acetic acid	300–500	5–16	corning glass
Li : ZnO	$Zn(CH_3CO_2)_2$, $LiCl_3$, isopropyl alcohol	300	8	pyrex glass
Tb : ZnO	$Zn(CH_3CO_2)_2$, $TbCl_3$, isopropyl alcohol, distilled water	270–400	4–16	pyrex glass
MgO	$MgC_{10}H_{14}O_{14}$, isopropanol	300–550	–	alumina
TiO_2	Ti powder, Con. H_2O_2 (Peroxo-Polytanic acid)	300–500	–	SnO_2 coated glass
TiO_2	$TiCl_3$, HCl, ethyl alcohol	370	–	quartz glass

Table II.1 *The deposition conditions for various thin film metal oxides prepared by using SP technique [65].*

II. 4 Models for film deposition by Spray Pyrolysis

Only very crude models about the mechanism of spray deposition and film formation have been developed up to now. There are too many processes that occur either sequentially or simultaneously during film formation by spray pyrolysis for these to be modeled in a straightforward manner. These include precursor solution atomization, droplet transport and evaporation, spreading on the substrate, drying and decomposition of the precursor salt. Understanding these processes will help to improve film quality. Thin-film deposition using spray pyrolysis can be divided into three main steps: atomization of the precursor solution, transportation of the resultant aerosol, and decomposition of the precursor on the substrate.

II. 4.1 Atomization of precursor solution

Atomization of liquids has been investigated for many years. The key is to understand the basic atomization process of the atomization device in use. In particular, it is important to know which type of atomizer is best suited for which application and how the performance of the atomizer is affected by variations in liquid properties and operating conditions. Air blast, ultrasonic, and electrostatic atomizers are normally used in spray pyrolysis techniques. Numerous reports were published on the mechanism of liquid atomization. Rizkalla and Lefebvre examined the influence of liquid properties on air blast atomizer spray characteristics [63]. Lampkin presented results concerning the application of the air blast atomizer in a spray pyrolysis set-up [64]. Recently, a theory of ultrasonic atomization was published [65]. Cone-jet and multi-jet modes are the most important modes for spray deposition. In the cone-jet mode the liquid is distorted at the tip of the tube type nozzle into a conical shape (Taylor cone). This cone is extended at its apex by a permanent jet of very small diameter. The jet usually emits charged mono-dispersed droplets. With increasing electric field, the jet may be split, forming a multi-jet mode where the number of jets increases with applied voltage.

To obtain uniformly distributed micrometer and sub micrometer size droplets, an ultrasonic nebulizer has been used. Generally the precursor solutions are vaporized with an ultrasonic nebulizer which is operated at a frequency varied from 2.56 to 40 MHz. The vapor generated is transported by the carrier gas, air, through a pipe to the heated substrate. To coat a large area, the spray jet is scanned continuously. The precursor solution is converted into small droplets by the ultrasonic waves, such droplets have very small sizes with a narrow size distribution and no inertia in their movement so that they can be transported the carrier gases without any heating. The solvent vaporizes as the droplets approach the substrate. The reactants diffuse to the substrate and a heterogeneous reaction occurs which led to the formation of thin solid films. The pyrolysis of an aerosol, produced by the ultrasonic spraying is known as the pyrosol process. The advantage in this method is that the gas flow rate is independent of the aerosol flow rate, which is not the case with pneumatic spraying.

II. 4.2 Aerosol Transport

In an aerosol the droplet is transported and eventually evaporates. During transportation it is important that as many droplets as possible are transported to the substrate without forming powder or salt particles. The thermophoretic force pushes the droplets away from a hot surface, because the gas molecules from the hotter side of the droplet rebound with higher kinetic energy than those from the cooler side. For example, at a surface temperature of 350 °C and a thermal gradient of 500 °C /cm it was calculated that the thermophoretic force is equal to the gravitational force for a droplet of 2 μm in diameter. Thermophoretic forces keep most droplets away from the surface in non-electrostatic spray process. However, most aerosols contain many droplets significantly larger than 2 μm. It follows that the authors overestimated the role of thermophoretic forces. Additionally, it was concluded that the film grows from the vapor of droplets passing very close to the hot substrate in a manner of chemical vapor deposition and droplets that strike the substrate form a powdery deposit (figure II.5). However, the authors have not considered the spreading of droplets on the substrate, which more significantly contributes to the film growth. In the spray pyrolysis process it is desired that the most droplets strike the substrate and spread. R. Rajan et al [65] have described the transport processes in corona spray pyrolysis. Here the droplets enter a corona discharge and are transported in an electric field to the substrate. The following forces were taken into account: gravitational, Stokes, thermophoretic, electric, and dielectric forces. The author has calculated that only droplets, with a radius larger than 5 μm, will contribute to film formation at a substrate temperature of 430◦C. This value depends on the composition of the solution, the applied voltage and the deposition temperature. The solvent is entirely vaporized in the smaller droplets that will consequently lead to powder formation. However, the authors have not considered formation of hollow particles during the transportation.

The aerosol droplets experience evaporation of the solvent during the transport to the substrate. This leads to a size reduction of the droplet and to the development of a concentration gradient within the droplet. The precursor precipitates on the surface of the droplet, when the surface concentration exceeds the solubility limit. Precipitation occurs due to rapid solvent evaporation and slow solute diffusion. This results in the formation of a porous crust and subsequently hollow particles, which are not desired because they increase the film roughness. The transfers of mass, momentum, temperature outside and around the droplet as well as effects of precursor precipitation were taken into account. The interactions between droplets were ignored. Rapid increases in droplet temperatures were observed at the beginning of evaporation and at the moment when precursor precipitation on the droplet surface starts. This temperature increase was due to heat evolved as a result of precipitation. At the beginning of this process the evaporation rate very quickly reaches a maximum, then decreases until precipitation takes place. This rate accelerates again simultaneously with droplet temperature when precipitation starts. Increasing the gas temperature caused a steeper concentration gradient inside the droplet. The effects of humidity of the ambient gas were found to be insignificant. Some authors have investigated powder production by spray pyrolysis using a temperature-graded laminar flow aerosol reactor. They presented calculations results for the evaporation rate and the change of the precursor concentration within the droplets. The predicted numerical simulation results were in good agreement with the experimental results. The simulations indicated that the solid part particles can be formed when the reactor temperature is low and constant or distributed in homogeneously, when the precursor solution concentration is high and when the flow rate of carrier gas is low. Undesired hollow particles are formed when the droplets are large and the droplet number concentration is low. Smaller droplets produce solid particles because the diffusion distance for the solute is shorter, leading to a more uniform concentration distribution within the droplet. Increasing the number of droplets results in a larger solvent vapor concentration in the carrier gas. Consequently, the evaporation rate decreases and precipitation is delayed. Therefore, an increase in the number of droplets decreases the probability of forming hollow particles. In the literature, a lot of authors have studied the behavior of an evaporating droplet in a non-isothermal field. An alcoholic solution of titanium tetraethoxide was atomized by an ultrasonic nebulizer. Nitrogen was used as carrier gas. The flow and temperature profiles of the carrier gas were calculated and then the motion and evaporation of the droplets simulated numerically. Measurements of deposition efficiency and film thickness distribution were compared with calculated particle trajectories. The comparisons have shown that the deposition efficiency and the area coated increase with the amount of sprayed solution and carrier gas flow rate, but decrease with nozzle-to-substrate distance.

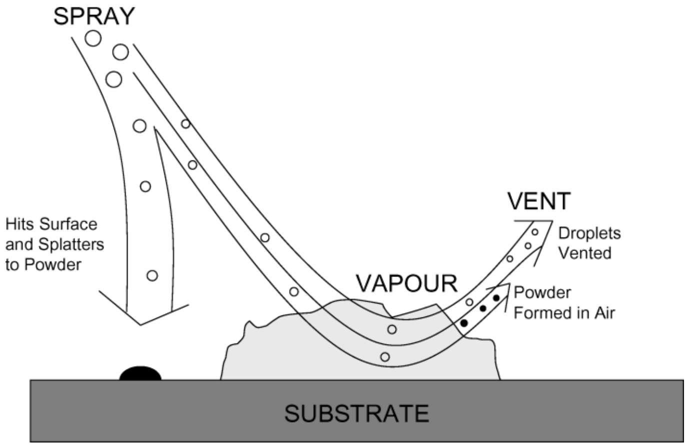

Figure II.5 *Aerosol transport.*

II.4.3 Decomposition of Precursor

Many processes occur simultaneously when a droplet hits the surface of the substrate: evaporation of residual solvent, spreading of the droplet, and salt decomposition. Many models exist for the decomposition of a precursor. Most of the authors suggest that only a kind of CVD process gives high quality films by spray pyrolysis. Ganan-Calvo proposed the following processes that occur with increasing substrate temperature [66].

In the lowest temperature regime (process A) the droplet splashes onto the substrate and decomposes (figure II.6). At higher temperatures (process B) the solvent evaporates completely during the flight of the droplet and dry precipitate hits the substrate, where decomposition occurs. At even higher temperatures (process C) the solvent also evaporates before the droplet reaches the substrate. Then the solid precipitate melts and vaporizes without decomposition and the vapor diffuses to the substrate to undergo a CVD process. At the highest temperatures (process D) the precursor vaporizes before it reaches the substrate, and consequently the solid particles are formed after the chemical reaction in the vapor phase. It is believed that the processes A and D lead to rough or non-adherent films. Adherent films were obtained by CVD at low temperatures (process C). However, type A or B allows formation of high quality adherent films too. Moreover, the process C can rarely occur in most spray pyrolysis depositions, because either the deposition temperature is too low for the vaporization of a precursor or the precursor salt decomposes without melting and vaporization.

Porous and amorphous CdS films were obtained below 300 °C. At high substrate temperatures (above 450 °C) powdery films were produced due to the vaporization and decomposition of the precursor before reaching the substrate. At intermediate temperatures (300–450 °C), both processes may occur. The authors suggest that at the optimum temperature the solvent evaporates close to the substrate, and the precursor is volatilized near the vicinity of the substrate and adsorbed onto the surface, followed by decomposition to yield a dense film with good adhesion. This would correspond again to a heterogeneous CVD reaction. It was estimated that the optimum temperature lies between 400 °C and 450 °C. The presence of large particles on the surface was attributed to very large droplets, which might not decompose through the CVD process route when they arrive at the substrate.

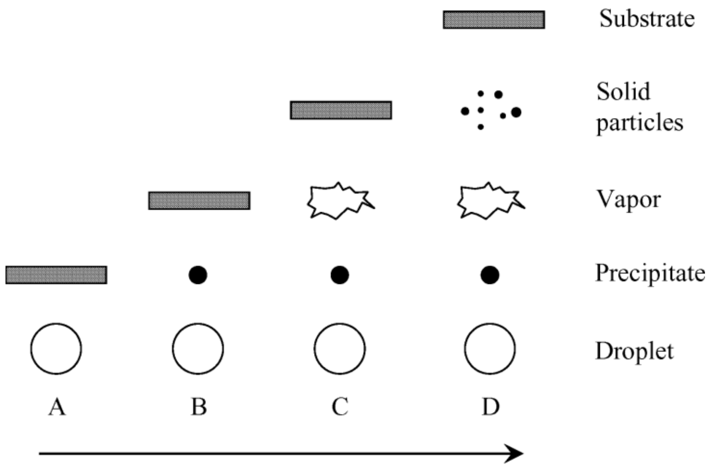

Figure II.6 *Description of the deposition processes initiated with increasing substrate temperature.*

II.5 CuO thin films preparation

The goal of the present study is the deposition and characterization of CuO thin films by spray ultrasonic pyrolysis technique. Influence of different parameters related to each this technique will be investigated. Experimental details of films preparation by this techniques and the various characterization techniques used in this thesis will be presented. Realization of Gas sensing system and fabrication of a gas sensor based on CuO thin films used for sensing organic vapor and gas will be also reported in the following sections.

In the contrary to the other deposition technique, ultrasonic spray pyrolysis has widely parameters to study. The most important parameters have been investigated in this study namely: substrate temperatures, flow rate, molarity of the solution and precursor slat. Five sets of samples were prepared. In each set only one parameter is varied while the rest of parameters were fixed. For the prepared sets the distance between atomizer and substrate is fixed at 4 cm. the temperature solution is fixed at room temperature (25°C). The dissolvent used for dissolved the salt source of copper is distillate water. The choice of distillate water is due to this abundance and the low cost. The total volume of the precursor solution is fixed to 40 ml. The precursor solutions are vaporized with an ultrasonic nebulizer which is operated at a frequency equal to 40 MHz. All the deposited CuO films are deposited at cleaned glass substrates. The glass substrates are cleaned following these steps:

1. The glass substrate were firstly cleaned ultrasonically in methanol to remove any impurity (grease o dust) stickled in the surface of the substrate three time several and for 10 min.
2. The glass substrates were secondly cleaned ultrasonically in distilled water to remove any trace of the methanol three several times and for 10 min.
3. The cleaned glass substrates are dried with dryer.

In tables II.2 (a-e) we have summarized the deposition parameters of each set. In the first and the second one we have varied the substrate temperature; in the thirdly set we have varied the salt molarity, the fourth we have changed the flow rate of the started solution while in the last set we have varied the copper salt used as source of copper. The deposition system of ultrasonic spray pyrolysis used for this study is shown in figure II.7.

Sample	Precursor salt	Molarity (ml/l)	Time deposition (min)	Flow rate (ml/h)	Substrate temperature (°C)
A	Copper chloride $CuCl_2.2H_2O$	0.05	20	20	280
B					300
C					350
D					400

***Table II.2-a** Deposition parameters of the first series of CuO samples.*

Sample	Precursor salt	Molarity (ml/l)	Time deposition (min)	Flow rate (ml/h)	Substrate temperature (°C)
A	Copper acetate $Cu(CH_3COO)_2$	0.05	20	20	280
B					300
C					350
D					400

***Table II.2-b** Deposition parameters of the Second series of CuO samples.*

Sample	Precursor salt	Molarity (ml/l)	Time deposition (min)	Flow rate (ml/h)	Substrate temperature (°C)
A	Copper chloride $CuCl_2.2H_2O$	0.01	20	20	300
B		0.02			
C		0.04			
D		0.06			
E		0.08			

Table II.2.c *Deposition parameters of the thirdly series of CuO samples.*

Sample	Precursor salt	Molarity (ml/l)	Time deposition (min)	Flow rate (ml/h)	Substrate temperature (°C)
A	Copper chloride $CuCl_2.2H_2O$	0.05	20	10	300
B				15	
C				20	
D				25	
E				30	

Table II.2-d *Deposition parameters of the fourthly series of CuO samples.*

Sample	Precursor salt	Molarity (ml/l)	Time deposition (min)	Flow rate (ml/h)	Substrate temperature (°C)
A	Copper chloride $CuCl_2.2H_2O$	0.05	15	20	300
B	Copper acetate $Cu(CH_3COO)_2$				

Table II.2-e *Deposition parameters of the fifth series of CuO samples.*

Figure II.7 *The deposition system of ultrasonic spray pyrolysis.*

II.6 Films characterization

Several techniques were used for the structural, morphological, optical and electrical characterization of the films, these techniques are described below:

II.6.1 The thickness measurement

The films thicknesses were measured by ellipsometry and from transmission excremental spectra data. In figure II.8 we have reported the theoretical calculation and the experimental data for CuO thin films deposited substrate temperature equal to 280°C using copper chloride. The optical transmission data for normal incidence, for an absorbing thin film on a non-absorbing substrate, is given by the following relation:

$$T = Ax/ B - Cx + Dx^2 \ (A1) \tag{1}$$

$$A = 16n_s (n^2 + k^2) \tag{2}$$

$$B = [(n + 1)_2 + k^2][(n + 1)(n + ns^2) + k_2] \tag{3}$$

$$C = [(n^2 - 1 + k^2)(n^2 - ns^2 + k^2) - 2k^2 (ns^2 + 1)]^2 \cos (\phi) -k [2(n^2 - ns^2 + k^2) + (ns^2 + 1) (n^2 - 1 + k^2)]^2 \sin \phi \tag{4}$$

$$D = [(n - 1)^2 + k^2][(n - 1)(n - ns^2) + k^2] \tag{5}$$

$$\phi = 4\pi nd / \lambda \tag{6}$$

$$x = \exp (-\alpha d) \tag{7}$$

$$\alpha = 4\pi k / \lambda \tag{8}$$

n and k are the real and imaginary parts of thin film refractive index, d is the film thickness and ns is the (real) substrate refractive index. The latter is assumed to be constant (i.e., = 1.51). The recorder experimental transmittances are fitted to the theoretical transmission (equ. A.1) by varying the values of n and d until both sides are reasonably equal. The values of n and d ensuring a well fitting are taken as the film thickness and refractive index.

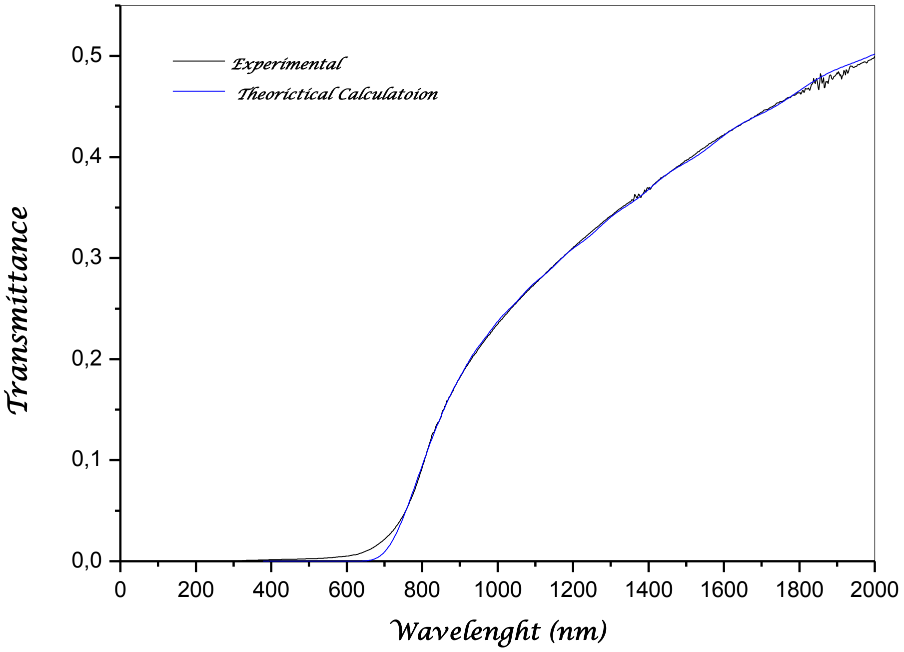

Figure II.8 *The theoretical calculation and the experimental data for CuO thin films deposited at 280°C using copper chloride.*

II.6.2 Structural properties

The structural properties of the films were studied by X-Ray Diffraction (XRD), using Philips X'Pert system with Cu-kα radiation of wavelength λ = 1.5418 Å. The diffractometer reflections were taken at room temperature and the 2θ value were varied from 20 to 90°. The micro-Raman measurements were performed at room temperature using the 514.5 nm line of an argon ion laser as the excitation source (Renishaw). The laser power was kept at 10 Mw. The structural parameters of the all deposited CuO films are estimated from the XPD pattern. The crystallites size, lattice strain, dislocation density, texture coefficient and number of crystallites is calculated by the formulas given below:

- The crystallites size was calculated from two formulas the Scherer's and Hall–Williamson equation formula [67] :

$$D = (0.94\,\lambda) / \beta\,(\cos\theta) \tag{9}$$

$$\beta \cos\theta / \lambda = 1/D + \varepsilon \sin\theta / \lambda \tag{10}$$

Where β is the FWHM (full width at half maximum) of diffraction peaks, θ is the Bragg angle, λ is the wavelength of the used X rays, D is the crystallite size and ε is the internal strain. D is estimated from the last square fit of β cos (θ) / λ vs. sin (θ) / λ of different peaks. The intercept of the equation plot with the y axis yields to the crystallite size.

- The texture coefficient (T_c) was calculated, which is defined [68,69]:

$$T_C = [\, I_{hkl} / I^0_{hkl}] / [\, (1/n) \sum (I_{hkl}/I^0_{hkl})] \tag{11}$$

Where I_{hkl} is the measured intensity of the plane (hkl) and I^0_{hkl} the standard intensity of the plane (hkl) taken from PDF card data, n is the reflection number.

- The lattice strain is calculated from two fowling equation [67] :

$$\varepsilon = \beta / 4 \tan\theta \tag{12}$$

$$\beta \cos\theta / \lambda = 1/D + \varepsilon \sin\theta / \lambda \tag{11}$$

Where β is the FWHM (full width at half maximum) of diffraction peaks, θ is the Bragg angle, λ is the wavelength of the used X rays, D is the crystallite size and ε is the internal strain. The strain is equal to the slope of the plot of β cos (θ) / λ vs. sin (θ) / λ of different peaks. In figure II.9 we have presented the plot of the Hall–Williamson equation for the sample deposited with molarity equal to 0.08 M.

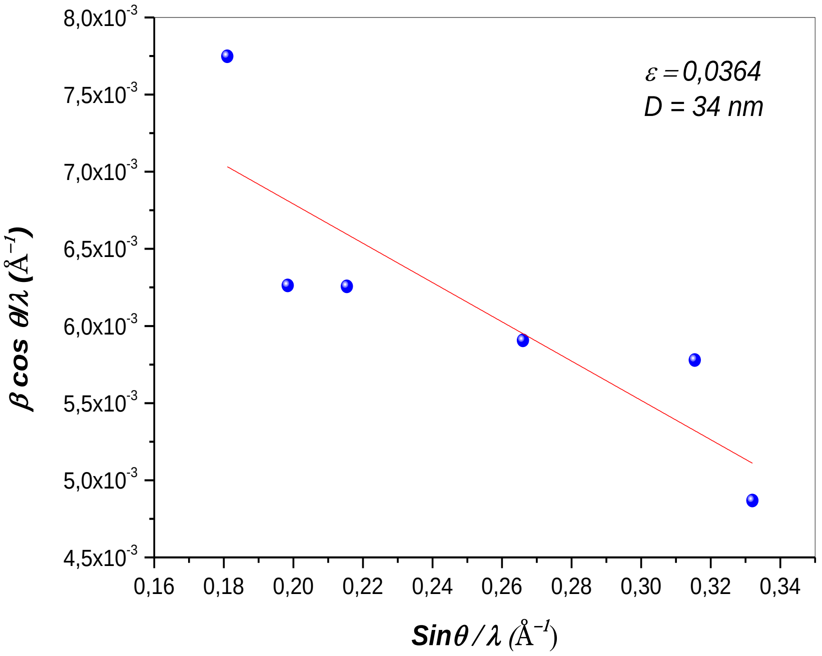

Figure II.9 *The plot of the Hall–Williamson equation for the sample CuO deposited with molarity equal to 0.08 M.*

- The dislocation density (δ) is calculated using this equation [67]:

$$\delta = 1/D^2 \quad (13)$$

Where δ is the dislocation density and D is the crystallite size.

- The number of crystallites (N) per unit area is calculated using[67] :

$$N = d/D^3 \quad (14)$$

Where N is the number of crystallites per unit area, d is the film thickness and D is crystallite size.

II.6.3 Films morphology

Films morphology was analyzed using scanning electron microscope Jeol 5400 SEM microscope and atomic force microscopy (AFM) Nanosurf easy scan 2. The grains size is estimated from the SEM images and the film roughness is obtained from AFM analysis.

II.6.4 Optical properties

The optical properties of the obtained films were studied using UV-Visible transmittance spectroscopy by means of Shimadzu 3101PC double beam spectrophotometer. The optical band gap, disorder (Urbach energy), Steepness coefficient, absorption coefficient and the refractive index was also measured using the giving expression:

- The absorption coefficient (α): in the spectral region of the light's absorption, was deduced from the Beer-Lambert law using the following expression [70] :

$$\alpha = -(1/d)\ln(100/T) \qquad (15)$$

Where α is absorption coefficient, d is the film thickness and T is the transmittance.

- The optical band gap (Eg) : The study of the spectrum of the absorption coefficient α of a semiconductor in the fundamental region and near the fundamental edge provides us with valuable information about the energy band structure of the material [70]. The absorption coefficient α can be divided into two regions the higher values and the low of the absorption coefficient region. In this region absorption coefficient takes the form [71]:

$$(\alpha h\nu) = A(h\nu - E_g)^r \qquad (16)$$

$$A = (4\pi\sigma / ncE_c) \qquad (17)$$

Where Eg is the optical energy gap of the material ,r is the power which characterizes the transition process c is the speed of light, σ is the minimum metallic conductivity (extrapolated dc conductivity at T=∞), Ec is a measure of the width of the tail states distribution and n is the refractive index.

In semiconductors there exist two types of band to band transitions (i) allowed and (ii) forbidden (forbidden transition take into account the small but finite momentum of photon these transitions are less probable). Direct band gap semiconductor transitions mostly occur between two bands of the same k values as. The allowed transition can occur in all values of k however forbidden can only occur at k ≠ 0. r = 2 and 2/3 for direct allowed and forbidden transitions, respectively. In indirect semiconductor, a phonon is involved in the transition in order to conserve momentum. In the indirect transitions, r = 1/2 and 1/3 for indirect allowed and forbidden transitions, respectively.

The usual method for the determination of the value of Eg involves plotting a graph of ($\alpha h\nu)^r$ against $h\nu$. Figure II.10 shows that plots of $(\alpha h\nu)^2 = f(h\nu)$ are linear function for CuO films . The linearity indicates the existence of the direct allowed transitions. Eg is determined by extrapolating the linear portion of the spectrum to $\alpha h\nu = 0$.

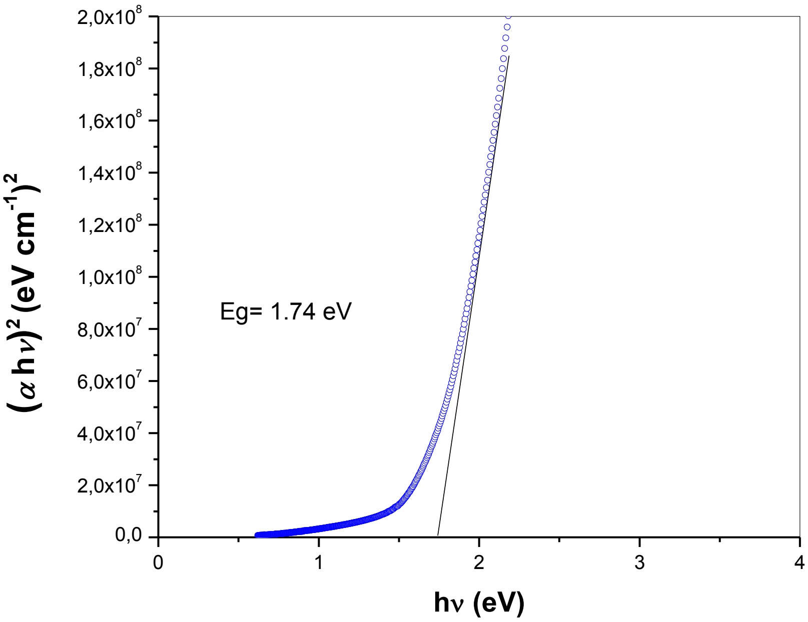

Figure II.10 *Typical variation of the quantity* $(ah\nu)^2$ *as a function of photon energy, for the sample prepared with 0.01 M used for the determination of the optical gap.*

- The disorder (E_{00}): the low absorption coefficient α region. The absorption coefficient of films shows a tail for sub-band gap photon energy. This tail is called the Urbach tail. The latter, which is closely related to the disorder in the film network, is expressed as [72] :

$$\alpha = \alpha_0 (h\nu / E_{00}) \qquad (18)$$

Where α_o is a constant and E_{00} is interpreted as the width of the tails of localized states in the gap region. To evaluate the values of α_o and E_{00}, one have to plot the variation of absorption coefficient α in logarithmic scale as a function of photon energy hν as shown in Figure II.11. The Urbach tail was determined from the slope of the variation of log (α) with the incident photon energy hν [71]. E_{00} can be estimated from the inverse slope of the linear plot of ln(α) versus hν.

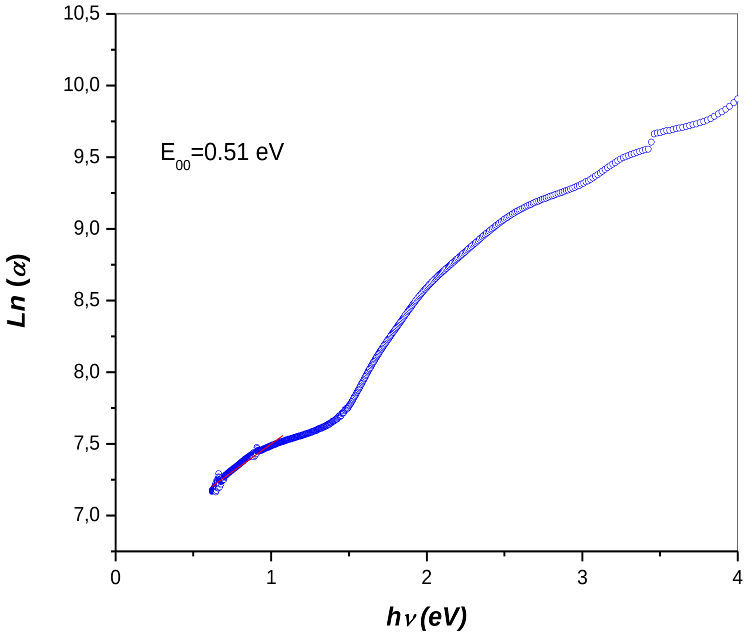

Figure II.11 *Variation of absorption coefficient α in logarithmic scale as a function of photon energy hν.*

- The steepness (σ_p): This parameter is characterized the width of the straight line near optical absorption edge is close related to the Urbach energy or the disorder (E_{00}) through the relation :

$$\sigma_p = kT/E_{00} \tag{19}$$

Where σ_p the steepness parameters, E_{00} is the Urbach energy, k is is the Boltzmann's constant and T is the absolute temperature.

- The refractive index: this optical constant is measured from ellipsometry and optical transmittance spectra data.

The estimated refractive indices were plotted as a function of wavelength in showing in figure II.12. These results showed that the refractive index obtained for all CuO thin films is the same in the wavelength range of $590 \leq \lambda \leq 2000$ nm and differs for wavelengths less than 590 nm. In the wavelength range between 590 and 1100 nm the refractive index was found to be ~1.60 regardless of thickness.

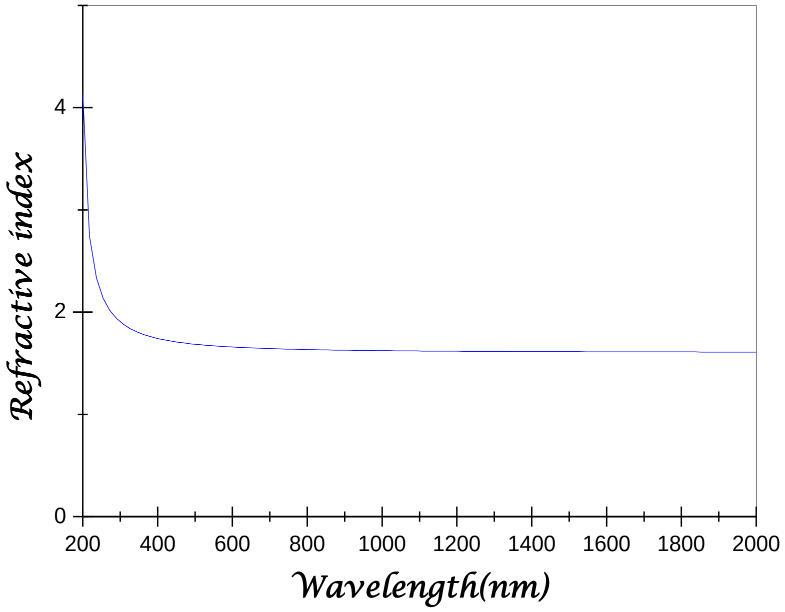

Figure II.12 *Variation of refractive index versus wavelength for CuO thin films deposited at 280°C using copper chloride.*

II.6.5 Electrical proprieties

The electrical measurements were performed at room temperature and in dark with two methods namely: The electrical D.C transport and effect Hall measurement.

- The dark conductivity is measured by the electrical D.C transport and the effect Hall measurement.
- The mobility and the free carriers concentration are determined By Hall measurement.

The electrical D.C transport characterization was carried using coplanar structures in samples with two evaporated golden strips used as electrodes as showing in figure II.13. The electrodes spacing is 5 mm. The applied voltage is varied from 0 to 20 V, Keithley electrometer 610 is used for current measurements. We have checked the ohmicity of this contact by plotting the IV characteristics. As shown in figure II.14, the linearity of the obtained characteristic curve indicates the contact ohmicity.

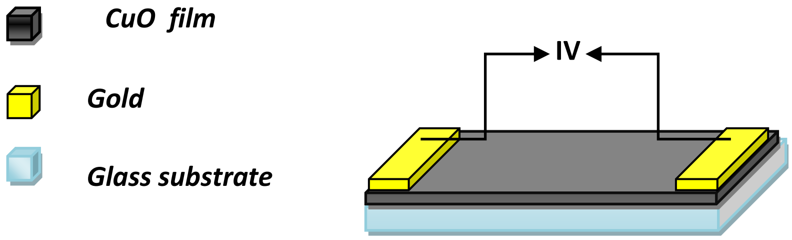

Figure II.13 *Schematic of coplanar structures*

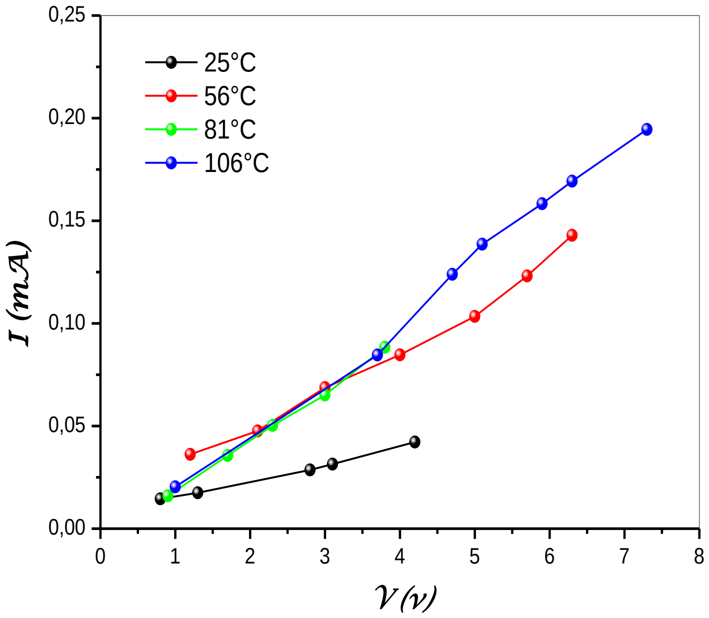

Figure II.14 *IV characteristic at different temperatures of measurement for the CuO films deposited at 280°C using copper chloride.*

- The activation energy (Ea): It is interesting to note that the conductivity appears to vary with inverse of temperature suggesting a thermally activated conduction mechanism. The activation energy and conduction of the films are related in following the Arrhenius equation:

$$\sigma = \sigma_0 \exp\left(-Ea/KT\right) \qquad (20)$$

Where Ea is the activation energy of conduction, σ_0 is pre-exponential factor, k is the Boltzmann's constant and T is the absolute temperature. The thermal activation energy can be estimated from the slope of the linear plot of ln (σ) vs inverse of temperature as showing in figure II.15.

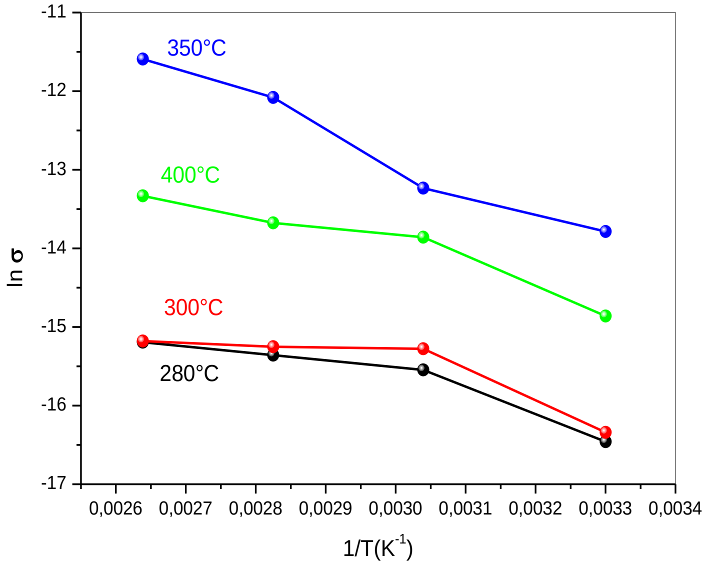

Figure II.15 *Variation of ln(σ) versus in inverse of temperature for CuO films deposited at different substrate temperatures.*

II.7 Fabrication of gas sensor

The aim of this present work is to produce a gas sensor using CuO thin films as sensitive layer. In figure II.16 we have represented a schematic of the fabricated gas sensor. CuO thin films were firstly deposited on glass substrates by spray pyrolysis at substrate temperature, deposition time and flow rate equal to 350°C, 5 min and 5ml/h respectively using copper chloride as precursor with 0.05 M molar concentration. The sensitive CuO layer is deposited using Holmarc ultrasonic spray pyrolysis system as shown in figure II.17. Then pre-patterned gold interdigitated electrodes were evaporated in the top of CuO sensing layer. The obtained gas sensor is used to sensing organic vapor and gas using two different gas sensing system fabricated at our laboratory.

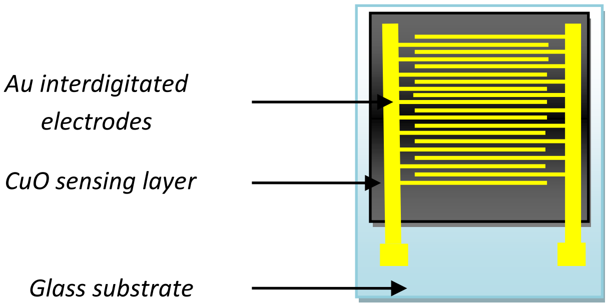

Figure II.16 *A schematic of the fabricated CuO based gas sensor.*

***Figure II.17** The deposition system of ultrasonic spray pyrolysis (Holmarc) used for elaboration of the sensitive CuO thin film.*

II.8 Gas sensing measurement

The organic vapor sensing for methanol and ethanol experiments were performed in a customized chamber with defined volume. The sensor sample was placed over a heated placed inside the chamber. A DC power supply was connected to the heater to control the operating temperature. A thermocouple was placed onto the top of the sensors surfaces to monitor real temperature. A schematic diagram of the gas system measurement for vapor is represented in figure II.18.

A concentration of organic vapor (methanol or ethanol) inside the system is achieved by injecting a known volume of liquid. This volume corresponding to ppm concentration of induced volume calculated using the following equation [73]:

$$Concentration\ (ppm) = (d \times V_{ing} \times R \times T) / (M \times P \times V_{ch}) \qquad (21)$$

Where d is the density of methanol (kg/m^3), V_{ing} the injecting volume of ethanol (ml), R is universal unit gas m^3·atm/(molk), T is the temperature (K), P is the pressure in the chamber (Pa), $V_{c\,h}$ is the chamber volume (m^3) and M is the molecular weight (g/mol).

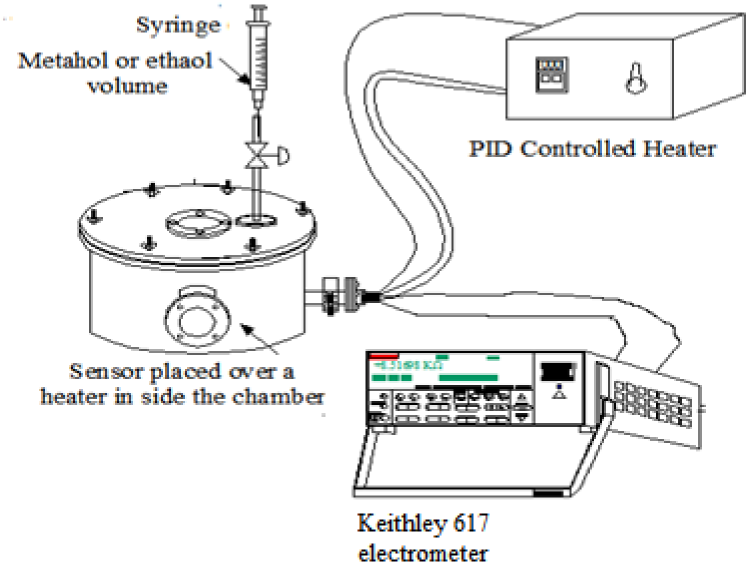

Figure II.18 *A schematic diagram of the gas system measurement for organic vapor.*

The gas sensing of CO_2 experiments is also performed in a customized chamber with defined volume. The sensor sample was placed over a heated placed inside the chamber. A DC power supply was connected to the heater to control the operating temperature. A thermocouple was placed onto the top of the sensors surfaces to monitor real temperature. Pressure meter is used to calculate the pressure inside the chamber in the presence of air after vacuum and CO_2 gas. The pressure under the air atmosphere is fixed to 2 x 10^{-2} hPa. A schematic diagram of the gas sensing system measurement is represented in figure II.19.

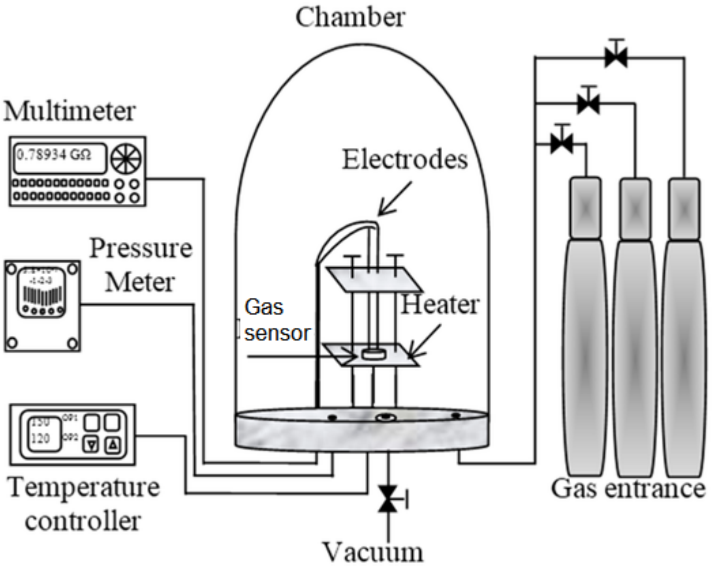

Figure II.19 *Schematic diagram of the gas sensing system.*

Gas response or the sensitivity (S) of the film sensor is defined as the ratio of change in the resistance of the sample when is exposure to gas and air on the resistance in air by the formula:

- In case of reduction (ethanol and methanol) :

$$S = \left| R_g - R_a \right| / R_a \times 100\ \% \qquad (22)$$

- In case of oxidation (CO_2 gas) :

$$S = \left| R_a - R_g \right| / R_g \times 100\ \% \qquad (23)$$

Where Rg and Ra are CuO film resistances measured in the presence of gas and air atmosphere, respectively. The resistance changes of the thin film CuO based conductometric sensor was recorded by Keithley 617 programmable electrometer as a function of time. The time taken for the sensor to attain 90% of the maximum change in resistance on exposure to the target gas is the response time. The time taken by the sensor to get back 90% of the original resistance is the recovery time. In figure II.20 we have represented a typical structure of a conductivity gas sensor.

In order to obtain the optimum operating temperature, the sensor was exposed to two organic vapors namely: methanol and ethanol towards concentration of 300 ppm with varying temperatures between 25 and 175 °C. Then the sensor is exposed to different vapor of concentrations at the same operating temperature. For the CO_2 gas sensing, the sensor was exposed to the pressure of CO_2 gas equal to 5 hPa with varying temperatures between 40 and 120 °C. Then the fabricated sensor exposed at different pressure of CO_2 gas at the obtained operation temperature.

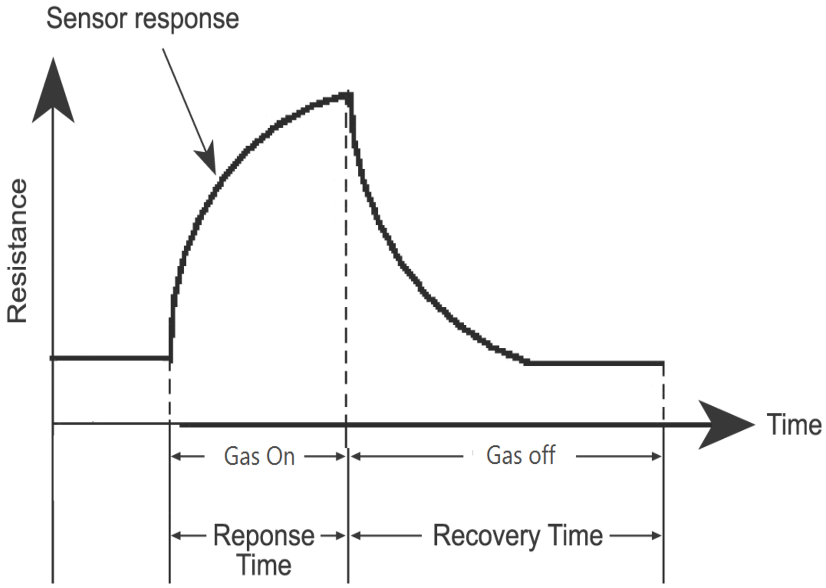

Figure II.20 *Typical structure of a conductivity sensor.*

II. 9 Solar cell production

At the end of this present work we attempted to produce a solar cell based on CuO thin films as a new absorber layer. In this part of study we have interesting to study the effect of the CuO film thickness by varying the deposition on the electrical behavior for the elaborated heterojunctions using two different window layers namely: zinc oxide (ZnO) and zinc sulfide (ZnS). The CuO/ZnO and CuO/ZnS heterojunctions were deposited via an ultrasonic spray pyrolysis onto industrial ITO substrates. In figure II.21 we represented a schematic cross section of the produced solar cells. To ensure an ohmic contact on the top of CuO layer, we have deposited gold by DC reactive sputtering, the ohmicity of these contacts was checked by the current–voltage characteristic is shown in figure II.22.

However we have focused to represente just the heterojunctions with best I-V characteristics and the preeminent solar cells parameters. The deposition conditions of this elaborated heterojunctions are regrouped in table II.3 (a-b).

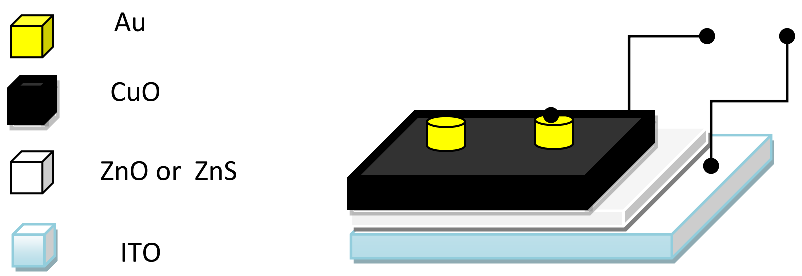

Figure II. 21 *A schematic cross section of the produced solar cells.*

Heretojunction	Deposition condition	ZnO	CuO
CuO/ZnO	Precursor	Zinc acetate ($Zn(CH_3COO)_2.2H_2O$)	Copper chloride ($CuCl_2.2H_2O$)
	Dissolvent	Methanol	Distillate water
	Molarity (mol/l)	0.1	0.1
	Substrate temperature °C	300	300
	Flow rate (ml/h)	4	10
	Deposition time (min)	10	40

Table II.3-a *Depositions condition of the CuO/ZnO heretojunction.*

Heretojunction	Deposition condition	ZnS	CuO
CuO/ZnS	Precursor	Zinc acetate ($Zn(CH_3COO)_2.2H_2O$) Thiourea (CH_4N_2S)	Copper chloride ($CuCl_2.2H_2O$)
	Dissolvent	Methanol	Distillate water
	Molarity (mol/l)	0.1	0.1
	Substrate temperature °C	300	300
	Flow rate (ml/h)	5	10
	Deposition time (min)	10	80

Table II.3-a *Depositions condition of the CuO/ZnS heretojunction.*

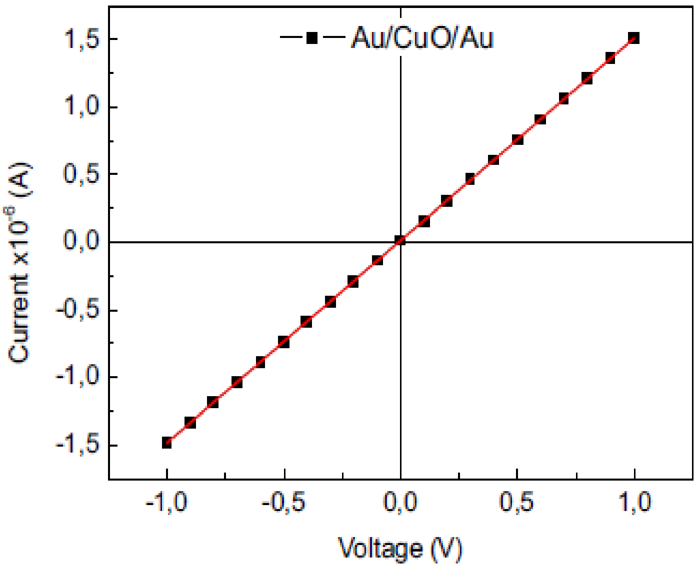

Figure II.22 *I–V characteristic of Au/CuO/Au structure.*

II.10 Current-Voltage Characteristic

The current-voltage (I–V) characteristics of the obtained hetero-junctions in the dark at room temperature are represented in Chapter IV. In figure II.23 we have shown the I-V characteristic of p-n heretojunction. The forward current varies exponentially with positive applied bias (V) and the characteristic can be described by the standard diode equation:

$$\mathrm{I} = \mathrm{I}_S \left(e^{\frac{qV_a}{nKT}} - 1 \right) \qquad (24)$$

Where k is the Boltzmann constant, T is the absolute temperature, and n is the junction ideality factor, Is the is the saturation current and Va is polarization tension.

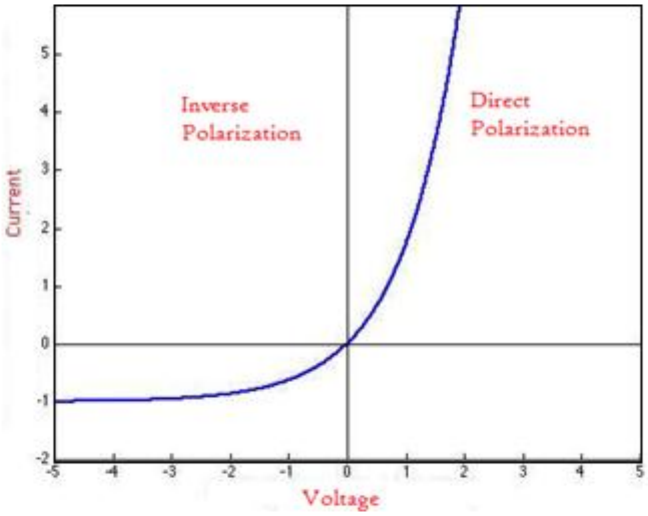

Figure II.23 *The I-V characteristic of p-n heterojunction.*

The estimated parameters characteristic of the elaborated heterojuctions is cited below:

- n is the ideality factor which is determined from the slope of the log (I)–V characteristic by the flowing equation:

$$n = {}^{q}\!/_{KT}\ \frac{d\ (V)}{d(\log(I))} \tag{25}$$

Its value is conventionally between 1 and 2, it depends strongly on the density of states at the interface and defects impairing the passage of electric current through the heterojunction.

- Is is the saturation current and it is the resulting current through the heterojunction in inverse polarization. The saturation current is obtained from the intersection of the straight line of log (I) at V= 0. For good heterostructures, the value turn to be negligible (~ µA or nA) compared with relative to the value in the direct polarization.

- Vth is the turn on voltage and it is defined as the built in potential, corresponds to a potential barrier the carrier has to overcome to contribute to forward current. It is determined from the inter-section of the linear portion of the forward I–V characteristic with the voltage axis.

- RR is rectification ratio and it is it gives the ratio between direct and reverse current at a voltage applied.

- The dynamic resistance is defined as Rd = ∂V/∂I, it depends heavily on the interface state and defects in the volume of materials. It represents the series resistance (Rs) in direct polarization and the shunt resistance (Rsh) in inverse polarization.

II.11 Solar cell parameters

Several factors affect a solar cell conversion efficiency value, including its the reflectance efficiency, the thermodynamic efficiency, the charge carrier separation efficiency, and the conduction efficiency values. Because these parameters can be difficult to measure directly, other parameters are measured instead, from the I-V curve of the solar cell under dark and light as shown in figure II.24, including:

- The open-circuit voltage (V_{OC}) is the maximum voltage available from a solar cell, and this occurs at zero current. The open-circuit voltage corresponds to the amount of forward bias on the solar cell due to the bias of the solar cell junction with the light-generated current.
- The short-circuit current (Isc) is due to the generation and collection of light-generated carriers. For an ideal solar cell at most moderate resistive loss mechanisms, the short-circuit current and the light-generated current are identical. Therefore, the short-circuit current is the largest current which may be drawn from the solar cell. The area of the solar cell. To remove the dependence of the solar cell area, it is more common to list the short-circuit current density (J_{sc} in mA/cm^2) rather than the short-circuit current.
- The fill factor (FF) is a parameter which, in conjunction with V_{oc} and I_{sc}, determines the maximum power from a solar cell. The FF is defined as the ratio of the maximum power from the solar cell to the product of V_{oc} and I_{sc}. Graphically, the FF is a measure of the "squareness" of the solar cell and is also the area of the largest rectangle which will fit in the IV curve (figure II.24).

$$FF = V_m \; I_m / V_{oc} \; I_{sc} \tag{26}$$

Where *FF* is the fill factor, V_{oc} is the open-circuit voltage, I_{sc} is the short-circuit current and V_m x I_m is maximum power.

- The efficiency (η) is the most commonly used parameter to compare the performance of one solar cell to another. Efficiency is defined as the ratio of energy output from the solar cell to input energy from the sun. In addition to reflecting the performance of the solar cell itself, the efficiency depends on the spectrum and intensity of the incident sunlight and the temperature of the solar cell. it is calculated using the flowing equation:

$$\eta = Voc\ Isc\ \ FF / P_{in} \tag{27}$$

Where η is the efficiency, V_{oc} is the open-circuit voltage, I_{sc} is the short-circuit current, FF is fill factor and P_{in} is the input power of the light.

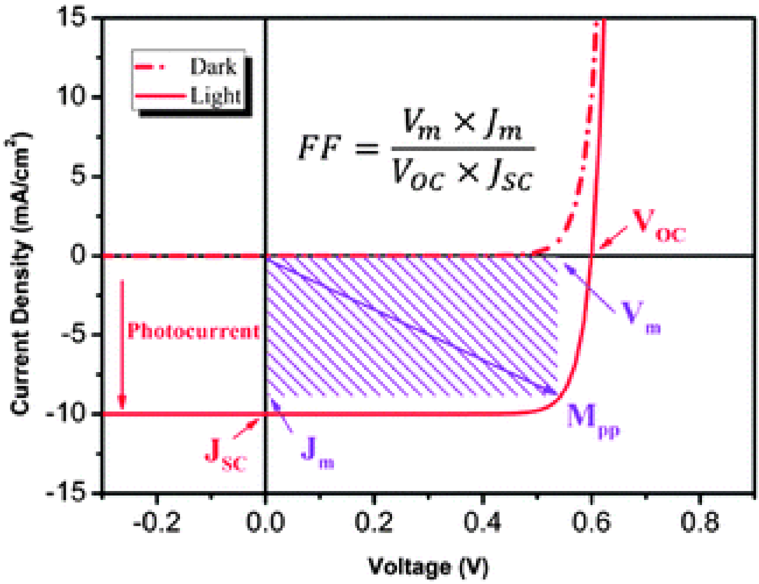

Figure II.24 *IV curve of a solar cell under dark and light.*

Chapter III

Results and Discussion: CuO thin films

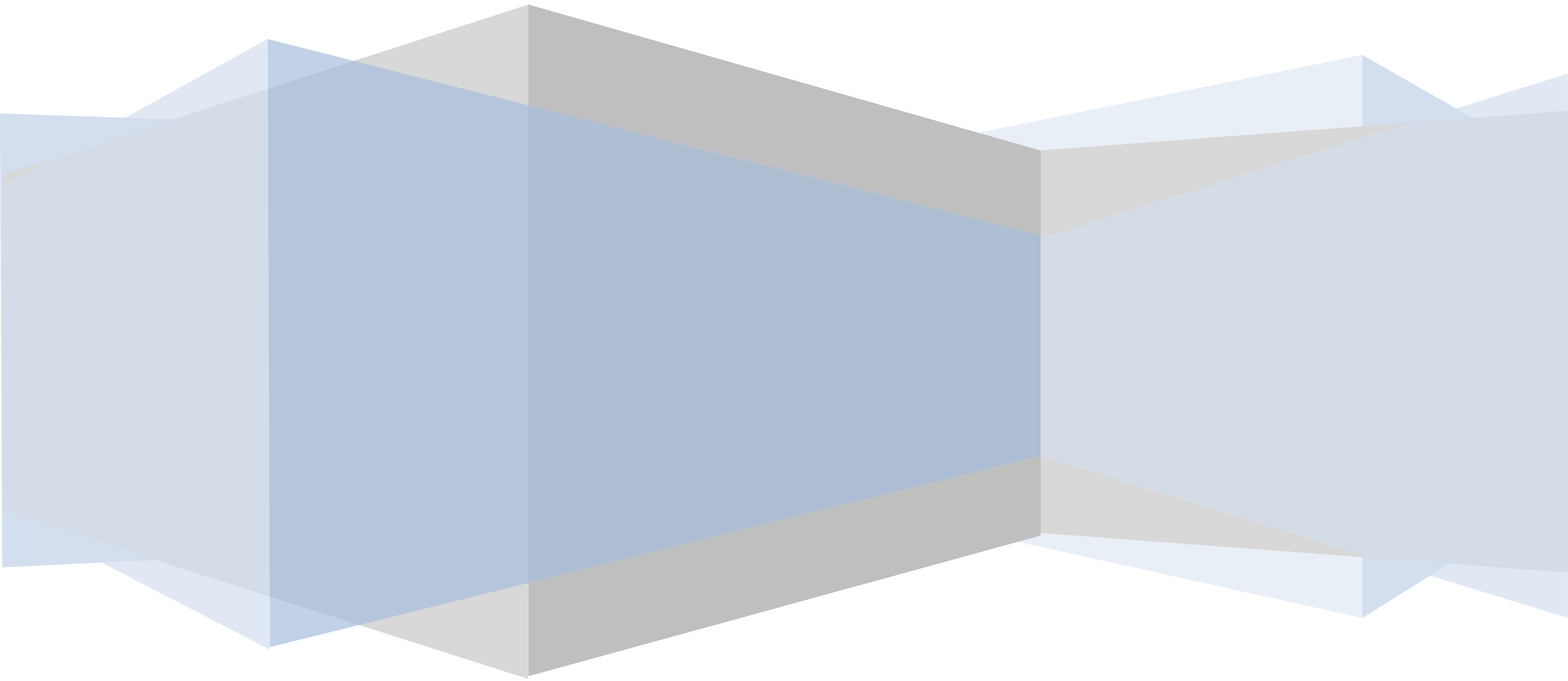

In this chapter, the results of the different investigation parameters are presented with discussion.

III.1 Influence of substrate temperature

In this section, we present the results of CuO films prepared with two different precursors namely: copper chloride ($CuCl_2.2H_2O$) and copper acetate $Cu(CH_3COO)_2$ at various substrate temperatures in order to investigate the effect of this parameter.

III.1.1 Copper chloride

Copper chloride is used as copper source with molarity equal to 0.05 M. The samples were deposited with various substrates temperature ranged from: 280 - 400°C.

III.1.1.1 Deposition rate

In figure III.1 we have reported the variation of growth rate as function of the substrate temperature. As can be seen, the film thicknesses decrease with the increase in substrates temperature. The films deposition rate starts with 274,96 nm/min at the beginning for the lower substrates temperature (280 °C) and decrease with substrate temperature rise to reach 216,20 nm/min for CuO films deposited at hither temperature (400 °C) . It is well known, that the increase of the substrate temperature improves the surface kinetic reaction of the substrate, which lead to thicker thin films. However, for CuO deposited thin films the thicknesses turn to reduce with increasing substrate temperature. In fact the deposition rate depends on the quantity of sprayed reactive species reaching the top of surface substrate. The increases in the substrate temperature enhance the evaporation of incoming species in one hand and the air convection around the heated substrate drifts away the droplets on the other hand. This leads to the reduction of the reactive species quantity on the growing surface. Biglin et al [74] have deposited CdS thin films by spray pyrolysis at different substrate temperature. They observed the same behavior where the evaporation phenomenon was found to cause CdS thin films thickness reduction.

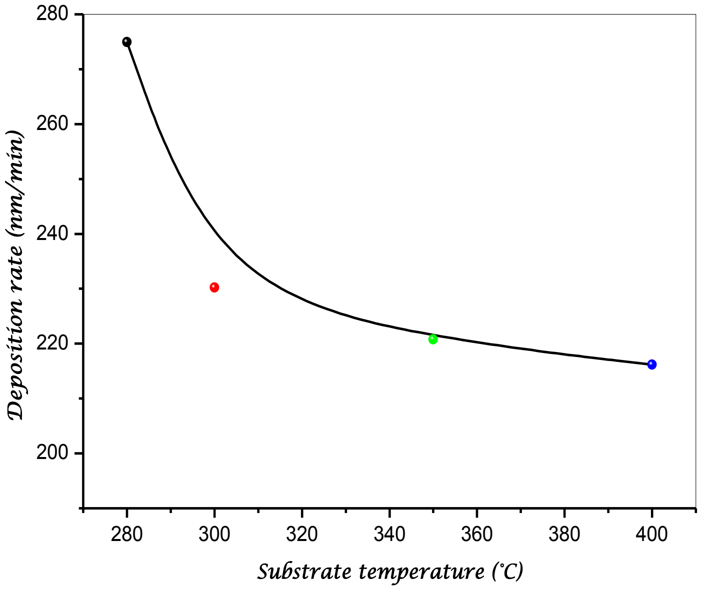

Figure III.1 *Variation of deposition rate as a function of substrates temperature.*

III.1.1.2 Structural properties

In figure III.2 we have regrouped the XRD diffraction patterns of different films. The influence of substrate temperature on the films can be clearly seen and suggests that the films structural proprieties are very sensitive to this parameter. The XRD pattern of the samples show fine crystalline structure with clear characteristic peaks of monoclinic CuO phase as found by comparison with standard JCPDS values (80-0076). The diffract-grams show prominent (200) and (111) atomic planes located at 2θ values of 35.5° and 38.9° for all the prepared films at various substrate temperatures. However, small features of other atomic planes are also observed situated in large diffraction angles indicating the polycrystalline nature of the as-prepared films. The films deposited at substrate temperature equal to 280 °C shows two intense peaks assigned to (111) and (200) respectively with the presence of small peaks related to (311) (220) and (004). With increasing substrate temperature (300 °C), the two important peaks $(\bar{1}11)$ and (200) became more intense, we notice also the emergence of other peaks related to (112) (020) and (202). With further increasing substrate temperature (350°C), we remark that the intensity of the (200) amplify strongly by contribution of $(\bar{1}11)$ peaks with the extinction of $(\bar{3}11)$ and (004) atomic plan. For the films elaborated at 400 °C, the intensity of the peaks (200) decrease remarkably with the presence of the single small peaks related to (112) and the extinction of the all other peaks.

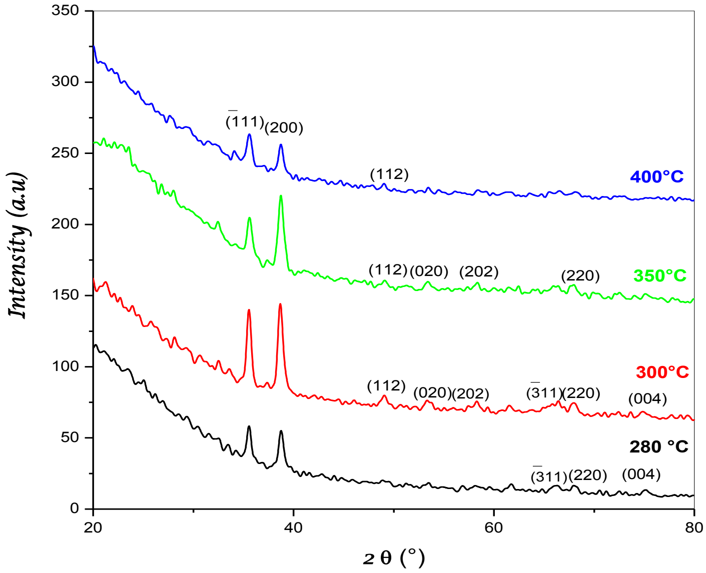

Figure III.2 *XRD diffraction patterns of CuO films prepared with different substrate temperatures*

As can perceive from the XRD spectra, the intensity of this peaks are affected by the change in substrate temperatures. To describe the structure and preferred orientation of the deposited CuO thin films in detail, the texture coefficient (T_C) was used, which is defined:

$$T_C = [\, I_{hkl} / I^0_{hkl}] / [\, (1/n) \sum (I_{hkl}/I^0_{hkl})] \qquad (11)$$

Where I_{hkl} is the measured intensity of the plane (hkl) and I^0_{hkl} the standard intensity of the plane (hkl) taken from PDF card data, n is the reflection number. In figure III.3 we have reported the variation of the texture coefficient estimated for the two prominent peaks namely (111) and (200) as function of substrate temperatures. As can be seen, the texture coefficient of the two atomic plans increase with increasing in substrate temperature to 300 °C. Above this temperature the texture coefficient is reduced considerably. The decrease in the Tc value with substrate temperature shows that films obtained have more randomly oriented grains. The Tc of the (200) plan is higher than the Tc of the $(\bar{1}11)$ plan in the investigated temperature, this indicated that all sample have preferred (200) orientation. Thus, it was clear from the calculated Tc that CuO films deposited at 300 °C have best crystallization level and preferred (200) orientation.

On other hand, we note that the variation in substrate temperature leads to the appearance and the disappearance of many small peaks as shown in figure III.2. At lower deposited substrate temperature we observed the appearance of (311) (220) and (004). However, with increasing substrate temperature above 350°C we notice the disappearance of these peaks and no change for other peaks. At higher substrate temperature, we remark the existence only of the (112) atomic plan and all the other peaks disappears. Thereafter, one can conclude that the (311) (220) and (004) emerge at lower substrate temperature contrary to the (112) (020) and (202) appearance at higher substrate temperature.

We emphasize that no peak corresponding to Cu_2O has been appeared in the XRD pattern of films deposited at various substrate temperature. While some authors have reported the presence of both CuO and Cu_2O phase for spray deposited CuO films [75,76]. Maruyama [77] has observed a mixture of Cu_2O and CuO phase in CVD grown copper oxide films prepared at a substrate temperature of 300 °C. Yoon et al. [78] have observed a dominant CuO phase in copper oxide thin films prepared using ion beam sputtering at a substrate temperature varied from 25 to 400 °C. It is important to note that films deposited with ultrasonic spray pyrolysis technique, copper oxide thin films with a predominant CuO phase has been successfully grown with substrates temperature of 300–400 °C.

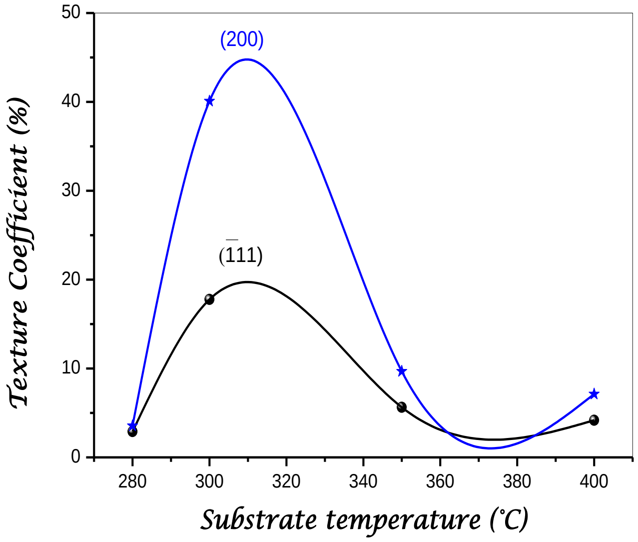

Figure III.3 *Variation of texture coefficient as various substrate temperatures.*

The films crystallites size was estimated from the most intense peak namely (111) and (002) by using Hall–Williamson equation. In figure III.4 we have reported the variation of crystallite size as a function of substrates temperature. It is evident from the figure that the films crystallites size is reduced with increasing the substrate temperature. This variation can be explained in terms of the decrease in film thickness. Akaltun [33] have investigated the effect of thickness on the structural proprieties of CuO thin films prepared by spray pyrolysis and he found increase of crystallite size from 8 to 18 nm for film thicknesses varied from 125 to 250 nm.

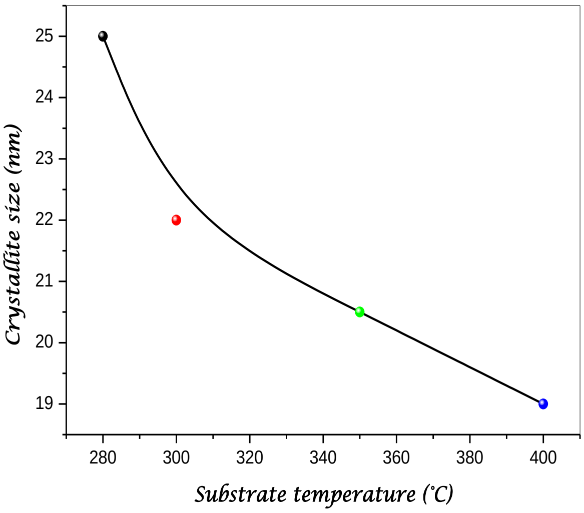

Figure III.4 *CuO films crystallite size dependence on substrate temperature.*

In table III.1 we have regrouped the values of strain (ε) for CuO deposited films at various substrate temperatures. This structural parameter was also calculated from Hall–Williamson equation. The strain values varied from 0.0217 to 0.0588 in the studied temperature range . As can be seen, the maximum strain value found for the films deposited at 300 °C. This can be explain by the appearance of all (hkl) plans characteristics of CuO phase in the same time which create a competition in the growth between this atomic plans and involve an augmentation of the strain in thin layer. Therefore, at higher substrate temperature the strain is found to decrease. This can be explained also by the disappearance of the (hkl) peaks as shown in XRD diffraction patterns.

A positive slope has been observed in the Hall equation plot for CuO films deposited at 280, 300 and 350 °C, which confirms the presence of tensile strain in the crystal lattice. However, for CuO thin films deposited at higher temperature (400 °C) a negative slope has been noticed indicating the presence of compressive strain in the crystal lattice. As can be seen, variation of the substrate temperature leads also to change in the type of strain.

Substrate temperature (°C)	Strain
280	0.0413
300	0.0588
350	0.0243
400	-0.0217

Table III.1 *Values of strain of the as-prepared CuO thin films with different substrate temperature*

As mentioned previously, CuO crystallizes in a monoclinic structure. This crystalline structure leads to nine optical and three acoustic phonon branches. The symmetries of the zone-center modes are Ag+ 4Au + 2Bg+ 5Bu. But only the three modes of Ag and 2Bg symmetry are Raman active. In figure III.5 we have presented the Raman spectra of the as prepared CuO films with various substrate temperatures. The Raman spectra are composed with three main photon modes Ag and 2Bg located at 296, 334 and 602 cm^{-1}. These peaks are largely reported in the literature [79,80]. This confirms the presence of a single phase CuO with monoclinic structure.

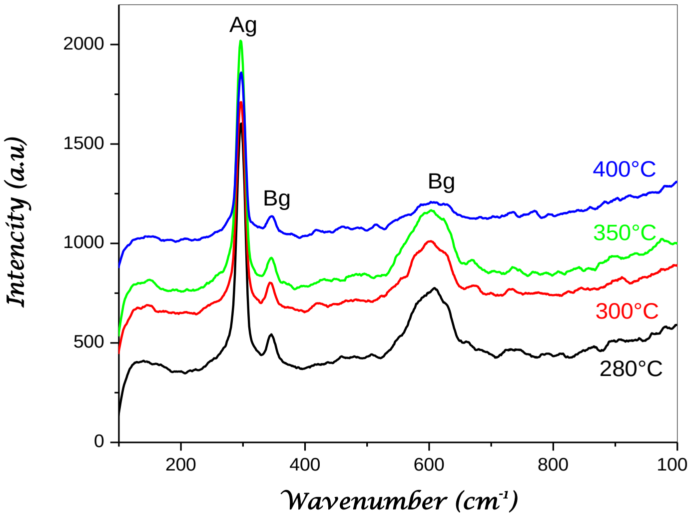

Figure III.5 *Micro Raman spectra of CuO thin films deposited with various substrate temperatures.*

In figure III.6 we have reported the variation of the intensity of Raman modes as function of substrate temperature. In the investigated temperature range, the intensity of the three Raman mode decrease with increasing substrate temperature, however the intensity of the Ag mode Raman is reduced noticeably. This can be attributed to the decrease in films thickness with increasing in substrate temperature. Chaturvedi and Sathe [81] have studied the variation of Raman modes in $PrMnO_3$ thin films by pulsed laser deposition as a function of thickness using Raman spectroscopy. They noted that the thickness decreases leads to the decrease in intensity of main Raman modes.

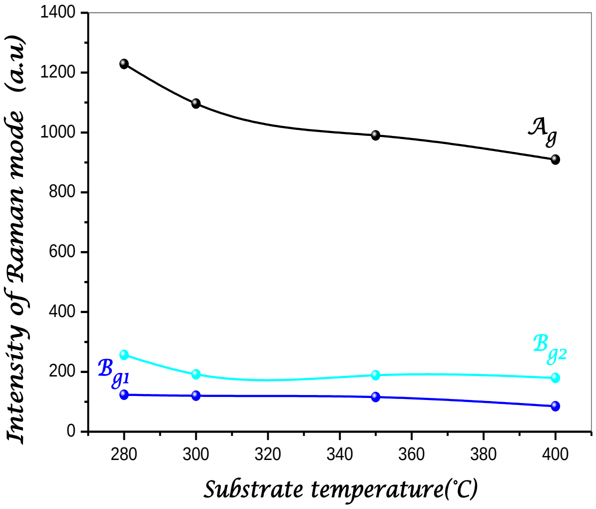

Figure III.6 *Variation of the three Raman modes intensity with various substrate temperatures.*

The variation of the peaks position correlates with the strain and the variation in the crystallite size. We note also from figure III.5 that the these peaks shift to lower frequency (red shift) with increasing in substrate temperatures compared to the films deposited at 280 °C. The variation of the position peaks can be related to the variation crystallite size. In figure III.7 we have reported peak position shift of Ag mode as function of crystallite size. It is evident from this figure that red shifts of the Raman frequencies increase with decreasing crystallite size; this is confirmed the values of crystallites size calculated from XRD spectra. The same variation is observed by Varghese Swamy et al [82]. They have found an increase in red shift for the A1g Raman mode, with decreasing crystallite size from 23 to 5 nm for nanocrystallite tin oxide (TiO_2). The decrease in crystallite size dimensions to the nanometer scale causes a wavenumber shift and broadening of Raman peaks as a result of phonon confinement. This has been observed for many small-sized semiconductor and oxide materials such as: Y_2O_3, CuO and TiO_2 fabricated by sol–gel techniques [83,84].

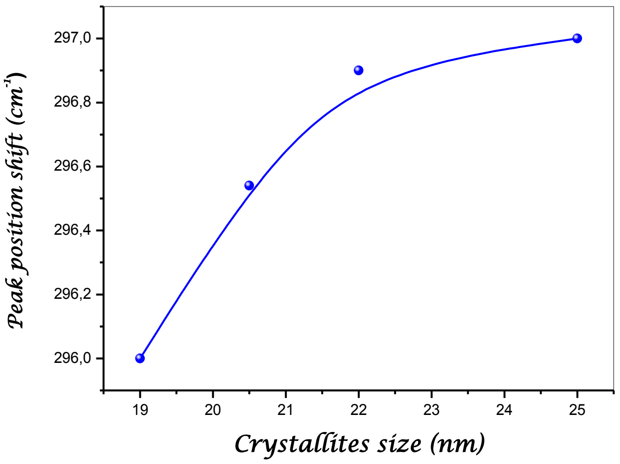

Figure III.7 *Variation of peak position shift as function of crystallites size.*

III.1.1.3 Optical properties

In figure III.8 we report the variation of the optical transmittance in the UV-VS-NIR of the deposited with different substrates temperature. It is clear that the deposited films exhibit a relatively high absorption ranged from 40 to 60 % for wavelengths greater than 600 nm. The reduction of the transparency in this range with the substrates temperature is due to film thickness increasing.

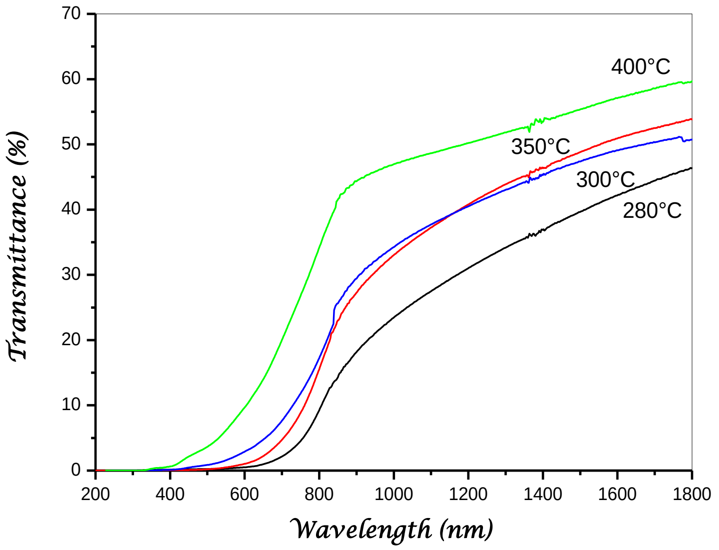

Figure III.8 *Transmittance in the UV-visible region range of CuO thin films prepared with various substrate temperature.*

In figure III.9 we have presented the variation of the optical band gaps as a function of substrates temperature. The optical band gap of the deposited films is increased with increasing the substrates temperature varying from 1.20 to 1.75 eV with increasing the substrates temperature from 280 to 400 °C.

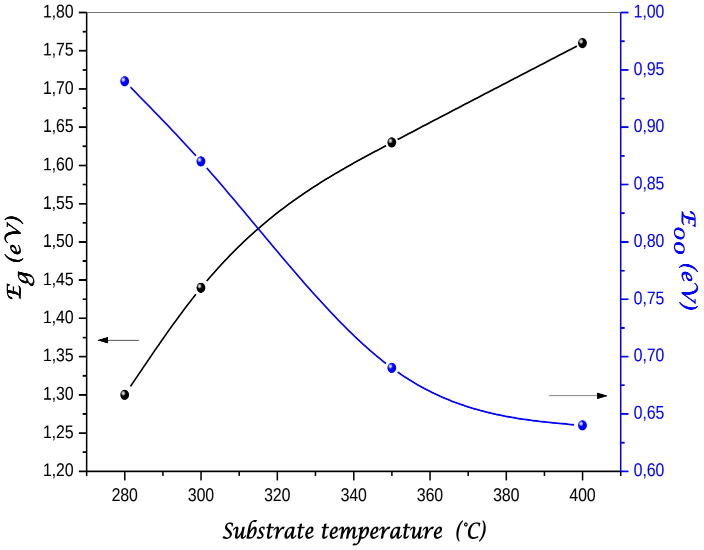

Figure III.9 *Influence of substrate temperature on CuO thin films optical band and disorder*

It is well known that localized states near the band edge causes the appearance of band tails in the films band diagram. These band tail states are responsible for the sub-gap absorption in the low energy range, the spectral dependence of the absorption edge follows the Urbach formula:

$$\alpha = \alpha_0 \, exp \, (h\nu/E_{00}) \qquad (18)$$

Where α_0 is the pre-exponential factor, hν the photon energy and E_{00} is the band tail width commonly called Urbach energy. The band tail width is also related to the disorder in the film network. The disorder is due to the presence of weakly bonded atoms. It corresponds to the deviation of bond distance and angle from their standard value in the crystalline structure. The Urbach energy or disorder can be estimated from the inverse slope of the linear plot of ln (α) versus photon energy (hν). The variation of the film disorder as a function of substrates temperature is represented in figure III.9. The disorder in the elaborated films is diminishing with increasing the substrate temperatures diverge from 640 to 960 meV. As can be seen the films became more organized with increasing the substrate temperature due to the diminution of the disorder in films. Urbach tail width found to be randomly affected by the substrate temperature as shown by Chamberlin et al. [62] for CdS thin films prepared by spray ultrasonic pyrolysis technique, where it has values in the range 122 - 188 meV for substrate temperatures in the range 164 - 350 °C. Melsheimer and Ziegler [42] observed a decrease in disorder with substrate temperature for spray-deposited tin dioxide thin films. For the elaborated films prepared at Ts = 420 - 500 °C, it decreases from 240 to 200 meV. On other hand the increase in optical band gap corroborates well this disorder reduction in films network. This indicates clearly that optical band gap in the obtained films is governed by the disorder. It can be deduced that an increase in the band tail width causes the reduction in optical gap.

In figure III.10 we have reported the variation of absorption coefficient (α) as function of the wavelength. It is clear that the prepared CuO films have a high absorption coefficient with a value of 10^4 (cm^{-1}) in the visible range of the wavelength. However, the films deposited at 300 °C show the highest absorption coefficient. The optical proprieties of this films revealed they are used as new activated layer in photovoltaic cells.

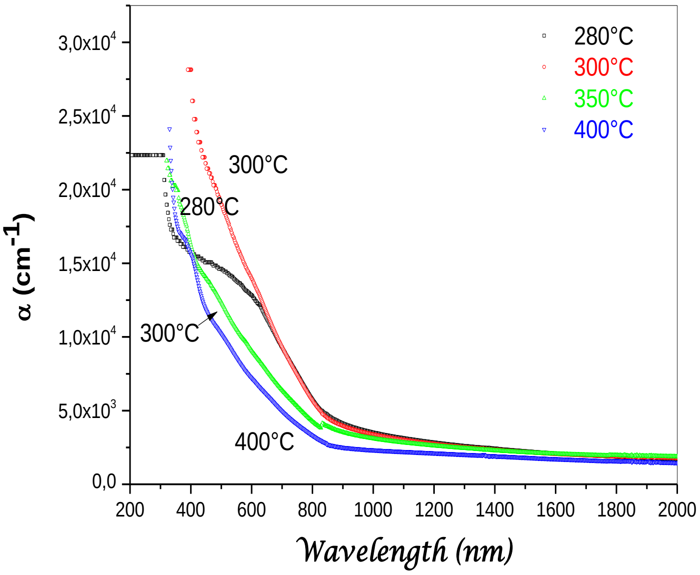

Figure III.10 *Variation of absorption coefficient versus wavelength.*

The variation of refractive index as function of the substrate temperature is reported in figure III.11. With increasing in the substrate temperature the value of refractive index increase from 1.53 to 1.63. This indicates that films became denser with increasing in substrate temperature. Xiaodong Wang [18] has deposited TiO_2-SiO_2 thin films by sol-gel method for different annealing temperature. They found that the refractive index increases with annealing temperature, from 1.75 to 1.86 at He-Ne laser wavelength of 633 nm.

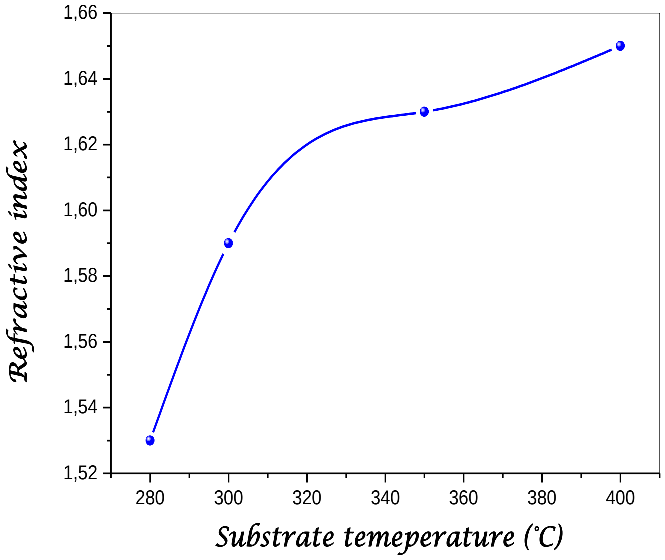

Figure III.11 *Variation of refractive index as function substrates temperature.*

III.1.1.4 Electrical properties

In figure III.12 we have reported the variation of the dark conductivities measured at ambient temperature. The conductivity changes in order of two decades. As can be seen the conductivity variation have a bell U shape behavior with maximum values found for the deposited films at 350 °C. It is well know that conductivity is altered by the substrate temperature. The conductivity increase with the substrate temperatures from 280 to 350 °C can be explained by decrease of the defect and disorder in the films with increasing the substrate temperature. But for the films deposited at 400 °C, the conductivity reduction can be related to films thickness decrease. Gopalakrishna et al [32] have deposited CuO films by spray pyrolysis at various substrate temperatures. They found that the resistivity of the films decrease from 10^4 to 53 (Ω.cm) with increasing substrate temperature from 250 to 350 °C then increase to 80 (Ω.cm) for film prepared at substrate temperature equal to 400 °C.

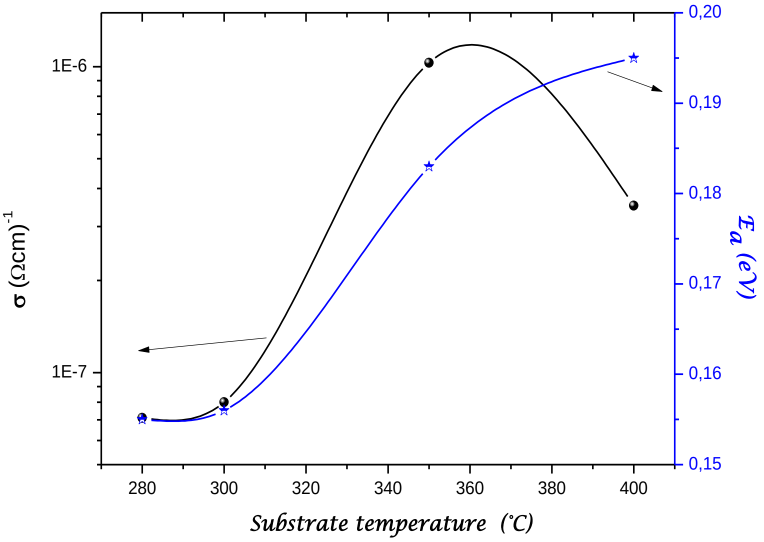

Figure III.12 *Variation of the dark conductivity and activation energy as function of the substrate temperatures.*

It is recognized that the conductivity increases with temperature indicating the semiconducting behavior of the films. It is interesting to note that the conductivity appears to vary with inverse of temperature suggesting a thermally activated conduction mechanism. The activation energy and conduction of the films are related in following the Arrhenius equation:

$$\sigma = \sigma_0 \exp(-Ea/kT) \qquad (20)$$

Where Ea is the activation energy of conduction, σ_0 is pre-exponential factor, k is the Boltzmann's constant and T is the absolute temperature. The thermal activation energy can be estimated from the slope of the linear plot of ln (σ) vs inverse of temperature. The activation energy variation as function of the substrate temperature is represented in figure III.12. As can be remarked, the activation energy is affected by the substrate temperature; it increases from 0,155 to 0,195 eV with increasing the substrate temperature. Singh et al [37] have deposited CuO thin films by spray ultrasonic pyrolysis. They investigate the effect of substrate temperature and found that the activation energy varied from 0.294 to 0.311eV.

The value of pre-exponential (σ_0) so can be used to determine the conduction mechanism. The value of this parameter can distinguish the conduction whether it is in extended states or in localized states. For extended state conduction, the value of so lies in the range 10^3–10^4 $(\Omega cm)^{-1}$, whereas for hopping conduction in localized states in band tails, the value of so is smaller than this range [85]. As shown in table III.2, the pre-exponential factors of different samples are estimated also from the slope of the linear plot of ln (σ) vs inverse of temperature.

The calculated values than 10^3 $(\Omega cm)^{-1}$ of σ_0 are lower. This indicates clearly that the dominant transport in CuO films is in the localized states present in band tails.

Substrate temperature (°C)	σ_0 $(\Omega.cm)^{-1}$
280	**8.89×10^{-6}**
300	**3.96×10^{-7}**
350	**3.2×10^{-2}**
400	**1.31×10^{-3}**

Table III.2 *Values of pre-exponential factors for various substrate temperature.*

It is well known that conductivity activation energy of a p-type semiconductor E_a corresponds to Fermi level E_f position regarding the bottom of valence band edge E_v. The band tail width E_{00} is correlated to the disorder and the larger the band tail the more disordered is the film network. Consequently, the variation of the activation energy is also related to the variation of the disorder in the film. In figure III.13 we have represented the variation of activation energy and the disorder as function of substrate temperature. The increase in activation energy correlates well with the disorder reduction in films networks. On other hand the increase in activation energy can be reflected by the decrease in the band tail width in films. As can be approved, the conduction mechanism in our deposited CuO thin films is situated in the localized states present in band tails which explains the low conductivity of the as-prepared films. Thus, in our case the activation energy is definite by the difference between the band tails width of the localized states and the energy Fermi position. As depicted in the figure III.14, is showing the activation energy for the conduction mechanisms in p-type semiconductor.

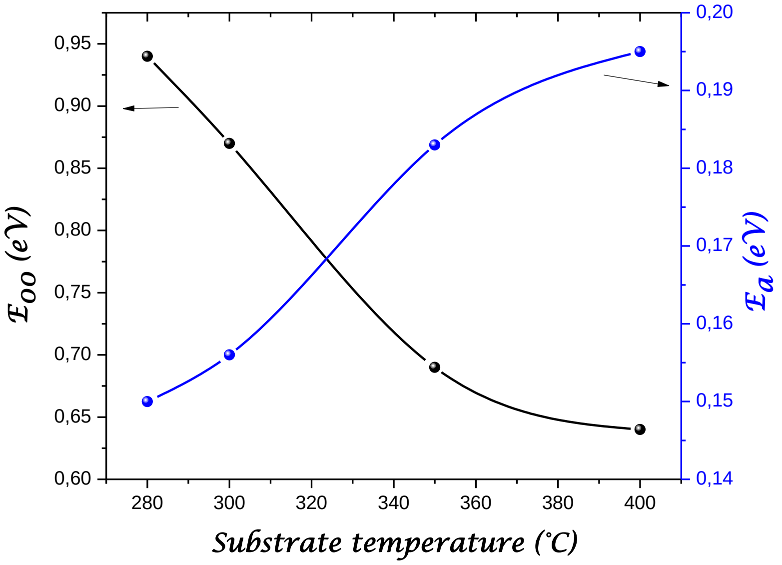

Figure III.13 *Variation of disorder and activation energy as function of substrate temperature.*

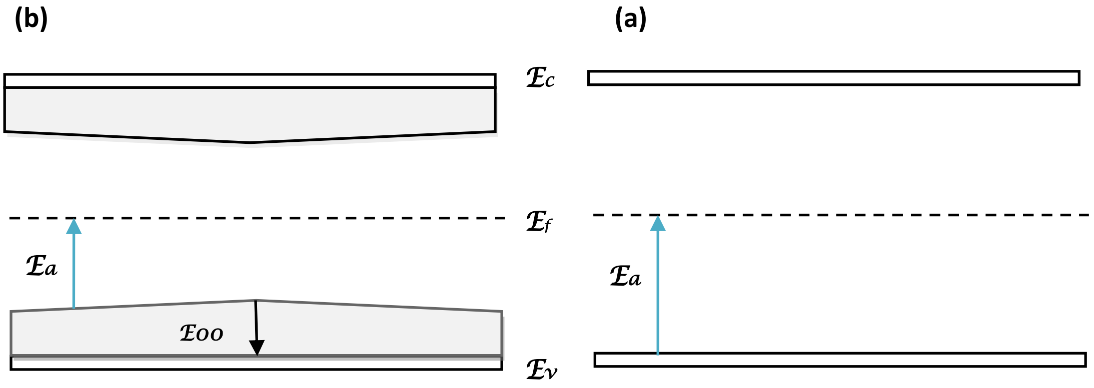

Figure III.14 *Schematic diagram of activation energy for the two conduction mechanism: (a) in localized state (b) in conduction state*

III.1.2 Copper acetate

In this part, copper acetate is used as copper source with molarity equal to 0.05 M. the used samples study are deposited with various substrates temperature ranged from : 280- 400°C.

III.1.2.1 Deposition rate

In figure III.15 we have reported the variation of the growth rate as function of substrate temperature. As can be seen, the deposition rate diminish from 65 to 50 nm/min in the investigate temperature range. Increasing in substrate temperatures causes to reduce of the quantity of reactive species and deteriorate the surface kinetic reaction of the substrate, which lead to decrease film thicknesses. We noted that films thickness condense with increasing in substrate temperature for the deposited CuO films deposited with the two precursor salt namely: copper acetate and chloride. As result this behavior is mostly and particularly attributed to the films deposited by spray ultrasonic pyrolysis deposition at higher substrate temperature. The same case is remarked for CdS thin films elaborated by chemical bath deposition at higher bath temperature and long deposition time. The reduction of the grow rate and the thickness saturation is due to the rarefaction or consumption of the reactive species such as Cd and S ions in the started solution.

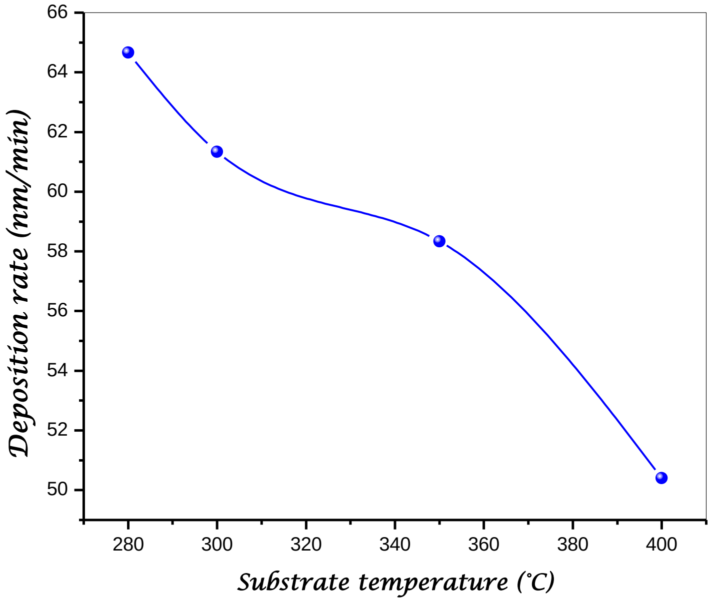

Figure III.15 *Variation of growth rate as function of substrate temperatures.*

III.1.2.2 structural properties

The XRD spectra of different films are reported in figure III.16. The influence of the deposition temperature on films structure can be divided as following:

- For substrate temperature varied from 280 to 350°C: Two most prominent peaks can be clearly seen at 2θ value 35.5° and 38.7° corresponding to atomic planes $(\bar{1}11)$ and (111), respectively of CuO phase. No peak corresponding to Cu_2O phase of copper oxide has appeared in the XRD pattern indicating the formation of pure CuO films. However the intensity of these two important peaks changed with the variation of the substrate temperature.
- For the films deposited at 400°C: The diffractogram shows the presence of single (111) atomic planes located at 38.7° and the peak $(\bar{1}11)$ disappears.

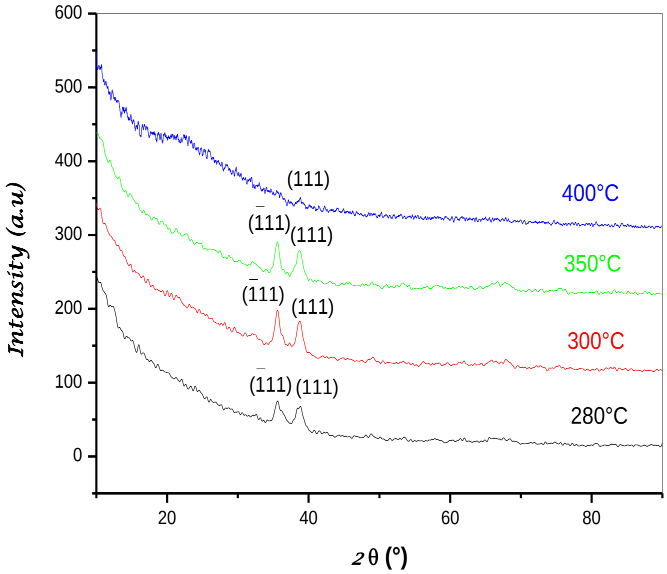

***Figure III.16** XRD diffraction patterns of CuO films prepared with different substrate temperatures.*

To determine the preferential orientation in CuO films from the XRD data, the texture coefficient was calculated. The texture coefficient (Tc) for the $(\bar{1}11)$ and (111) atomic planes at various substrate temperature is showing in figure III.17. As can be seen, the Tc of the two atomic plans have the same behavior, it is maximum for substrate temperature equal to 300°C.

For the films prepared at 280°C, the samples show a (111) preferred orientation. With increasing substrate temperature the Tc of the two atomic plans equalized indicates a random distribution of grains in the film. At substrate temperature equal to 350°C, the preferred orientation of the CuO films change from (111) to $(\bar{1}11)$. As result, for lower substrate temperature, the films showed a (111) preferred orientation and a $(\bar{1}11)$ preferred orientation for the sample deposited at higher substrate temperature. All films are polycrystalline and the calculated texture coefficient shows that the CuO films elaborated at 300°C have the best crystallinity.

It is remarkable to note from the comparison of our observed and their reported from the XRD analysis that, the nature of salt solution used as Cu source for deposition CuO film by spray pyrolysis technique might be responsible in change of copper oxide phases and the variation of structural proprieties of single phase CuO.

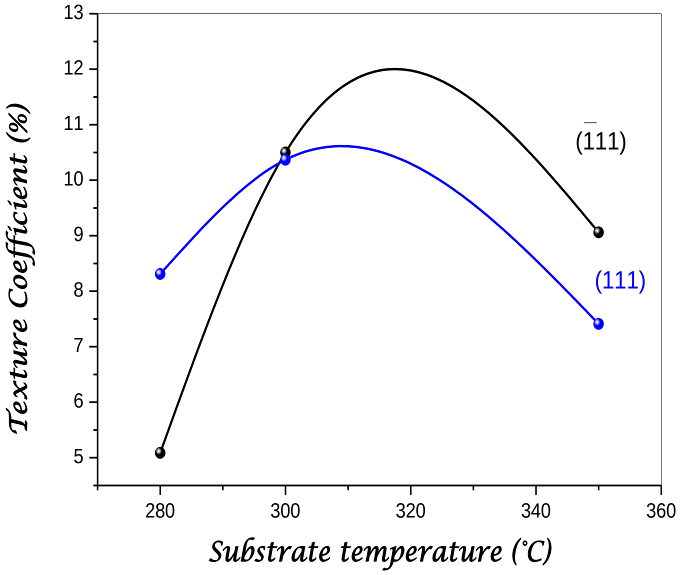

Figure III.17 *Variation of texture coefficient as function of substrate temperatures.*

The films crystallites size was estimated from the most intense peak namely $(\bar{1}11)$ and (111) by using Debye Scherrer formula (see chapter II). In figure III.18 we have represented the variation of the crystallites size as function of the substrate temperature. It is clear from this figure that crystallites size increase with increasing substrate temperature. The calculated crystallites size enlarges from 9 to 40 nm in the investigated temperature range. It is well know that the increase in substrate temperature improve the crystallinity and leads to the formation of bigger crystallites size. The nucleation step is highly sensitive to the substrate temperature. At hot surface substrate, atoms have larger kinetic energy which leads to wide nucleation and higher condensation of atoms in consequence growth of bigger crystallites size. Therefore, at low substrate temperature the nucleation center are fewer with less kinetic energy this leads to the growth of small crystallites size. In the same figure III.18 we have represented the variation of strain with various substrate temperatures. It is evident from this figure that the strain is reduced with increasing the substrate temperature. As can be noted the increase in substrate temperature improves the crystallinity and so the amount of the defects in the films. On other hand the increase in the crystallites size correlates well with the strain reduction in films. This indicates clearly that the obtained strain film is controlled by the value of the calculated crystallites size. In additional, the growth of lager crystallite size leads to grain boundaries reduction and consequently the reduction of defects in the structure. Grain boundaries are 2D defect in the crystal structure; it tends to decrease the film crystallinity. So, the reducing in crystallite size is a common way to improve the strain in films, as described by the Hall–Petch relation. It can be deduced an increase in the crystallite size causes the reduction in the strain.

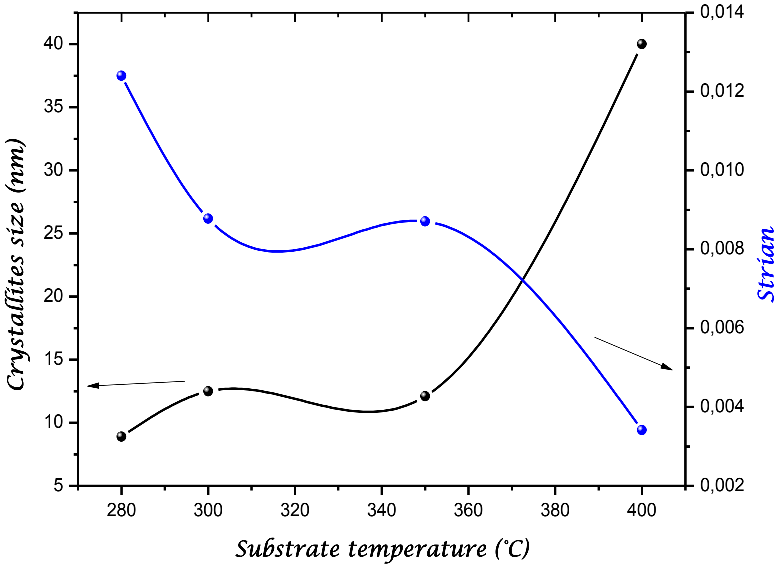

Figure III.18 *Variation of crystallites size and strain as function of substrate temperature.*

Dislocations are the imperfections in a crystal associated with the mis-match of the lattice in one part of the crystal with respect to another part. The dislocation density (δ) is calculated from the equation (13). In table III.3 we have illustrated the calculated dislocation density for different substrate temperatures. The dislocation density in our case is found to be decreases with substrate temperatures. The decrease in dislocation density indicates decrease in concentration of lattice imperfections and formation of high quality films. The decrease in the dislocation density and increase in the crystallites size values with increase in substrate temperature also gives the evidences of the obtained strain and crystallite size.

Substrate temperature (°C)	*Dislocation density (line/m^2)*
280	**15.6 x 10^3**
300	**6,4 x 10^3**
350	**6,2 x 10^3**
400	**0,6 x 10^3**

Table III.3 *Values of dislocation density at different substrate temperature.*

III.1.2.3 Optical properties

In figure III.19 we have represented the diverse spectrum of transmittance in the UV-VIS-NIR range with different substrate temperatures. The films transparency varied wildly, in the investigated temperature range. It is seen that the films become more transparent with the increase in substrate temperatures. For wavelength above 800 nm the transmittance of the whole films is ranged from 30 to 70 %. This variation is in same rage reported in the literature [26-35]. CuO thin films are used as an absorber layers in solar cells. The high absorption of this layer in visible range is one of the required proprieties devices. The film transparency increases with increasing substrate temperature. This behavior is due to the decrease in films thicknesses.

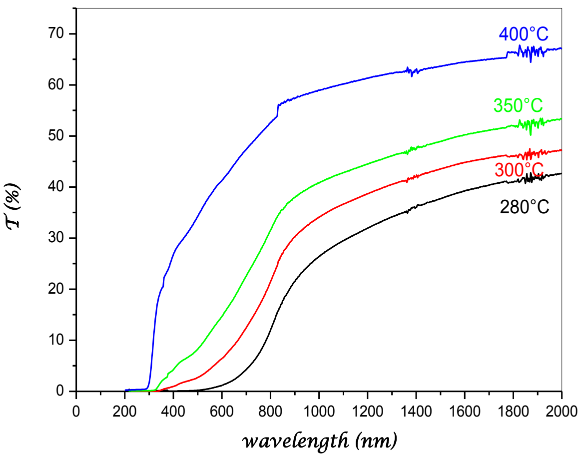

Figure III.19 *Transmittance spectrum in UV-VIS-NIR range of CuO films deposited with various substrate temperature.*

The optical band of films is deduced from the transmittance spectra (as mentioned in chapter II). The obtained results are shown in figure III.20. As can be seen, the optical band gap enlarges with increasing substrate temperature. It is varied from 1.25 to 1.50 eV for substrate temperature ranging from 280 to 400 °C. In figure III.20 we have represented the variation of the steepness (σ_p) as function of substrate temperatures. The steepness parameters (σ_p) is inversely proportional to the disorder in film. As mentioned above the variation of optical band gap is related to the variation of disorder. The increase in optical band gap corroborates well the disorder reduction in films network. As result, the variations of the optical band gap and the steepness have the same behavior. This confirms also the increase in optical band gap with substrate temperature increasing. The increase in the steepness indicates that the disorder in films is reduced with substrate temperature. This is consistent with the decrease is the values of the defects of the strain calculated from XRD patterns. In this case, the variation of the optical gap is governed by the film disorder.

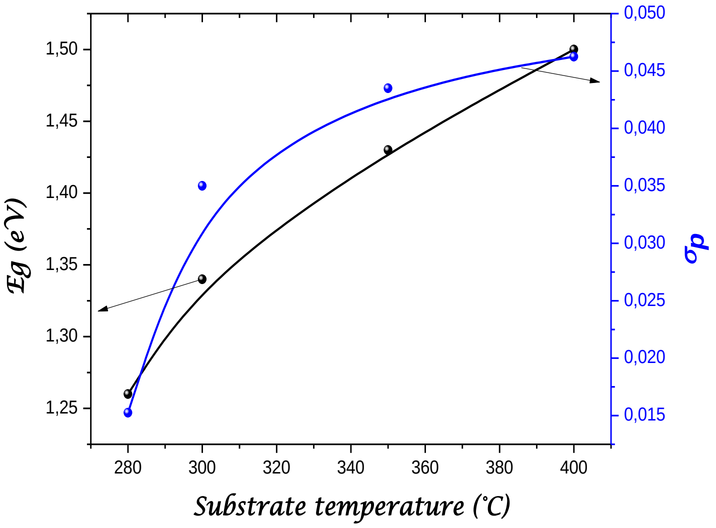

Figure III.20 *Variation of optical band gap and steepness as function of substrate temperature.*

In figure III.21 we have reported the variation of absorption coefficient (α) as function of the wavelength. It is clear that the prepared CuO films have a high absorption coefficient with a value of 10^5 (cm^{-1}) in the visible range of the wavelength. The values of absorption coefficient decrease with increasing substrate temperatures.. The values of the optical band gap and absorption coefficient calculated of all deposited films are suitable for the use of these layers in solar cells.

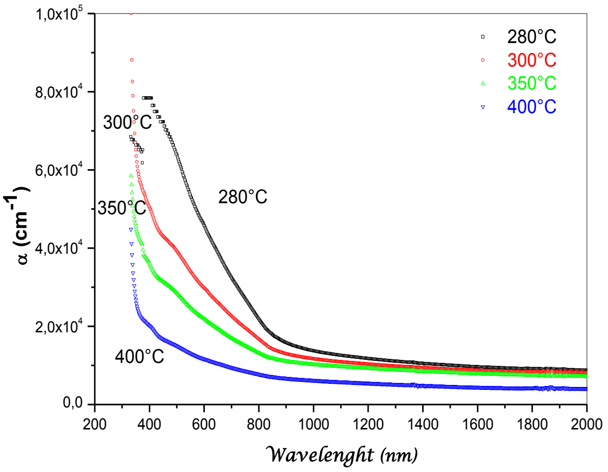

Figure III.21 *Variation of absorption coefficient as function of wave number.*

The variation of refractive index as function of the substrate temperature is reported in figure III.22. With increasing in the substrate temperature, the value of refractive index increase from 2 to 2.22. As can be seen refractive index is slightly altered by substrate temperature. However, the deposited CuO films became denser with increasing substrate temperature.

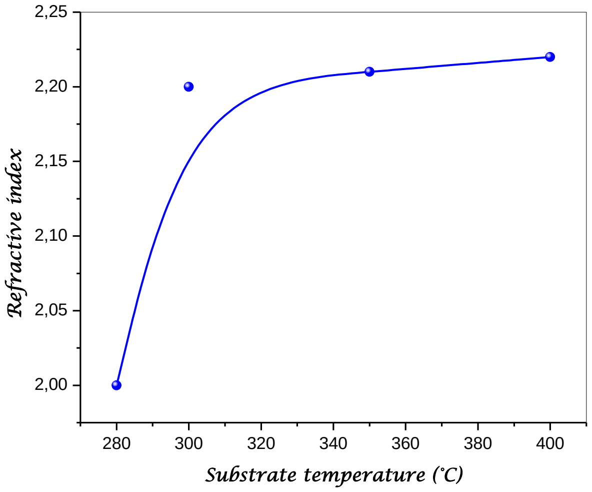

Figure III.22 *Variation of refractive index versus substrate temperature.*

III.1.2.4 Electrical properties

In figure III.23, we have represented the measured dark conductivity in different films deposited with various temperatures. As seen the conductivity variation have a bell U shape behavior. In the investigate temperature range, the variation is in order of four decades. This indicates the extreme sensitivity of the electrical transport in CuO films to substrate temperature. The minimum of conductivity is measured in films deposited at 400 °C, with conductivity equal to 10^{-7} $(\Omega cm)^{-1}$, however the highest conductivity is measured in film deposited at 300 °C with value of 10^{-2} $(\Omega cm)^{-1}$.

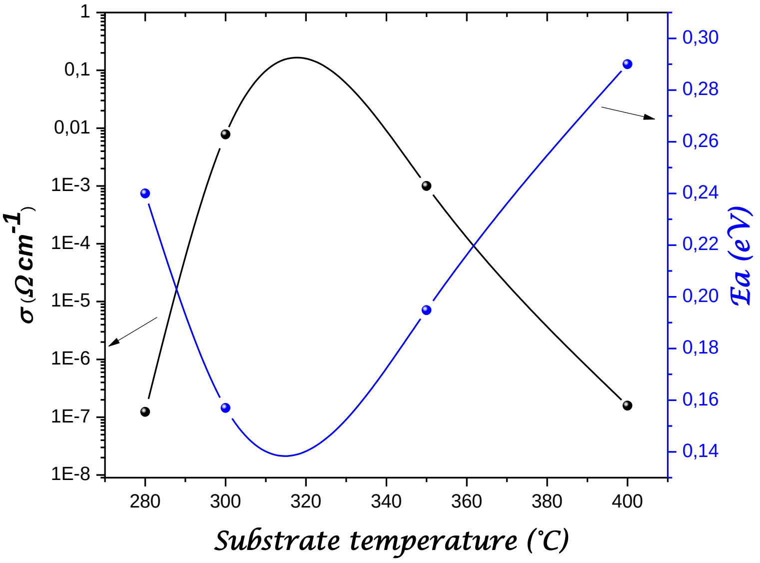

Figure III.23 *Variation of the dark conductivity and activation energy as function of the substrate temperatures.*

The dark conductivity and the activation energy are expressed by the Arrhenius equation. In general, these two quantities have an opposite behavior. In figure III.23 we have reported the variation of activation energy as function of various substrate temperatures. As remarked the variations have a U shape behavior also. It is varied from 0.157 to 0.290 eV in the investigated temperature range. The maximum value of activation energy is measured in films deposited at 400 °C with a lower conductivity. This indicates that the activation energy varied contrary with the conductivity of films this variation corroborates well with the Arrhenius equation. Therefore, the reduction of the activation energy is reflected by the Fermi level approaching to the valence band bottom, this results in an increase in the hole concentration and consequently the enhancement in the conductivity.

As mentioned previously, the value of pre-exponential so can be used to determine the conduction mechanism located in localized states or state conduction. As shown in table III.4, the pre-exponential factors of different samples are estimated also from the slope of the linear plot of ln (σ) vs inverse of temperature. The calculated values of σ_0 are lower than $10^3(\Omega\text{cm})^{-1}$. It is know that the conduction is state conduction, the value of σ_0 in ranged from $10^3 - 10^4$ $(\Omega\text{cm})^{-1}$. This indicates clearly that the dominant transport in CuO films is in the localized states present in band tails.

Substrates temperature (°C)	σ_0 $(\Omega cm)^{-1}$
280	**0.135**
300	**7.389**
350	**19.29**
400	**0.025**

Table III.4 *Values of pre-exponential factors for various substrate temperatures.*

III.2 Molarity effect

In this section we present the results of the influence of Cu salt molarity on the films properties. The used samples in this study are deposited with copper chloride ($CuCl_2.2H_2O$) as precursor with varying molarity from 0.01 to 0.08 M.

III.2.1 Deposition rate

In figure III.24 we have reported the variation of the growth rate as a function of molarity. The deposition rate increase by two factor with increasing in the molarity of the precursor solution. Increasing of precursor molarity causes availability in Cu concentration this yields to facility formation of CuO phase and enhancement of the deposition rate. Shabu et al [35] have deposited CuO films by spray pyrolysis for various molar concentrations. They observed that films thicknesses increase from 1.34 to 1.94 µm with increasing molarity from 0.1 to 0,2 M.

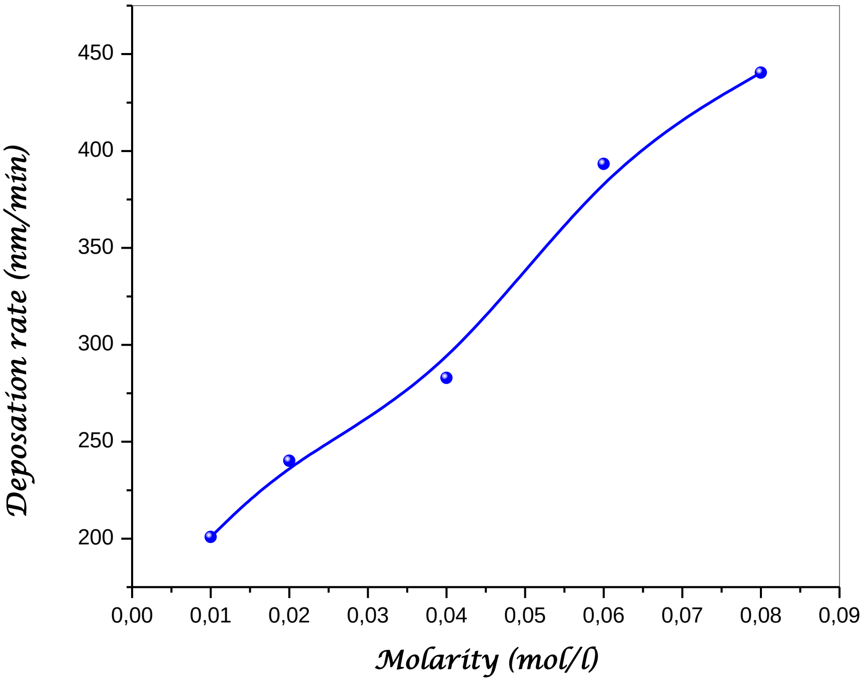

Figure III.24 *Variation of growth rate as function of molarity.*

III.2.2 Structural properties

In figure III.25 we have reported the XRD pattern of prepared CuO thin films at a constant substrate temperature of 300°C for different precursor concentrations ranged from 0.01 to 0.08 M. Prepared thin film sample using 0.01 M and 0.02 M shows two important peaks were observed at 35.5° and 38.6° corresponds to the $(\bar{1}11)$ and (111) diffraction planes. With increasing the molarity to 0.04 M, the two dominant peaks assigned to $(\bar{1}11)$ and (111) became finer and more intense. We notice also the emergence of some small peaks related to (-202) (202) (020) $(\bar{2}22)$ (113) $(\bar{1}13)$ $(\bar{3}11)$ and (311) planes .With further increasing of precursor concentration, the deposited films contain also all the cited (hkl) plan however we notice the change in the intensities of the dominant and smallest peaks. All the apparent atomic plans revel that the deposited films are composed of a single CuO phase with monoclinic crystal structure.

The most attractive feature on copper oxide thin films prepared by various deposition techniques, from the structural point of view, is its polymorphism. Indeed, to obtain a pure Cu_2O phase with cubic structure or a pure CuO phase with monoclinic structure is difficult, the mixture of this two phases are generally present. Balamurugan and Mehta [11] reported a mixture of Cu_2O and CuO phase by an activated reactive evaporation technique. Nair et al. [14] could only achieve a deposition of Cu phase along with a minority Cu_2O phase at room temperature by the chemical deposition technique. However in the present study, spray pyrolysis technique with specially designed spray nozzle and the optimized deposition parameters yield to only the single tenorite CuO phase with monoclinic structure at the lowest deposition temperature of 300°C. This is comparable to the results reported by Gopalakrishna et al. [32], Morales et al. [86], Senthil Kumar et al. [87] and Cho et al. [88] for CuO films prepared by spray pyrolysis technique. In spray pyrolysis deposition technique, the influence of the deposition parameters on film formation, particularity the role of the precursor concentration, is extremely critical. Several authors have deposited CuO films using this technique with precursor concentration ranged from 0.1 to 0.5 M at fixed substrate temperature varied from 350 to 400°C to ovoid the mixture of two copper oxide phases (Cu_2O and CuO) and to obtain films with single CuO phase. Hence from our result, we have successfully deposited films with pure CuO phase and monoclinic structure at very lower molarity equal to 0.01 M.

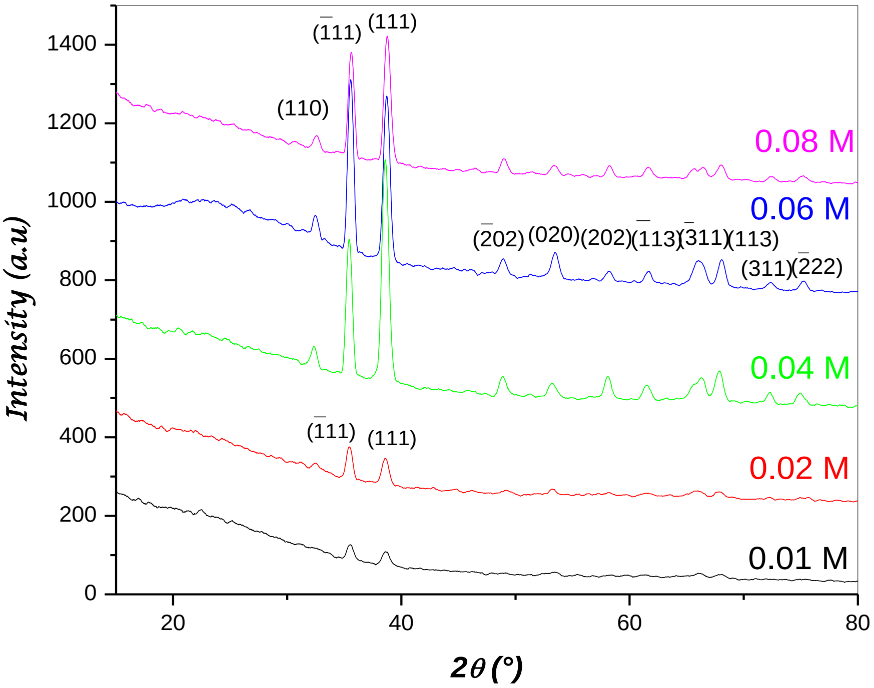

Figure III. 25 *XRD diffraction of CuO thin elaborated with different molarities.*

Based on the above result of XRD we remark that the preferred orientation in the deposited CuO thin films is effected by the variation of the solution molarity. We have calculated the texture coefficient for the two dominated atomic plan $(\bar{1}11)$ and (111) to discuss more distinctly. In figure III.26 we have represented the variation of the texture coefficient of the two plane $(\bar{1}11)$ and (111) as a function of Cu slat molarity. The texture coefficient of the $(\bar{1}11)$ plan variation with various molarities has similar behavior of the variation of the Tc (111) plane, as can be seen from this figure. For the films deposited with lower molarity we noticed that the films have lowest texture coefficient and the sample shows a $(\bar{1}11)$ preferred orientation this reveal an abundance of grains oriented in a given (hkl) direction. By increasing molarity to 0.04 M, the texture coefficient of the two atomic plan increases strongly however the (111) orientation became the most dominant. With increasing the morality to 0.06 M the texture coefficient of the two planes decreases similarly, this indicates that presence of randomly orientation of the crystallites. There was a clear reduction in Tc with a further increase in morality to 0.08 M. However, the Tc of (111) plane is higher than the Tc of $(\bar{1}11)$ plane. This indicate the (111) orientation becomes again the most dominant.

All films have a polycrystalline nature and the calculated texture coefficient shows that the CuO films elaborated with precursor concentration equal to 0.04 M have the best crystallinity. Shabu et al [35] have deposited CuO thin films using $Cu(CH_3COO)_2.H_2O$ as Cu source by varying the molarity from 0.15 to 0.2 M , they found that the grains are abundantly oriented along the $(\bar{1}11)$ plane. They notice no change in preferred orientation with increasing the molarity of the solution.

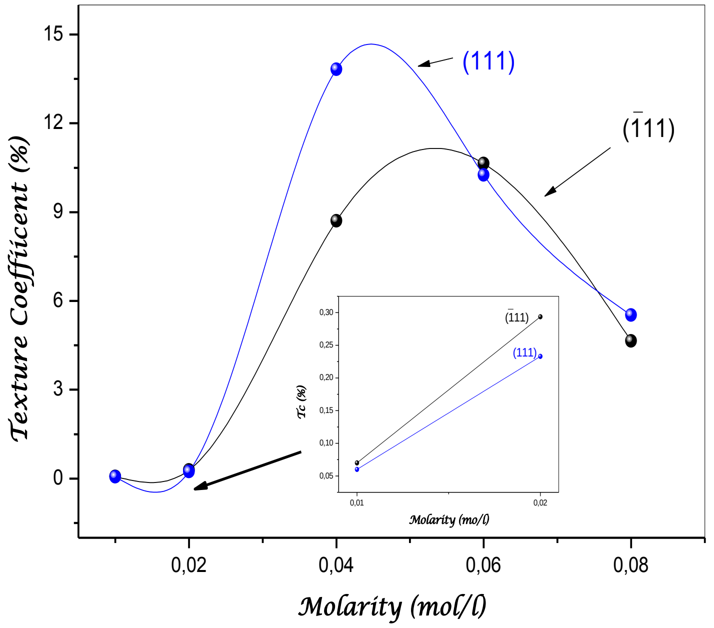

Figure III.26 Variation of the texture coefficient for CuO films elaborated with different molarities.

The films crystallites size was estimated from XDR patterns by using Hall–Williamson equation. In figure III.27 we have represented the variation of crystallites size as a function of different concentration of morality. It is apparent from the figure that crystallites size enlarged with increasing the solution molarity. This variation can be related to the increase in film thicknesses. In addition, the increase in the molarity leads to increase in Cu concentration which results a higher condensation of Cu atoms and faster nucleation in consequence a growth of bigger crystallite size. In same figure III.27 we have reported the variation of the dislocation density for various molarities. As can be noticed the dislocation density decrease with increasing the molarity form 0,01 to 0,08 M. This may be due to the decrease in the grain boundaries because of the enlargement in the crystallites size of the film with increasing the concentration of precursor solution.

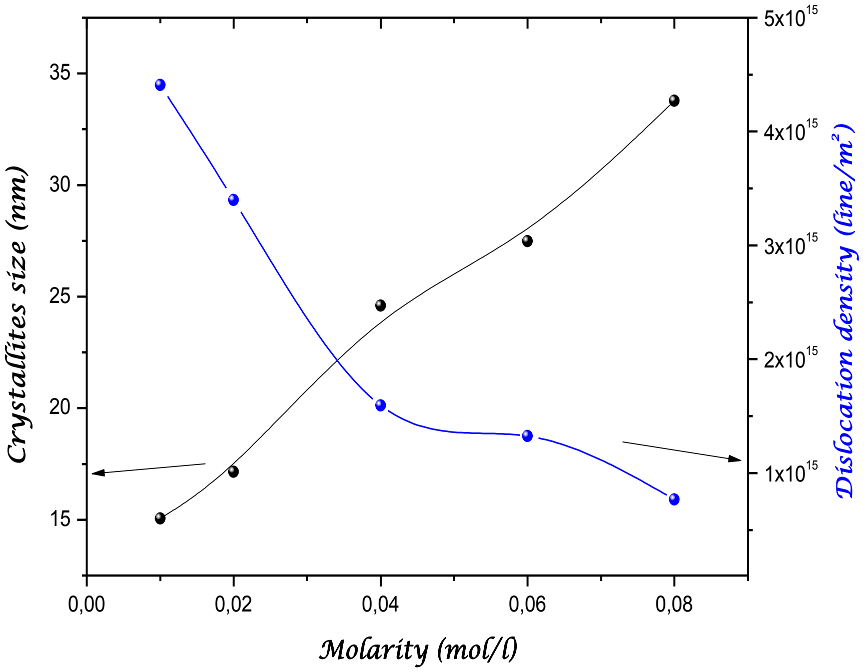

Figure III.27 *Variation of the crystallites size and dislocation density as function of different slat molarity.*

In figure III.28 we have regrouped the values of strain (ε) for CuO deposited films at various substrate temperatures. The strain was also calculated from Hall–Williamson equation. A negative slope has been observed in the Hall equation plot for all the deposited CuO films, which confirms the presence of compressive strain in the crystal lattice. The compressive strain values augment from 0,005 to 0,034 with increasing the precursor concentration. This can be related to the increase in film thicknesses. The enrichment of the Cu concentration leads to formation of faster crystal growth and enhance the density of nucleation for a single crystal as result a hence in film thicknesses as explained before. However we noticed the defect increase in the films network. This can be construed by the fact, the low deposition rate leads the formation of more organized films with less thickness conversely the higher growth rate produce more disordered and thicker films which create more defects in films.

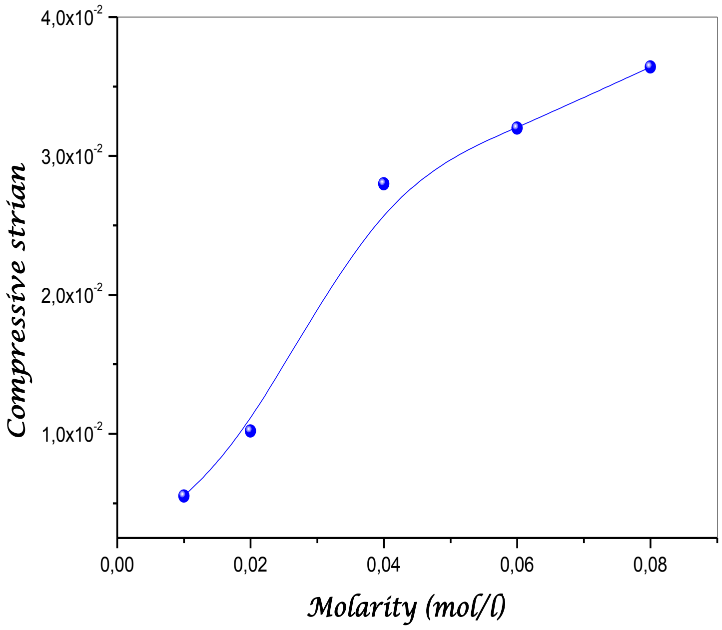

Figure III.28 *Variation of compressive strain versus le concentration of the precursor solution.*

As mentioned above (chapter I), CuO crystallizes in a monoclinic lattice with four formula units in the crystallographic primitive cell and belongs to the space group symmetry of C_{2h}^{6}. The metal cation copper forms four coplanar bonds with oxygen, which again self coordinated by four copper atoms. The factor group analysis yields [89]:

$$Cu: \Gamma = 3\,Au + 3Bu$$

$$O: \Gamma = Ag + 2Bg + Au + 2Bu$$

$$\Gamma_{CuO}^{tot} = 4Au + 5Bu + Ag + 2Bg$$

Of these, 1Au and 2Bu are the acoustical modes, so that the total vibration modes and their activity are [33–35]:

$$\Gamma_{CuO}^{vib} = 3Au + 3Bu + Ag + 2Bg$$

Thus, three modes are Raman active (Ag, Bg) and six infrared (Au, Bu) active modes are to be expected in the spectra of CuO [79,80]. In figure III.29 we have shown the Micro- Raman spectra of CuO thin films coated on glass substrate using different precursor concentrations. The Raman spectrums for the deposited films are composed with three main photon modes

Ag and 2Bg located at 296, 346 and 602 cm^{-1}. Observed locations of the peaks are comparable to the previously reported results. The strongest Ag mode at 294 cm^{-1}, arising from the extension vibration of the monoclinic structure, is well resolved, which indicates that the samples are monoclinic phase. This confirms the presence of a single phase CuO with monoclinic structure.

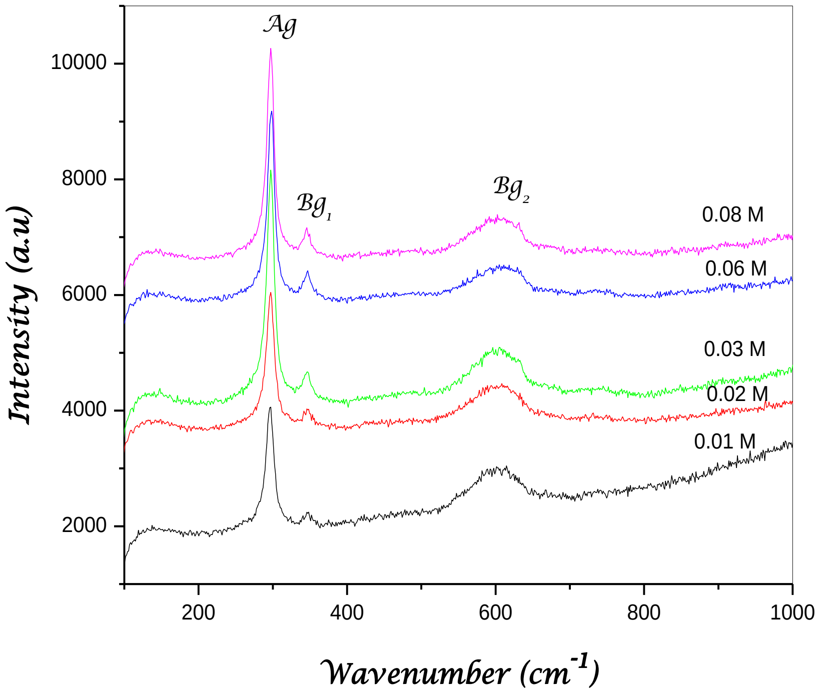

Figure III.29 *Micro Raman spectra of CuO thin films deposited with various molarities.*

Comparing the Raman spectrums recorded from the deposited CuO with various molarities, some differences can be seen between these spectrums for example: the relative intensities, line width and position of the three modes Raman. One can easily see that the Raman peak of the Ag mode of CuO is largely affected by the variation of the concentration of precursor. In order to see this change more clearly, we have correlated in figure III.30 the variation of intensity Ag mode with different Cu salt molarity. With increasing molarity the intensity of Ag mode became more intense. This can be related the increase in film thicknesses. As can be deduced before, we have noted the decrease the intensity of Ag modes with the reduction in thickness for the CuO films deposited at various substrates temperature.

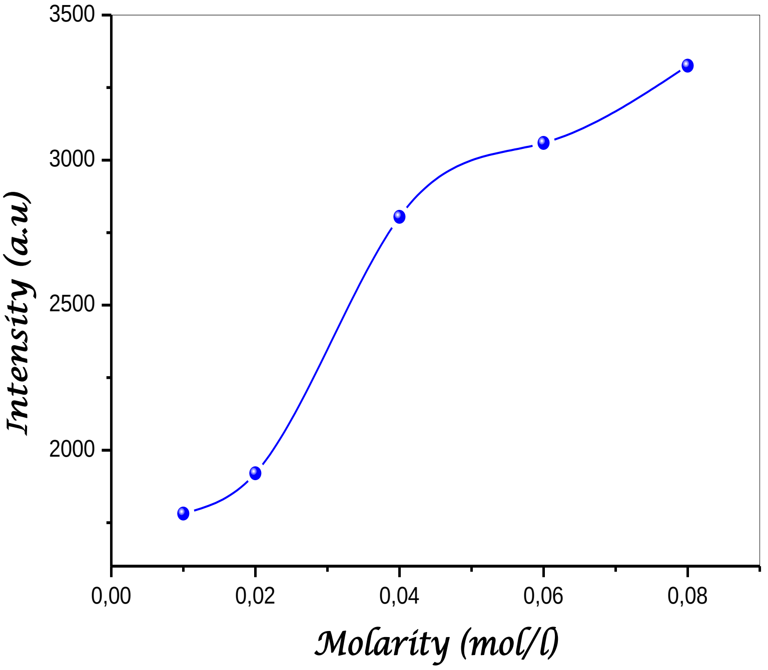

***Figure III.30** Variation of Ag Raman mode intensity for CuO films deposited with different molarities.*

It has been reported that the presence of strain in film and the variation in value crystallites size affects the crystalline structure and results in shifts and broadening of the Raman peaks of thin films. Comparing the Ag Raman mode spectra for the deposited CuO with the lower molarity to the other films elaborated with diverse molarities. In order to know the origin of this shift we have represented the variation the strain with the peak position shift of the Ag mode as showing in figure III.31. We can clearly see that the Raman peak of the Ag mode of CuO shifts towards higher wavenumber (blue shift) with increasing the molarity of the solution and it is showing in the inset in figure III.30. With increasing the strain in film the position peak of Ag mode to shift higher wavenumber. This confirmed that the Raman shift observed in our case is related to the increasing in the strain in the films. It is well known that any changes in lattice parameters due to applied strains would result in a shift in the frequency of most Raman active modes of the crystal. Such a shift in peak wave number is generally linear with strain. Raman mode wavenumber generally shifts to higher or lower wavenumber under the effect of compressive or tensile strains, respectively. As we have deduced the strain from XRD diffraction spectra, the strain applied in films is compressive which confirmed by the Raman shift to the higher wavenumber. Miyagawa et al [90] have prepared PbO thin films by using physical vapor deposition. They examined the relation between peak shift of PbO thin films and applied tensile strain and found that the peak shift to the lower wave number under tensile strain.

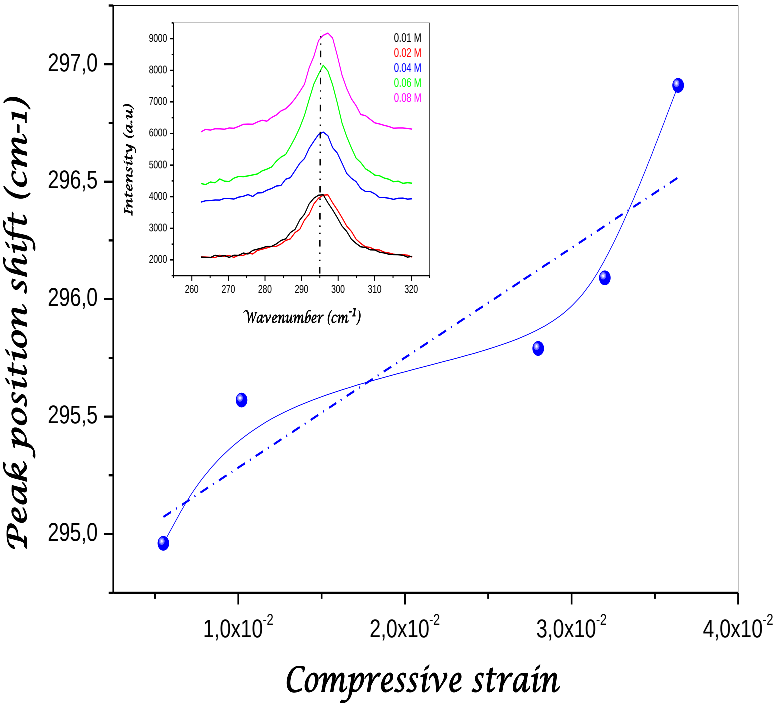

Figure III.31 *correlation between the variation of compressive strain and shift Raman.*

III.2.3 Surface morphology and composition

The films surfaces were studied by scanning electron microscopy. The observations by SEM indicate the film surface homogeneity, the shape of the grains and aggregates of grains boundaries. SEM micrographs were taken for CuO films deposited with molarity equal to 0.01 M and 0.08 M are embedded in figure III.32. The SEM micrographs show that deposited films are homogenous, dense and compact. However, the films deposited with lower precursor concentration are smoother than the films deposited with higher molarity. This can be related to the increase in film thicknesses. This confirms the extinction of interference fringes in transmittance spectra.

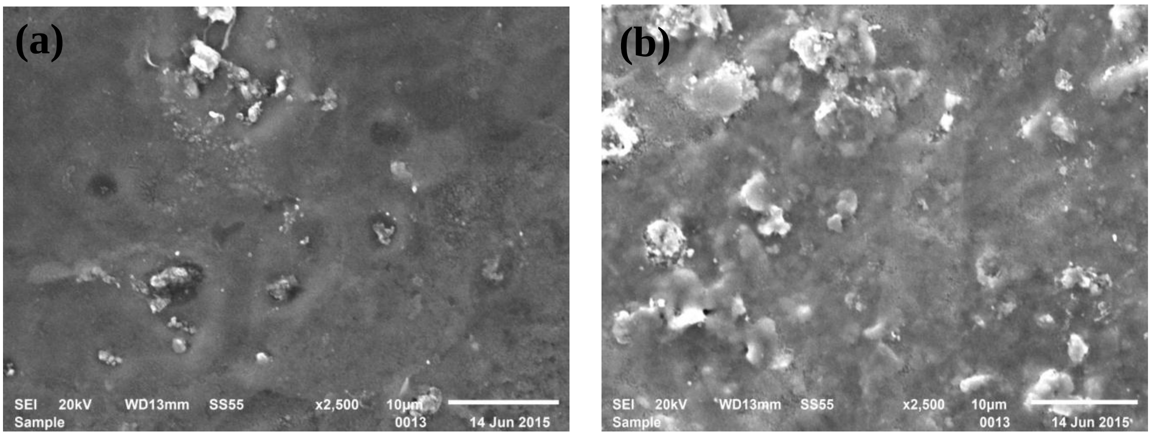

***Figure III.32** the SEM images for CuO films deposited with: (a) 0.01 M and (b) 0.08 M.*

In figure III.33 we have reported the typical EDS spectra for the deposited film CuO with 0.01 M and 0.08 M at substrate temperature equal to 300°C. It is evident from spectra, the presence of two Cu and O elements constituting the film and also the presence of other elements in the spectrum originated from the substrate glass. In table III.5 we have illustrated the quantitative analysis extracted from EDS spectra. It is apparent from this table that the variation of concentration precursor deeply effects the composition of the deposited CuO films. It is found that the amount of Cu increase with increasing the solution molarity. For the CuO film elaborated with 0.01 M, the ratio O:Cu is equal to 3.71. Consequently, an O-rich cupric oxide films had been formed. Meanwhile, the ratio O:Cu is above 0.97 for the deposited CuO films with 0.08 M which is less than the unity. Thus, a Cu-rich cupric oxide films had been formed. The increase in concentration molarity leads to enhancement the solution with Cu atoms. So, the film deposited with lower precursor concentration guide to the formation of O-rich cupric oxide however the elaborated CuO films with higher molarity produce a Cu-rich cupric oxide. Ooi et al [26] have elaborated copper oxide thin films with by reactive radio frequency sputtering at various oxygen percentage flow rates R(O_2). They found that the compositions of the elaborated films changed, the films deposited at lower oxygen percentage are rich on Cu however the films deposited with higher oxygen percentage are rich on O, the ratio Cu:O is varied from 3.38 to 0.72 with oxygen percentage flow rates R(O_2) changed from 10 to 50%.

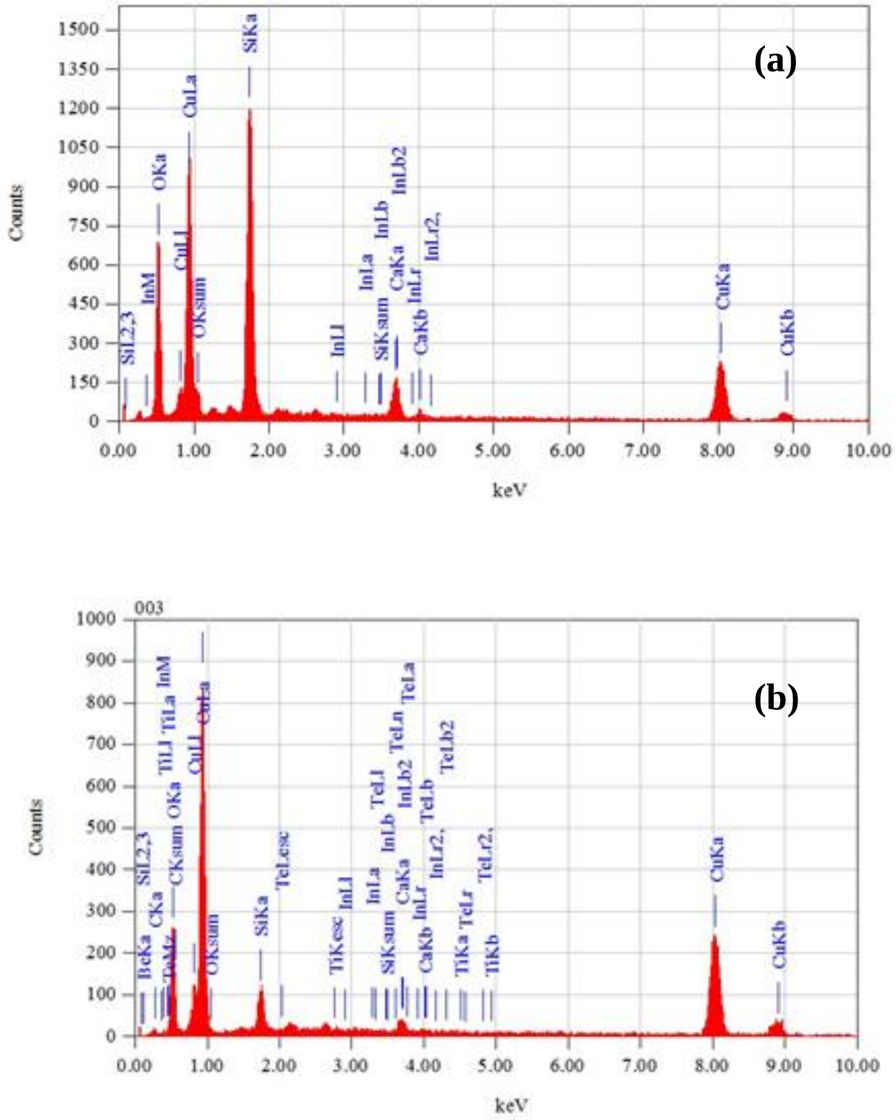

Figure III.33 *Typical EDS spectra for the deposited film CuO with: (a) 0.01 M and (b) 0.08 M.*

Molarity	Atomic percentage (%)		O:Cu
	Cu	O	
0.01	15.30	56.84	3.71
0.08	44.98	46.26	0.97

Table III.5 *Element composition from EDS for the CuO films elaborated with 0.01 and 0.08M.*

III.2.4 Optical properties

The optical transmittances in the wavelength UV-VIS-IN range of different samples are reported in figure III.34. The film transparency decreases from 70 to 30 % with increasing the molarity of the precursor solution. This behavior can be due to two reasons:

i. The increase in the films thickness.
ii. The increase in film surface roughness.

The transmittance is a function of $e^{-\alpha d}$, where d is the thickness and α is absorption coefficient. Hence, an increase in the thickness is then followed by reduction in the transmittance. Consequently, the reduction in the film transparency can be attributed to the increase in thickness. As can be seen, we note the absence of interference fringes in the deposited films. The presence of interference fringe is due to multiple reflections at films/substrate and films/ air interface. These reflections appear only when the films are thick enough and mainly when the film surface is smooth. However, the rough surface film favors the light scattering at the surface which reduces the reflection and then the extinction of interference fringes this indicates that the surface of all the deposited films is rough.

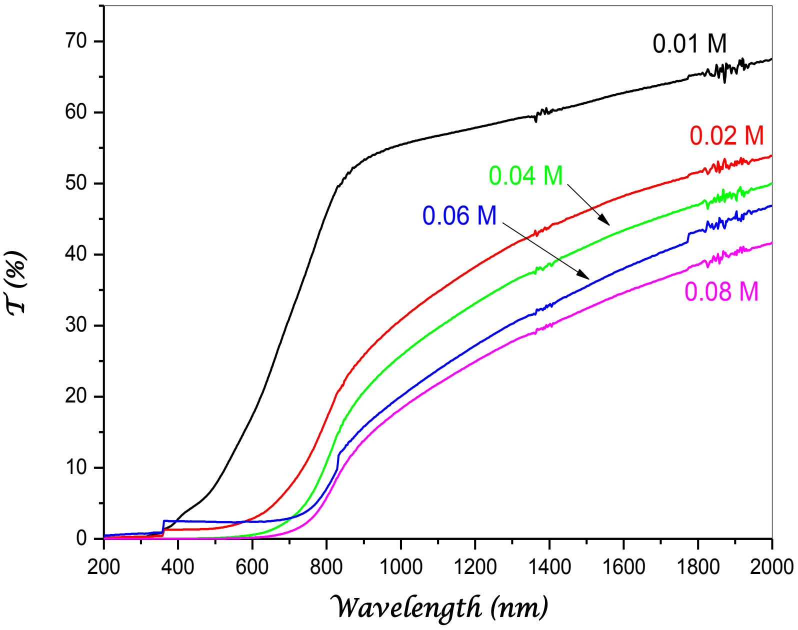

Figure III.34 Transmittance spectra of CuO films elaborated with various molarities.

The most important feature in this figure is the shift of the absorption band edge toward the highest wavelengths. This shift is translated as optical band gap strangulation as seen in figure III.35. With increasing the molarity concentration of precursor solution, the optical band gap reduce from 1.74 to 1.10 eV. While, this diminution can be also relate to the increase of the disorder in film networks. The variation of the film disorder as a function of molarity is represented in figure III.35. As can be seen the films become more disordered with increasing the concentration molarity, it is increased from 510 to 770 meV. On the other hand the variation of the optical band gap and the disorder varied conversely, showing the variation of the optical band gap is controlled by the disorder.

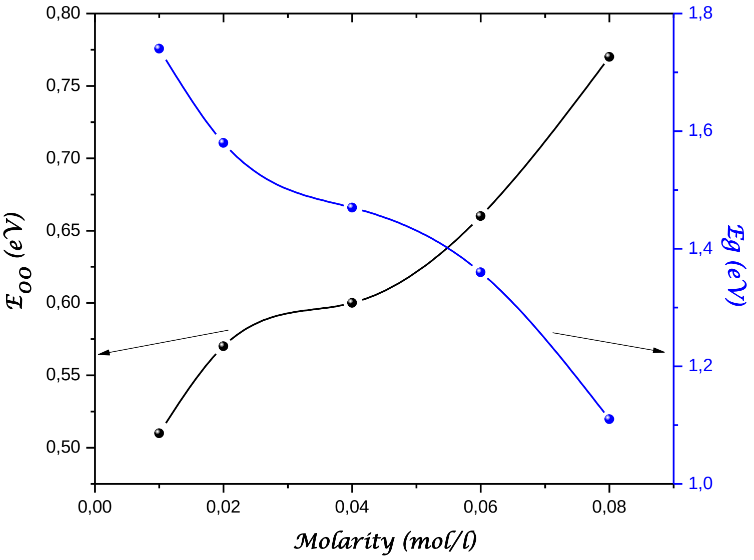

***Figure III.35** Variation of optical band gap and the disorder as function of the molarity.*

In figure III.36 we have shown the variation of the growth rate and the disorder in the films as function of solution molarity. As can be concluded from this figure, the variation of growth rate and the film disorder has similar behavior. This suggests that the disorder in film network is related to the rapid growth rate. With increasing the deposition rate, the atoms arrived on the surface substrate have not the time to organized which leads to growth of a disordered films.

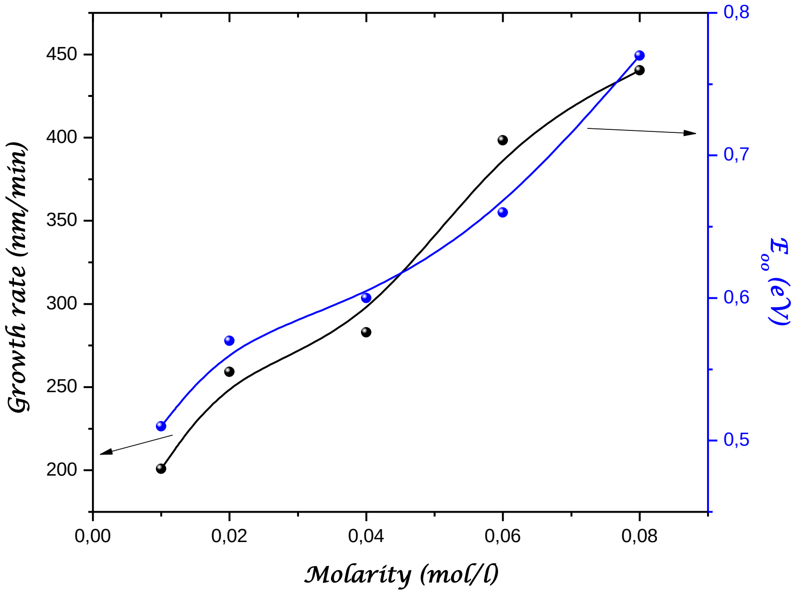

Figure III.36 *Variation of growth rate and disorder in CuO film network.*

In figure III.37 we have shown the variation of the strain and the disorder in films networks as function of molarity. We observe the film strain increase with the disorder this suggests that the strain and the disorder in film network may have the same origin related to the fast growth rate at higher concentration molarity.

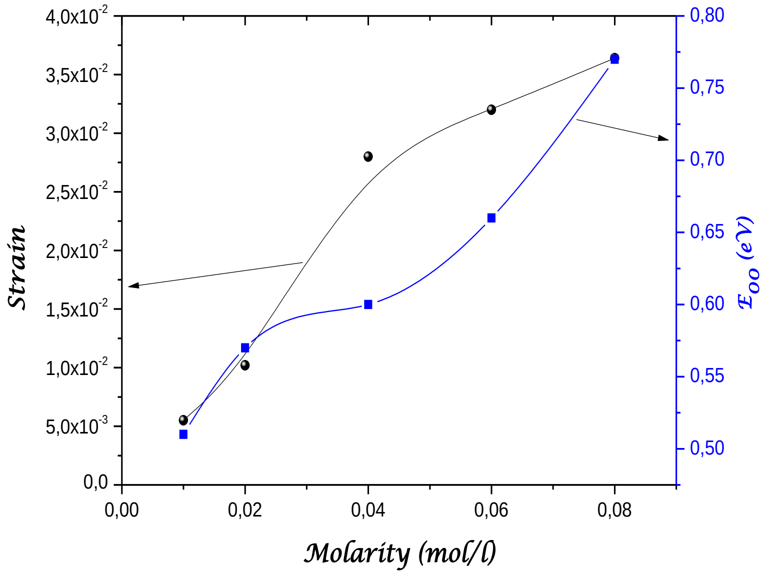

Figure III.37 *Variation of strain and disorder in CuO film network.*

III.2.5 Electrical properties

The electrical conductivity was characterized by mean of Hall effect measurements in order to determine the dark conductivity, free carriers concentration and mobility. In figure III.38 we have shown the variation of the dark conductivity and free carriers concentration as function of solution molarity. As can be seen, the conductivity increases with increasing the concentration molarity. In the investigate molarity range, the conductivity is varied in order of three decades. This indicates that the molarity effect the electrical transport in CuO thin films. We note also that the free carriers concentration augment from 4.96 x 10^{12} to 7.88 x 10^{13} cm^{-3}. It is well known that, the conductivity of semiconductor can be expressed:

$$\sigma = n\,\mu\,q \tag{28}$$

Where n is the free carrier concentration, µ is mobility and q is the elementary electronic charge. From this equation the electrical conductivity in semiconductor is proportional to the product of the carriers concentration and the mobility. The increase of these two parameters (n and µ) improves the conductivity in films. As can be seen, the electrical conductivity follows faithfully the trend of the carriers concentration. This indicates clearly that the conductivity is rather controlled by the free carrier concentration than by their mobility.

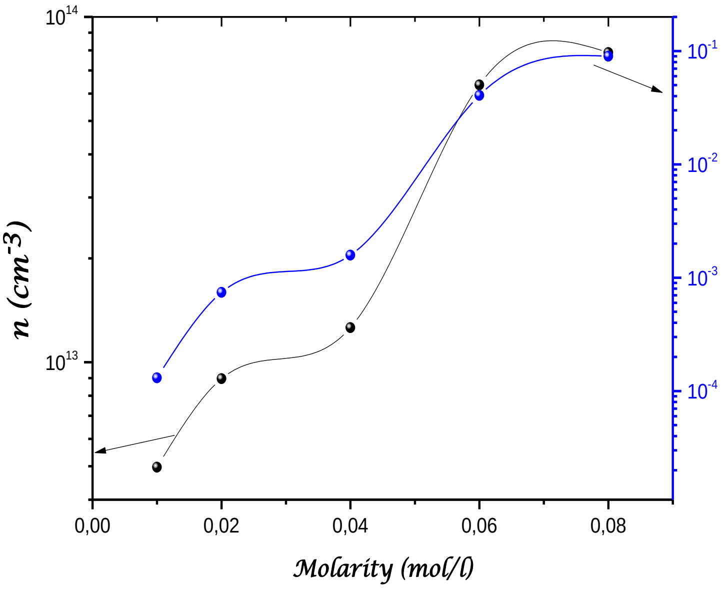

Figure III.38 *Variation of the dark conductivity and free carriers concentration of CuO thin films elaborated with various.*

It is well know that the mobility can be altered by the crystal structure. The mobility is enhanced with increasing the crystallites size. In figure III.39 we have reported the variation of the crystallite size and the mobility in the deposited CuO films with various molarities. The mobility increases from 16 to 60 (V/cm^2s) with increasing in crystallite size. The increasing in crystallite size is followed by decrease in grain boundary. It is notable that the electrical transport properties of films are governed by carrier trapping at the grain boundaries and the effect of grain boundaries on transport in other semiconductors, especially polycrystalline films, has been extensively studied.

A polycrystalline film material contains a large number of micro crystallites separated by grain boundaries that plays an important role in determining the film conductivity. The incomplete atomic bonding at a grain boundary can act as trap centers and build a local space charge. This charge then impedes the transition of charge carriers from one crystallite to another. Trapping states reduce free carriers, as a consequence, more free carriers become immobilized. In other words, larger crystallite size results in a lower density of grain boundaries, which behave as traps for free carriers and as barriers for carrier transport in the film. Hence, an increase in crystallites size can causes a decrease in grain boundary scattering, which leads to an increase in the electrical conductivity and mobility.

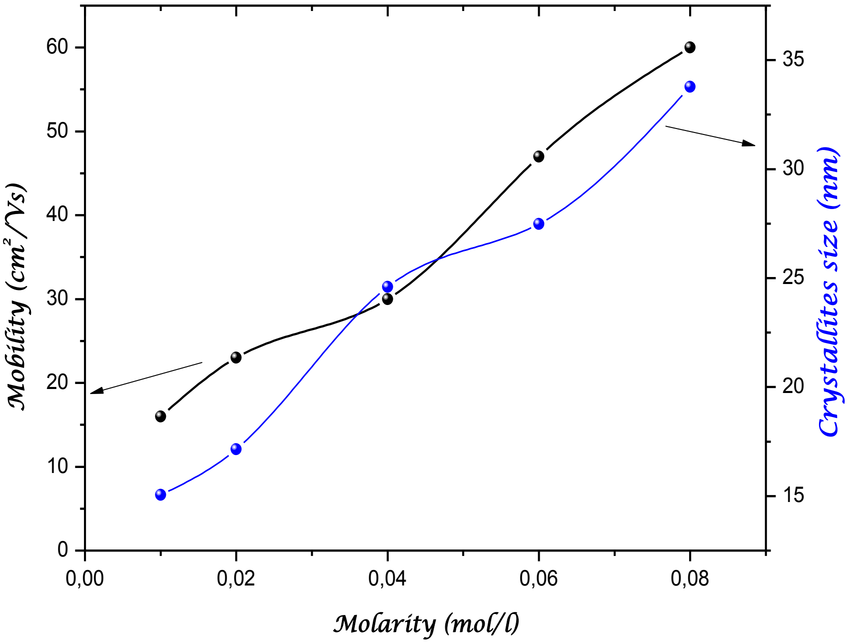

Figure III.39 *Variation of mobility and crystallites size as function of the molarity.*

III.3 Influence of flow rate

In this section we present the result of the flow rate influence on the CuO thin films prepared by spray pyrolysis.

III.3.1 Deposition rate

In figure III.40 we have reported the prepared films deposition rate variation as a function of flow rate. The latter is estimated from the ratio of film thickness on the deposition time fixed at 20 min. As can be seen, the influence of flow rate on deposition rate can be divided into two regions:

- Low flow rate (10 to 20 ml/h): the variation of the deposition rate is almost constant and equal to 200 nm/min.
- High flow rate (25 to 30 ml/h): the deposition rate increase considerably and varied linearly with the flow rate augmentation. We note also this change is produced above a critical value equal to 20 ml/h.

Generally, in the whole commonly used deposition techniques, film growth steps namely nucleation, condensation and subsequent growth, are mainly controlled by two major parameters: the substrate temperature which controls the species energy and motion onto the substrate and the flux of arriving species on the substrate. In the case of spray pyrolysis, arriving species rate is controlled by the flow rate of the solution feeding the nozzle. The substrate temperature is extensively studied in the literature, while, to our knowledge, the flow rate influence is less studied.

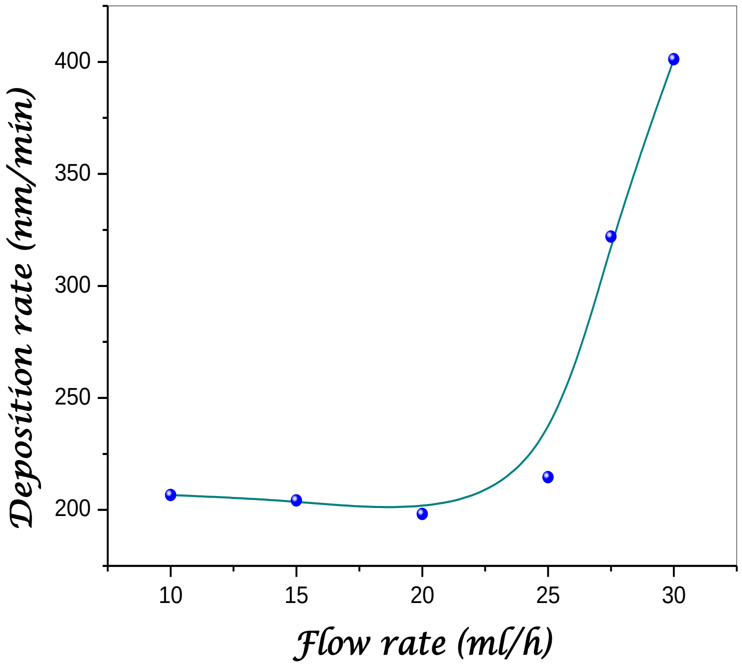

Figure III.40 *Variation of deposition rate as a function of solution flow rate.*

III.3.2 Structural properties

The XRD spectra recorded in different films are shown in figure III.41. In the whole spectra, only two peaks assigned respectively to the planes (111) and (002) assigned to CuO tetragonal structure are present (PDF card # 45-0937). No peaks related to Cu_2O phase are seen. Dominant CuO phase has been also reported in different studies [91,92] where (002) preferential orientation is observed, while Koseet al. [93] have observed the (111) preferential orientation. However, in our case, an inversion in the preferential orientation with varying the flow rate is seen.

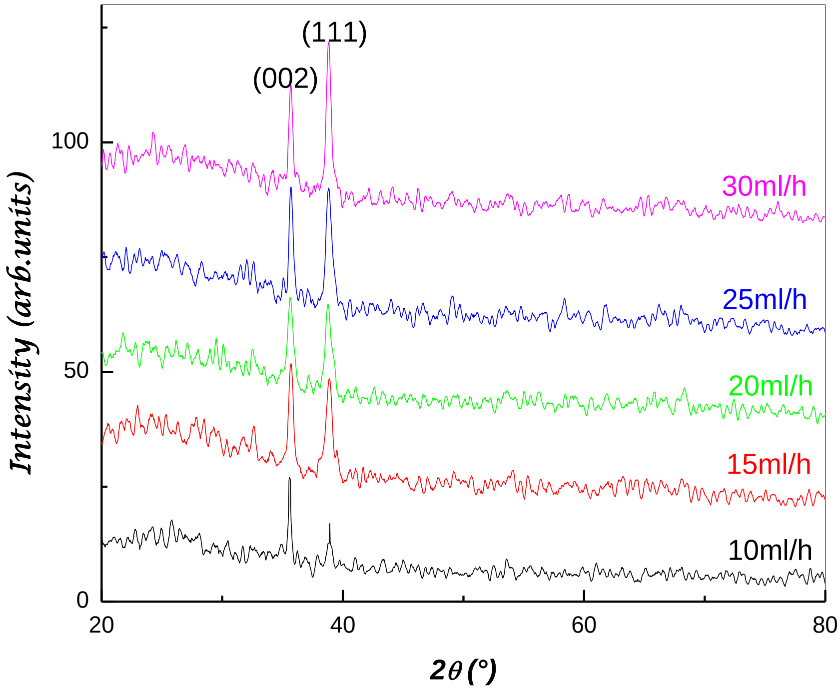

Figure III.41 *XRD diffraction pattern of CuO thin films prepared with different solution flow rates.*

In figure III.42 we have reported the variation of the texture coefficient as function of the flow rate. We deduce that CuO film starts with preferential orientation (002) at low flow rate to become along the direction (111) above 25 ml/h. We speculate that the change in the growth direction may originate from the variation in the growth rate. At low growth rate the plane (002) is formed; while at faster growth rate the plane (111) is formed indicating that the latter plan requires less formation energy than the plane (002). This is consistent with the commonly observed (111) preferential orientation observed in CuO films formed with conditions involving low energy such as sol–gel or low substrate temperatures [94–97].

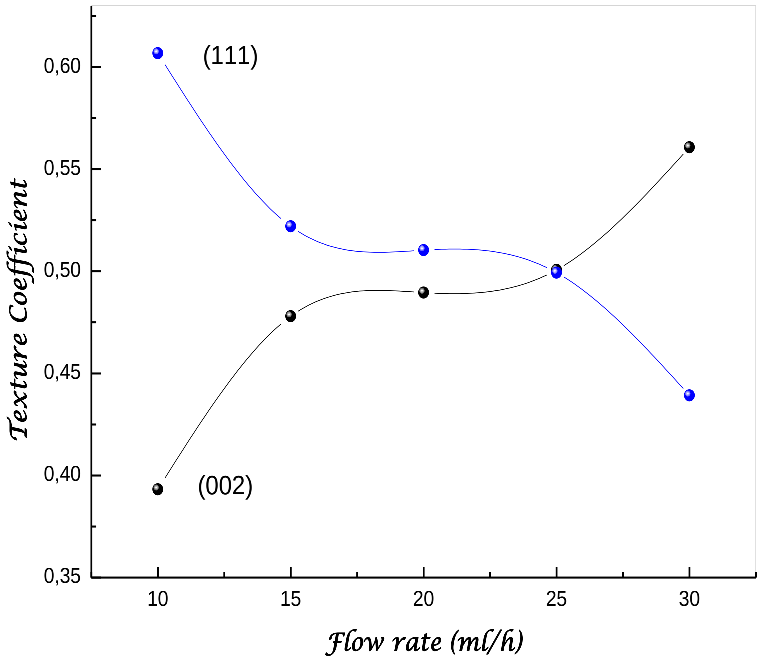

Figure III.42 *Variation of the texture coefficient for the direction (002) and (111) as a function of the solution flow rate.*

The films crystallites size and internal lattice strain have estimated from Hall–Williamson equation. The variations of the crystallites size together with the film strain are reported in figure III.43. The obtained films have a polycrystalline nanostructure, the obtained crystallites size are ranged from 60 to 10 nm. As seen, the crystallites size is reduced with increasing the flow rate. Indeed at low flow rate the deposition rate is low; thereafter the film formation process is slow yielding to larger crystallites formation. On the other hand an increase in the flow rate causes the rise of internal strain in the formed crystallites. Above 25 ml/h flow rate we noticed a strain relaxation and an increase in the crystallites size; this can be due to the change in growth direction at this flow rate as suggested the calculated texture coefficient.

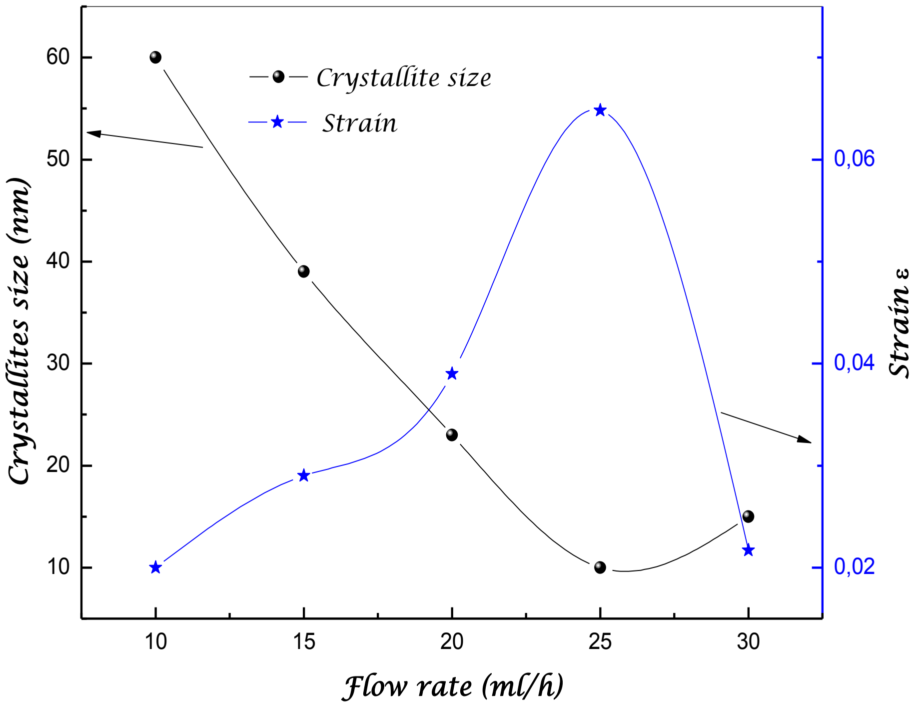

Figure III.43 *Crystallites size and internal stress in grain as a function of flow rate.*

In figure III.44 we have represented the Raman spectra of the as-prepared CuO thin films with different flow rates. The Raman spectra are composed with three main phonon modes Ag and 2Bg located at 297, 334 and 608 cm^{-1}. These peaks are largely reported in the literature. This confirms the presence of a single phase CuO with a monoclinic structure as deduced from XRD analysis.

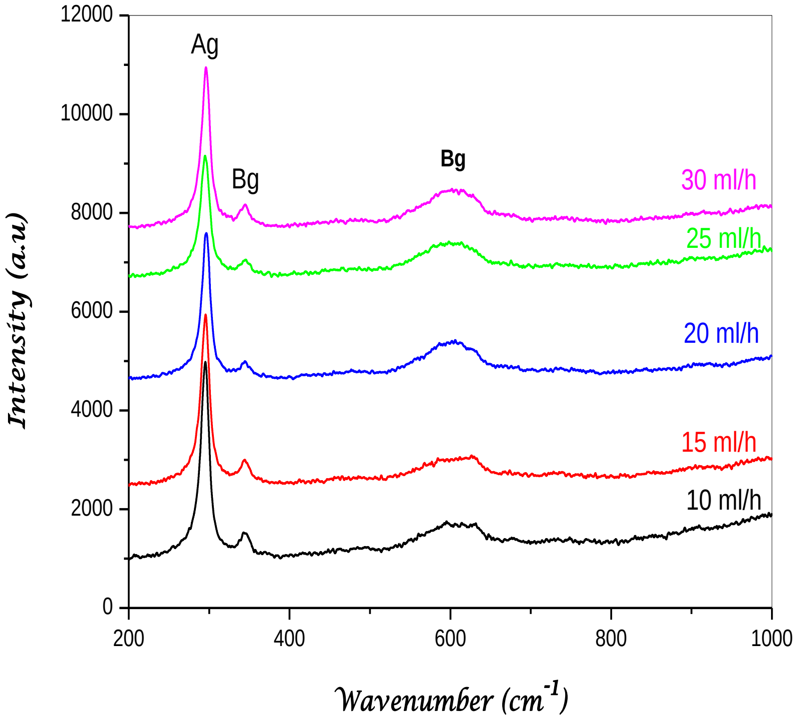

Figure III.44 *Micro-Raman spectra of CuO deposited with various flow rates.*

It is evident from the figure with increasing the flow rate the position and the intensities and the position of the peaks for the three Raman modes is changed. In the figure III.45 we have shown the variation of peak position shift and the strain as function of the flow rate for the Ag Raman mode. It is well know that the Ag mode is the most Raman mode which characterizes the monoclinic structure in a single CuO phase. The position of the intense peak Ag is strongly dependent of several factors such as strain, crystallites size, disorder and the crystallinity of the films. However, this factors effect differently with the parameters study. It is clearly seen from this figure that the peaks position shit with the variation of the flow rate. Moreover, the variation of peak position shift follows faithfully the trend of the strain. So, the presence of the strain in the films is responsible of the shift of the Ag mode Raman.

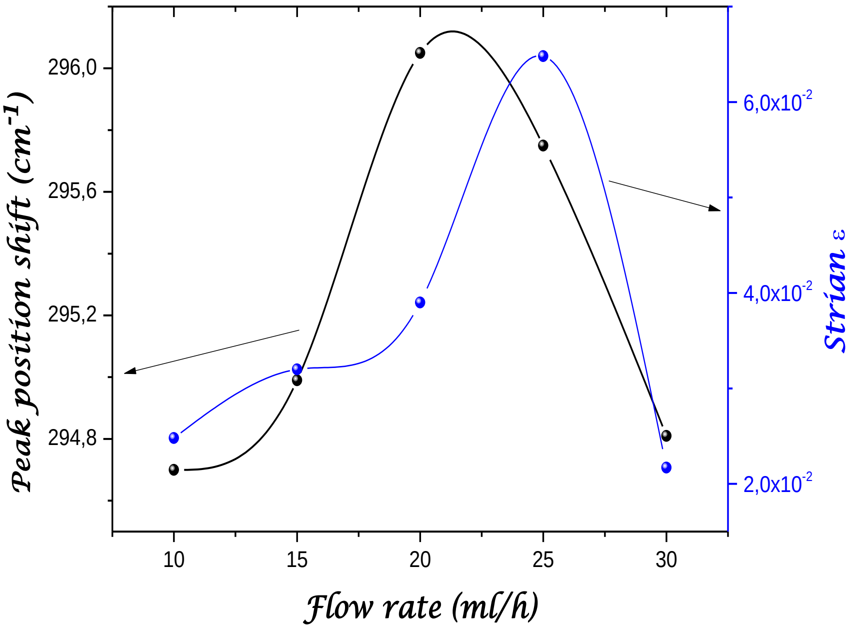

Figure III.45 *Variation peak position shift and the strain versus flow rate.*

III.3.3 Optical properties

The transmittance spectra in UV–visible region of the prepared CuO films are shown in figure III.46. The films deposited with low flow rates exhibit higher transparency due to their low thickness. It can be seen that when the flow rate increases the transmittance decreases until 20 ml/h, and increases again with further flow rate increase. It is well argued that the deposition rate may alter the nucleation step, at low deposition rate the nuclei size is larger than in rapid growth rate one [98]. Moreover, larger nuclei yield to a rougher film surface. Thereafter, the films prepared at 20 ml/h have a rougher film surface due to its lower deposition rate. The surface roughness causes the scattering of incident light [99], this explains then the low transmittance measured in the film prepared at 20 ml/h.

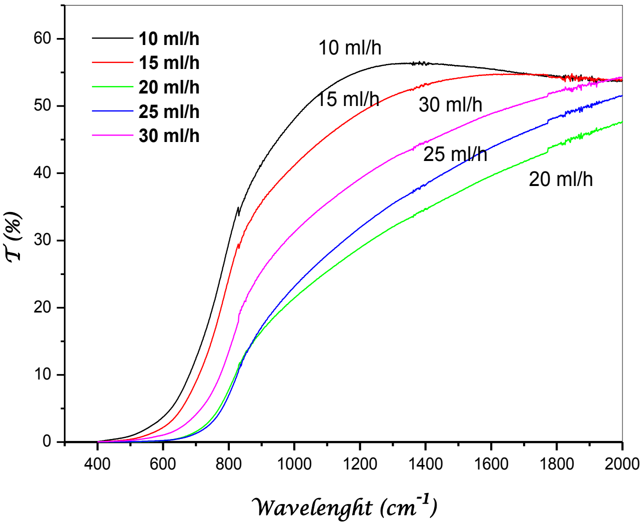

Figure III.46 *UV–visible transmittance spectrum of CuO thin films deposited using different flow rates.*

As can be seen from the figure III.47, the variation of optical band gap decrease from 1.62 to 1.40 eV with increasing flow rate from 10 to 25 ml/h and increase to 1.46 eV at flow rate equal to 30 ml/h. The calculated optical band gaps are in suitable rang for the solar cells which can be used as an active absorber layer. However, film prepared at flow rate of 25 ml/h have an optical band gap close to 1.4 eV required for solar cells since it matches well with solar spectrum. This variation can be related to the variation of the disorder in films. In same figure we have reported the variation of the disorder as function of flow rate. At low deposition rate the incoming species on surface substrate have enough time to find a favorable site and to form a more organized material. In contrary, higher deposition rate case leads to much disordered network due to the fast film formation. Thus, the observed enhancement of the network disorder with increasing the flow rate can be explained in terms of deposition rate variation. An increase in the band tail width is followed by the reduction in the optical band gap. This suggests that the variation of the optical gap is governed by the disorder in the film network.

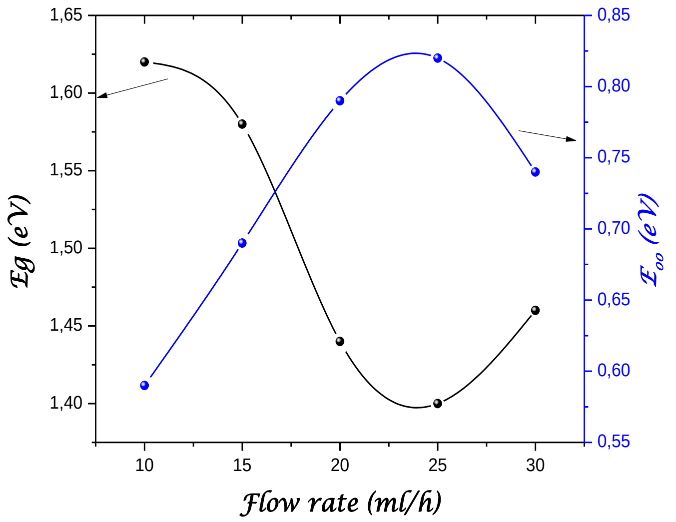

Figure III.47 *Variation of the optical band gap and disorder in film network as a function of the flow rate.*

In figure III.48 we have reported the variation of the strain and disorder in network films as function of the flow rate. As can be seen, the disorder follows faithfully the trend of the strain. This indicated that the appearance of strain in films is probably due to the presence disorder in films. As mentioned above, the deviation of bond distance and angle from their standard value in the crystalline structure engender the presence of weakly bonded atoms which favorite the creation of the disorder. This disorder can produce the deformation in lattice parameters and leads the formation of the strain.

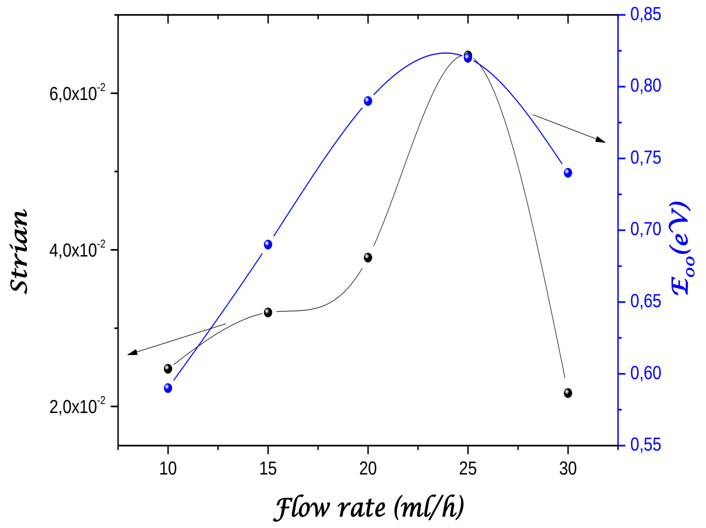

Figure III.48 *Variation of strain and disorder in films versus flow rate.*

The variation of refractive index as function of the flow rate is reported in figure III.49. With increasing in the flow rate of the solution the value of refractive index increase reliably from 1.62 to 1.82. As can be seen refractive index is altered by the flow rate. This can be explained to the increase in film thicknesses.

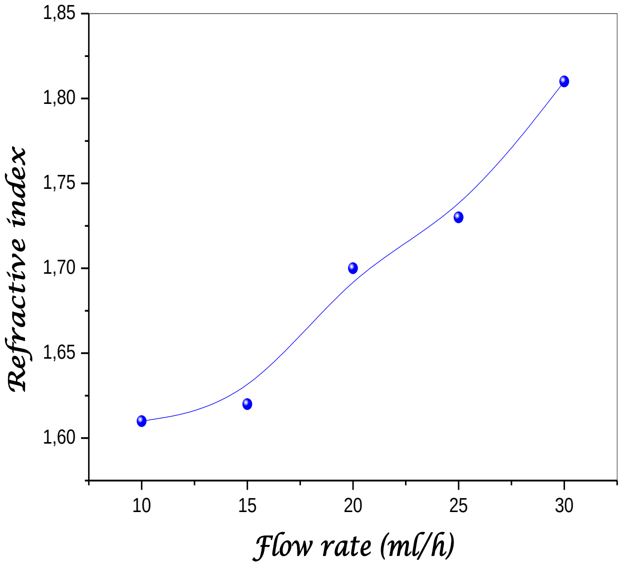

Figure III.49 *Variation of refractive index of CuO thin films deposited at various flow rate.*

III.3.4 Electrical properties

The films electrical conductivity was characterized by mean of Hall Effect measurements in order to determine the dark conductivity, free carriers concentration and mobility. In figure III.50 we have reported the electrical conductivity variation together with the free carriers concentration as a function of solution flow rate. As can be seen, the electrical conductivity follows faithfully the trend of the carriers concentration. Indeed, the electrical conductivity in semiconductors is proportional to the product of the free carrier concentration (n) and the mobility (μ). The carriers concentration varies by three decades while the mobility variation is less than one decade (see figure III.51). This indicates clearly that the conductivity is rather controlled by the free carrier concentration than by their mobility. The whole prepared films have p-type conductivity according to Hall constant sign. With increasing flow rate above 20 ml/h, the conductivity is enhanced by one decade due to the increase in the free carriers concentration . As mentioned above, the increasing in the flow rate causes the formation of disorder in film network. This disorder yields to the appearance of defects such as copper vacancy or oxygen in interstitial sites. These defects act doping impurities in film network [49], causing an increase in free carriers concentration and consequently the conductivity.

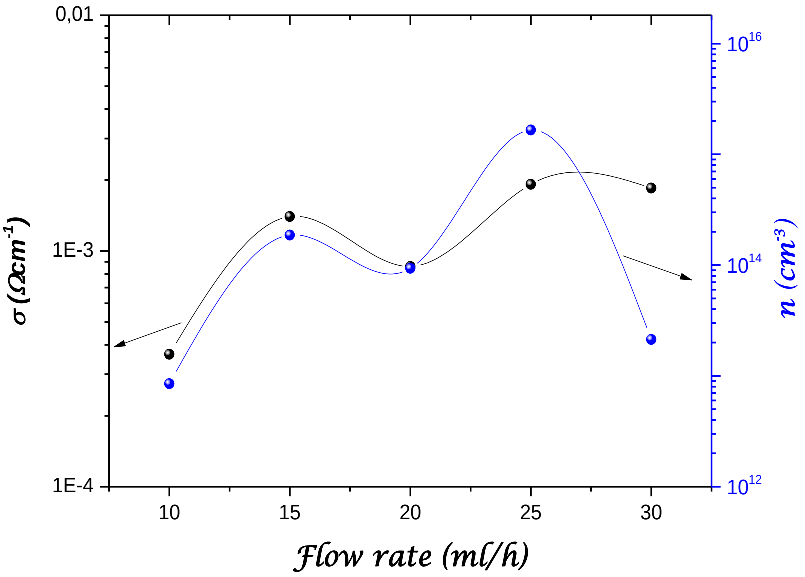

Figure III.50 *Dependence of the CuO film conductivity and free carrier concentration upon the flow rate.*

In figure III.51 we have represented the variation of the carriers mobility for various flow rate. The mobility increases with increasing the flow rate of the precursor solution. It is varied from 11 to 540 (cm^2/Vs) in the investing flow rate rang. The value of the mobility for CuO thin films deposited with spray pyrolysis reported is ranged from 0.01 to 10 (cm^2/Vs). However the measured mobility in our case is very higher. CuO is one material which is attracting attention due to its electrical and optical properties. As a metal oxide p-type semiconductor, it has the highest known hole mobility at room temperature (500 cm2/Vs), which might be particularly favorable for p-channel TFTs.

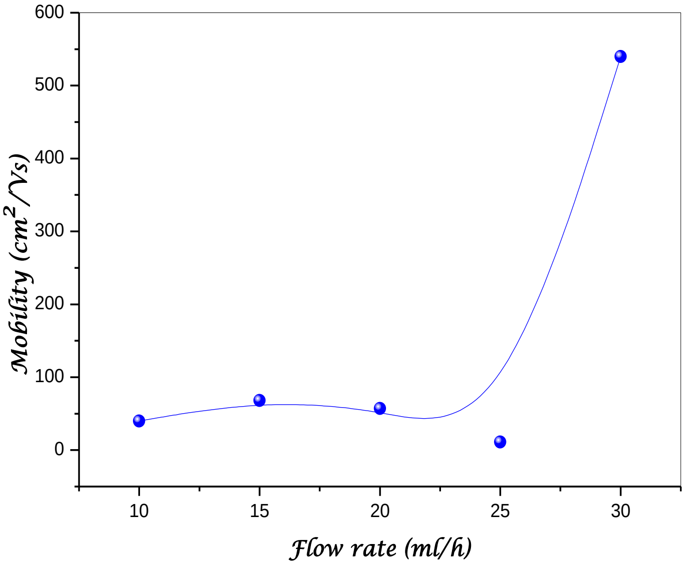

Figure III.51 *Variation of the carrier mobility versus the solution flow rate.*

III.4 Influence of Cu slat source

In spray deposition technique several Cu salts have been used. In order to investigated the influence of Cu salt nature, we have prepared CuO thin films with two Cu slat namely copper chloride ($CuCl_2.2H_2O$) and copper acetate ($Cu(CH_3COO)_2$). All the other parameters were fixed: the molarity was 0.05 M for the different slats; the substrate temperature, the flow rate and time deposition are equal to 300°C, 10 ml/h and 15 min respectively.

III.4.1 Deposition rate

As can be seen in table III.6, for deposition time equal to 15 min, the film thickness or the deposition rate is Cu salt dependent. The deposition rate for the films deposited with copper chloride is three times greater than the growth rate for the prepared CuO films with copper acetate. Few studies have been devoted to the influence of the Cu salt on CuO thin films priorities. The formation of the films is produced by the pyrolytic reaction on the top surface of substrate. The CuO phase is formed by the reaction between the copper ion Cu^{2+} from the solution and the O atom from air. When we used copper chloride, the reaction on surface is spontaneous however the reaction between the reactive spices is slow in the case of the solution prepared with copper acetate. The variation of the deposition rate can be explained by the difference of concentration of free copper ions Cu^{2+} in the two used started solution. To more understand this difference we measured the pH of the two different solutions. The measured the pH of the solution prepared with copper chloride and copper acetate are found equal to 4.45 and 5.73, respectively. Hidmi [100] have study the thermodynamic speciation of copper in solution as a function of pH at a temperature equal to 25°C, the result are showing in figure III.52.

As can be seen the pH of the solution affect largely the species formed or present in the start solution. At lower pH ranged from 3 to 7, we noted the presence of three species namely: copper ion Cu^{2+}, complex $Cu(OH)^+$ and copper hydroxide $Cu(OH)_2$ but the concentration of this different species are strangely changed with the variation of the pH solution in this rang. The concentration of copper ion Cu^{2+} is higher at value of pH varied from 3 to 5.2 above this value the concentration of copper ion is reduce however the concentration of the complex $Cu(OH)^+$ increases. That means some quantities of copper ions Cu^{2+} is changed to complex $Cu(OH)^+$. Moreover, we note also the formation of the copper hydroxide $Cu(OH)_{2(aq)}$ and $Cu(OH)_{2(s)}$ is started at pH solution equal to 5 and 5.5, respectively with low concentration.

consequently, in our case, the solution prepared with copper chloride with lower pH (4.45) we suggest the presence of higher concentration of copper ion Cu^{2+} and a lower concentration of complex $Cu(OH)^+$ however the solution prepared with copper acetate with pH (5.73) we propose the presence of lower concentration of copper ion Cu^{2+} and higher the concentration of $Cu(OH)^+$ with the presence of the copper hydroxide $Cu(OH)_{2(aq)}$ and $Cu(OH)_{2(s)}$. As result, we notice the reduction of copper ion Cu^{2+} is the started solution using copper acetate is due to the consumption of Cu^{2+} for the formation of the complex $Cu(OH)^+$ and copper hydroxide $Cu(OH)_{2(s)}$. The diminution of the concentration of Cu^{2+} leads to the reduction of the formation of CuO phase thus decrease in films thickness. This is consistent with result of the section dealing with the influences of the molarity of the solution.

Salt nature	Film thickness (nm)	Deposition rate (nm/min)
$CuCl_2.2H_2O$	2880	192,06
$Cu(CH_3COO)_2$	1009	67,31

Table III.6 *Deposition rate and film thickness of CuO films using different sources.*

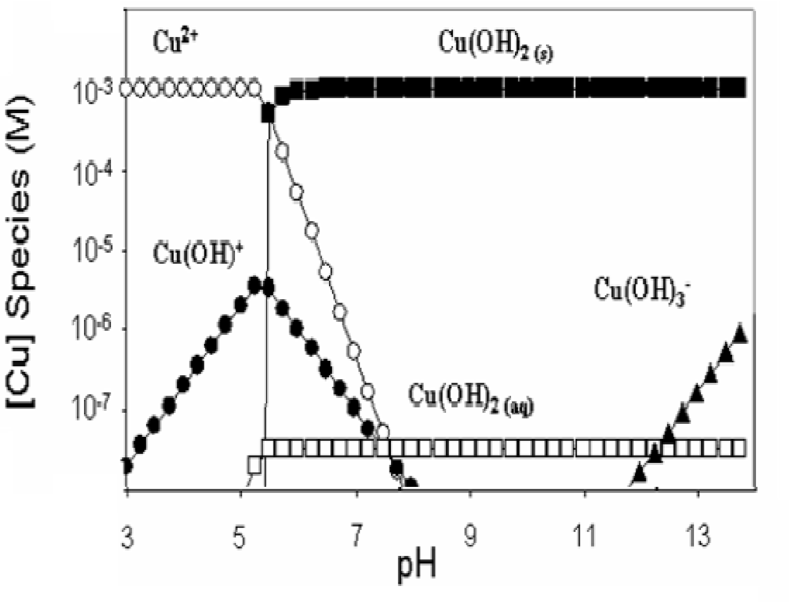

Figure III.52 *Thermodynamic speciation of copper calculated using as a function of pH.*

III.4.2 Structural properties

In figure III.53 we have represented the XRD diffraction patterns of the CuO films elaborated using different Cu source. The crystalline structure is strongly depended to the salt nature. The films prepared using copper acetate ($Cu(CH_3COO)_2$) is amorphous this is evident from the absence of the peaks in the spectra of the films . This is consistent with the broad peak situated in the small diffraction angles. The presence of the amorphous phase can be related to the low deposition time (15 min). This is reliable with results of the section (part B), we have noticed the CuO films have a monoclinic crystalline structure at substrate temperature and deposition time equal to 300°C and 20 min, respectively. However, the CuO films deposited using copper chloride ($CuCl_2.2H_2O$) the spectra showed the presence of two dominant peaks associated to (111) and (200) and the appearance of other miniature peaks related (110) (020) (202) and (113). The presence of all this peaks confirms the presence of a single CuO phase with monoclinic structure. The observed intensity of the peaks indicated that films growth along (200) direction.

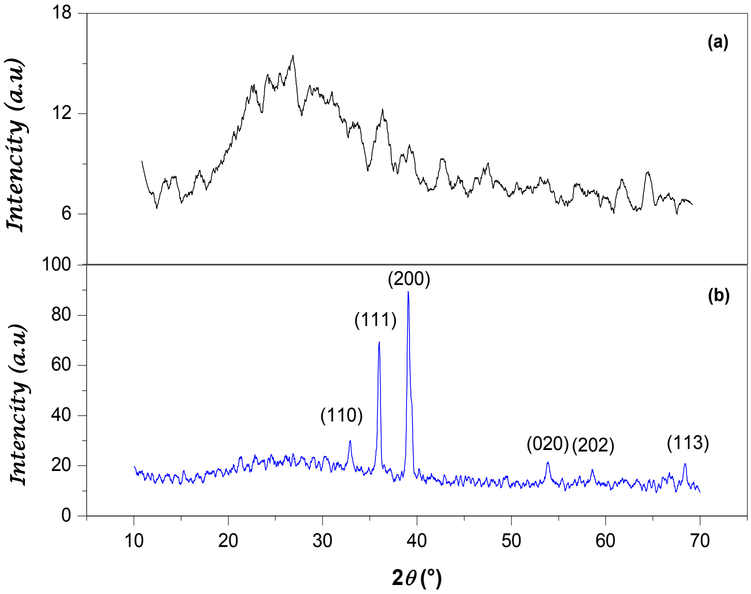

***Figure III.53** XRD pattern of the deposited CuO films using different salt nature : (a) copper actate and (b) copper chloride.*

In table III.7 we have regrouped the calculated structural parameters for the all (hkl) plan of the CuO films deposited using copper chloride. As can be seen in the table the dislocation density and the strain augment with the appearance of the small peaks related to (110) (020) and (113). We noticed also the strain increase with increasing the density dislocation in the films. Dislocation density is defined as the length of dislocation lines per unit volume of the crystal, and it indicates the amount of defects as a result the augmentation of the strain in films.

2θ (°)	(hkl)	Crystallite size (nm)	Number of crystallites/unit area (10^{-3} nm^{-2})	Strain ε (10^{-4})	Dislocation density δ (10^{-4}) (line/m^2)
32.50	(110)	44	30.93	10.54	12.96
35.67	(111)	31	88.90	8.89	10.02
38.98	(200)	25	162.47	9.41	14.98
53.87	(020)	23	219.65	10.75	18.32
67.80	(113)	26	143.36	11.74	19.78

Table III.7 *structural parameters of CuO films deposited using copper chloride.*

Table III.8 we have represented the structural parameters estimated from the all (hkl) atomic plan for the CuO films elaborated with cooper chloride.

Salt nature	Crystallite size (nm)	Number of crystallites/unit area (10^{-3} nm^{-2})	Strain ε (10^{-4})	Dislocation density δ (10^{-4}) (line/m^2)
$CuCl_2.2H_2O$	30	85.66	8.41	12.41 10^4

Table III.8 *Structural parameters estimated from the all (hkl) atomic plan for the CuO films elaborated with cooper chloride.*

In figure III.54 we have shown the Micro- Raman spectra of CuO thin films deposited at 300°C using different Cu source. The Raman spectrums for the deposited films are composed with three main photon modes Ag and 2Bg. In table III.9 we have reported the intensity, the position peaks and the width at half maximum of the three Raman modes for the CuO films elaborated using different slat. It is well known that Raman scattering modes is sensitive to the degree of crystallinity in a sample. Typically, a crystalline material yields a spectrum with sharp and intense Raman peaks, whilst an amorphous material will show broader less intense Raman peaks. From this table we noticed that the intensity of the mode Ag and the first mode Bg decreases with the use of copper acetate this can be related the difference in film thicknesses and the crystalline structure of the deposited films. These two Raman modes are particularly reported that are the most important Raman modes which indicate the formation of a single CuO phase. However, the intensity of the second modes Bg increase and shifted to lower wavenumber. In most spectra shown in the literature, this signal is weakness than in our case and it is located at as a rather feeble signal at about 620 cm^{-1} [101]. A likely reason for the stronger of the latter signal and the red shift of this Raman mode is related to the presence of disorder in CuO films prepared using copper acetate. The amorphous phase is characterized by short range order and lower crystallinity so this engender and favorite to produce a disordered films. In addition, the increase in the FWTH of the three Raman modes for the CuO films deposited with copper acetate is attributed to the amorphous phase. For this reasons, we can concluded that the Ag mode and the first Bg is sensitive to the crystallinity in the films and the second mode Bg is more sensitive the disordered films. Shighesato et al [102] have deposited WO_3 by evaporation and investigated the crystallinity of amorphous tungsten oxide at various substrate temperatures. They found that the peak at 807 cm^{-1} was sensitive to the degree of crystallinity of a-WO_3 and the FWHM of this peak decreased by 35% when the substrate temperature was raised from 40 to 145 °C due to the improve of the crystallinity of the sample.

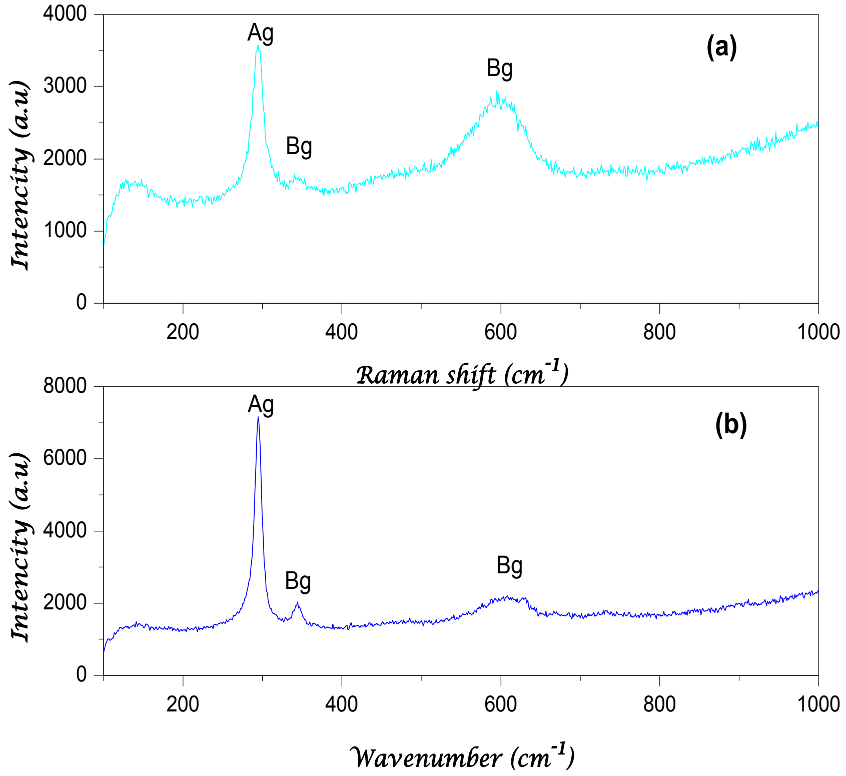

Figure III.54 *Micro Raman spectra of CuO thin films deposited with various Cu sources (a) copper acetate and (b) copper chloride*

Salt nature	Raman mode	Peaks position (cm^{-1})	Intensity	FWHM (cm^{-1})
$CuCl_2.2H_2O$	Ag	294	5092	8.56
	Bg	344	430	9.45
	Bg	609	1133	21.44
$Cu(CH_3COO)_2$	Ag	294	1859	11.89
	Bg	344	112	13.78
	Bg	597	1344	29.08

Table III.9 *Intensity peaks position and width at half maximum of the three modes Raman.*

III.4.3 Films morphology and composition

The films morphology is studied by means of SEM. The SEM images of CuO films deposited using different Cu source, were shown in figure III.55. The morphology of the deposited films is strongly depended to the salt nature. The films deposited using copper chloride as Cu source are dense and homogenous surface with random distributed grains. The estimated grains size for the SEM images is equal to 268 nm. This values is very bigger than the calculated from XRD pattern. While the films elaborated using copper acetate are characterized by a rough, granular surface, consisting of crystallites distributed randomly with the presence of a needle structures.

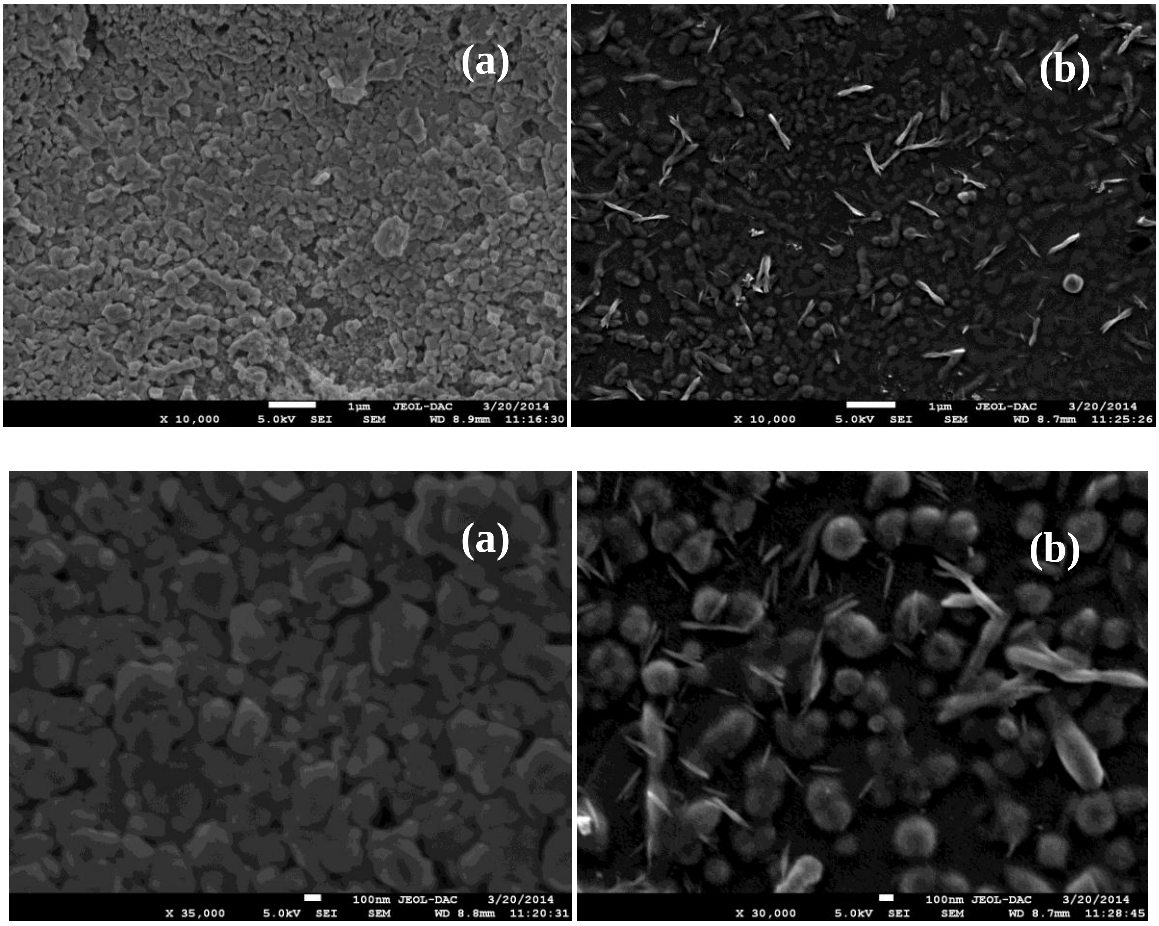

Figure III.55 *typical SEM images of CuO films deposited using different of Cu slat source (a) copper chloride and (b) copper acetate.*

In figure III.56 we have reported the typical EDS spectra for the deposited film CuO using two different salt natures at substrate temperature equal to 300°C. It is evident from spectra, the presence of two Cu and O elements constituting the film. In table III.10 we have illustrated the quantitative analysis extracted from EDS spectra. It is apparent from the table that the use of different Cu source effects the composition of the CuO films. For CuO film elaborated using copper chloride, the ratio O:Cu was 0.26; consequently, the a Cu-rich cupric oxide films have been formed. Meanwhile the ratio O:Cu for the deposited CuO films using copper acetate as Cu source was 1.04 which is more than the unity, thus, the a O-rich cupric oxide films have been formed. This confirms the calculated deposition rate for the deposited CuO films and the difference of the free concentration copper ion Cu^{2+}, because the increase in concentration of Cu atoms in films improve the reaction between the two elements copper and oxygen for the formation of CuO phase. As a consequence, the increase in the films thickness. CuO is intrinsically a p type semiconductor due to the existence of Cu vacancies. However, recent theoretical calculations indicate that although Cu vacancies are the most stable defects in CuO. Otherwise, oxygen vacancies defects are weakly reported in literature while their formation energy is not much different from formation energy of Cu vacancies. The presences of these two defects are much correlated with the composition of the films. As can be seen the films prepared using cooper chloride the major defect present in the films is O vacancy on the other hand the films prepared using cooper acetate indicate the existence of Cu vacancy is dominated.

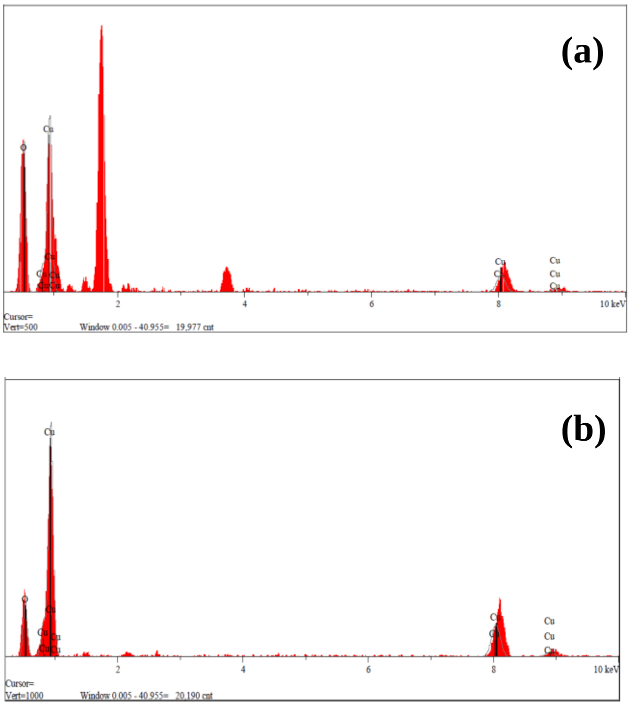

Figure III.56 *Typical EDS spectra for the deposited film CuO using different salt nature: (a) copper acetate (b) copper chloride.*

Salt nature	Atomic percentage (%)		Ratio O:Cu
	Cu	O	
$CuCl_2.2H_2O$	78.88	21.13	0.26
$Cu(CH_3COO)_2$	49.05	50.96	1.04

Table III. 10 *Atomic percentage of Cu and O for CuO films elaborated with different Cu source.*

III.4.4 Optical properties

The optical transmittance spectra in wavelength recorded in films deposited with different slat are shown in figure III.57. The transmittance is about 60 % for the films deposited with copper acetate ($Cu(CH_3COO)_2$) and around 50 % for films prepared using copper chloride ($CuCl_2.2H_2O$). The difference in the transmittance can be attributed to the variation in film thicknesses.

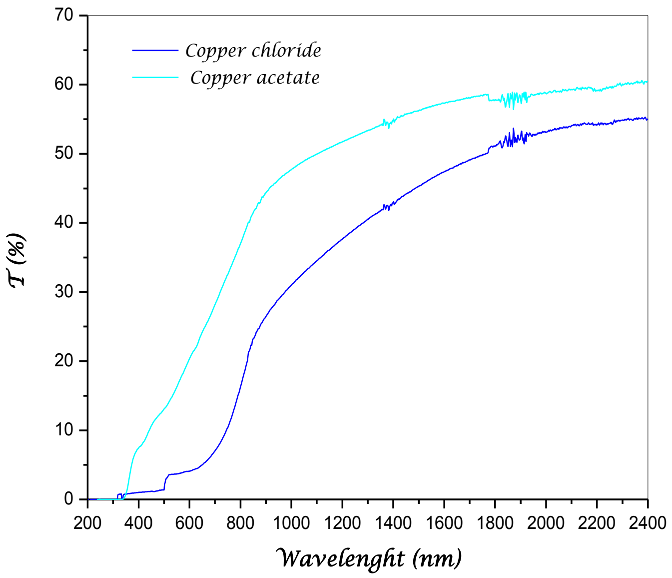

Figure III.57 *transmittance spectra of CuO films deposited using different salt.*

The optical gap values deduced from the transmittance measurements are shown in table III.11. As can be seen from this table, using $Cu(CH_3COO)_2$ as source of Cu yields to films with narrower band gap. While films prepared using $CuCl_2.2H_2O$ as Cu source exhibits a larger optical band gap. The diffidence in value of optical gap can be related to the disorder in films. The films deposited using $Cu(CH_3COO)_2$ are more disordered this can be associated to the presence of the amorphous phase in the deposited films. This confirms the presence of amorphous phase as deduced from XRD analysis. So the variation of the optical band gap correlated well with the variation of Urbach energy.

Salt nature	**Eg (eV)**	**E00 (eV)**
$CuCl_2.2H_2O$	1.47	0,4
$Cu(CH_3COO)_2$	1.30	0,75

Table III.11 *Optical band gap and band tail or disorder in CuO films prepared with different Cu salt sources.*

In figure III.58 we have reported the variation of absorption coefficient with the photon energy of CuO films elaborated with acetate copper and copper chloride. It is evident from this figure that the absorption coefficient of the all deposited CuO films is suitable to be used selective absorber material in photovoltaic cells. The CuO films deposited with copper acetate show a higher absorption coefficient than the films prepared using copper chloride. This explain also the calculated optical band gap.

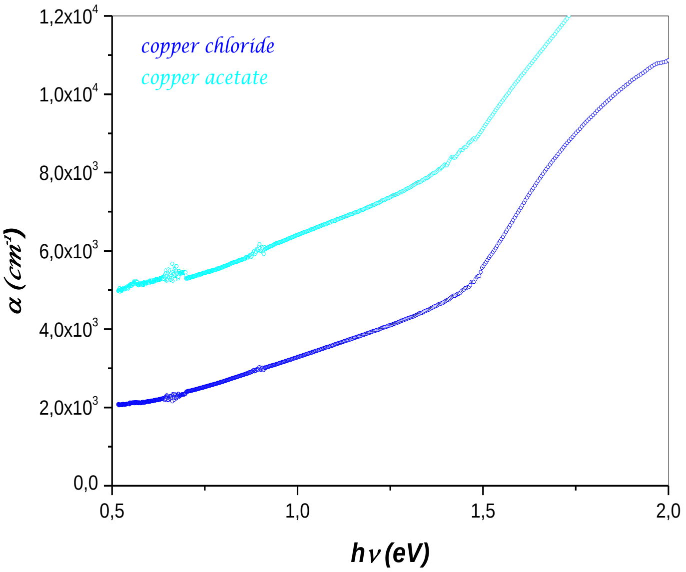

Figure III.58 *Variation of the absorption coefficient as function of the deposited CuO films elaborated with various Cu sources.*

III.4.5 Electrical properties

In table III.12 we have represented the value of free carries concentration, the conductivity and the mobility of the CuO films deposited using the two different salt. As can be observed the electrical proprieties is largely sensitive to slat nature. The electrical conductivity follows faithfully the variation of the carriers concentration. This indicates clearly that the conductivity is rather controlled by the free carrier concentration. The whole prepared films have p-type conductivity according to Hall constant sign. However the conductivity of the films deposited using copper acetate is relatively higher than the films elaborated using copper chloride. In additional, the free carriers concentration in film prepared with copper chloride is three decades lower than in film prepared with the copper acetate.

It is well known that the electrical proprieties are altered by the films composition. It has been widely reported that in CuO films excess oxygen ions or copper ion vacancy in the films are the mains source acceptor or donor defects which affect the conductivity and the free carriers. We have found that the films deposited using copper acetate are O-rich CuO films but the films elaborated with copper chloride are Cu-rich CuO films. As can be suggested that CuO films excess O ion are more conductor with higher free carriers concentration and the CuO films excess Cu ion are more resistive with lower free carriers concentration. This confirms that Cu vacancy is the most important defect in CuO films which affect drastically the conductivity. V. F. Drobny et al [103] have deposited copper oxide films by reactive sputtering at different partial pressure of oxygen. They have noticed that for copper oxide films composited with a single phase CuO the resistivity reduce from 10^3 to 0.1 (Ωcm) with increasing the oxygen percentage. This lowering of resistivity through doping the films with excess oxygen leads to more effectively producing more copper ion vacancies and a p-type semiconducting material.

On other hand the mobility in the films prepared using copper chloride is greater about two decades than the value found for the films elaborated by copper acetate. The conductivity is also affected by the films structure and the crystallinity. The films deposited using copper chlorides are crystalline in nature with monoclinic structure conversely to the films prepared by copper acetate which are amorphous. The crystalline phase is characterized by long- range order with well-defined orientation of crystallite and more ordered films. However, the amorphous phase is distinguished by short long range with random orientation and disordered films. This characteristic of each phase affect the mobility of the free carrires on the films networks. In the crystal structure the free carriers are free to move contrary in amorphous phase they are trapped due to the presence of defect and disorder in the films which leads the reduction of their mobility. As can be concluded the mobility is also controlled by the crystallinity of the films.

Salt nature	n (cm^{-3})	σ $(\Omega cm)^{-1}$	μ ($cm^2V^{-1}S^{-1}$)
$CuCl_2.2H_2O$	9.37 10^{13}	1.46 10^{-4}	7.87
$Cu(CH_3COO)_2$	7.37 10^{17}	3.46 10^{-3}	0.029

***Table III.12** Electrical conductivity, free carriers concentration and mobility of CuO films deposited using different Cu source.*

Chapter IV

Applications of CuO thin films

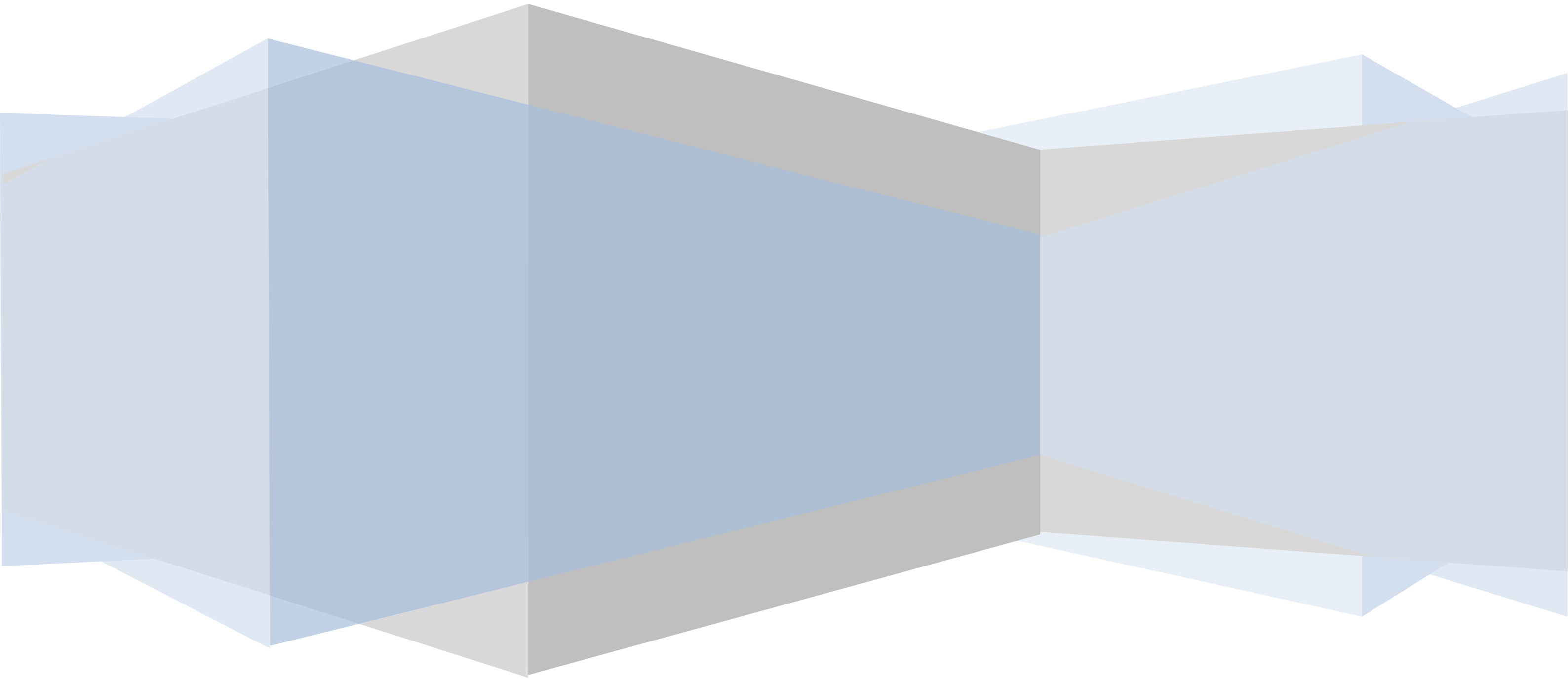

Gas and organic vapor sensing

In the present chapter, firstly, we present the result of CuO films characterization for application as sensitive layer and in the second part, the gas sensing performance of CuO based sensor towards organic vapor (methanol and ethanol) and CO_2 gas.

IV.1 CuO sensitive layer characterization

In this section we present the structural, optical and electrical characterizations of the CuO thin film as attractive sensitive layer, deposited by ultrasonic spray pyrolysis technique using copper chloride with solution molarity equal to 0.05 M at substrate temperature and deposition time fixed at 350 °C and 5 min, respectively.

IV.1.1 Film thickness

Film thickness was estimated from fitting optical transmission data. In Figure IV.1 we have present the theoretical calculation (blue one) and the experimental data (red one). The film thickness was found to be 158 nm. It well known that sensitive layer thickness affects strongly the performance of the gas sensor. It have been previously demonstrated that the fabricated sensor with more thinner activate layer presents ~~a~~ higher sensitivity, good response and recovery times. This justified the choice of the experimental parameters specially the deposition time.

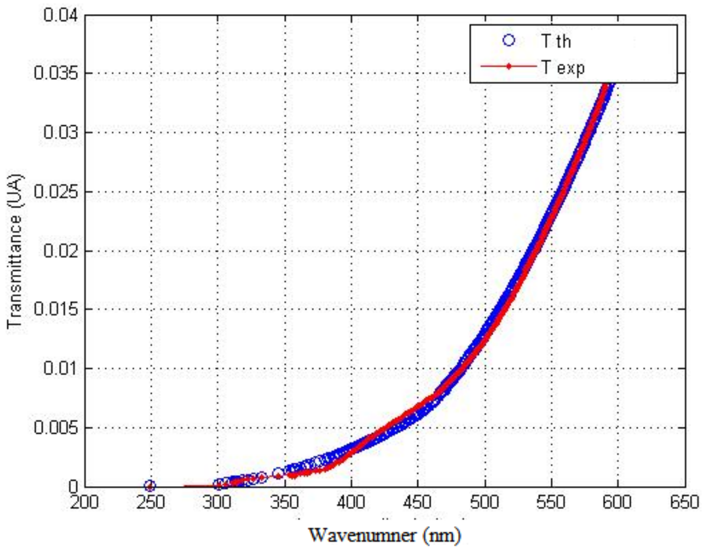

Figure IV.1 *Theoretical calculation and the experimental transmittance spectra of CuO thin film.*

IV.1.2 Structural properties

Figure IV.2 shows the Raman spectrum of the as-prepared CuO thin film. The Raman spectrum is composed with three main phonon modes (Ag and 2Bg) located at 297, 344 and 598 cm^{-1}. These peaks are largely reported in the literature. This confirms the presence of a single phase CuO with a monoclinic structure.

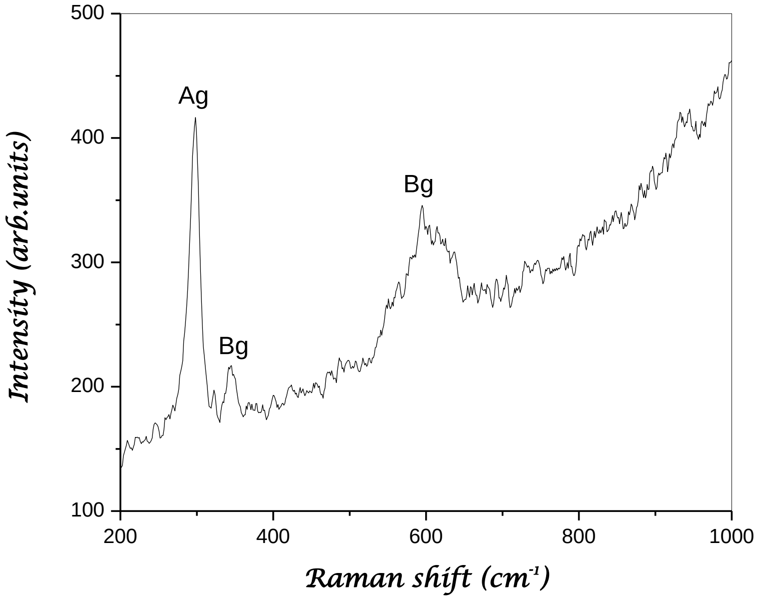

Figure IV.2 *Micro-Raman spectrum of the sensitive layer CuO.*

IV.1.3 Film morphology and composition

In figure IV.3 we have represented the SEM micrographs of the sensitive layer CuO films. The SEM images revealed that the film surface is smooth and dense with the random distributions of grains size. We have observed also the presence of pores at all films surface of the deposited film. While, the grains distribution and size are not uniforms. The estimated grains size is about 50 nm.

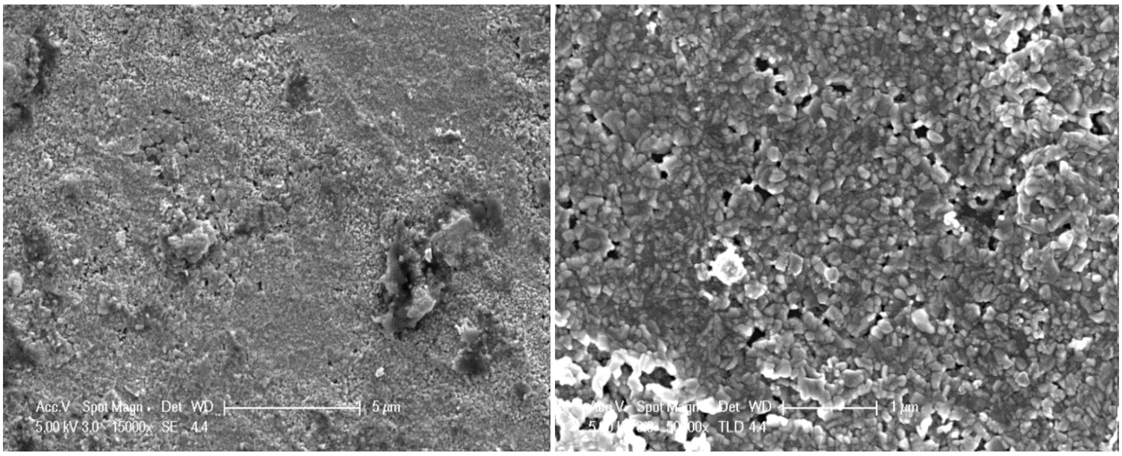

***Figure IV.3** The SEM images of the sensitive layer CuO thin film.*

The EDS spectrum of the deposited CuO films is shown in figure IV.4. The analysis indicates the presence Cu and O elements forming the CuO layer. However, the appearance of other elements (such as Si, Ca, Na, O and Mg) originates from the used glass substrate. The elements composition suggests that the deposited film is close stochiometric with Cu: O ratio equal to 1.09.

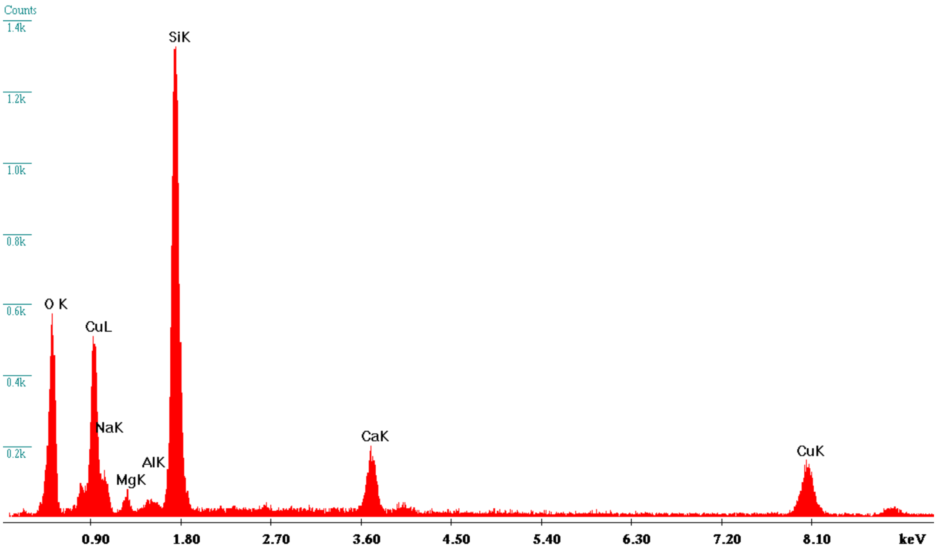

***Figure IV.4** The EDS spectrum of CuO film.*

In figure IV.5 (a and b) we have presented typical two dimensional (2-D) and three dimensional (3-D) AFM image of CuO film deposited on glass substrate. The (3-D) image indicates that the film surface exhibits hills and valley like structures, which are uniformly distributed over the entire substrate surface. The 2-D images show compact and granular morphology with presence of pores in the surface; this is benefit to the gas sensor sensitivity improvement. Porous materials have been extensively investigated, it is well recognized that porous material, due to the high specific surface, is most suitable for application in the fields of photocatalysis and gas sensing.

Atomic force microscopy (AFM) is proved to be a useful tool for surface roughness determination. There are several roughness parameters that are used to fully characterize the surface. The most common ones being the arithmetic roughness (Ra) and the root mean square roughness (Rq). The estimated value of this two parameters Ra and Rq are equal to 45.35 nm and 50.67 nm, respectively. As can be seen, our CuO films show large roughness. In the literature, it is well recognized that the sensitivity, response and recovery times are the main parameters to characterize the sensor performance. Moreover, these parameters are close related to the roughness of the activated layer. Several authors have focused their study to improve the surface roughness in order to enhance the interaction between gas-surface which leads to the sensor sensitivity increase.

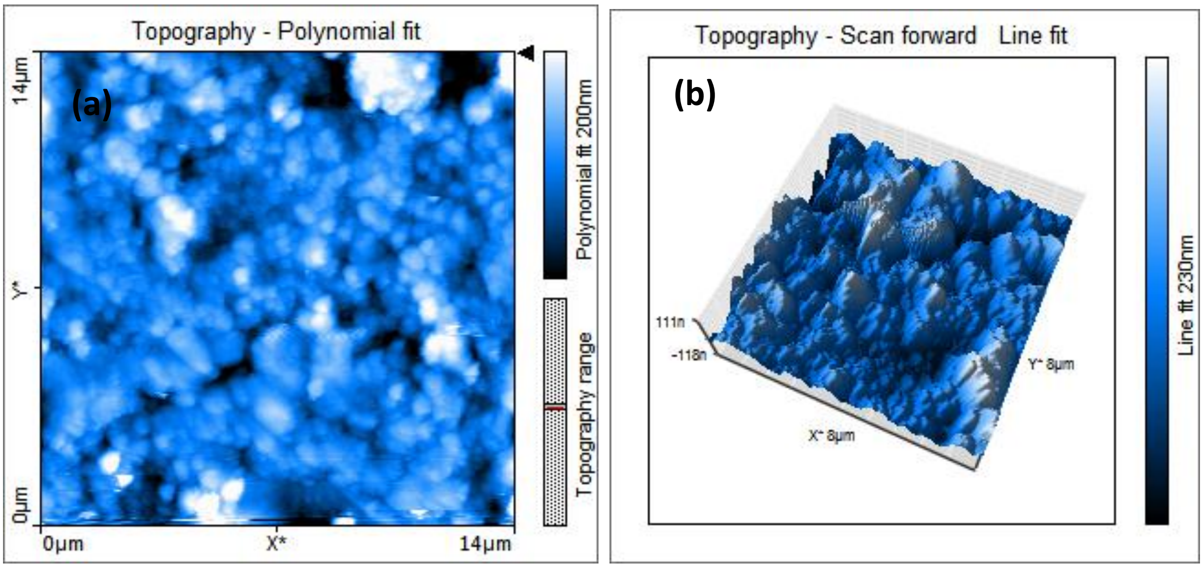

Figure IV.5 *The AFM images of the deposited CuO film (a) 2-D , (b) 3-D.*

IV.1.4 Optical properties

The transmittance spectrum in UV–visible region of the prepared CuO film is shown in figure IV.6. The measurements were performed in the UV-VI-IN, corresponding to the wavelength range: 200 - 1000 nm. The films transmittance decreases with wavelength. The film behaves as transparent material in the 800-1000 nm wavelength range. On the other hand, in the visible region films transmittance values decreases sharply in the wavelengths range less than 800 nm due to their highly absorbing properties which represent the fundamental absorption region.

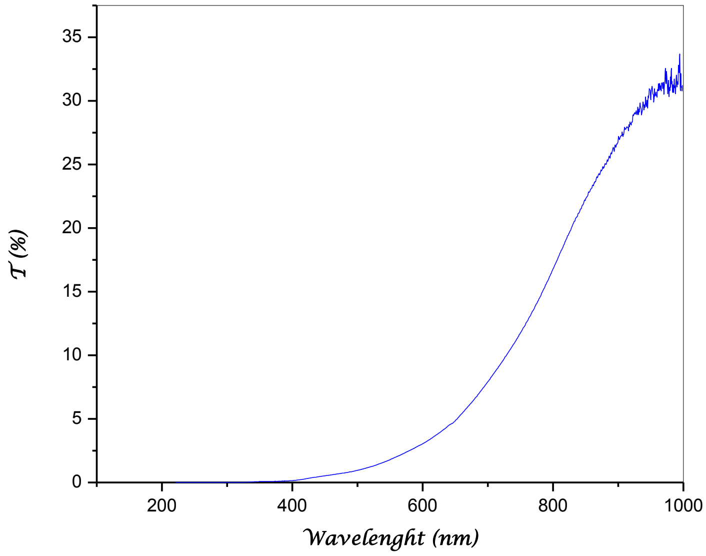

Figure IV.6 *Transmittance spectrum of CuO thin film.*

Film optical band gap is estimated from the plot (αhν)^2 as a function of photon energy (hν), according to Tauc formula for direct band gap semi-conductors as shown in figure IV.7. The obtained optical gap is equal to 1.30 eV which is in good agreement with CuO band gap values reported in the literature [26].

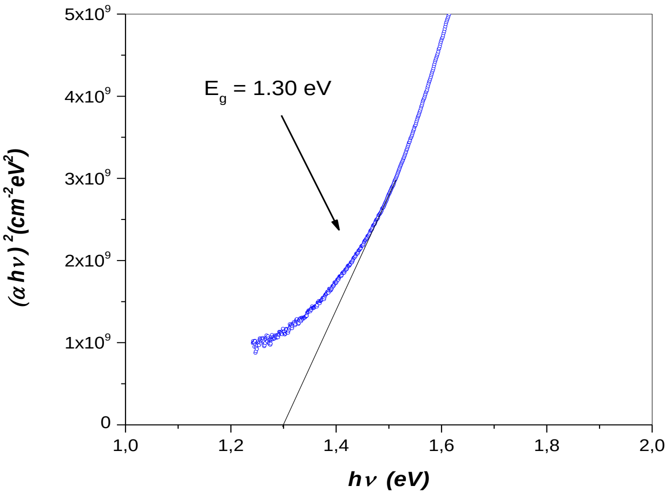

Figure IV.7 *the plot (αhν)^2 as a function of photon energy (hν) of CuO thin film.*

Refractive index was estimated from fitting optical transmission data. The estimated refractive indices were plotted as a function of wavelength in figure IV.8. In the wavelength range between 550 and 600 nm the refractive index was found to be ~2.29.

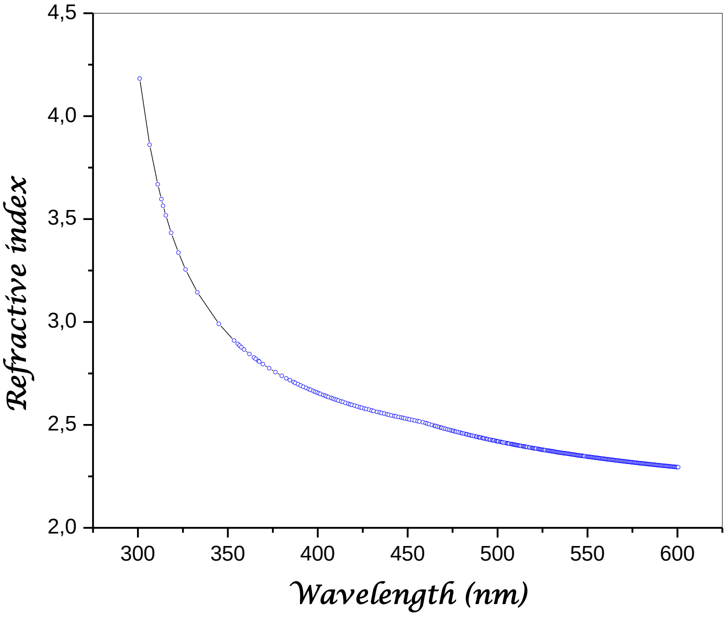

Figure IV.8 *The estimated refractive indices were plotted as a function of wavelength for the deposited CuO thin film.*

IV.1.5 Electrical properties

In Figure IV.9 we have presented ln(σ) vs. 1000/T curves for CuO thin films. As can be seen, the dark conductivity follows the Arrhenius behavior with increasing measurement temperature. This indicates that CuO film electrical conductivity is thermally activated. The activation energy of electrical conduction has been calculated from the local gradient of ln (σ) vs. 1000/T plots. The obtained result is equivalent to 0.6 eV.

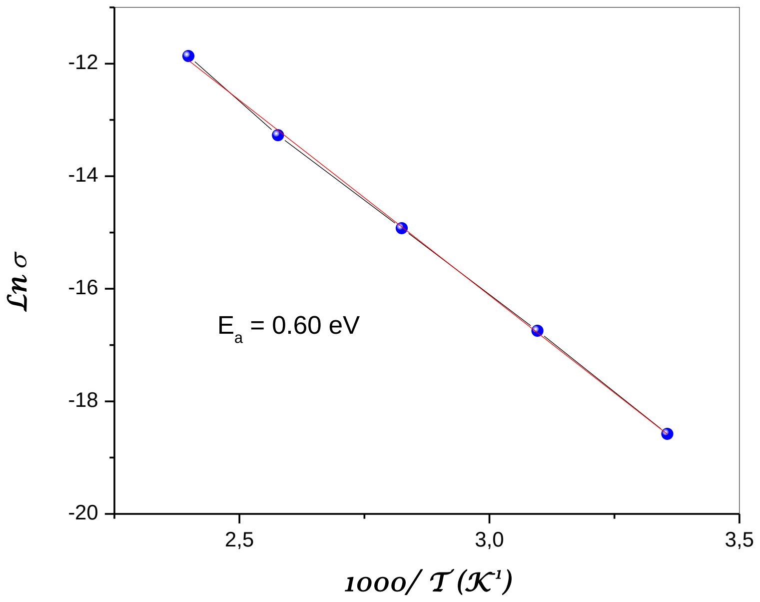

Figure IV.9 *Ln (σ) versus 1000/T plot for the CuO thin films*

In order to determine the conductivity type of the deposited film we have calculated the ratio 2Ea/Eg, where Ea is the electrical activation energy and Eg is the film optical gap deduced from the optical transmittance spectrum. It is well known that conductivity activation energy of a semiconductor Ea corresponds to Fermi level Ef position regarding the bottom of conduction band edge (Ec) (Ea = Ec - Ef). Since the band gap energy Eg is equal to the difference Ec - Ev, then the ratio 2Ea/Eg can be an easy tool used for the determination of Fermi level position in the forbidden region [70]. If this ratio is close to the unity, this means that the Fermi level is located at the midgap position and the semiconductor is intrinsic. However, the reduction of this ratio means that Fermi level moves towards the minimum Ev in p-type semiconductor band edge and the material contains donor (or acceptor) impurities. As can be seen, the ratio 2Ea/Eg is equal to 0.92 and it is almost identical to unity, this means that Fermi level is located nearby to the midgap position indicating that ours deposited CuO thin film is close to be intrinsically p-type semiconductor or slightly p-doped semiconductor with lower hole concentration. In figure IV.10 we have reported a schematic drawn of bands structure in p-type semiconductor and the deposited CuO thin films.

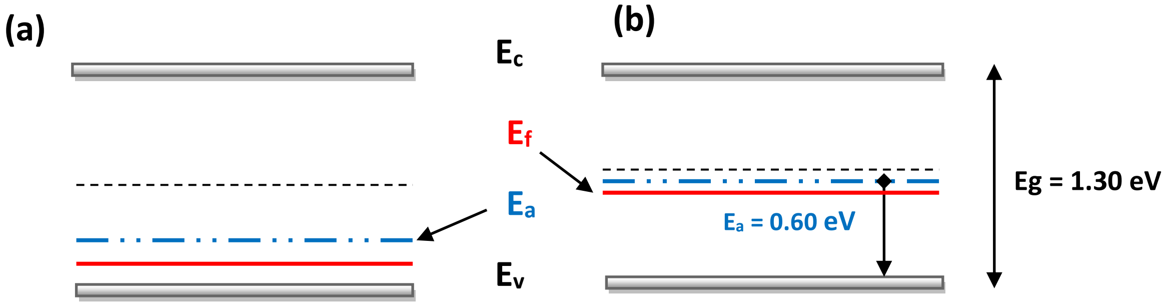

Figure IV.10 *Band diagram for: (a) P-type semiconductor (b) the deposited CuO thin film.*

IV.2 Gas sensing performance

In this section we present the result of the realized gas sensor based on CuO thin film. The gas sensor fabrication and measurement procedures are described in the Chapter II. In order to characterize sensor performance towards methanol and ethanol vapor and CO_2 gas a set of characteristics parameters are investigated namely: operation temperature, sensitivity, detection limit, response and recovery times. The characteristic of CuO based sensor are presented below.

IV.2.1 Methanol sensing

IV.2.1.1 Operation temperature

The semiconductor based sensor response is greatly influenced by its operating temperature. In fact, the adsorption of gases is directly related to the operating surface temperature of the sensing layer. In order to determine this temperature, sensor is exposed to 300 ppm of methanol vapor at different temperatures ranged between 25 and 125 °C, the obtained responses are shown in figure IV.11. A typical operation temperature corresponds to maximum response is widely reported in literature. In our case, the evolution of the sensor response indicates that this maximum is located around 50 °C. This operating temperature (50 °C) is lower compared to other reported working temperature for sensing ethanol vapor ranged from 200 to 400°C [104-105]. However, we note also that CuO based sensor exhibits a good sensitivity at lower operation temperature equal to 25 °C (room temperature). This low operating temperature may lead to sensor power consumption reduction, thus making the device more stable, low cost with a longer life [105].

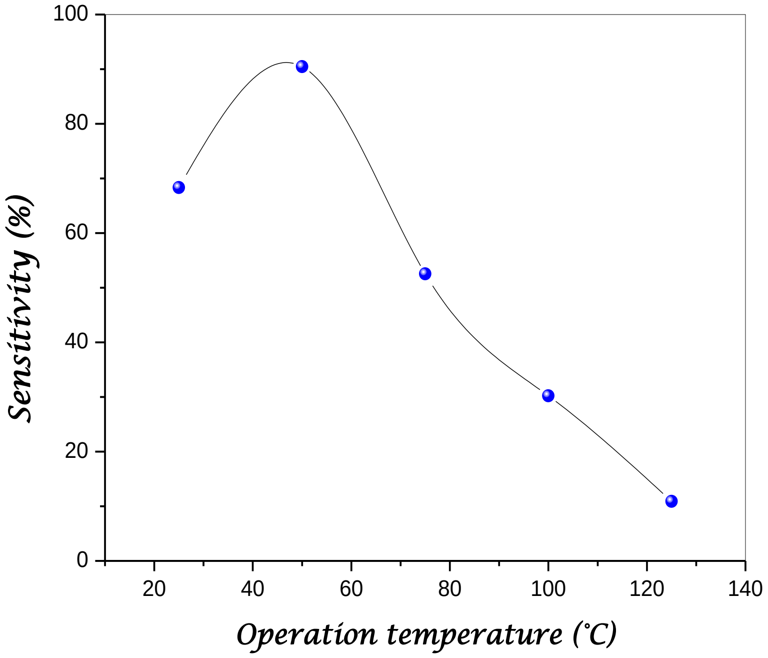

Figure IV.11 *Sensor response curves of CuO based sensor towards methanol (300 ppm) at different operating temperatures.*

IV.2.1.2 Sensitivity

The film sensitivity is the relative change of measured signal during vapor or gas exposure. The gas response of the sensor is defined as the ratio of change in the resistance of the sample when exposed to methanol vapor on the resistance in air by the formula:

$$S = \left| R_g - R_a \right| / R_a \times 100\ \% \qquad (22)$$

Where R_g and R_a are CuO film resistances, measured in methanol vapor and in air atmosphere, respectively.

In figure IV.12 we have shown the dynamic response of sensor resistance vs. time for 300 ppm ethanol at the operation temperature 50 °C. It is evident from the figure that the resistance decreases when the sensing layer is exposed to methanol vapor reveals that R_g is lower than R_a. The sensor exhibits a high sensitivity equal to 90% at operation temperature and equal to 68 % at room temperature. It is well-known that the behavior of the CuO gas sensor is greatly influenced by its operating temperature, adsorption and desorption of oxygen molecules or atomic on the surface of the sensing film which leads to electrical resistance change. When the sensing film is exposed to a reducing gas (donor electron) such as methanol, the interaction of methanol molecules with the surface chemisorbed oxygen species takes place, thereby releasing electrons. Consequently, the type of semiconductor will decide the behavior of the resistance variation. Hence, if the semiconductor is an n-type, the released electrons yield to resistance reduction. While in the case of p-type semiconductors, the released electrons recombine with holes to decrease the semiconductor electrical conductance and consequently the gas sensor resistance increases.

As mentioned above CuO is a p-type semiconductor due to the presence of Cu vacancy. Thereafter, if the Cu defects concentration is low, the holes concentration in CuO film is then also lower than in a p-type semiconductor which is conformed from the composition analysis of the deposited film. When the sensitive CuO layer is in contact with methanol vapor, the electrons coming from gas, reduce quickly the small holes density by recombination until saturation, then the large density of electrons will dominate. Consequently, the CuO thin films change from p-type to n-type when it is exposed to a reducing gas such as methanol.

For comparison with our work, the responses of various CuO based gas sensor for methanol sensing which have been developed by other groups using different fabrication techniques, are summarized in table IV.1. As can be deduced, our thin film CuO based sensor has the lowest operating temperature (50 °C) as well as the highest response (90 %). This difference may be due to the fact that in our sensor, the resistance is rather controlled by the free electron than by holes. Since the later have lower mobility, this explains then the noticed higher response in our case.

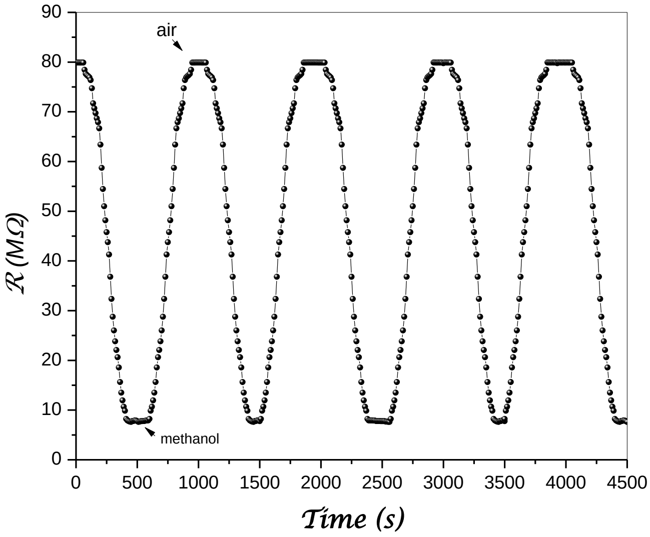

Figure IV.12 *Dynamic response of CuO based sensor towards methanol at the optimum operating temperature of 50 ◦C*

Fabrication technique (morphology)	**Operating temperature (◦C)**	**Concentration (ppm)**	**Sensitivity (%)**	**References**
DC-magnetron sputtering (thin films)	350	700	17	[108]
Chemical solution (nanosheet)	320	500	37.5	[109]
Chemical solution (nanoparticles)	320	500	25	[109]
Spray pyrolysis (thin films)	50 25	300	90 68	This work

Table IV.1 *Sensor response of CuO based sensor towards methanol vapor on various fabrication techniques and morphologies.*

IV.2.1.3 Response and recovery times

The response and recovery times are defined as the time required to reach 90% of the final signal level and the time to return to the initial value respectively. These are important characteristics of a gas sensor. The sensing layer exhibits response and recovery times of

2.45 min and 2.02 min respectively. For comparison with our work, a CuO based sensor fabricated by Mitesh et al [108] exhibits a response time and recovery time equal to 3.91 min and 4.25 min towards 2500 ppm of methanol vapor. The response and recovery times are found longer than ours. The long response and recovery times is probably the result of complex mechanisms related to adsorption and desorption of molecules when the layer is exposed to vapor of methanol. The kinetics of each of these mechanisms is strongly influenced and controlled by the morphology and deposition conditions of the film. Modification of these conditions to obtain more porosity and decrease of the layer thickness may be a suitable method to improve the response time.

IV.2.1.4 Detection limit

The response of the sensing layer as a function of methanol concentration ranging from 20 to 500 ppm was studied at the optimum temperature of 50 °C is shown in figure IV.13. An increase of the sensitivity is evident when the concentration of methanol increases. This is due to the increase in the flux of molecules arriving at the adsorption sites. The sensitivity of our sensor remains significant even for the lowest methanol concentrations equal to 20 ppm.

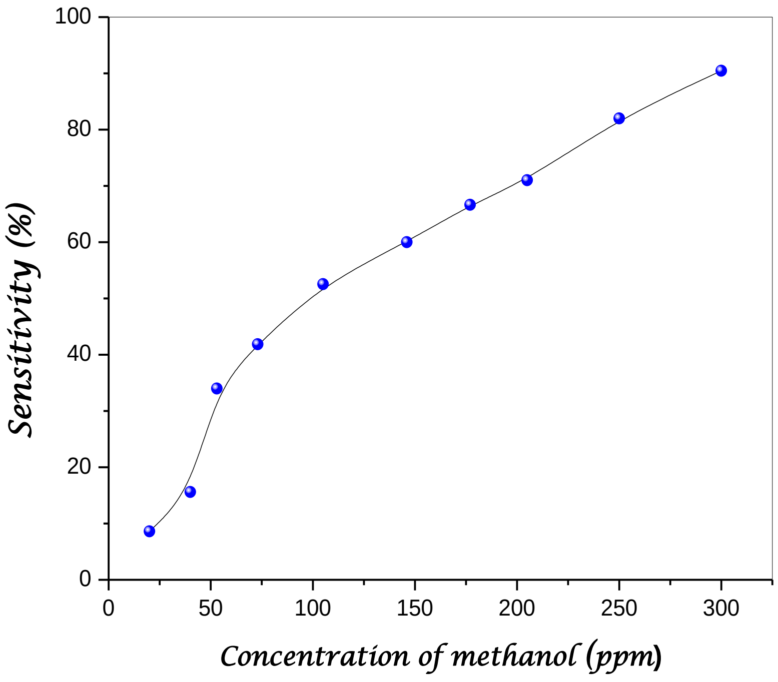

__Figure IV.13__ Variation of the sensitivity as function of concentration of methanol vapor.

IV.2.2 Ethanol sensing

IV.2.2.1 Operation temperature

In figure IV.14 we have reported the variation of the sensor response of the CuO based sensor at different operation temperature. The operation temperature was varied from 100 to 175°C. As can be seen, the sensor exhibits higher sensitivity about 45 % for operation temperature equal to 150°C towards 300 ppm of ethanol vapor. However, both of the sensors responses were reduced significantly as the operating temperature was further increased. This operation temperature is lower than that reported ones in the literature for sensing ethanol [104-106].

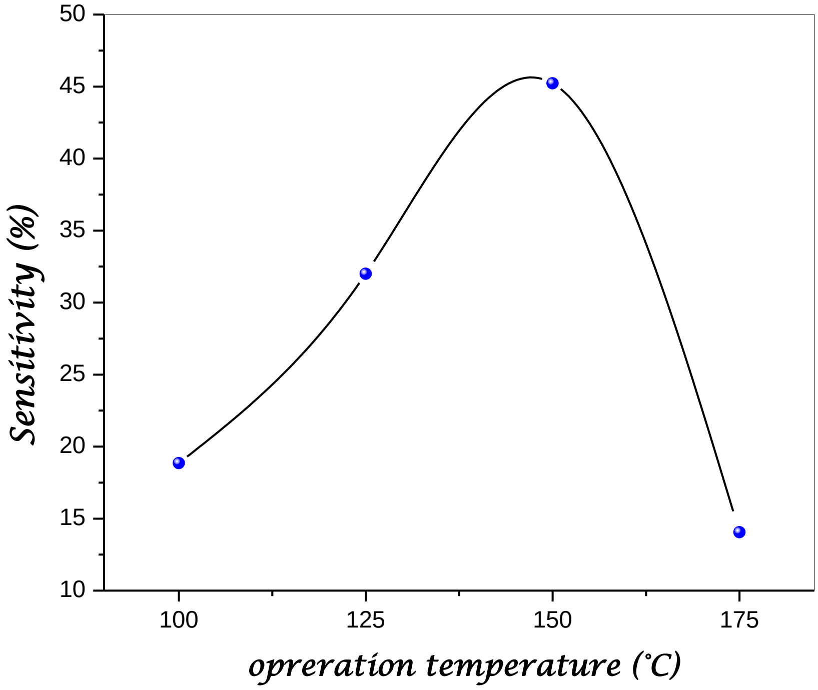

Figure IV.14 *Sensor response curves of CuO based sensor towards ethanol (300 ppm) at different operating temperatures.*

IV.2.2.2 Sensitivity

In figure IV.15 we have shown the sensor based on CuO resistance vs. time for 300 ppm ethanol vapor at the optimum temperature 150°C. The dynamic responses of the CuO sensors towards ethanol vapor showed good sensor response, repeatability and reversibility. We noticed also that the resistance of the sensor decrease when the sensing layer is exposed to ethanol vapor. In addition, the same behavior is observed for the both reducing gases namely: ethanol and methanol vapor.

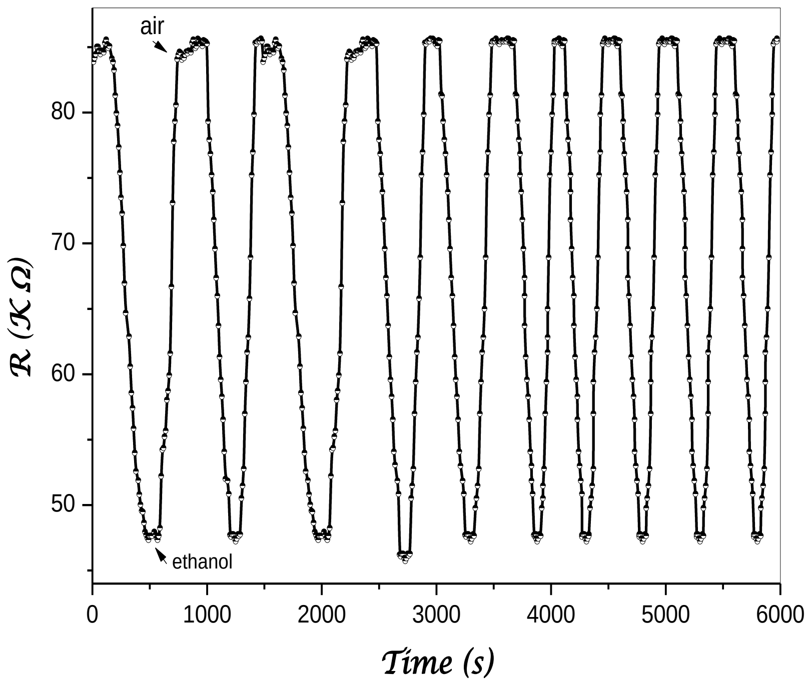

Figure IV.15 *Dynamic response of CuO based sensor towards 300 ppm of ethanol at the optimum operating temperature of 150 ◦C.*

In figure IV.16 we have reported the variation of the resistance change of the CuO based sensor towards ethanol vapor versus time. It can be deduced that the resistance of the sensor increase in the presence of ethanol during a few second and turns to decrease with increasing the time. The increase in the resistance firstly is due the interaction of the reducing gas with low holes concentration of the p-type semiconductor then the resistance decreases due to the change of the semiconductor type with increasing the electrons concentration of the reducing gas (ethanol).

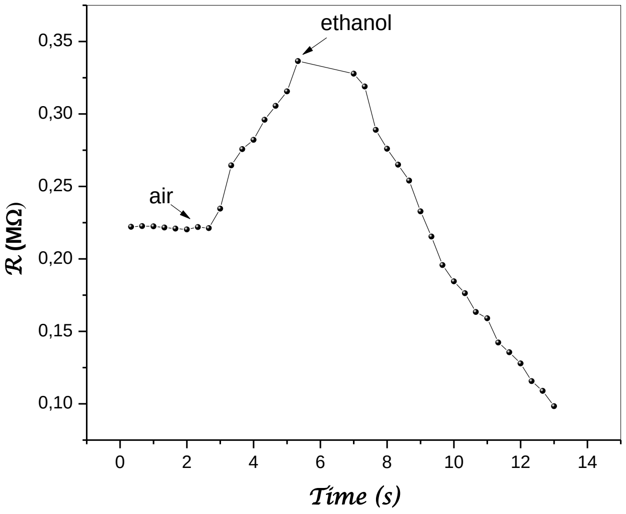

Figure IV.16 *Variation of the resistance change of the CuO based sensor towards ethanol vapor versus time.*

For comparison with our work, the responses of CuO based sensor (without any additional catalytic layers) which have been developed by other groups using different fabrication techniques are regrouped in table IV.2. It is observed that our CuO based sensor has the lowest operating temperature (150 ◦C) as well as a high response (45 %). The superior performance of our CuO sensors is mainly due to our films morphology.

Fabrication technique (morphology)	Operating temperature (◦C)	Concentration (ppm)	Sensitivity (%)	References
Thermal oxidation (nanowires)	200	100	10	[110]
DC sputtering (nanowires)	300	1000	27	[111]
Hydrothermal (nanorods)	400	100	50	[112]
This work	150	300	45	-

Table IV.2 *Sensor response of CuO based sensor towards ethanol vapor on various fabrication techniques and morphologies.*

IV.2.2.3 Response and recovery times

The sensing layer exhibits response and recovery times of 2.98 min and 2.11 min respectively. The CuO based sensor fabricated by Mitesh.al [108] exhibit a response time and recovery time equal to 4.11 min and 4.06 min towards 2500 ppm ethanol vapor. The response and recovery times were almost 2 times larger than ours.

IV.2.2.4 Detection limit

The response of the sensing layer as a function of ethanol concentration ranging from 20 to 500 ppm was studied at the optimum temperature of 150 ◦C is shown in figure IV.17. The sensitivity of our sensor remains significant even for the lowest ethanol concentrations equal to 25 ppm. At higher concentration of ethanol the sensitivity increases by 70 %.

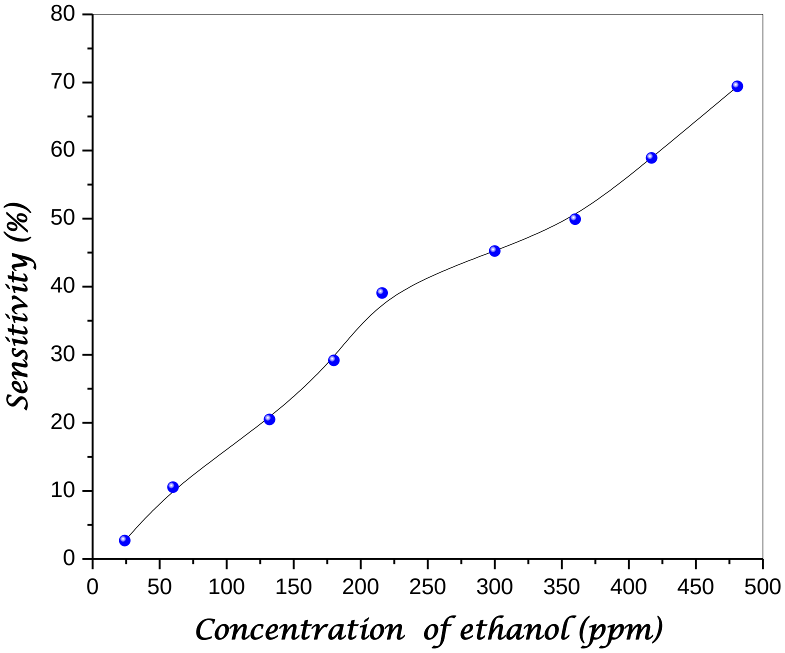

Figure IV.17 *Variation of the sensitivity as function of concentration of ethanol vapor.*

IV.2.3 Carbon dioxide (CO_2) detection

IV.2.3.1 Operation temperature

Figure IV.18 we have represented the response of the sensitive layer at operating different temperatures. The measurements were performed at intervals between 40 ◦C and 120 °C. The carbon dioxide pressure was fixed at 5 hPa. The curve shows a classical evolution with a maximum at around 60 °C. Below 60 °C, the decrease of the response with the temperature, is due to the surface desorption of the adsorbed species which are responsible for changing the response factor. The sensitivity of sensor depends strongly on the operating temperature. In table IV.3 we have represented the operation temperature of different metal oxides for CO_2 detection. As can be seen, CO_2 detection needs a higher operation temperature for all the metal oxide. The obtained operation temperature for our fabricated gas sensor is low compared to the reported ones in the literature. Some authors suggest the mixture of these metal oxides to reduce the detection temperature. This phenomenon is generally explained by the thermally activated adsorption and desorption of oxygen at the surface of the sensing layer. Other models take in account the width of a depletion layer between the semi-conducting grains which is temperature dependent. The temperature that gives the optimal response depends on the composition and the doping of the used sensitive semiconductor layer. For a given material, the grain size the grain boundaries and the porosity have also a great influence on the optimal temperature.

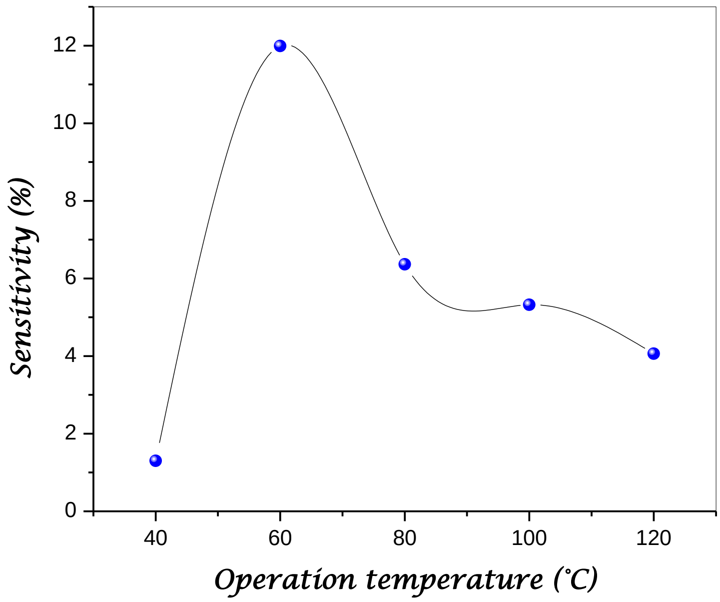

Figure IV.18 *Sensor response curves of CuO based sensor towards CO_2 pressure equal to 5 hPa at different operating temperatures.*

Metal oxide	Operation temperature (°C)
MgO	867
ZrO_2	624
PbO	501
CaO	900
In this works	60

Table IV.3 *Operation temperature of various metal oxides for CO_2 detection.*

IV.2.3.2 Sensitivity

In figure IV.19 we have reported the resistance variation of the CuO based sensor at the operation temperature of 60°C with alternating air with pressure above 2 x 10^{-2} hPa and air + CO_2 with pressure equal to 5 hPa. The positive response observed (i.e., Rair > RCO_2) is representative of the interaction of CO_2 with sensitive CuO layer. The sensitivity measured for our sensor is above 9%. Very few studies have been reported for CO_2 sensing in the case of CuO based sensitive layer. However, several studies have focused on the use of various metal oxides mixture in addition to CuO for the elaboration of p-n heterojunction or multilayer such as: ZnO, SnO_2, TiO_2, $BaTiO_3$, La_2O_3 and $Cu_xFe_{3-x}O_4$ to improve of the sensitivity towards CO2 gas [55-59].

In n-type oxide semiconductor, such as SnO_2, ZnO, and In_2O_3, the oxidation reaction at the surface between the reducing gas and the negatively charged surface-adsorbed oxygen (O^- or O^{2-}) leads to the injection of electrons from the surface to the semiconducting core. This decreases the sensor resistance in proportional to gas concentrations. In contrast, in a p-type semiconductor, such as the CuO of the present study, the electron injection originated from the reaction between the reducing gas and the negatively charged surface oxygen increases the sensor resistance by decreasing the major charge carrier (hole) concentration. However, the sensor resistance decreases when exposures to ethanol and methanol vapor, as observed in figure IV.15 and figure IV.12.

When the CuO based sensor is exposed to CO_2 gas, the resistance of the sensor decreases also. Actually, the temporary resistance decreases immediately after the exposure to oxidizing gas is a characteristic of p-type semiconductor. The reduction of sensor resistance upon exposure to CO_2 gas can be explained by the increase in the holes concentration due to the increased formation of negatively charged oxygen upon exposure to the oxidizing gas (CO_2).

These two opposite behaviors indicate that the interaction between the gas and the surface of the CuO based sensor is not so simple; the interactions can either be oxidative or reductive depending on the type of gas (reducing or oxidizing). To our knowledge, this is the first report showing that CuO based gas sensor exhibits a change in type of the semiconductor in the presence of reducing gas. However, the exposure to an oxidizing gas does not alter the p-type semiconducting of our gas sensor.

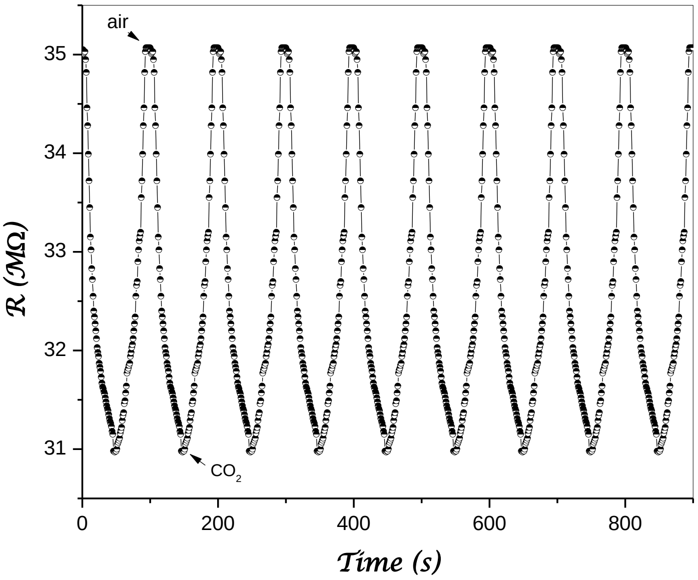

Figure IV.19 *Transient resistance of CuO thin film deposited on screen printed gold electrodes. P_{air} = 2 x 10 hPa and P_{CO2}= 5 hPa at 60°C.*

In figure IV.20 we have reported the sensor resistance change versus time for different CO_2 pressure. It evident from the figure that the resistance turns to decrease when the sensor is exposited to the CO_2 gas, furthermore the resistance diminution enhances with increasing CO_2 pressure.

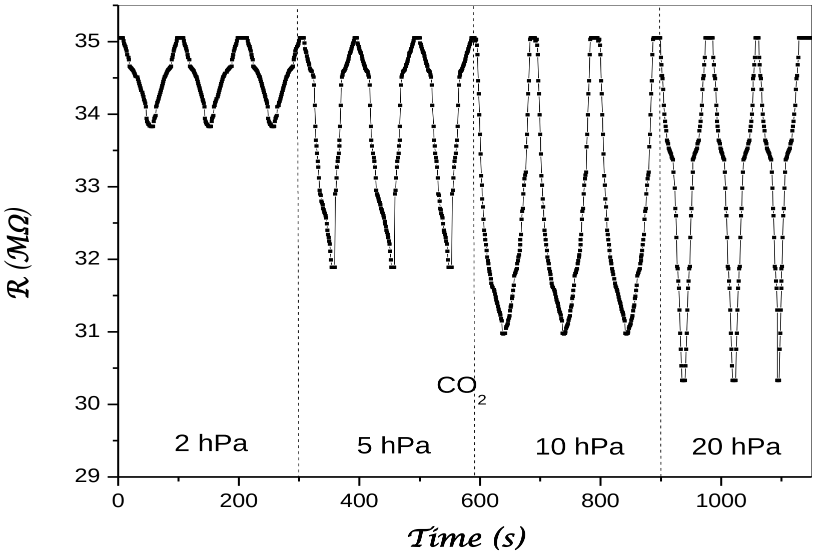

Figure IV.20 *The resistance change versus time at different pressure of CO_2 gas.*

To have more insight on this variation, we have represented the variation of the sensitivity as function of the CO_2 pressure as shown in figure IV.21. As can be seen, the CuO based sensor sensitivity increases with increasing the CO_2 concentration. It can be seen that the responses of sensor are almost linear for lower concentrations and exhibits a tendency to saturate at higher concentrations. The sensor sensitivity rises from 4.67 to 13.46 % with increasing the CO_2 concentration. According to Scott theory [59], the sensor response (S) is represented by the following equation:

$$S = A P_g^b \tag{29}$$

Where Pg is the target gas partial pressure that is directly proportion to its concentration, and the sensor response is characterized by the pre-factor A and exponent b. One can thus easily understand that the sensor response rises continuously with the increase in CO_2 concentration, as observed above.

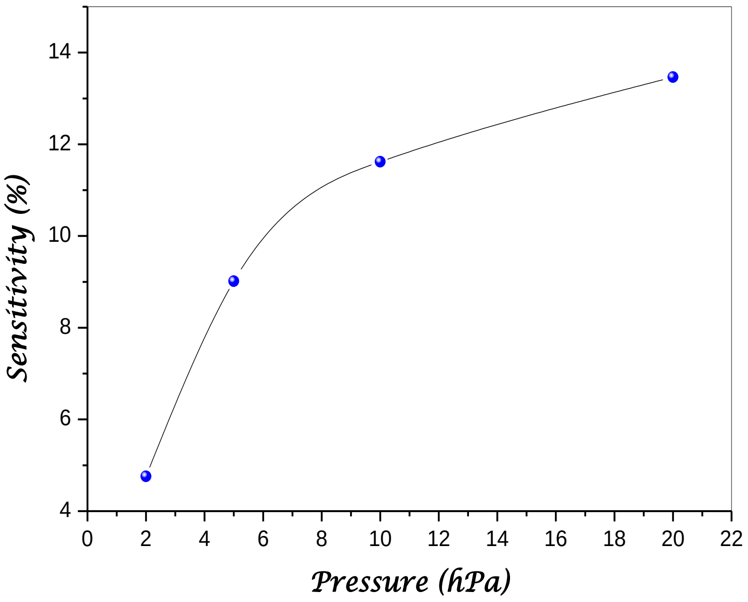

Figure IV.21 *The variation of the sensitivity as function of the CO_2 pressure.*

IV.2.3.3 Response and recovery times

The response and recovery time are important characteristics for gas sensors, they are a consequence of the surface framework accessibility to the sensing gas. Furthermore, the response time includes the gas diffusion toward the sensing surface to react with the chemisorbed oxygen ions, and the subsequent re-oxidation process of the sensing surface to produce oxygen species. The response and recovery time were defined as the time required for the gas sensor to achieve 90% of the total resistance change in the case adsorption and desorption, respectively. In figure IV.22 we have reported the relationship between CO_2 concentrations, the response and recovery time for the gas sensors at operating temperature of 50 °C. The response time was more effected than the response time at each CO_2 concentration. A short response time is useful for the CO_2 detecting for industrial application. The response time is ranged from 29 s to 41 s, whereas the recovery time is ranged from 30 s to 35 s under the studied CO_2 pressure range. However, we noticed that this two parameters decrease with increasing the CO_2 concentration. The increase of the CO_2 concentration leads to improve the response and recovery times, it evident that when the sensor detected more gas particles the phenomena of adsorption and desorption became easier due to the availability of CO_2 particles in the atmosphere.

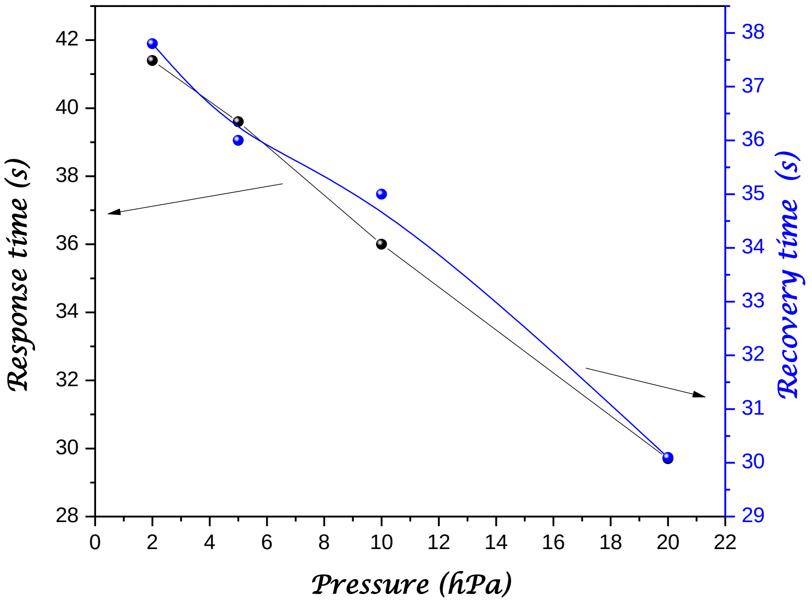

Figure IV.22 *Variation of response and recovery times at operation temperature for different CO_2 pressure.*

Solar cells

In the following section we present the films characterization of the different materials used for fabricated the heterojuctions such as: zinc oxide (ZnO), zinc sulfide (ZnS) and cupric oxide (CuO) and the IV characteristic of the realized solar cells.

IV.3.1 Structural properties

In figure IV.23 (a and b) we have regrouped the XRD diffraction patterns of different films used for the heterojunction based solar cells. The diffraction peaks identification of the deposited ZnO and ZnS thin films on ITO glass (figure IV.23-a) indicates that the deposited ZnO films is characterized by a polycrystalline phase, which is manifested by the three major peaks of the wurtzite structure (100), (002) and (101) and a cubic structure for the ITO films (PDF card # 45-0937). However no significant peak of diffraction relative to the ZnS phase is identified indicating the later has an amorphous structure. The XRD diffraction of CuO films deposited on glass is shown in figure IV.23-b. The CuO films are polycrystalline monoclinic structure with two preferential orientations corresponding to the reflection planes (002) and (111). No peaks corresponding to the Cu_2O are detected, suggesting that the deposited films are exclusively formed with pure CuO phase. With the increase of the deposition time, the emergence of other peak characteristic of CuO phase is observed. This change indicates the film crystallinity improvement.

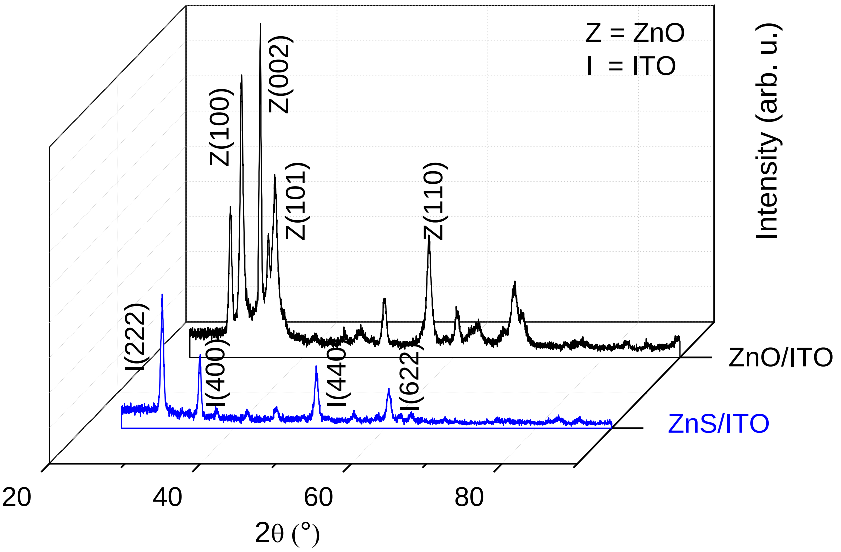

Figure IV.23-a *XRD diffraction patterns of ZnO and ZnS films deposited on ITO glass at 300°C.*

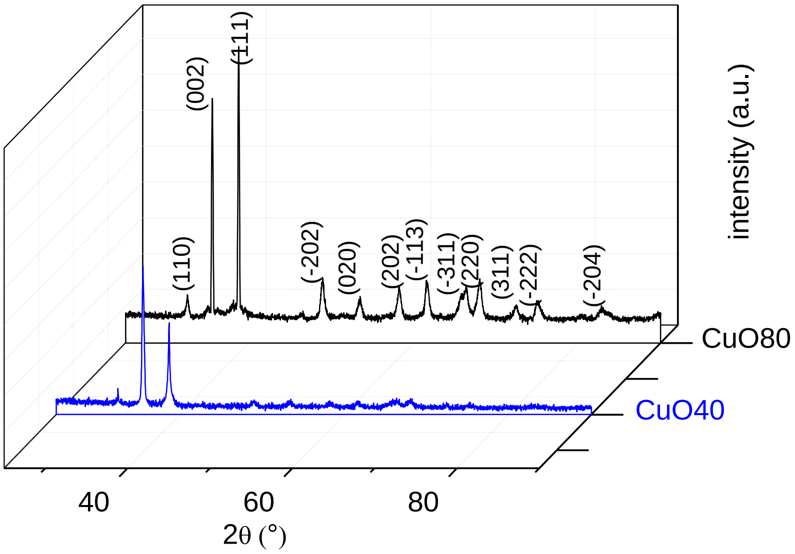

Figure IV.23-b *XRD diffraction patterns of CuO films prepared at 300°C.*

The calculation of the structural parameters and the films thickness of the different deposited thin films are regrouped in the table IV.4.

	(hkl)	D (nm)	ε ($\times10^{-3}$)	δ ($\times10^{14}$ lines/m^2)	d (nm)
ZnO	(002)	20	45	13	116
ZnS	/	/	/	/	123
CuO40	(111)	29	57	10	647
CuO80	(111)	46	35	5	1069

***Table IV.4** The structural parameters and the films thickness of the deposited thin films.*

IV.3.2 Films morphology

The films morphology is studied by means of SEM. The SEM images of the deposited films were showing in figure IV.24. For the two different window layers ZnS and ZnO ,we observe that the elaborated ZnO films deposited on ITO glass substrate has a dense and rough surface with identical average grains size distributed almost uniformly over the all surface (figure IV.24-a). However, the deposited ZnS film on ITO glass substrate reveals a smooth, continuous surface, where it is difficult to distinguish the grains size, confirming the amorphous structure of the deposited layer (figure IV.24-b) as suggested by XRD analysis. For the two CuO absorber layer (CuO40 and CuO80) deposited on glass substrate, we observe that the deposited films are granular, porous, dense, with randomly distribution of grains size (figure IV.24 (c and)). We also observe that an increase in deposition times from 40 to 80 minutes induces a significant improvement in films crystallinity. The films surface becomes less porous with larger grain sizes.

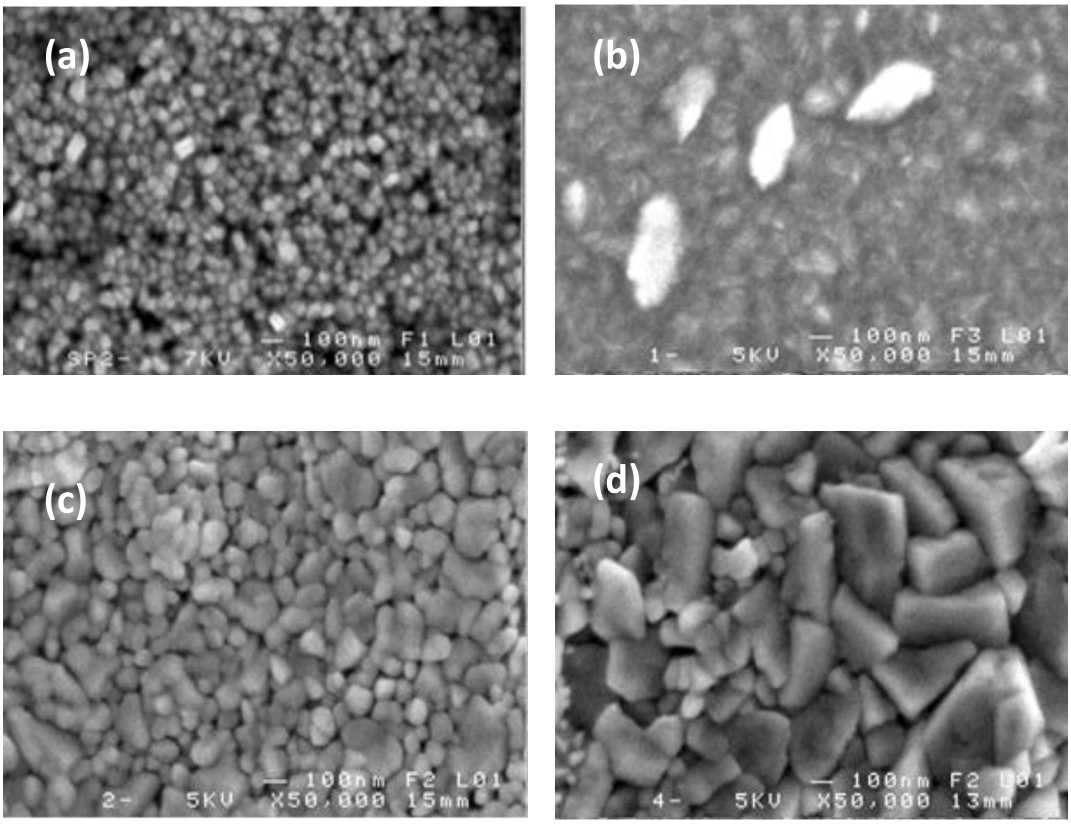

Figure IV.24 *SEM images for the different deposited thin films: (a) ZnO on ITO glass substrate (b) ZnS on ITO glass substrate (c) CuO40 and (d) CuO80.*

IV.3.3 Optical properties

In figure IV.25 (a and b) we have reported the transmittance spectrum of the elaborated thin films deposited at 300°C. ZnO and ZnS films have a good transparency (~ 80%) in the visible range of the wavelength (figure IV.25-a). We noticed that ZnS film has less homogeneity and uniformity compared to ZnO film. The transmittance spectra of CuO films deposited on glass at different times are shown in figure IV.25-b. Since, they are used as absorber layer, the CuO films exhibit a high absorption in the visible wavelengths range (λ <800 nm). Beyond 800 nm, their transmittance reaches the order of 25% for CuO film deposited for 40 min and gradually decreases with increasing thickness for CuO film elaborated for 80 min.

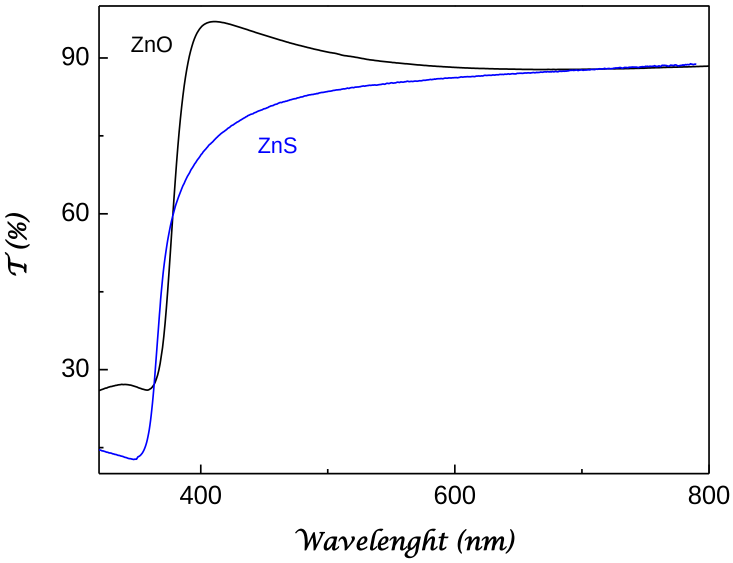

Figure IV.25-a *Transmittance spectrum of the two window layers ZnO and ZnS thin films.*

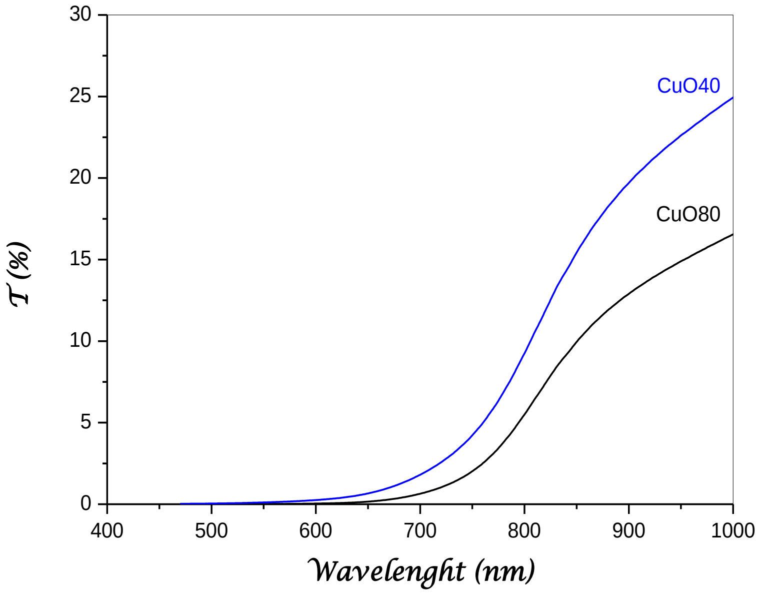

Figure IV.25-b *Transmittance spectrum of the absorber layers CuO thin films.*

The calculated band gap and disorder in the films network of the prepared thin films are illustrated in table IV.5. As can be seen, the deposited ZnO and ZnS present a large band gap, this good transmittance in visible range of the spectrum solar confirms their used as window layer in solar cells. In addition the calculated band gaps for the elaborated CuO films prove also the good applicability of these materials as an activated layer for photovoltaic cells.

	Eg (eV)	E_{00} (eV)
ZnO	3.31	0.035
ZnS	3.43	0.098
CuO40	1.42	0.070
CuO80	1.40	0.056

Table IV.5 *The calculated band gap and disorder of the prepared thin films.*

IV. 4 Solar cells characteristics

In this section we present the current-voltage characteristic of the fabricated p-CuO/n-ZnO and p-CuO/n-ZnS heterojunctions as well as their performance.

IV.4.1 Current-Voltage characteristic

In figure IV.26 (a and b) we have reported the I-V characteristic curve of the two realized p-CuO/n-ZnO and p-CuO/n-ZnS heterojunctions. As can be seen, the I-V characteristic of the heretostructures measured in dark and at room temperature show rectifying properties, indicating the junction formation. The significant reverse current is due to the minority charge carrier concentration which increases by oxygen vacancies and/or impurities. The forward current varies exponentially with positive applied bias (V) and the characteristic can be described by the standard diode equation:

$$\mathrm{I} = \mathrm{I}_S\left(e^{\frac{qV_a}{nKT}} - 1\right) \tag{24}$$

Where k is the Boltzmann constant, T is the absolute temperature, and n is the junction ideality factor, Is the is the saturation current and Va is polarization tension.

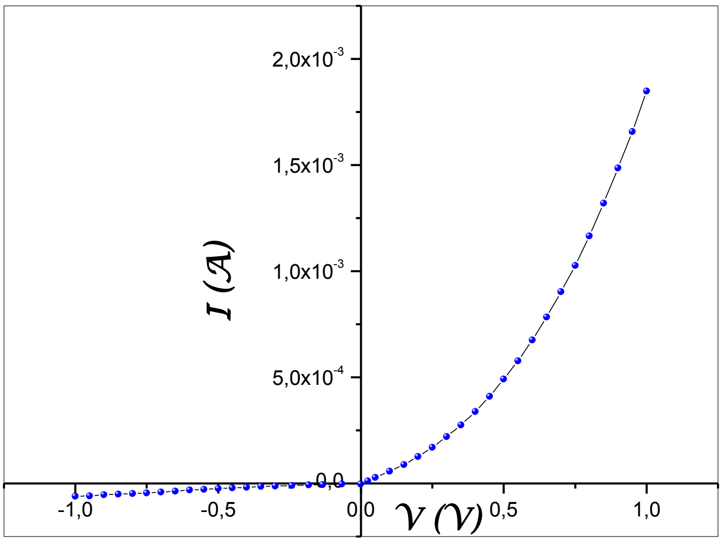

Figure IV.26-a *I-V characteristic curve of the heretojunction p-CuO/n-ZnO.*

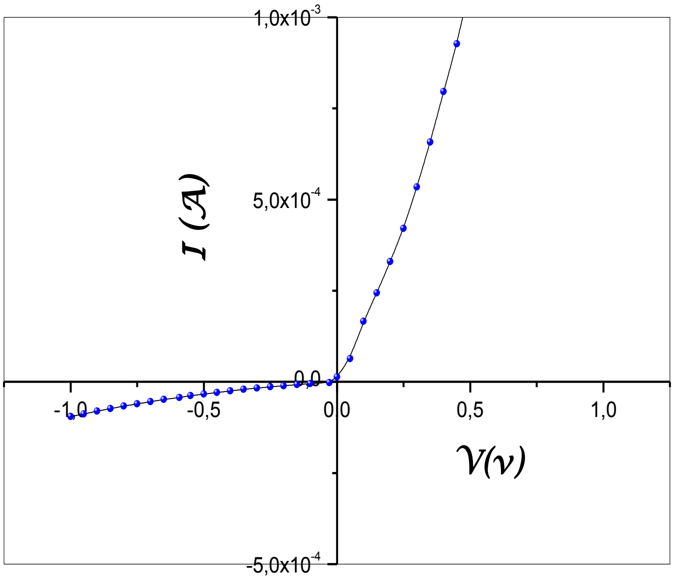

Figure IV.26-b *I-V characteristic curve of the heretojunction p-CuO/n-ZnS.*

In the table IV.6 we have reported the calculated parameters characteristic of the both heretojunctions CuO/ZnO and CuO/ZnS. The values of ideality factor (n) are greater than 2 for both heterostructures this indicate that the mechanism of the current transport cross the junction is not due to the thermal injection over barrier or diffusion [113]. In such a case, several conduction mechanisms have been proposed. The built in potential (Vth) of CuO/ZnO diode is equal to 0.81V with a highest rectification ratio (η) above 28%, thus surpassing that of CuO/ZnS diode (25%). The value of the series resistance (Rs) of CuO/ZnO diode is lower than CuO/ZnS diode this can the related to the nature of amorphous phase of ZnS films. Generally, for heterojunction diode, the structural imperfections at grain boundaries as well as the interface deteriorate its quality [114]. These imperfections are essentially caused by lattice mismatch and change of the preferential crystalline direction.

	CuO/ZnO	**CuO/ZnS**
n	3.46	3.49
V_{th} (V)	0.81	0.10
η (%)	28	25
I_{sc} (A)	1.26×10^{-4}	5.19×10^{-4}
R_s (KΩ)	0.32	0.34
R_{sh}	13	56

***Table IV.6** The parameters characteristic of the heretojunction CuO/ZnO and CuO/ZnS.*

IV.4.2 Solar cell parameters

In figure IV.27 we have reported the I-V characteristic of the both CuO/ZnO and CuO/ZnS solar cells under illumination. The parameters extracted from this figure are regrouped in the table IV.7. The obtained results show that the performance of our diodes under illumination does not exceed about 7×10^{-4} % with low open circuit voltage. We note that for heterostructures CuO/ZnS present the best the photovoltaic effect, it can be related the corresponding to the best crystallized CuO layer with higher thickness. However, these results are the same order of magnitude as those reported in reference [115]. However, it is possible to improve this performance by improving the properties of CuO films and by adjusting other deposition parameters. The effect of annealing can also enhance the efficiency of the solar cells.

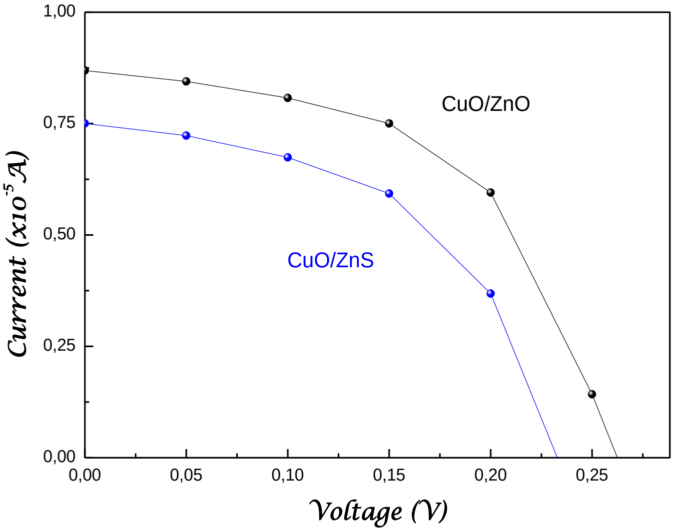

Figure IV.27 *I-V Characteristic of CuO/ZnO and CuO/ZnS solar cells under illumination.*

	J_{cc} (mA/cm^2)	V_{oc} (V)	FF	η (%)
CuO/ZnO	1.94	0.23	0,52	5.2×10^{-4}
CuO/ZnS	2.28	0.26	0,53	7×10^{-4}

Table IV.7 *The parameters of the fabricated solar cells.*

Conclusion

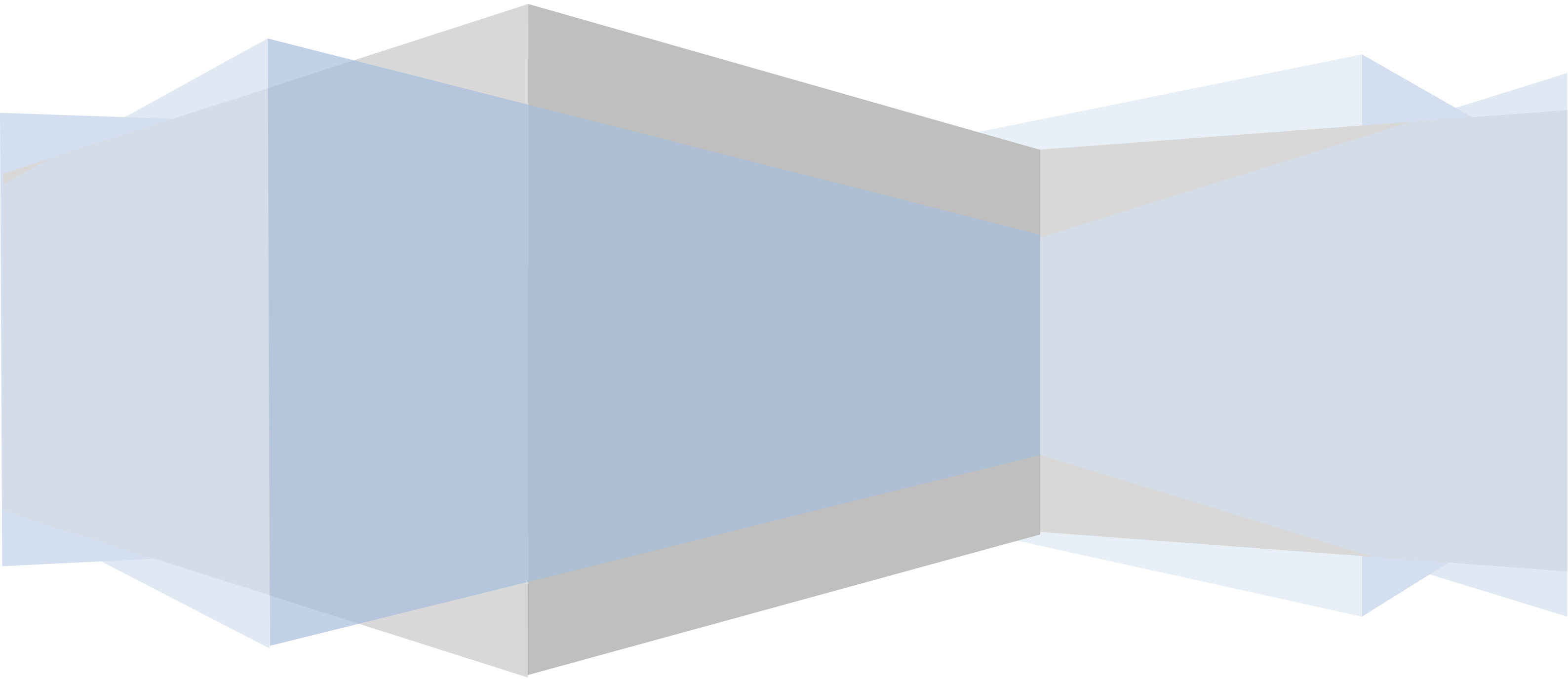

Conclusion

CuO thin films were deposited by spray ultrasonic pyrolysis. The CuO films are deposited with different deposition conditions in order to optimize these parameters for elaborate a CuO films with good quality which can be used in several applications such as: solar cells and gas sensor. The investigated parameters in this study were substrate temperature, flow rate, molarity and nature salt. From the investigation of substrate temperatures using copper chloride as precursor, the deposition rate decrease with increasing the substrate temperature; this is due to the evaporation of reactive species droplets and the thermal convection. The films structure reveals that all deposited films crystallize in monoclinic structure. The calculated texture coefficient reveals that CuO films deposited at 300°C have best crystallization level along preferred orientation (200). The crystallite size decreases from 25 to 19 nm in the investigated substrate temperature. The Raman spectra are composed with three main photon modes Ag and 2Bg located at 296, 334 and 602 cm^{-1} indicating a single CuO phase film formation. The intensity of the three Raman mode decrease with increasing the substrate temperature, due to the reduction in films thicknesses. The decrease in crystallite sizes lead to red shift of the Ag Raman mode. The optical band gap increases with substrate temperature from 1.20 to 1.75 eV, this is related to the decrease in the film disorder from 640 to 960 meV. The electrical conductivity varied from 10^{-5} to 10^{-7} $(\Omega cm)^{-1}$ and the activation energy ranged from 0.294 to 0.311eV. However, the films deposited with copper acetate at higher substrate temperature films grows with low deposition rate. The XRD analysis indicates that the obtained films have a monoclinic structure. The calculated texture coefficient shows that at lower substrate temperature, the films growth along (111) preferred orientation, contrary to preferred orientation $(\bar{1}11)$ found for that deposited at higher substrate temperature. The best crystallinity is found for films prepared at 300°C. The increase of crystallite size and the decrease in strain confirms the crystallinity improvement of films deposited with increasing the substrate temperature. The enlargement in optical band gap corroborates well with the increasing in steepness parameter which leads to reduce the films disorder with increasing the substrate temperature. The electrical conductivity is varied from 10^{-2} to 10^{-7} $(\Omega cm)^{-1}$. The high electrical conductivity is obtained for film deposited at 300 °C. Finally, we can conclude that films elaborated at substrate temperature equal to 300°C have the best optoelectronic proprieties for solar cells conversion.

Increasing salt concentration augment the deposition rate due to the rise of Cu concentration which leads to enhance CuO deposition rate. XRD analysis indicates that all deposited film are polycrystalline in nature with monoclinic structure. The calculated texture coefficient showed that the best crystallinity is found for film deposited with 0.04 M. CuO films deposited with larger salt molarities are characterized by larger crystallites size relatively to those prepared with small molarities. The lattice strain increase with precursor concentration, it can be related to the increase in films network disorder. The intensity of Ag mode increase with the molarity due to the larger films thicknesses. The peak position of Ag Raman mode shifts towards higher wave numbers due to the presence of compressive strain in the film. The SEM micrographs show that deposited films are homogenous, rough and compact. However films deposited with higher precursor concentration are more dense and compact than the ones deposited with lower molarity. The EDS spectra analysis confirms that the films deposited with higher molarity leads to the formation of Cu-rich cupric oxide films, however the films elaborated with lower salt concentration produces an O-rich cupric oxide films. With increasing the molarity, the optical band gap decreases from 1.8 eV to 1.1 eV while the value of the disorder increase from 510 to 770 meV. The Hall effect measurements indicate that the electrical conductivity and the free carriers concentration increase from 1.34 x 10^{-4} to 9 x 10-2 $(\Omega.cm)^{-1}$ and 4.96 x 10^{12} to 7.88 x 10^{13} cm^{-3} with the salt concentration. The electrical conductivity follows faithfully the carriers concentration evolution. The mobility also increase from 16 to 60 (V/cm^2s) due the crystallite size enlargement.

We have also investigated the influence of the sprayed flow rate on CuO thin films properties. We found that at low flow rate the variation of the deposition rate is almost constant equal to 200 nm/min. While, at high flow rate the deposition rate increase considerably. XRD analysis indicates that all deposited films are polycrystalline with monoclinic structure. At low growth rate films exhibit texturation along (002) plane; while at faster growth rate the deviation to plane (111) is observed indicating that the latter plan requires less formation energy than (002) plane. The obtained films have a polycrystalline nanostructure, the obtained crystallite sizes are ranged from 60 to 10 nm. On the other hand an increase in the flow rate causes the rise of internal strain due to the reduction in crystallites size. The optical band gap varied from 1.40 to 1.62 eV in the investigated range of flow rate. This variation can be related to the disorder in films. This suggests that the variation of the optical gap is governed by the disorder in the film network. The measured electrical conductivity is controlled by the free carrier concentration than by their mobility. The carrier mobility is varied from 11 to 540 (cm^2/Vs) in the investing flow rate range. However, the measured mobility in our case is very higher. Film prepared at 25 ml/h have an optical band gap close to 1.4 eV required for solar cells since it matches well with the visible solar spectrum region.

From the investigation of the precursor salt nature, we inferred that the deposition rate of films deposited using copper chloride is three times larger than those resulting from copper acetate. This is probably due to the formation of copper hydroxide $Cu(OH)_2$ which leads to the reduction of the free copper ion Cu^{2+} in the precursor solution prepared by copper acetate. Films deposited with copper acetate are amorphous; however films prepared with copper chloride are polycrystalline with monoclinic structure and presented (200) as preferred orientation. Raman spectra analysis indicates the presence of the three Raman mode Ag and 2Bg located at 294, 344 and 609 cm^{-1} characterize a single CuO phase. The intensity of the two Raman modes Ag and the first Bg mode are higher for the films deposited with copper chloride due to the crystallinity of the deposited films. However the intensity of the second modes Bg increase and shifted to lower wave numbers, it is probably due to the amorphous phase and the disorder in the films network. From the optical band gap calculation we concluded that the use of copper chloride yields to the large band gap of 1.47 eV. However, the films deposited using copper acetate are more disordered due the presence of amorphous phase and confirm the XRD results. SEM images of CuO films deposited using copper chloride as Cu source are dense and homogenous with good adherence with random distributed grains. The mean grains size estimated from the SEM images is equal to 268 nm. While, films elaborated using copper acetate are characterized by a rough and granular surface, consisting of crystallites distributed randomly with the presence of a needle structures. The quantitative analysis extracted from EDS spectra indicates that CuO films elaborated using copper chloride are Cu-rich cupric oxide. Meanwhile, an O-rich cupric oxide had been formed when using copper acetate precursor. The Hall effect measurements indicate that films deposited with copper acetate are more conductor and the free carriers concentration is larger, this is due to the presence of Cu vacancy defect. This is consistent with the fact that Cu vacancy is the most important defect responsible for the p-type conductivity in CuO thin films. However the mobility of films deposited with copper chloride is higher by two decade due to film crystallinity. We can concluded that copper chloride precursor is preferred to realize CuO thin films for solar cell application. However, the use of copper acetate can be favorable for CuO sensing application.

At the end of the present work we have addressed an attempt to produce a gas sensor and solar cells based on CuO thin films. The obtained CuO based gas sensor show a high sensitivity equivalent to 90% at lower operation temperature equal to 50°C. The sensing layer exhibits response and recovery times of 2.45 min and 2.02 min, respectively. The sensitivity of our sensor remains significant even for the lowest methanol concentration equal to 20 ppm. For ethanol sensing, the CuO based gas sensor show a sensitivity equal to 45% towards 300 ppm concentration of ethanol at operation temperature equal to 150°C. The sensing layer exhibits response and recovery times of 2.98 min and 2.11 min respectively. At higher ethanol concentration the sensitivity enhances by 70%. The realized CuO based gas sensor show also a relative gas response equal to 9% at lower operation temperature above 60°C for CO_2 at 5 hPa. The response and recovery times are ranged from 29 to 41 s and 30 to 35 s for different CO_2 pressure. The sensitivity increases from 4.67 to 13.46 % with increasing the CO_2 pressure from 2 to 20 hPa. Modification of experimental conditions in order to obtain more porosity with thinner thickness may be a suitable method to improve the performance of our sensor, particularly response and recovery times. The obtained solar cells devices based on CuO/ZnO and CuO/ZnS heterostructures have a low efficiency, while the best one is found equal to 7×10^{-4} % and a fill factor of about 0.53 for solar cell fabricated with ZnS as window layer and the thicker CuO absorber layer. Since different layers are involved in the solar cells operating, it difficult to diagnostic the efficiency issue. A careful attention can be made in the preparation of different layers and interfaces is necessary. This is an ambitious task which is a perspective and will be a continuity of the present thesis.

References

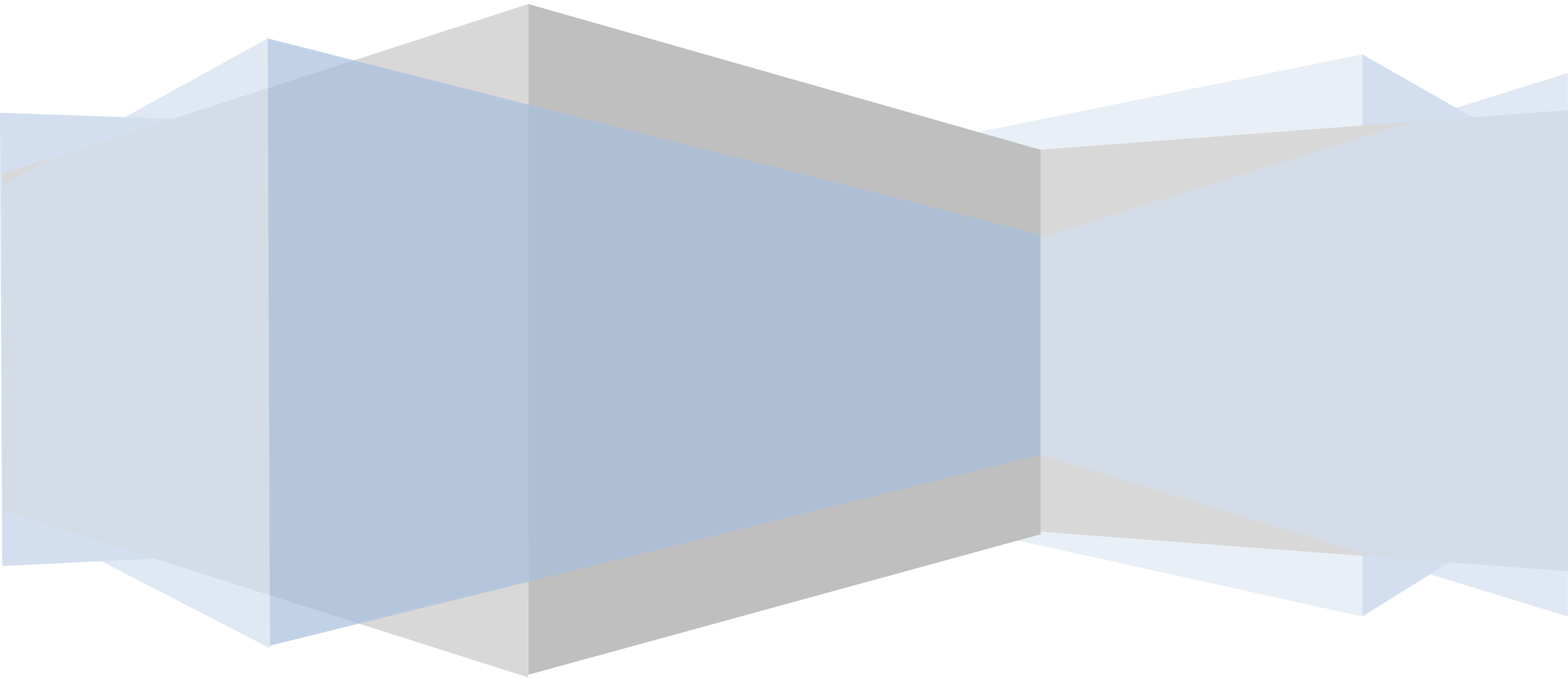

References Introduction

[1] A .De Vos, J. Phys. Appl. Phys. 13 (1980) 839.
[2] V. M. Fthenakis, Renew.Sust.Energ.Rev.8 (2004)303.
[3] B. J. Stanbery, Crit. Rev.Solid Stat. 27 (2002).73
[4] R. W. Collins, A. S. Ferlauto, G. M.Ferreira, C.Chen, J.Koh, R. J.Koval, Y. Lee, J. M.Pearce, and C. R.Wronski, Sol.Energ.Mat.Sol.C.78 (2003) 143.
[5] C. Wadia, A. P. Alivisatos, and D. Kammen, Environ. Sci. Technol. 43 (2009) 2072.
[6] F. Marabelli, G. B. Parravicini, and F. Salghetti-Drioli, Phys. Rev. B 52 (1995) 1433.
[7] T. V. Pham, M. Rao, P. Andreasson, Y. Peng, and J. Wang, Appl. Phys. Lett.102 (2013) 32101.
[8] W. Shockley and H. J. Queisser, J. Appl. Phys. 32 (1961)510.
[9] A. Mittiga, E. Salza, F. Sarto, M. Tucci, and R. Vasanthi, Appl. Phys. Lett.88 (2006)163.
[10] S. Asbrink and L. J. Norrby, Acta Crystall. B26 (1970) 8.
[11] B. Balamurugan,B.R. Mehta Thin solid films 396 (2001) 90
[12] L.S. Huang, S.G. Yang, T. Li, B.X. Gu, Y.W. Du, Y.N. Lu, S.Z. Shi, J. Cryst. Growth 260 (2004) 130.
[13] E.R. Kari, K.S. Brown, Choi, Chem. Commun 23 (2006) 3311.
[14] M. T. S. Nair, L. Guerrero, O. L. Arenas, and P. K. Nair, Appl. Surf. Sci., 150 (1999) 143
[15] N. Serin, T. Serin, S. Horzum, Y. Celik, Semicond. Sci. Technol. 20 (2005) 398.

[16] E.H. Nicollian,. J.R Brews,”*MOS Physics and Technology*”. Wiley, New York (1982)

[17] A.S. Grove “ *Physics and Technology of Semiconductor Devices*” Wiley, New York (1967)

[18] F.J. Arregui. “*Sensors Based on Nanostructured Materials*” Berlin Springer (2008).

[19] S. M. Wilhelm,Y. Tananizawa, and N. Hachemn, Corrosion Science, 22 (1982)791.

[20] Y.S. Gong, C. Lee, C.K. Yang, , J. Appl. Phys. 77 (1995) 5422.

[21] L.S. Huanga, S.G. Yanga, T. Lia, B.X. Gua, Y.W. Dua, Y.N. Lub, S.Z. Shit, J. Cryst. Growth 260 (2004)130.

[22] J.H. Lee, B.W. Yeo, B.O. Park; Thin Solid Films 457 (2004) 333.

[23] C. Luyo, I. Fabregas, L. Reyes, J.L. Solis, J. Rodriguez, W. Estrada, R.J. Candal, Thin Solid Films 516 (2007) 25.

[24] S. Kose, F. Atay, V. Bilgin, I. Akyuz, , Mater. Chem. Phys. 111 (2009) 351.

[25] K. Santra, C.K. Sarkar, M.K. Mukherjee, B. Ghosh, Thin Solid Films 213 (1992) 226.

[26] P.K. Ooi, S.S. Ng, M.J. Abdullah, H. Abu Hassan, Z. Hassan Materials Chemistry and Physics 140 (2013) 243.

[27] V. Dhanasekaran , T. Mahalingam, R. Chandramohan, Jin-Koo Rhee , J.P. Chu d Thin Solid Films 520 (2012) 6608.

[28] S. C. Ray, Solar Energy Materials & Solar Cells 68 (2001) 307.

[29] L. D. Valladares , D. H. Salinas, A. B. Dominguez, D. A. Najarro ,S.I. Khondaker , T. Mitrelias, C.H.W. Barnes , J. A. Aguiar , Y. Majima Thin Solid Films 520 (2012) 6368.

[30] I.A .Ezenwa, Chem. Phys, 50 (2012) 41.

[31] I. Singha, R.K. Bedi Applied Surface Science 257 (2011)7592.

[32] D. Gopalakrishna, K. Vijayalakshmi ,C. Ravidhas , J Mater Sci: Mater Electron, 08 (2012) 667.

[33] J. Moralesa, L. Sa´ncheza,, F. Martı´nb, J.R. Ramos-Barradob, M. Sa´nchezb Thin Solid Films 474 (2005)133.

[34] A. H. Mashhad-Toroghi , N. Shahtahmasebia, E. Azhira, P. Madahia, M. Mashreghi Thin Solid Films 15 (2012) 852.

[35] R. Shabu , A. Moses Ezhil Raj , C. Sanjeeviraja, C. Ravidhas Materials Research Bulletin 68 (2015) 1.

[36] L. Guo, M. Zhao, D.M. Zhuang, M. Jie Cao, L. Ouyang, X. Li,R. Sun, Z. Ga, Applied.Surface. Semiconductor. 359 (2015) 40.

[37] I. Singha, R.K. Bedi, Appl. Surf. Sc. 257 (2011) 7592.

[38] Y. Gu¨lena, F.Bayansalb, B.S-ahinb, H.A.C- Etinkarab, H.S.Guderb Ceramics International 39 (2013) 6475.

[39] V. Saravanakannan, T. Radhakrishnan Mater. Res. Bull. 6 (2014) 306.

[40] Y. Akaltun Thin Solid Films 594 (2015) 30.

[41] A. T Ravichandran, K Dhanabalan,., R Chandramohan,., A Vasuhi, and. N.Parameswaran, Thin Solid Films 21 (2014) 007.
[42] F.K Mugwang, P.K Karimi, W.K Njoroge, O Omayio and S.M Waita,Int. J. Thin Film Sci. Tec. 1 (2013) 15.
[43] M. Li Flora, R. Waddingham , I .William. Milne J, A. Flewitt ,S.Speakman ,J. Dutson , S. Wakeham , M. Thwaites Thin Solid Films 520 (2011) 1278.
[44] V. Dhanasekaran, T. Mahalingam Journal of Alloys and Compounds 539 (2012) 50.
[45] W. Y. Ching, Y.-N. Xu, K. W. Wong, Phys. Rev. B 40, (1989)7684.
[46] C.Y.Chiang, Y. Shin and S. Ehrman Journal of The Electrochemical Society, 159 (2012) 227.
[47] A. Kargar, Y. J.Sung J. Kim,T. Riley ,X. Pan, D.Wang, ASC Nano 12 (2011) 11112.
[48] J. Wu, Engineering and Applied Science 154 (2010) 233.
[49] R.Naeema, R. Yahyaa, A. Pandikumarb, N. M. Huangb,M. Misrana, Z. Arifina, M. Mazhar Materials Today Communications 4 (2015) 141.
[50] H. Kidowaki, T. Oku, T. Akiyama Journal of Physics: Conference Series 352 (2012) 12022.
[51] E. O. Omayio, P. M. Karimi, W. K. Njoroge, F. K. Mugwanga Int. J. Thin Film Sci. Tec. 2 (2013) 25
[52] J.P. Kim, E. Sick Pak, T. Eun Hong, J.S.Bae, M. Gyu Ha, J. Sung Jin, E. D. Jeong , K. S. Hong Ceramic Processing Research 13 (2012) 96.
[53] T. Oku , R.Motoyoshi, K.Fujimoto,T.Akiyama, B. Jeyadevan, J.Cuya Journal of Physics and Chemistry of Solids 72 (2011) 1206.
[54] R.Palitha Wejisundera, Ceramics Silikáty 54 (2010) 19.
[55] A. Bhaumik , A. Haque , P. Karnati , M.F.N. Taufique , R. Patel , K. Ghosh Thin Solid Films 33 (2014) 455.
[56] T. Ishihara, K. Kometani, Y. Nishi, Y. Takita, Sens. Actuators B 28 (1995) 49.
[57] Y. Zeng, T. Zhang, H. Yang, L. Qiao, Q. Qi, F. Cao, Y. Zhang, R. Wang, Appl. Surf. Sci. 255 (2009) 4045.
[58] S. Aygun , D. Cann, J. Phys. Chem. B 109 (2005) 7878.
[59] L. Presmanes, A. Chapelle, F. Oudrhiri-Hassani, A. Barnabé, P. Tailhades Applied Surface Science 4715 (2011) 256.
[60] D. H. Trinh, T. Kubart, T. Nyberg, M. Ottosson, L. Hultman, H. Högberg, Thin Solid Films 23(2008) 8352.
[61] A Rydosz , ASzkudlarek Sensors 15 (2015) 20069.

[62] R.R. Chamberlin, J.S. Skarman, J. Electrochem. Soc. 113 (1966) 86.

[63] A.A. Rizkalla and A.H. Lefebvre, J. Eng. Power, 97 173 (1975).

[64] C.M. Lampkin, Progress in Crystal Growth and Characterization of Materials, 4 (1979) 405.

[65] R. Rajan and A.B. Pandit, Ultrasonics, 39 (2001) 235.

[66] A.M. Ganan-Calvo, J. Davila, and A. Barrero, J. Aerosol Sci., 28 (1997) 249.

[67] G.K. Williamson, W.H. Hall, Acta Mater. 1 (1953) 22.

[68] C.S. Barrett, T.B. Massalski, Structure of Metals, Pergamon, Oxford, (1980) 204.

[69] V. Bilgin, S. Kose, F. Atay, I. Akyuz, J. Mater. Sci. 40 (2005) 1909.

[70] M. Pinczlits, G. Spingholz and G. Bauer, Appl. Phys. Lett , 73(1998) 250.

[71] F.Urbach, Phys 92 (1953) 1324.

[72] V.F. Drobny, D.L. Pulfrey, 61 (1979) 89.

[73] T. Nakamoto, M. Yosihioka, Y. Tanaka, K. Kobayashi, T. Moriizumi, S. Ueyama and W. S. Yerazunis, Sens. Actuators B, 116 (2006)202.

References Chapter III

[74] P.K. Nair, M.T.S Nair, V.M. Gaecia, O.L Arenas, Y. Pena, A. Castillo. Solar Energy Mater and Solar Cells Soc. 313(1998) 52.

[75] S. Kose, F. Atay, V. Bilgin, I. Akyuz, Mater. Chem. Phys. 111 (2009) 351.

[76] J. Morales, l. Sanchez, F. Martin, J.R. Barrado, M. Sanchez, Electrochem. Acta 49 (2004) 4589.

[77] T. Maruyama, Jpn. J. Appl. Phys. 37(1998) 4099.

[78] K.H. Yoon, W.J. Choi, D.H. Kang, Thin Solid Films 372 (2000) 250.

[79] I. Singh, G. Kaur, R.K. Bedi, Appl. Surf. Sci. 257 (2011) 9546.

[80] H. Fan, B. Zou, Y. Liu, S. Xie, Nanotechnology 17 (2006) 1099.

[81] A.Chaturvedi , C.Sathe, Int. J.of Mater., Mechanics and Manufacturing 2 (2014) 1.

[82] V. Swamy, B. C. Muddle , Q. Dai, Appl. Phys. Lett. 89 (2006) 163.

[83] J.Cheng, Z. Ma, Zhao, L. Qi, Chem. Mater. 7 (1995) 663.

[84] S. P. S. Porto, P. A. Fleury, T. C. Damen, Phys. Rev. 154 (1967) 522.

[85] E.A. Davis, N.F. Mott, Phil. Mag. 22 (1970) 903.

[86] J. Morales, L. Sánchez, F. Martín, J.R. Barrado, M. Sánchez, Thin Solid Films 474 (2005) 133.

[87] A. S. Kumar, K. Perumal, P. Thirunavukkarasu, Optoelectron. Adv. Mater. Rapid Commun. 4 (2010) 831.

[88] M.Y. Cho, M.S. Kim, K.G. Yim, D.Y. Lee, J.S. Kim, J.Y. Leem, J. Nanosci. Nanotechnol. 8 (2011) 7479.

[89] K. Mageshwari, R. Sathyamoorthy, Mater. Sci. Semicond. Process. 16 (2013) 337.

[90] H. Miyaga, J. of Mater. Sci.34 (1999)105.

[91] J.H. Lee, B.W. Yeo, B.O. Park, Thin Solid Films 457 (2004) 333.

[92] C. Luyo, I. Fabregas, L. Reyes, J.L. Solis, J. Rodriguez, W. Estrada, R. J. Candal, Thin Solid Films 516 (2007) 25.

[93] Y.S. Kim, I.S. Hwang, S.J. Kim, C.Y. Lee, J.H. Lee, Sens. Actuators B 135 (2008) 298

[94] V. Dhanasekaran, Mater. Sci. Semicond. Process. 30 (2013) 436.

[95] L. D.Valladares, D. H.Salinas, A. B. Dominguez, D. A.Najarro, S.I. Khondaker, T. Mitrelias. W. Barnes, J. A. Aguiar, Y. Majima, Thin Solid Films 520 (2012) 6368.

[96] T. Okun, R. Motoyoshi, K. Fujimoto, T. Akiyama, B. Jeyadevan, J. Cuya, J. Phys. Chem. Solids 72 (2011) 1206.

[97] H. Moualkia, S. Hariech, M.S. Aida, N. Attaf, E.L. Laifa, J. Phys. D: Appl. Phys. 42 (2009) 135404.

[98] S. Schröder, A. Duparré, L. Coriand, A. Tünnermann, D.H. Penalver, J.E. Harvey, Opt. Express 19 (2011) 9820.

[99] T. Yu, C.H. Sow, A. Gantimahapatruni, F.C. Cheong, Y. Zhu, K.C.Chin, X. Xu, C.T. Lim, Z. Shen, J.T.L. Thong, A.T.S. Wee, Nanotechnology 16 (2005) 1238.

[100] L.Hidmi, and M.Edwards, Environment Science and Technology, 33

(1999) 2607.
[101] H. Hagemann, H. Bill, W. Sadowski, E. Walker, and M. Francois, Solid State Commun. 73 (1990) 447.
[102] Y. S higesato, A. Murayama, T. K amimori, K.M atsuhiro Appl. Surf. Sci. 33 (1988) 804.
[103] V. F. Drobny , D. L. Pulfey Thin Solid Films 61 (1979) 89.

[104] Y.S. Kim, I.Hwang, S.Kim, C.Lee, J.Lee, Sensors and Actuators B 135 (2008) 298.

[105] A. S. Zoolfakar, M. Z.Ahmad , R. A. Rani , J. Z. Ou , S. Balendhran, S. Zhuiykov, K.Latham, W. Wlodarski, K.Kalantar Actuators B 185 (2013) 620.

[106] M.L. Zhong, D.C. Zeng, Z.W. Liu , H.Y. Yu, X.C. Zhong, W.Q. Qiu Acta Materialia 58 (2010) 5926

[107] I.D .Kim, A. Rothschild; B.H. Lee, D.Y. Kim, H.L.Tuller, Nano Lett., 6 (2006) 2009.

[108] M. Mitesh Parmar, K.Rajanna ,International Journal sensing materials 4 (2011) 710

[109] X. Gou, G. Wang, J. Yang, J. Park, D. Wexler, Journal of Materials Chemistry 18 (2008) 965.

[110] L. Liao, Z. Zhang, B. Yan, Z. Zheng, Q.L. Bao, T. Wu, C.M. Li, Z.X. Shen, J.X. Zhang, H. Gong, J.C. Li, T. Yu, Nanotechnology 20 (2009) 345.

[111] H.T. Hsueh, S.J. Chang, F.Y. Hung, W.Y. Weng, C.L. Hsu, T.J. Hsueh, S.S. Lin, B.T. Journal of the Electrochemical Society 158 (2011) 106.

[112] C. Wang, X.Q. Fu, X.Y. Xue, Y.G. Wang, T.H. Wang, Surface Nanotechnology 18 (2007) 78.

[113] R. Rediker,S.Stopek,J.H.R.Ward, Solid State Electron.7 (1964) 621.

[114] H. Matsuura, T.Okuno , H.Okushi, K.Tanaka, Journal Applied Physic. 55 (1984) 1012.

[115] H.Kidowaki, T.Oku and T. Akiyama IJRRAS 13 (2012) 67.

Publications

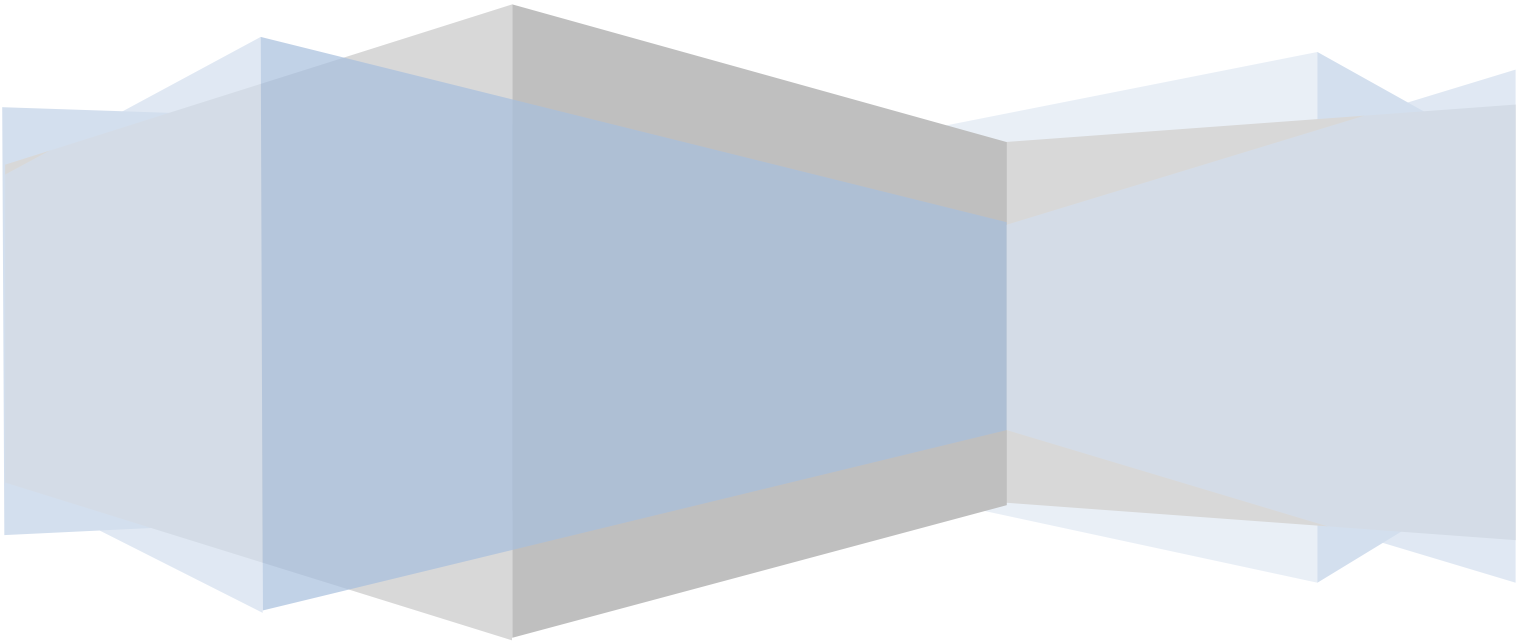

Gap states density measurement in copper oxide thin films

Article *in* Materials Science in Semiconductor Processing · April 2016

Impact Factor: 1.96 · DOI: 10.1016/j.mssp.2016.01.007

4 authors, including:

Meryem Lamri zeggar
University of Constantine 1
7 PUBLICATIONS **12** CITATIONS
SEE PROFILE

M.s. Aida
University of Constantine 1
134 PUBLICATIONS **1,123** CITATIONS
SEE PROFILE

Materials Science in Semiconductor Processing 45 (2016) 32–35

Contents lists available at ScienceDirect

Materials Science in Semiconductor Processing

journal homepage: www.elsevier.com/locate/mssp

Gap states density measurement in copper oxide thin films

M. Lamri Zeggar, M. Messaoudi, M.S. Aida*, N. Attaf

Laboratoire Couches mince et interface faculte des Science, Université frères Mentouri Constantine –Constantine, Algerie

ARTICLE INFO

Article history:
Received 31 October 2015
Received in revised form
26 December 2015
Accepted 14 January 2016

Keywords:
Density of states
Thin films
Spray pyrolysis
Solar cells

ABSTRACT

The density of gap states near the Fermi level have been measured in copper oxide (CuO) thin films deposited by spray pyrolysis technique. The measurement method is based on the exploitation of the current–voltage characteristics of the space charge limited current (SCLC) measured in a sandwich Au/CuO/Au structure. The measured gap states density is equal to $1.5 \times 10^{14}\ \text{cm}^{-3}$ and $2.0 \times 10^{14}\ \text{eV}^{-1}$ respectively in films prepared at 300 and 400 °C substrate temperature, while the defect position are located at 16 and 20 meV above Fermi level. The carriers mobility and concentration are also determined from SCLC, the obtained results are in good agreement with Hall effect measurement ones.

1. Introduction

A large research activity have been devoted to new materials investigation for low cost thin films solar cells. Generally solar cell device is based on pn homo-junction or an heterojunction between two semiconductors with different gaps. Thin films based heterojunction solar cells is formed with a stack of buffer layer (such as CdS or ZnS) and an absorber layer. The commonly used absorber layers are CuIn(Ga)Se, Cu_2ZnSnS_4, CuO and SnS films. The incident photons are wholly absorbed and converted to free carriers in this layer. Thereafter solar cells performance i.e photocurrent , open circuit voltage and efficiency are close related to the electronic properties of the absorber layer. The presence of electronic defects in the band gap is crucial and may be a serious drawback of cells conversion, they hinder photo-generated charges collection through their recombination. Therefore, determination of the density of states (DOS) localized in the material band gap is an ambitious task and their diagnostic is important for the study of material dedicated to photovoltaic conversion. Several techniques have been used for DOS measurement in semiconductors such as: field-effect measurements [1], capacitance measurements [2], space charge limited current (SCLC) [3], deep-level transient spectroscopy (DLTS) [4] and photoluminescence (PL) measurements [5]. Among these techniques the space charge limited conduction (SCLC) technique has been extensively used for measurement of the DOS for amorphous hydrogenated silicon (*a*-Si:H) [6], organic semiconductors [7] and nano-cluster carbon [8]. The experimental measurement requested by this technique is simple and easy , it needs less equipments by comparison to the other techniques. It is based only on the exploitation of the current–voltage characteristics. Copper oxide (CuO) has emerged as a promising material as absorber layer in solar cell [9,10]. CuO is a monoclinic semiconductor with an optical band gap ranged from 1.21 to 1.55 eV [11] which matches well with the solar spectrum and enjoys a high absorption coefficient in visible region which is suitable for solar energy conversion. Moreover, it is a p type semiconductor and is considered as a good partner to CdS or ZnS to form with an heterojunction necessary for thin films solar cells production [12]. On the other hand it is composed of inexpressive, no-toxic and available elements. To our knowledge no studies have been devoted to investigation of gap state density in CuO. The present work deals with the estimation of the density of localized state near the Fermi level and the carrier mobility in CuO thin films deposited by ultrasonic spray pyrolysis, using the space charge limited conduction (SCLC) measurements.

2. Experimental details

Copper oxide thin films have been prepared by ultrasonic spray pyrolysis. The precursor solution was prepared by dissolving 0.05 M copper chloride ($CuCl_2.2H_2O$) in distilled water. The precursor solution is sprayed, using an ultrasonic generator with a frequency of 40 KHz, in fine droplets of 40 μm diameter on heated glass substrate in ambient air. Films are formed by pyrolytic reactions. During deposition, the substrate temperature is kept at 300 and 400 °C. This temperature range is chosen to ensure a complete precursor decomposition and to avoid the presence of chloride in films network. Deposition time was fixed equal to 30 minutes.

---

* Corresponding author.
E-mail address: aida_salah2@yahoo.fr (M.S. Aida).

http://dx.doi.org/10.1016/j.mssp.2016.01.007
1369-8001/

Films thicknesses were determined by ellipsometry measurements. Films structural properties were determined by XRD using Philips X'Pert system with Cu K_α radiation ($\lambda_{Cu}=0.154$ nm). The space charge limited conduction (SCLC) measurements was carried using sandwich structure (Au/CuO/Au). The bottom contact layer, with a thickness of 200 nm, was deposited by DC sputtering of a high purity gold target, using 2.5 KV DC bias, on glass substrate surface prior to CuO deposition. The top contact, formed with 2 mm^2 area Au dots, were deposited on CuO film surface by the same sputtering system. The contacts were ohmic in nature. Currant-voltage (I–V) characteristic were measured by Keithley electrometer 610 in dark and ambient temperature. The applied voltage is varied from 0 to 40 V.

Space charge limited current (SCLC) phenomenon occurs in semiconductors and insulator once the number of carriers injected into the sample exceeds the traps concentration in the sample. In this situation, the electric field in the sample becomes non-uniform, and the current no longer follows Ohm's law. Therefore, at voltages below traps filling limit, the semiconductor exhibits an ohmic behavior. However, at voltages where the injected charges are comparable to the thermal ones, the semiconductor current -voltage characteristic changes from ohmic to SCLC and its behavior obeys to the called the Mott-Gurney law given by [13]:

$$J = 9\varepsilon_s \mu V^2/8d^3 \qquad (1)$$

where ε_s and μ are the permittivity and the mobility of the material respectively, d is the sample thickness and V is the applied voltage.

Assuming an uniform distribution, the density of state near the Fermi level is calculated from sample J–V characteristic in the SCLC regime using de Boer method [14]. Taking two points (J_l,V_1) and (J_2,V_2) on the measured J-V-curve in the SCLC regime ,the Fermi level shift (due to the applied bias) $\Delta E_F=E_{F2}-E_{F1}$ corresponding to voltage change $\Delta V=V_1-V_2$ is calculated according to the following relation [14]

$$\Delta E_F = KT \ln\left(J_2.V_1/J_1.V_2\right) \qquad (2)$$

Where J_1, and J_2 are the current densities measured at the bias V_1 and V_2 respectively

The defect density average N_s in the band gap between E_{F1} and E_{F2} is given by [14] :

$$N_s = 2e_s\Delta V/ed^2\Delta E_F \qquad (3)$$

where ε_s is the permittivity of the material, d is the sample thickness, ΔV and ΔE_F

the bias increment and the corresponding Fermi level respectively and e is the elementary electrical charge.

The trap density was calculated using Eqs. 2 and 3. Films should be thick enough (higher than 1 μm) to have an accurate measurement of the gap density [14].

Hall effect measurements were carried in a dark and at ambient temperature using Van der Paw structure.

3. Results and discussion

In Fig. 1 we have reported a typical XRD spectrum of CuO thin film prepared by spray pyrolysis with substrate temperatures 300 and 400 °C. As can be seen, two peaks assigned respectively to the planes (111) and (002) of CuO tetragonal structure are present (PDF card #45-0937). No peaks related to Cu_2O phase are seen. Dominant CuO phase has been also reported in several studies [15–17] where (002) preferential orientation is observed.

Increasing substrate temperature reduces the diffraction peaks intensities, this is due to film thickness reduction . As shown in Table 1, the thickness of CuO film deposited at 300 °C substrate temperature is equal to 2800 nm, however the film prepared at 400 °C is thinner with 1800 nm. The reduction of films thickness with increasing substrate temperature is due to air convection around the substrate that may carry droplet away from the substrate. The same conclusion has been reported in ZnO thin films prepared by spray pyrolysis [18].

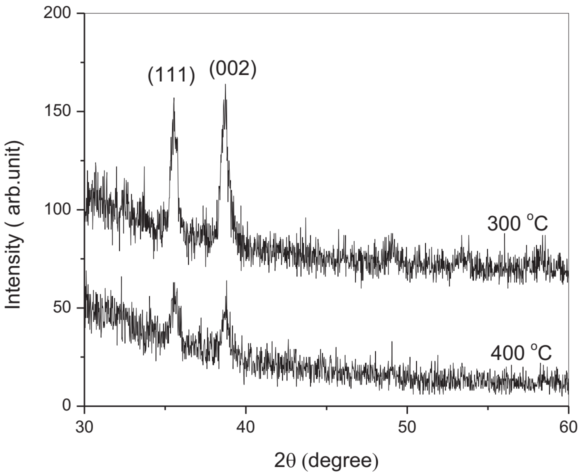

Fig. 1. XRD pattern of CuO thin film deposited by spray pyrolysis with substrate temperatures of 300 and 400 °C .

Table 1
Optical band gap, conductivity, defect density and position in films deposited at 300 and 400 °C substrate temperature.

Substrat Temperature (°C)	Eg (eV)	Conductivity $(\Omega\ cm)^{-1}$	DOS $(cm^{-3}eV^{-1})$	Position ΔE_F (meV)
300 °C	1.37	6.64×10^{-4}	1.5×10^{14}	16
400 °C	1.41	6.90×10^{-2}	2.2×10^{14}	20

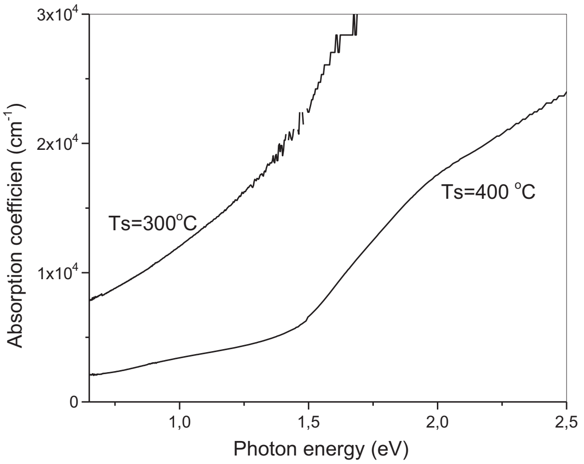

Fig. 2. Absorption coefficient as a function of photon energy of CuO films prepared with 300 and 400 °C substrate temperatures.

In Fig. 2 we have reported the variation of the optical absorption coefficient, of different CuO films, calculated from films transmittance in the visible range. As can be seen, the film deposited at 300 °C exhibits a lager absorption coefficient than the film prepared at 400 °C substrate temperature. This is consistent, as shown in Table 1, with the narrower band gap measured in this film. This suggests that 300 °C substrate temperature is suitable to produce CuO thin films candidate as absorber layer in thin films solar cell.

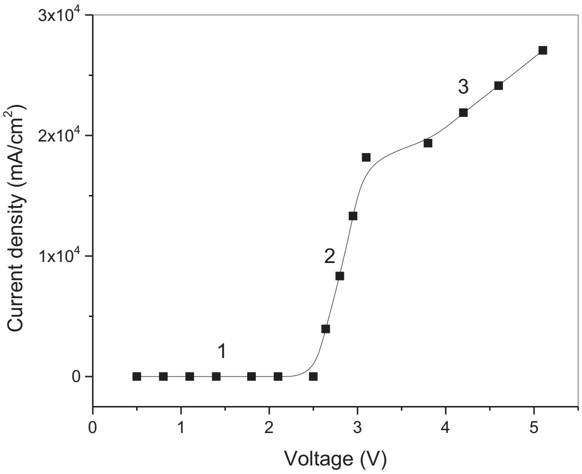

Fig. 3. Current–voltage characteristic of Au/CuO/Au structure in dark and at ambient temperature three different regimes are visble: 1- ohmic 2- SCLC and 3- trap free current regime.

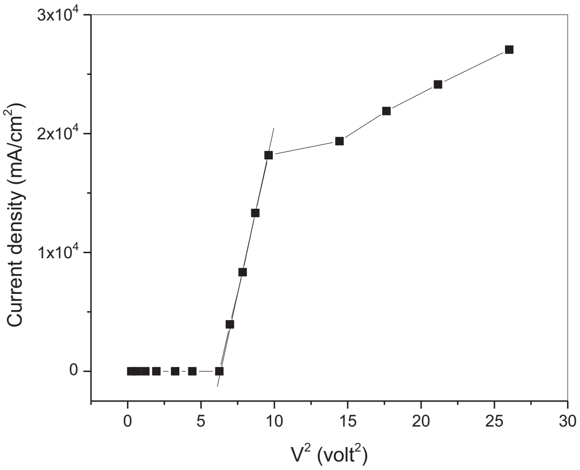

Fig. 4. Variation of current as a function of the square of voltage.

In Fig. 3 we have drawn the current voltage characteristic of CuO sample, the curve exhibits three different regions. At voltages below the traps filling limit voltage (regime labeled 1 in Fig. 3), the sample exhibits an ohmic characteristic. In this regime only the thermal carriers contribute in the current transport. With bias increasing, the current behavior changes, it began to increase sharply, this regime labeled 2 corresponds to the departure from the ohmic regime and the so called SCLC regime is established. In this situation the injected carriers become comparable to the thermally excited ones.

With further voltage increasing , the regime of trap free appears (regime labeled 3 in Fig. 3). The voltage V_{SCLC}, at which the transport regime changes from ohmic to SCLC, occurs when the injected charges concentration is comparable to the thermal excited ones. it can be expressed as [12]:

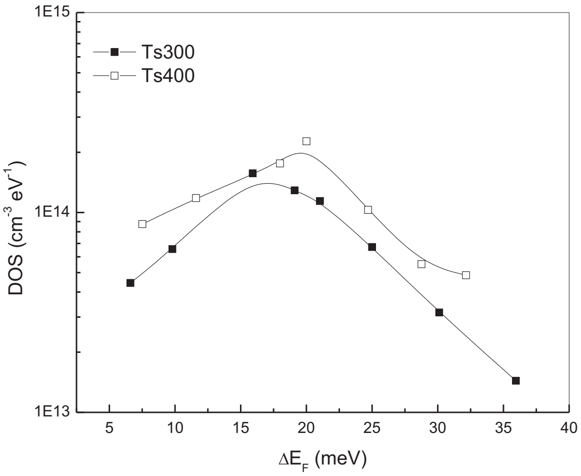

Fig. 5. Density of gap states in the midgap of CuO films prepared at 300 and 400 °C.

$$V_{SCLC}=\frac{e\,.n_0.\,d^2}{\epsilon} \tag{4}$$

where n_o is the thermally excited carriers concentration , d is film thickness, ε is the material permittivity and e is the electronic charge .

In SCLC regime, the density current–voltage characteristics can be expressed using Eq. (1). According to this relation, in SCLC regime, the current varies quadratically as function of voltage. In Fig. 4 we have drawn the current variation as a function of V^2, the observed linear variation confirms the establishment of the SCLC behavior. The slope of this variation yields information about the mobility. This method has been widely used to estimated the mobility in organic semiconductors [19–22].

The density of localized states near Fermi level are estimated using the Eq. (2) and Eq. (3). The obtained results are reported in Fig. 4. The calculated defect density in CuO films prepared at 300 and 400 °C substrate temperatures, are equal to $1.5\times10^{14}\,\mathrm{cm}^{-3}$ and $2.2\times10^{14}\,\mathrm{cm}^{-3}$ respectively (Table 2). The maximum defects density is located at 16 meV above Femi level position in film prepared at 300 °C and at 20 meV in the film prepared at 400 °C. These defects may originate from the dangling bonds caused by oxygen vacancies or oxygen atoms in interstitial position. The presence of these defects is reported in the literature in CuO thin films [23–25]. Calculations reveal that midgap states can be introduced by oxygen vacancies and antisites defects [24]. Although Cu vacancies are the most stable defects in CuO, theoretical calculations indicate that , they do not introduce states within the band gap, but in a shallow levels that act as acceptor impurities [25]. The gap state defects are slightly larger in the film prepared at 400 °C substrate temperature than in the film prepared at 300 °C, this can be attributed to the increase in the oxygen vacancy, due to its volatility, with increasing substrate temperature. (Fig. 5).

In Table 2 we have reported the calculation results of the free carriers concentration and mobility. Once knowing the V_{SCLC} with corresponds to the departure from the ohmic to the SCLC regime

Table 2
Values of mobility and carriers concentration deduced from SCLC and Hall effect measurements.

Substrate Temperature (°C)	Film Thickness (nm)	Carriers Mobility ($V^{-1}cm^2s^{-1}$)		Carriers Concentration (cm^{-3})	
		SCLC	Hall effect	SCLC	Hall effect
300	2800	14.7	17.4	6.7×10^{14}	3.2×10^{14}
400	1800	10.2	12	2.6×10^{16}	10^{16}

with is equal to 2.4 V, the free carriers concentration can be easily estimated using Eq. (4). While the carrier mobility is estimated from the slope of the variation

J–V^2 characteristics in the SCLC regime according to Eq. (1). The dielectric constant ε_{CuO} was taken equal to 18.1 [26].

The obtained results are compared to the calculated values from the Hall effect measurement, as reported in Table 1, the derived results from the SCLC measurement are comparable to Hall effect ones. The large free carriers density measured and calculated in the film prepared at 400 °C (Table 2) explains the higher electrical conductivity measured in this film, about two orders of decade larger than in the film prepared at 300 °C (Table 1).

4. Conclusion

In the present work we have determined the density of states located in the band gap of CuO thin films prepared by ultrasonic spray pyrolysis. The defects density was deduced from the current–voltage characteristic in the SCLC regime using de Boer model. The defects are located near the Fermi level with a concentration in the order of $10^{14}\,\mathrm{eV}^{-1}\,\mathrm{cm}^{-3}$. Substrate temperature increase slightly the defect concentration due to the increase in oxygen defects. The voltage corresponding to SCLC regime establishment of was used to calculate the density of free carriers and the slope of I–V curve in SCLC regime was used to estimate the carriers mobility. A good agreement between SCLC analysis and Hall effect measurement is observed. In conclusion SCLC can be a powerful tool for semiconductor electrical characterization.

References

[1] H.S. Soh, C. Lee, J. Jang, M.Y. Jung, S. Sung, Appl. Phys. Lett. 63 (1993) 779.
[2] S.C. Deane, M.J. Powell, J. Appl. Phys. 74 (1993) 6655.
[3] S. Nespurek, J. Sworakowski, J. Appl. Phys. 51 (1980) 2098.
[4] C.E. Michelson, J.D. Cohen, Phys. Rev. B 41 (3) (1990) 1529–1541.
[5] E.C. Le Ru, J. Fack, R. Murray, Phys. Rev. B 67 (2003) 245318.
[6] A. Abd El-Mongy, Phys. Status Solidi (A) 136 (1993) 113.
[7] C. Krellner, S. Haas, C. Goldmann, K.P. Pernstich, D.J. Gundlach, B. Batlogg, Phys. Rev. B 75 (24), 245115.
[8] S.D.E.,B.S. Satyanarayana, M. Rao, V.H.S. Moorthy, Rom. J. Phys. 57 (2012) 657.
[9] L. Chabane, N. Zebbar, M. Lamri Zeggar, M.S. Aida, M. Kechouane, M. Trari, Mater. Sci. Semicond. Process. 40 (2015) 840.
[10] Saeid Masudy-Panah, K. Radhakrishnan, Hui Ru Tan, Ren Yi, Ten It Wong, Goutam Kumar Dalapati, Solar Energy Mater. and Solar Cells, 140, 2015, 266.
[11] D.P. Singh, O. Srivastava, J. Nanosci. Nanotechnol. 9 (2009) 5345.
[12] R. Shabu, A. Moses Ezhil Raj, C. Sanjeeviraja, C. Ravidhas, Mater. Res. Bull. 68 (2015) 1.
[13] M.A. Lampert, P. Mark, in: Current Injection in Solids, Academic, New York, 1970.
[14] W. de Boer, J. De Phys. Colloque C4 42 (1981), C.4-45 1.
[15] M. Lamri Zeggar, L. Chabane, M.S. Aida, N. Attaf, N. Zebbar, Mater .Sci. Sem. Process. 30 (2015) 645.
[16] J.H. Lee, B.W. Yeo, B.O. Park, Thin Solid Films 457 (2004) 333.
[17] C. Luyo, I. Fabregas, L. Reyes, J.L. Solis, J. Rodriguez, W. Estrada, R.J. Candal, Thin Solid Films 516 (2007) 25.
[18] A. Zaier, F. OumElaz, F. Lakfif, A. Kabir, S. Boudjadar, M.S. Aida, Mater. Sem. Sci. Proc. 12 (2009) 207.
[19] O.G. Reid, K. Munechika, D.S. Ginger, Nano Lett. 8 (6) (2008) 1602.
[20] K. Ul-Haq, M.A. Khan, J. Xueyin, Z. Zhilin, Z. Xiaowen, Z. Liang, L. Jun, J. Semicond. 30 (2009) 114009.
[21] L. Bosano, S.A. Carter, J.C. Scott, G.G. Malliaras, P.J. Brock., Appl. Phys. Lett. 74 (1999) 1132.
[22] Z.B. Wang, M.G. Helander, M.T. Greiner, J. Qiu, Z.H. Lu, J. Appl. Phys. 107 (2010) 034506.
[23] I. Singh, R.K. Bedi, Appl. Surf. Sci. 257 (2011) 7592.
[24] M.A. Mäki-Jaskari, Model. Simul. Mater. Sci. Eng. 14 (2006) 207.
[25] W. Dangxin, Z. Qiming, T. Meng, Phys. Rev. B 73 (2006) 235206.
[26] Z. Zhangab, P. Wang, J. Mater. Chem. 22 (2012) 2456.

Materials Science in Semiconductor Processing 40 (2015) 840–847

Contents lists available at ScienceDirect

Materials Science in Semiconductor Processing

journal homepage: www.elsevier.com/locate/matsci

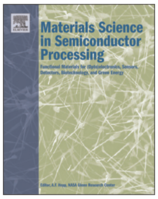

Effects of CuO film thickness on electrical properties of CuO/ZnO and CuO/ZnS hetero-junctions

L. Chabane [a], N. Zebbar [a,*], M. Lamri Zeggar [b], M.S. Aida [b], M. Kechouane [a], M. Trari [c]

[a] *Department of Materials & Compounds, Faculty of Physics, USTHB, BP 32, 16111 Algiers, Algeria*
[b] *LCM et Interface, Faculty of Sciences, University of Constantine, 25000 Algeria*
[c] *Laboratory of Storage and Valorization of Renewable Energies, Faculty of Chemistry, (USTHB), BP 32, 16111 Algiers, Algeria*

ARTICLE INFO

Article history:
Received 26 May 2015
Received in revised form
16 July 2015
Accepted 26 July 2015

Keywords:
Hetero-junction
Thin films
Spray pyrolysis
Solar cells

ABSTRACT

It is known that the quality of the diode and the transport of the charge carriers across the junction may be greatly influenced by the quality of the interface, and depends on the crystallinity of thin layers. In this work, we have prepared the p-CuO/n-ZnO and p-CuO/n-ZnS hetero-junctions by ultrasonic spray pyrolysis at 300 °C under atmospheric pressure. We have investigated the influence of the thickness of CuO film on the electrical properties of the hetero-junctions. The X-ray diffraction indicates that both the CuO and ZnO thin films grow according to polycrystalline nature while ZnS films show a quasi-amorphous nature. The current voltage temperature (I–V–T) and capacitance voltage (C–V) characteristics reveal that CuO/ZnS is an abrupt junction, whereas the data of CuO/ZnO hetero-junctions suggest that the potential barrier heights are spatially non-uniform (junction not abrupt). The electrical behavior of the junction is strongly affected by the defect state distribution at the hetero-interface. The recombination process involving the interface states predominates at low forward bias ($V < 0.5$ V), whereas trap assisted multi-step tunneling capture emission (MTCE) prevails in the higher bias region ($V > 0.5$ V) on the thin CuO side. The junction parameters (ideality factor, rectification ratio, built in potential etc…) are of the same order of magnitude for both heterojunction diodes i.e. ZnO/CuO and ZnS/CuO.

1. Introduction

In recent years, the p–n hetero-junctions based on transition metal oxides and metal sulfides semiconductors have attracted considerable attention in different fields due to the favorable properties of these materials for various technological applications, such as optics, optoelectronics, photovoltaic, electrochemical, photo-catalysis and so on. ZnO and ZnS are wide band gap transparent conducting materials exhibiting many interesting properties, essentially, n-type conductivity, direct band gap (~3.37 eV at room temperature) and high exciton binding energy (~60 and 55 meV for ZnO and ZnS respectively), making the excitons thermally stable at room temperature [1,2]. Among the metal oxide semiconductors, CuO is p-type semiconductor, with a narrow band gap of 1.2 eV, an excellent stability and good electrical properties [3]. It is attractive as a selective solar absorber since it has high solar absorbency and a low thermal emittance [4]. These three semiconductors are attractive for many applications, because they are inexpensive, abundant, and non-toxic.

Thin films and hetero-junctions of semiconductors have been elaborated by different methods like thermal evaporation [5], magnetron sputtering [6], vapor liquid solid (VLS) method [7], pulsed laser deposition [8], sol gel process [9] and ultrasonic spray pyrolysis [10]. The last method has some advantages for producing thin films, such as the simplicity and low cost.

Even though, p–n hetero-junction constitutes the vital part of vast majority of electronic devices, the p-CuO/n-ZnO thin-films hetero-junction have not been studied enough and even less the p-CuO/n-ZnS hetero-junctions. Previous works [11–14] were mainly focused on the application of ZnO/CuO hetero-contact for CO, H_2, gas sensors or humidity sensing, and recently Zhang et al. [15] have investigated the ethanol gas-sensing properties of flower-like p-CuO/n-ZnO hetero-junction nanorods. However, the efficiency of the hetero-junctions and current transport mechanism are limited by the inevitable presence of defects at the interface and in volume. The level of understanding hetero-junction behavior is far from complete. Baek et al. [16] and ÖzyurtKuş et al. [9] have studied the current transport mechanism of n-ZnO/p-CuO hetero-junction.

In this paper, we investigate and compare the electrical

---

[*] Corresponding author. Fax: +213 21 24 80 08.
E-mail addresses: lamia007ch@hotmail.com (L. Chabane), nacbar2003@yahoo.fr (N. Zebbar).

http://dx.doi.org/10.1016/j.mssp.2015.07.080
1369-8001/

behavior of p-CuO/n-ZnO and p-CuO/n-ZnS hetero-junctions prepared by ultrasonic spray pyrolysis technique and deposited in the same conditions of temperature and pressure. The current transport mechanism in hetero-contacts is studied through dependent temperature current–voltage and capacitance–voltage characteristics.

2. Experimental

The CuO/ZnO and CuO/ZnS hetero-junctions were deposited via an Ultrasonic Spray Pyrolysis (USP) onto industrial ITO substrates. The samples were elaborated under atmospheric pressure at 300 °C. ZnO films were prepared by dissolving zinc acetate ($Zn(CH_3COO)_2 \cdot 2H_2O$) in methanol solution at a concentration of 0.1 M. On the other hand, the precursor solution of ZnS was obtained by dissolving zinc acetate (0.1 M) and thiourea (0.1 M) in methanol. Then, the solutions were thoroughly mixed by magnetic stirring (10 min), until homogeneous transparent solutions were obtained. For good quality of polycrystalline films, the solutions were sprayed during 10 min, the flow rate was controlled by a flow-meter and maintained at 4 and 5 mL/h for ZnO and ZnS, respectively, with an ultrasonic frequency of 40 kHz.

CuO has been sprayed on deposited ZnO and ZnS films. The solution was prepared by dissolving ($CuCl_2 \cdot 2H_2O$) in distilled water. The molarity, the mixture time and the solution flow rate were 0.1 M, 30 min and 10 mL/h, respectively. The deposition time varied from 20 to 80 min.

The surface morphology of the films was observed by scanning electron microscopy (SEM, Instrument JSM-6360). The crystal nanostructure of CuO/ZnO hetero-junction was determined by X-ray diffraction (XRD, D-Advance Bruckeraxs), with Cu Kα radiation ($\lambda = 1.540598$ Å) operating at 45 kV and 40 mA in the 2θ range (10–110°) with step of 0.02°. The optical parameters of the films were investigated by 3101 PC Shimadzu spectrophotometer. The thickness of the films was determined by ellipsometry using SEMILAB GES-5E Spectroscopic Ellipsometer. The current–voltage (I–V) and capacitance–voltage (C–V) characteristics were measured under vacuum ($\sim 5 \times 10^{-5}$ mbar) by a pico-ammeter (Keithley 617) and Hp 4192A LF Impedance Analyzer respectively.

The schematic structure of p-CuO/n-ZnO (ZnS) hetero-junction diode is shown in Fig. 1(a). To ensure an ohmic contact on the CuO layer, we have deposited gold by DC reactive sputtering, the ohmicity of these contacts was checked by the current–voltage characteristic (Fig. 1(b)).

3. Results and discussions

The main objective of this work is devoted to the effect of the CuO film thickness on the electrical and capacitive properties of the hetero-junctions p-CuO/n-ZnO and p-CuO/n-ZnS. We have considered four samples from each hetero-junction, CZO20, CZS20, CZO40, CZS40, CZO60, CZS60, and CZO80, CZS80 corresponding to 20, 40, 60 and 80 min deposition time of CuO films, respectively.

3.1. Films properties

Fig. 2 shows SEM images of ZnO, ZnS and CuO40 films; the surface of ZnO film (Fig. 2(a)) has a dense and rough appearance, consisting of crystallites with similar size, distributed uniformly. However, the aspect of ZnS film (Fig. 2(b)) is distinguished by a fully continuous and smooth surface which does not emerge crystallite, in agreement with the quasi amorphous nature observed by XRD analysis. The CuO film (Fig. 2(c)) is characterized by a rough, granular and porous surface, consisting of large crystallites distributed randomly. The conversion efficiency mainly depends on the surface morphology and roughness that play an important role for improving the absorber efficiency. Fig. 3 shows the XRD diffraction patterns of CuO80/ZnO/ITO and CuO80/ZnS/ITO hetero-junctions which indicate the presence of hexagonal ZnO würtzite phase and monoclinic CuO phase (PDF card #45-0937). The other peaks are assigned to the cubic phase of ITO (PDF card #45-0937) with the absence of characteristic peaks of ZnS phase. The XRD patterns reveal an amorphous nature of ZnS layer and indicate that the CuO and ZnO films have polycrystalline nature, where the predominant crystalline orientations are (002) and (111) for CuO and (100), (002) and (101) for ZnO. The average crystallite size (D) was calculated from the Scherrer's equation [17], using the most intense diffraction peak of each phase namely (002) for ZnO, (002) for CuO20 and CuO40, and (111) for CuO60 and CuO80 (Table 1 and SM).

$$D = \frac{(0.9\lambda)}{\beta cos(\theta_{hkl})} \tag{1}$$

Where β the full width at half maximum (FWHM) of the peaks and θ the diffraction angle. The average grain size of deposited films in the directions indicated previously, varies from 16 to 46 nm (Table 1). The increase in the grain size with raising the deposition time (thickness) suggests the improvement of the CuO films crystallinity.

The transmittance spectra of ZnO, ZnS films are represented in Fig. 4. The average transmittance light exceeds 80% in the visible range, while CuO (Fig. 4, Inset) presents a low transmittance rate

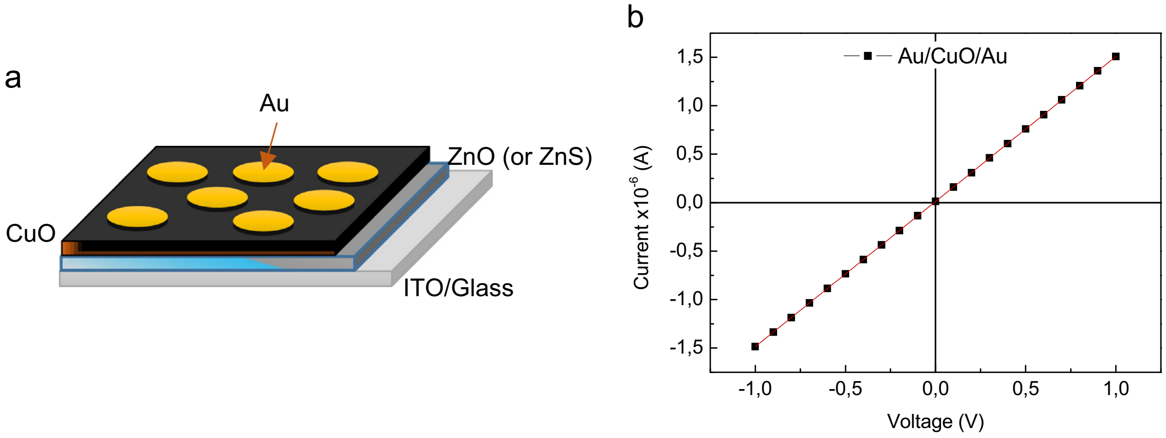

Fig. 1. (a) Schematic structure of Au/p-CuO/n-ZnO (ZnS) hetero-structure, (b) I–V characteristic of Au/CuO/Au structure.

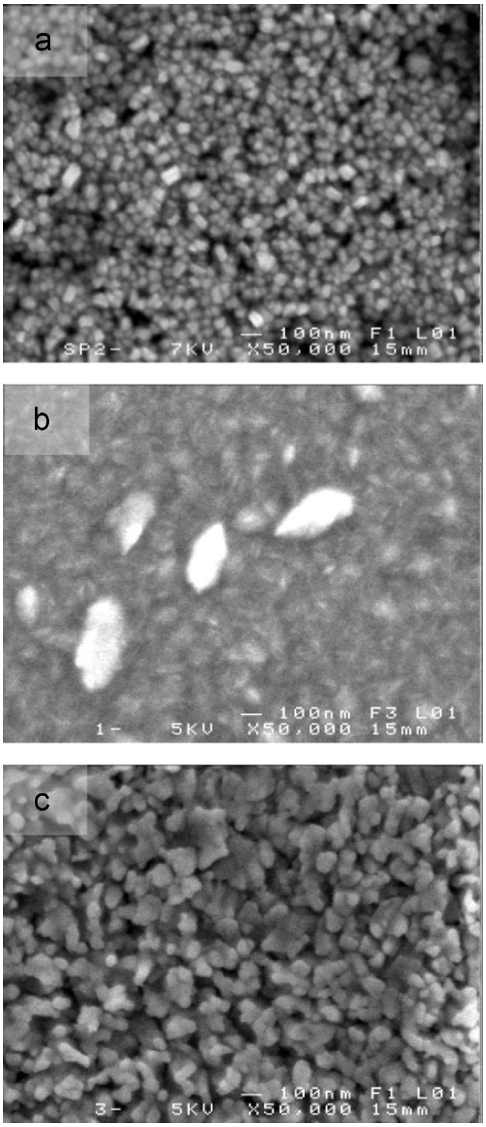

Fig. 2. SEM images of: (a) ZnO layer, (b) ZnS layer and (c) CuO40 layer.

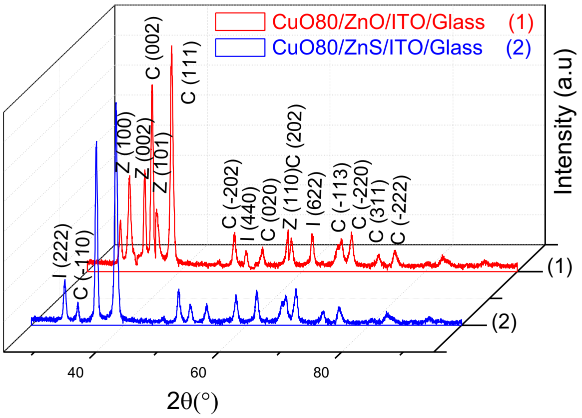

Fig. 3. XRD patterns of CuO80/ZnO and CuO80/ZnS heterojunction deposited onto ITO substrate (C=CuO, Z=ZnO, I= ITO).

Table 1
Characteristics parameters of ZnO, ZnS and CuO thin layers: Deposition time (t_d), thickness (Th), intense diffraction peak (hkl)/average grain size (D), optical band gap (E_g), Urbach energy (E_{00}), resistivity (ρ) and activation energy (E_a).

	t_d (min)	Th (nm)	$(hkl)/D$ (nm)	E_g (eV)	E_{00} (eV)	ρ (kΩ cm)	E_a (eV)
ZnO	10	124	(002)/20	3.29	0.041	0.8	0.28
ZnS	10	130	/	3.40	0.081	1.0	0.30
CuO20	20	163	(002)/16	1.40	0.035	41.0	0.72
CuO40	40	275	(002)/29	1.46	0.034	28.5	0.48
CuO60	60	370	(111)/36	1.43	0.050	1.4	0.30
CuO80	80	474	(111)/46	1.46	0.034	1.2	0.20

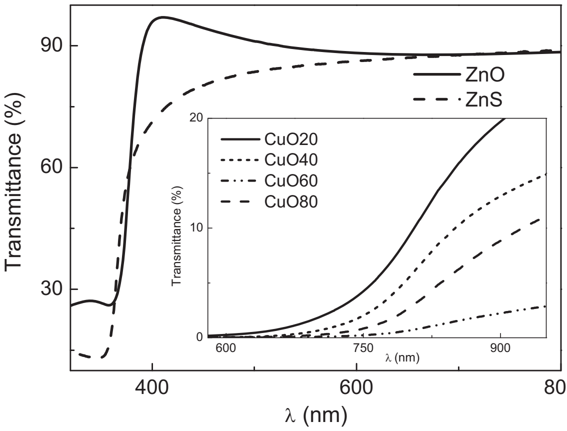

Fig. 4. Optical transmittance spectra of ZnO, ZnS and CuO thin films at various thickness in inset.

(5–18%) and high absorbance rate. The optical band gap (Eg) was evaluated from the plot $(\alpha h\nu)^2$ versus the photon energy ($h\nu$), according to the Tauc formula for direct band gap semiconductor [18].

$$(\alpha h\nu)^2 = A(h\nu - E_g) \tag{2}$$

Where α is an absorption coefficient and A is a constant. We estimated the band tail width E_{00} (Urbach energy) from the following expression [19]:

$$\alpha(h\nu) = \alpha_0 e^{E_{00}/h\nu} \tag{3}$$

Where α_0 is the pre-exponential factor. The optical gap E_g and Urbach energy (E_{00}) of ZnO and ZnS are reported in Table 1. It is clear that the band tail width of ZnS (0.081 eV) is large compared with that of ZnO (0.041 eV), thereby confirming the XRD results. For CuO layers, the values of E_g and E_{00} (Table 1) are in the range (1.40–1.46 eV) and ~0.34 meV respectively. Statistically, an increase in the grain size with thickness is followed by the slight widening in the optical band gap (Table 1). This suggests that the variation of the optical gap is governed by the improvement of the crystallinity in the film network.

3.2. Hetero-junctions properties

The electrical properties of the hetero-junction are focused on the characterization of the interface p-CuO/n-ZnO (or n-ZnS), including the transport phenomena through this interface.

3.2.1. Current–voltage characteristics

The *I–V* characteristic of the obtained hetero-junction in the dark at room temperature (Fig. 5) shows rectifying properties, indicating proper formation of the junction. The significant reverse current is due to the minority charge carrier concentration which increases by oxygen vacancies and/or impurities [14]. The forward current varies exponentially with positive applied bias (V) and the characteristic can be described by the standard diode equation [20]

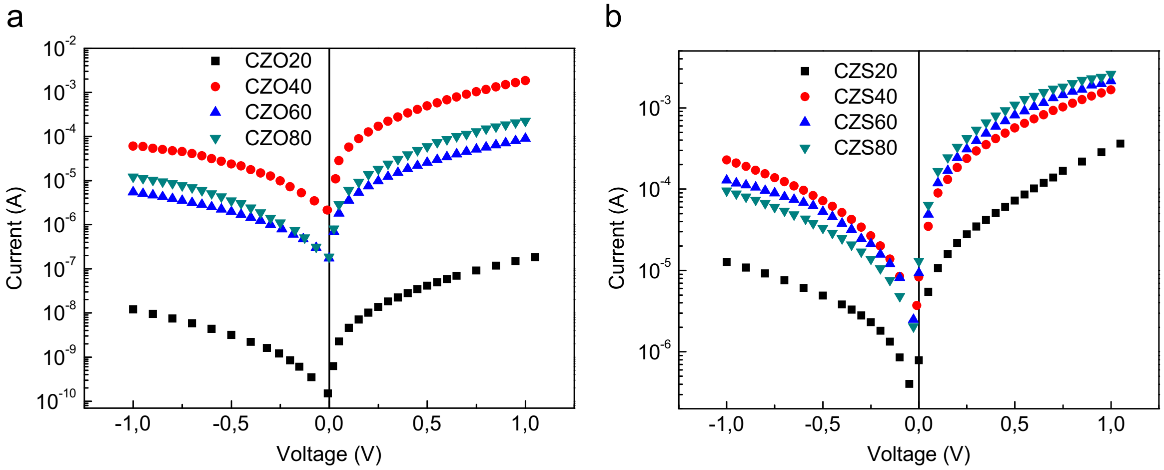

Fig. 5. Semi-logarithmic scale representation of the room temperature current–voltage characteristics of: (a) CuO/ZnO heterojunctions, (b) CuO/ZnS heterojunctions.

$$I = I_S(e^{qV/nKT} - 1) \qquad (4)$$

Where k is the Boltzmann constant, T the absolute temperature, and n the junction ideality factor, which is determined from the slope of the $\log(I)$–V characteristic $n = \frac{q}{KT}\frac{dV}{d(\log I)}$. The saturation current (I_s) obtained from the intersection of the straight line of $\log(I)$ at $V=0$, is found to vary exponentially with $(-1/T)$ according to the relation [20]:

$$I_s \propto e^{(-E_a/KT)} \qquad (5)$$

Where E_a is the activation energy of the charge carrier in the forward bias.

The turn on voltage (V_{th}), defined as the built in potential, corresponds to a potential barrier the carrier has to overcome to contribute to forward current. It is determined from the intersection of the linear portion of the forward I–V characteristic with the voltage axis [21]. The large ideality factor (>2) (Fig. 6(a)) indicates that the mechanism of the current transport across the junction is not the thermal injection over barrier or diffusion [21]. In such a case, several conduction mechanisms have been

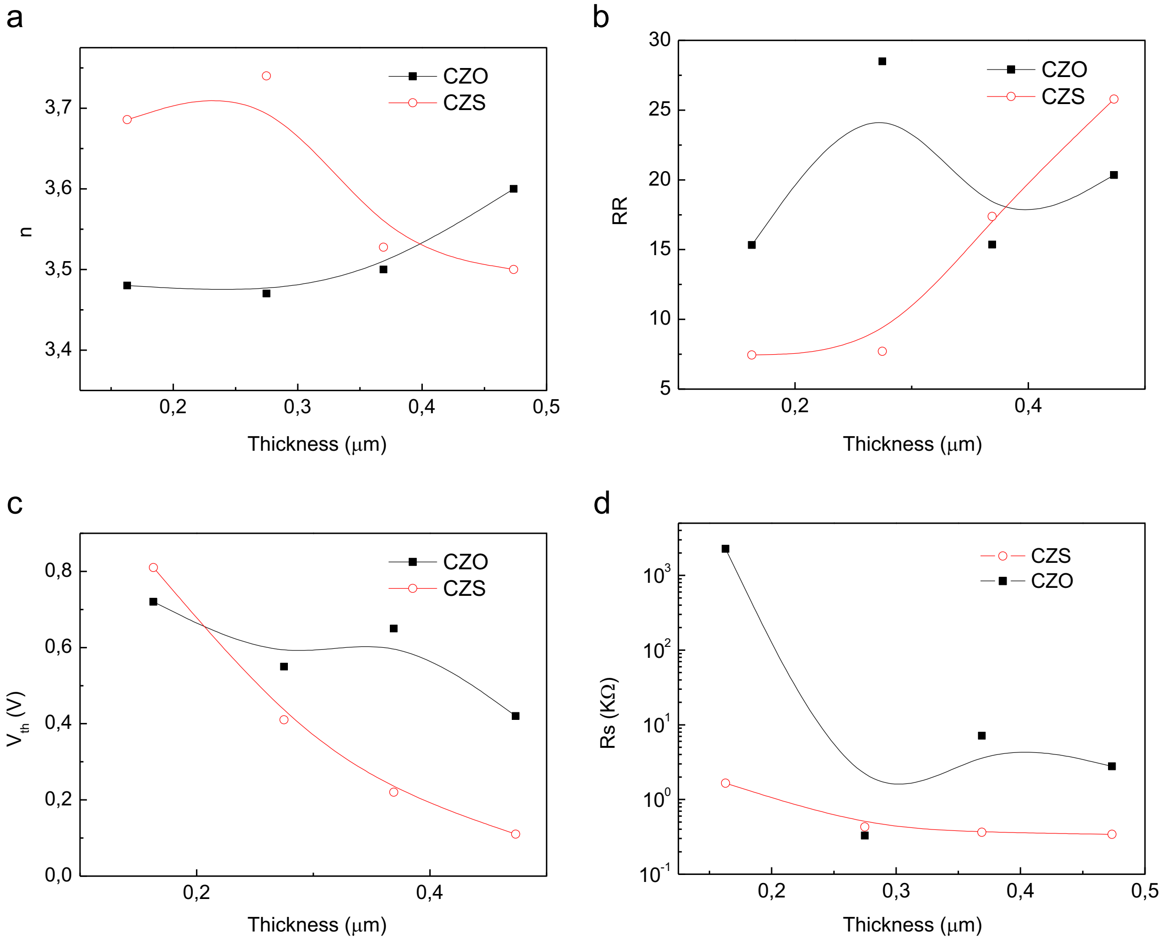

Fig. 6. Variation of heterojunction parameters vs. thickness: (a) Ideality factor (n), (b) Rectification Ratio (RR), (c) Turn on voltage (V_{th}) and (d) Series resistance (R_s).

proposed. For the CZO hetero-junction, similar results are reported for CuO/ZnO hetero-contacts elaborated by solid state synthesis routes and by sputtering, respectively [11,14]. The forward current (Fig. 5) is greater than the reverse one by a factor ranging from 15 to 28 and 7 to 25, for CZO and CZS hetero-structure respectively, while the turn on voltage V_{th} varies in the range (0.5–0.85 V) (Fig. 6(c)). The variation of hetero-junction parameters with the CuO thickness (Fig. 6) is not similar for CuO/ZnO and CuO/ZnS. The decrease of the potential barrier V_{th} and series resistance (R_s) with increasing the CZS thickness, accompanied by a slight decrease of the ideality factor n, induce an increase in the rectification ratio RR, with an improvement of the diode quality. The ZnS film has an amorphous nature. So, one can associate the diode improvement to changes in the physical properties of CuO layer (and/or interface), especially the crystallinity and electrical conductivity, which are improved when the thickness increases (Table 1). Per against, for CZO samples, we do not observe a significant variation of the characteristic of the hetero-junction parameters with the CuO thickness, the order of magnitude of the parameters is almost the same as for the hetero-contact CuO/ZnS (Fig. 6(a and b)). It is noted that the best CZO diode is that corresponding to CuO40 film (~0.28 μm), with the lowest ideality factor (n=3.47) and a series resistance R_s of 0.32 kΩ (Fig. 6(d)). The built in potential V_{th} of this diode is equal to 0.81 V with a highest rectification ratio (28%), thus surpassing that of CZS diode (25%). Generally, for hetero-junction diode, the structural imperfections at grain boundaries as well as the interface deteriorate its quality [23]. These imperfections are essentially caused by lattice mismatch and change of the preferential crystalline direction. The XRD patterns of CuO40 and ZnO films indicate that the [002] direction prevails over others (Table 1 and SM) and this may explain the good behavior of CZO40 hetero-junction. Rediker et al. [21] reported that the rectification is most probably due to the impurity distribution in the re-crystallized region. The presence of imperfections induces a creation of allowed states essentially at the interface, which limit the current flow through the hetero-junction. The analysis of I–V–T characteristics is useful to identify the transport mechanisms controlling the conduction. Fig. 7 shows the semi-logarithmic plot of the I–V characteristics of CZO80 and CZS80 hetero-junctions at temperature ranging from 25 to 120 °C. The plot of the forward current (Fig. 7(a)) consists of two distinct regions, at low applied bias (< 0.5 V) the current varies linearly with applied voltage because the electrical field due to the injected carriers is negligible, compared to the applied bias. The nature of metallic contact and the presence of interface defects induce generally a deviation from the ohmic behavior [10]. Beyond 0.5 V, the current varies exponentially with applied bias ($\propto e^{\beta V}$), where β= 2.47 and 2.59 for CZO80 and CZS80 respectively is temperature independent (Fig. 7). This particularity of relative temperature invariance of β is consistent with the current due to a tunneling (or multi-tunneling) process [21-23]. According to this hypothesis, the saturation current I_s (Eq. (4)) obtained by extrapolating the forward characteristics (I–V–T) to zero voltage (Fig. 7), should change exponentially with temperature according to relation (5). The temperature dependence of I_S (for $V > 0.5$ V) is represented in Fig. 8. For CZS samples, the variation is really well governed by the relation (5) except for CZS20. However, for CZO samples, I_s does not change exponentially with ($-1/T$), except for CZO40. Therefore, it is almost certainly that the barrier is not linear, we have neglected the changes in the density of states and their population with temperature [21]. Even so, we can solved this in-coincidence by considering the multi-tunneling capture-emission mechanism (MTCE) instead of the multi-tunneling model studied by Matsuura et al. [23], and Song et al. [6], that combine the thermal transport mechanism and tunneling transport mechanism. The values of activation energy (E_a) of the saturation current, deduced from the linear fit of data in Fig. 8 according to relation (5), are shown in Fig. 8 and Table 2.

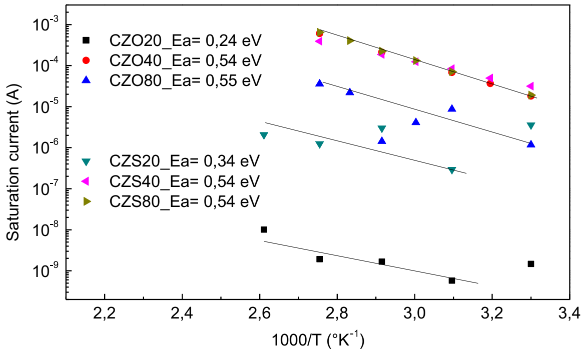

Fig. 8. Temperature dependence of saturation current Is of CZO and CZS for different thickness.

The activation energy of saturated current is closely related to the defects at the interface CuO/ZnO (or ZnS) (Fig. 8) is reduced (0.54–0.24 eV) with decreasing the CuO thickness; this may be due to the increase of interfacial states. It is well known that thinner layers contain more structural defects than thicker one.

From Fig. 9, we can observe that the reverse current (in all hetero-junctions) is strongly dependent on the temperature and slightly non-saturating with applied reverse bias. Bergmann et al.

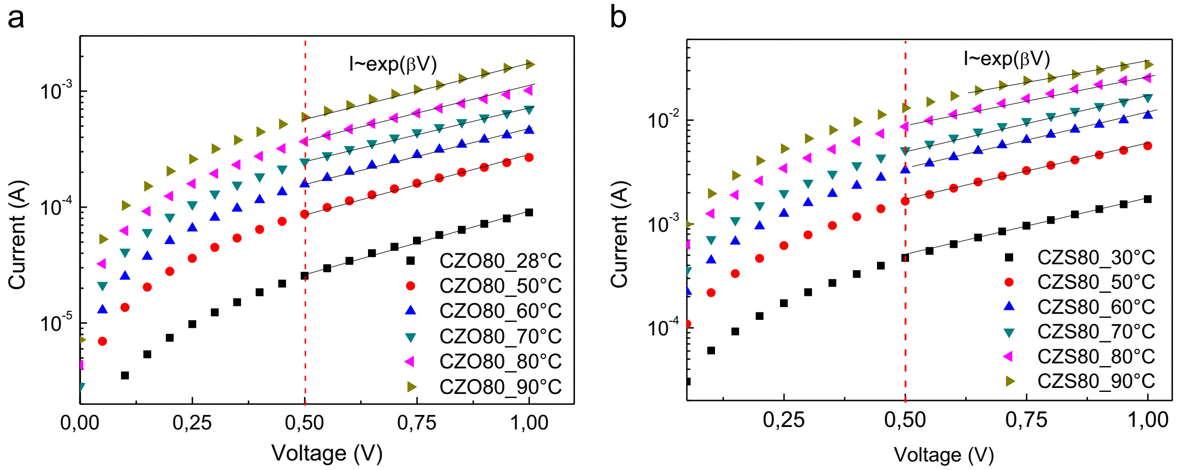

Fig. 7. I–V–T characteristics in forward bias of (a) CuO80/ZnO and (b) CuO80/ZnS heterojunctions.

Table 2
The valence band offset (ΔE_V) and the activation energy (E_a) of saturation current of CZO and CZS heterojunctions.

	ΔE_V (eV)	E_a (eV)
CZO20; CZS20	1.64; 1.83	0.24; 0.33
CZO40; CZS40	1.58; 1.77	0.54; 0.53
CZO60; CZS60	1.61; 1.80	0.50; 0.49
CZO80; CZS80	1.58; 1.77	0.55; 0.55

[24] have explained the existence of the reverse current in the hetero-junctions by the generation of minority carriers in the space charge region and may be accompanied by the flow due to the inter-band tunneling of the minority carriers. Weitering et al. [25] attribute the non-saturation of the reverse current with applied voltage to the spatial non homogeneity of the barrier height. It is clear that the predominance of any given mechanism is governed by the life time of the minority carrier [24] and the thermal energy given by the elevation of temperature.

One can see from Fig. 8 that the activation energy (E_a) of the saturation current (I_S) for the hetero-junctions CZO and CZS, eg. CZO20, CZO40, CZS80 is nearly the same. Fig. 10 shows that the electrical behavior of the hetero-junction diodes (CZO20 and CZS20) is also similar, be it for CuO deposited on polycrystalline ZnO or on amorphous ZnS layers. Such result suggests that the conduction mechanism is mainly controlled by the defects profile in the bulk CuO layer and/or interface state between CuO and ZnO (S) layers. In the low applied bias region ($-0.5<V<0.5$ V), the activation energies of forward and reverse currents have nearly the same values: 0.6 eV and 0.78 eV ($\sim E_{g,\mathrm{CuO}}/2$) for CZO20 and CZS20 hetero-junctions respectively. This implies that the carrier transport mechanism, in this bias region, is the same from either side (reverse and forward bias), and is strongly influenced by the interface recombination centers. For higher applied bias (>0.5 V), the E_a values for CZO(S)20 are less than (E_F-E_V) of CuO layer (Table 2), stating that the presence of defects in the bulk CuO layer, introduces energy levels near the valence band, and controls the charge carrier transport through the samples.

Fig. 11 presents the energy band diagram of CZO(S)20 hetero-junction; the discontinuity of conduction and valence bands are expressed by

$$\Delta Ec = \chi_{\mathrm{ZnO(S)}} - \chi_{\mathrm{CuO}} \tag{6}$$

$$\Delta Ev = Eg_{\mathrm{ZnS}} - Eg_{\mathrm{CuO}} - \Delta Ec \tag{7}$$

Where $\chi_{\mathrm{ZnS}} = 3.9$ eV [26], $\chi_{\mathrm{ZnO}} = 4.32$ eV [27] and $\chi_{\mathrm{CuO}} = 4.07$ eV [28] are the electron affinities of ZnS, ZnO and CuO, respectively, the energy band gap of CuO (1.40 eV) and ZnO(S) (3.29 eV) were determined from the optical measurement (Table 1), the ΔEv values are reported in Table 2.

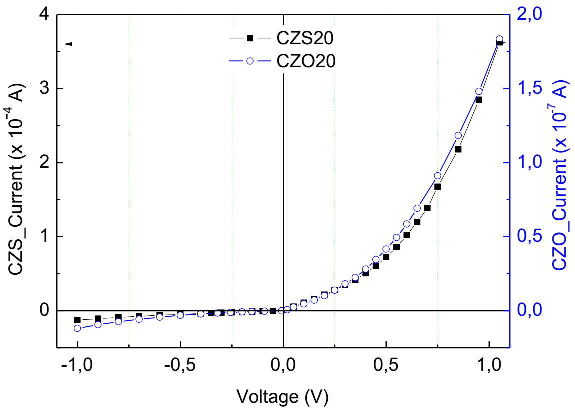

Fig. 10. Linear scale of current–voltage characteristics of CZO20 and CZS20 heterojunctions at room-temperature.

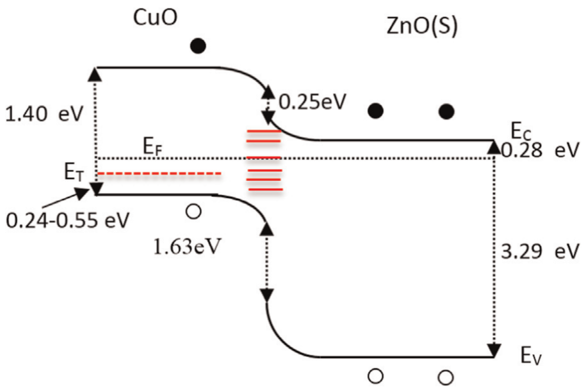

Fig. 11. Proposed Energy band diagram of CZO(S) heterojunction.

The activation energy (E_a) of p-CuO and n-ZnS layer is determined from the current–temperature measurements in coplanar configuration (not reported here) and the barrier potential from capacitance measurements.

3.2.2. Capacitance–voltage characteristics

The capacitance measurements i.e. capacitance vs. voltage, can be used to obtain the parameters characterizing the junction, such

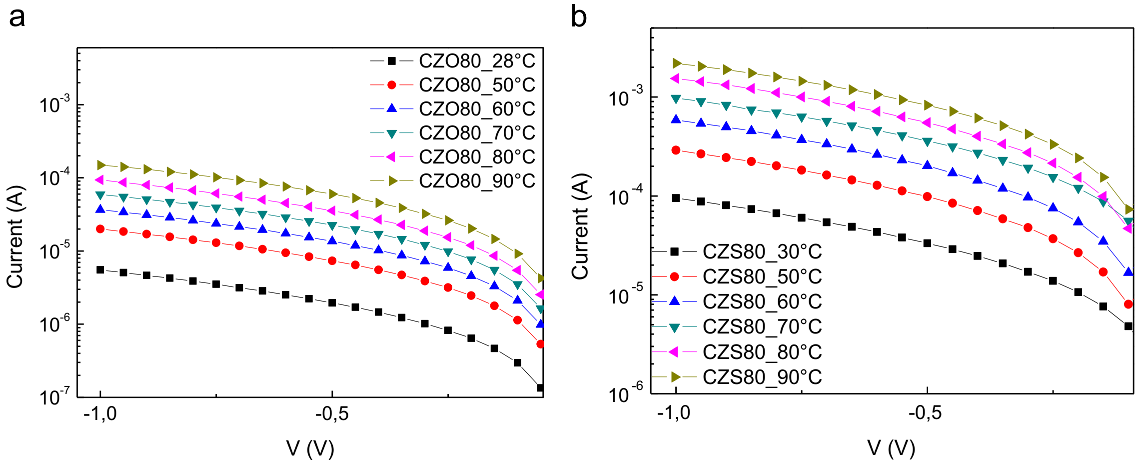

Fig. 9. *I–V–T* characteristics in reverse bias of (a) CuO80/ZnO and (b) CuO80/ZnS heterojunctions.

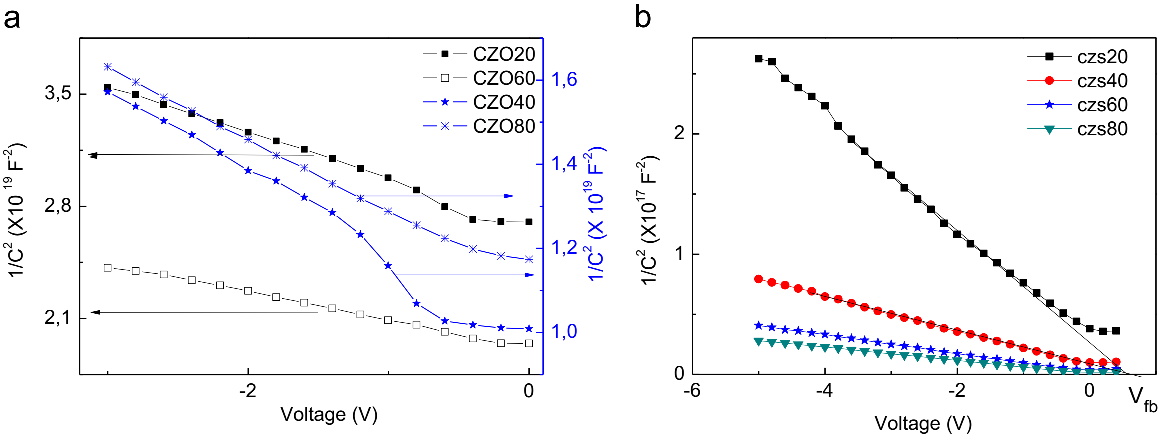

Fig. 12. C^{-2}–V characteristics of (a) CuO/ZnO and (b) CuO/ZnS heterojunctions.

as the flat band potential (V_{fb}) of the hetero-junction, the doping density of one-side and the depletion width on both side of the junction. The depletion capacitance can be expressed by the following relation [20]

$$\frac{1}{C^2} = \frac{2(N_a\varepsilon_{\mathrm{CuO}} + N_d\varepsilon_{\mathrm{ZnO(ZnS)}})(V_{fb} - V_a)}{S^2 q N_a N_d \varepsilon_{\mathrm{CuO}}\varepsilon_{\mathrm{ZnO(ZnS)}}} \tag{8}$$

Where S and q are respectively the surface area of the diode and the charge carrier, V_a the applied reverse bias voltage, $\varepsilon_{\mathrm{CuO}}$ and N_a are the dielectric permittivity and acceptor carrier concentration of p-CuO layer respectively, $\varepsilon_{\mathrm{ZnO(ZnS)}}$ and N_d are the dielectric permittivity and donor carrier concentration of n-ZnO (or n-ZnS) film. N_a of CuO film and V_{fb} of hetero-junction can be easily determined from the slope and the extrapolation of linear part of C^{-2}–V characteristic to the potential axis, respectively.

Fig. 12 shows the C^{-2}–V dark characteristic (at room temperature) of CZO and CZS hetero-junctions. We confirm that the CZO junction is not abrupt and presents a high density of interface states. The V_{fb} values determined from capacitance measurements (Fig. 12) are high compared with those obtained from the I–V curves. Therefore, the depletion capacitance of CZO cannot be well described by Eq. (4). However, for CZS hetero-junction the capacitance varies as $V^{1/2}$ under reverse applied bias, thus indicating an abrupt junction. Using the constants: $\varepsilon_{\mathrm{CuO}}=18.1\varepsilon_0$, $\varepsilon_{\mathrm{ZnS}}=8.3\varepsilon_0$, $\varepsilon_0= 8.85\times10^{-12}$ F/m, the measured values: $S=3.14\times10^{-6}$ m^2, $\mathrm{Nd}_{\mathrm{ZnS}}=10^{21}$ m^{-3}, and the slope of C^{-2}–V curve, the acceptor density N_a of the CuO films can be calculated. The value of N_a ranges from 6×10^{20} to 3×10^{22} m^{-3} corresponding to the thicknesses domain [124–474 nm]. The potential V_{fb} for CZS hetero-junction; substantially corresponds to the values of V_{th} deduced from the I–V characteristic, the variation of $\mathrm{Na}_{\mathrm{CuO}}$ and $\mathrm{V}_{\mathrm{fbCZS}}$ according to the CuO thickness are shown in Fig. 13.

4. Conclusion

In this work, the p–n hetero-junctions diodes of CuO/ZnO and CuO/ZnS were fabricated using the spray pyrolysis, a simple and low cost technique. This deposition method provides textured and rough surfaces that can favor multiple internal reflections, leading to increased solar absorption. Both the hetero-junctions showed an obvious rectifying behavior over the thickness range [124–474 nm]. Then, we have compared the electrical behavior of CuO/ZnO and CuO/ZnS hetero-junctions. The dependence of the dark current–voltage (I–V–T) characteristics on the temperature showed a recombination process, which predominates at low forward bias ($V<0.5$ V). The multi-tunneling capture-emission mechanism (MTCE) process dominates in the higher bias region ($V>0.5$ V) and is closely related to the bulk defects profiles in CuO thin film rather than the interface states whatever the thickness. The reverse current follows the characteristics of generation current in the space charge region and confirms the domination of the recombination process at low bias voltages ($-0.5<V<0.5$ V). The capacitance–voltage characteristics indicate that CZS is an abrupt junction unlike CZO. Based on this study, although the ZnS film is amorphous and resistive, the parameters of CZS hetero-junction (ideality factor, flat band tension, rectification ratio, etc…) can readily be controlled by adjusting the deposition time of CuO films, which influences mainly the crystallinity and conductivity of the films. For CZO hetero-junction, the best performance of the diode is obtained for CuO deposition time of 40 min.

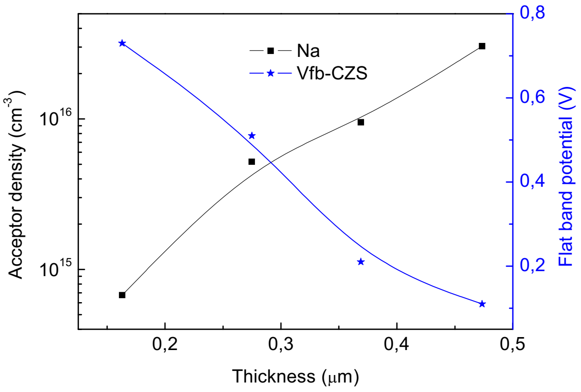

Fig. 13. Variation of acceptors density of p-CuO layers and flat band potential of CZS heterojunctions vs. thickness.

Acknowledgments

The financial support of this work was provided by the Faculties of Physic USTHB (Algiers) and Sciences UC1 (Constantine) (Grant no. R3).

Appendix A. Supplementary material

Supplementary data associated with this article can be found in the online version at http://dx.doi.org/10.1016/j.mssp.2015.07.080.

References

[1] C. Jagadish, S.J. Pearton, Thin Films and Nanostructures, Elsevier, Amsterdam, 2006.

[2] B. Urbaszek, C.M. Townsley, X. Tang, C. Morhain, A. Balocchi, K.A. Prior, R. J. Nicholas, B.C. Cavenett, Phys. Status Solidi B 229 (2002) 549–552.

[3] F. Marabelli, G.B. Parravicini, F. Salghetti-Drioli, Phys. Rev. B 52 (1995) 1433–1436.

[4] T. Maruyama, Sol. Energy Mater. Sol. Cells 56 (1998) 85–92.

[5] M.F. Kotkata, Sh. A. Mansour, Thin Solid Films 518 (2010) 3407–3412.

[6] D. Song, D.H. Neuhaus, J. Xia, Armin G. Aberle, Thin Solid Films 422 (2002) 180–185.

[7] P. Klason, M.M. Rahman, Q.H. Hu, O. Nur, R. Turan, M. Willander, Microelectron. J. 40 (2009) 706–710.

[8] F.H. Hsu, N.F. Wang, Y.Z. Tsai, M.P. Houng, Sol. Energy 86 (2012) 3146–3152.

[9] F. ÖzyurtKuş, T. Serin, N. Serin, J. Optoelectron. Adv. Mater. 11 (2009) 1855–1859.

[10] N. Zebbar, Y. Kheireddine, K. Mokeddem, A. Hafdallah, M. Kechouane, M. S. Aida, Mater. Sci. Semicond. Process. 14 (2011) 229–234.

[11] K.K. Baek, H.L. Tuller, Solid State Ion. 75 (1995) 179–186.

[12] Y. Ushio, M. Miyayama, H. Yanagida, Sens. Actuators B 12 (1993) 135–139.

[13] Y. Hu, X. Zhou, Q. Han, Q. Cao, Y. Huang, Mater. Sci. Eng. B 99 (2003) 41/43.

[14] S. Aygün, D. Cann, Sens. Actuators B 106 (2005) 837–842.

[15] Y.B. Zhang, J. Yin, L. Li, L.X. Zhang, L.J. Bie, Sens. Actuators B: Chem. 202 (2014) 500–507.

[16] K.K. Baek, H.L. Tuller, Sens. Actuators B 1344 (1993) 238–240.

[17] L. Sagalowicz, G.R. Fox, J. Mater. Res. 14 (1999) 1876.

[18] J. Tauc, R. Grigorovichi, A. Vancu, Phys. Status Solidi B 15 (1966) 627.

[19] M.V. Kurik, Phys. Status Solidi A 8 (1971) 9.

[20] S.M. Sze, Physics of Semiconductor Devices, John Wiley and Sons, New York, 1981.

[21] R. Rediker, S. Stopek, J.H.R. Ward, Solid State Electron. 7 (1964) 621–629.

[22] A.N. Banerjee, S. Nandy, C.K. Chattopadhyay, Thin Solid Films 515 (2007) 7324–7330.

[23] H. Matsuura, T. Okuno, H. Okushi, K. Tanaka, J. Appl. Phys. 55 (1984) 1012–1019.

[24] Y.V. Bergmann, V.I. Korol’Kov, Y.M. Makushenko, V.G. Nikitin, A.A. Yakovenko, Sov. Phys. Semicond. 10 (1976) 4.

[25] H.H. Weitering, J.P. Sullivan, R.J. Carolissen, R. PérezSandoz, W.R. Graham, R. T. Tung, J. Appl. Phys. 79 (1996) 7820–7829.

[26] B. Sharma, R. Purohit, Semiconductor Hetrojunctions, Pergamon Press, Oxford, 1974.

[27] Z. Guo, D.X. Zhao, Y.C. Liu, D.Z. Shen, J.Y. Zhang, B.H. Li, Appl. Phys. Lett. 93 (2008) 163501.

[28] M.T.S. Nair, L. Guerrero, O.L. Arenas, P.K. Nair, Appl. Surf. Sci. 150 (1999) 143–151.

Materials Science in Semiconductor Processing 30 (2015) 645–650

Contents lists available at ScienceDirect

Materials Science in Semiconductor Processing

journal homepage: www.elsevier.com/locate/mssp

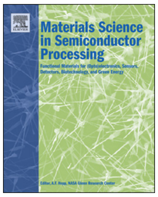

Solution flow rate influence on properties of copper oxide thin films deposited by ultrasonic spray pyrolysis

M. Lamri Zeggar [a], L. Chabane [b], M.S. Aida [a,*], N. Attaf [a], N. Zebbar [b]

[a] *Laboratoire de Couches Minces et Interfaces Faculté des Sciences Université de Constantine 1, Algeria*
[b] *Laboratoire Couches Minces Faculté de Physique Université USTHB bab Ezzouar, Algeria*

ARTICLE INFO

Available online 8 October 2014

Keywords:
Thin films
Semiconductor oxides
Spray pyrolysis
Solar cells

ABSTRACT

The present work is an investigation of the solution flow rate influence on copper oxide (CuO) thin film properties deposited by ultrasonic spray pyrolysis. A set of CuO thin films were deposited, with various solution flow rates, on glass substrate at 300 °C. The precursor solution is formed with copper salt dissolution in distilled water with 0.05 molarity. The solution flow rate was ranged from 10 to 30 ml/h. Films composition and structure were characterized by means of XRD (X Rays diffraction) and Raman scattering. The optical properties were studied using UV–visible spectroscopy. The electrical conductivity, carrier mobility and concentration were determined by Hall Effect measurements. The obtained results indicate that flow rate is a key parameter controlling CuO films growth mechanism and their physical properties. The prepared films are mainly composed with a CuO monophase, the crystallite size is reduced with increasing the flow rate. A ZnO/CuO heterojunction structure has been realized and its rectifying behavior is tested.

1. Introduction

It is well recognized that metal oxides play an important role in several areas of physics, chemistry and materials science. Currently, they found a wide application domains in microelectronics, piezoelectricity, photovoltaics, gas sensing and photocatalysis fields [1–4]. Among these metal oxides, copper oxide (CuO) is a promising material due to its low cost, non-toxicity and abundant availability of copper.

Copper oxide exists in two stable phases namely: CuO and Cu_2O with different proprieties [5]. CuO phase has a relatively low band gap (1.2–1.9 eV), it is a p-type semiconductor with a monoclinic structure. While Cu_2O phase is known to be a p-type semiconductor with cubic structure and a large direct band gap 2–2.6 eV. Both these oxides have found special interest for several applications such as: photocatalysis [6], high Tc superconductors [7], lithium batteries [8,9], magnetic storage [10], gas sensor [11] and solar cells [12].

Several techniques have been used to deposit CuO thin films namely: thermal oxidation [13], dip coating [14], chemical vapor deposition [15], plasma evaporation [16], electrodeposition [17], spray pyrolysis [18,19] and reactive sputtering [20]. Among these techniques, spray pyrolysis is a very attractive and versatile technique; it has been widely used to produce adherent, homogenous and stochiometric thin films. Ultrasonic spray pyrolysis technique has been extensively used for metal oxide thin films deposition [21–24]. It is a simple easy, low cost technique and do not require any sophisticated or vacuum equipments; it is also compatible with thin films materials mass production.

It is well recognized, that thin films physical properties are close related and largely influenced by the used technique and deposition conditions. Therefore, deposition

---

* Corresponding author.
E-mail address: aida_salah2@yahoo.fr (M.S. Aida).

http://dx.doi.org/10.1016/j.mssp.2014.09.026
1369-8001/© 2014 Elsevier Ltd. All rights reserved.

parameters effect has been widely studied and optimized in order to produce CuO thin films with suitable properties for the application in hand. The most studied parameters are: precursor concentration [25] substrate temperature [26,27] and doping [28,29]. However fewer studies have been devoted to the influence of solution flow rate in ultrasonic spray pyrolysis technique.

Generally, in the whole commonly used deposition techniques, film growth steps namely nucleation, condensation and subsequent growth, are mainly controlled by two major parameters: the substrate temperature which controls the species energy and motion onto the substrate and the flux of arriving species on the substrate. In the case of spray pyrolysis, arriving species rate is controlled by the flow rate of the solution feeding the nozzle. Substrate temperature is extensively studied in the literature, while, to our knowledge, the flow rate influence is less studied. The lack of investigation related to this parameter is the motivation of the present study.

In the present work, CuO thin films have been deposited by ultrasonic spray pyrolysis. Solution flow rate effect on structural, morphological, optical and electrical proprieties of CuO films have been investigated. CuO is known to be a good ZnO partner to form an heterojunction used for gas sensor or solar cells application. Thereafter, preparation and characterization of ZnO/CuO heterojunction has been addressed at the end of this work.

2. Experimental details

CuO thin films were grown onto glass substrate, using a homemade spray ultrasonic system [22]. A solution of 0.05 morality was prepared by dissolving $CuCl_2.2H_2O$ precursor in distilled water. The total solution of 50 ml was sprayed during 20 min on heated glass substrates by ultrasonic nebulizer system (Sonics). The obtained stream is formed with uniform and fine droplets of 40 μm average diameter [30]. The substrates temperature was fixed at 300 °C. A set of samples was prepared by varying the solution flow rate from 10 to 30 ml/h with a step of 5 ml/h.

Films structural properties were determined by XRD using Philips X'Pert system with Cu Kα radiation ($\lambda_{Cu}=0.154056$ nm). The diffractometer reflections were taken at room temperature and the 2θ value were varied in the range 20–80°. Films morphology was analyzed using scanning electron microscope Jeol 5400 SEM microscope. The micro-Raman measurements were performed at room temperature using the 514.5 nm line of an argon ion laser as the excitation source (Renishaw). The laser power was kept at 10 mW. The optical transmission in the UV–visible range (200–2000 nm) measurements was performed using Shimadzu UV-3101 PC spectrophotometer. Films thicknesses and optical band gaps were estimated from fitting optical transmission data. Films electrical characterization was performed using Hall Effect measurement system, at room temperature (27 °C), to determine carriers concentration, mobility and electrical conductivity. ZnO/CuO heterojunction has been realized using CuO films prepared with a flow rate of 10 ml/h. ZnO films were also prepared by ultrasonic spray using the same deposition system. The sprayed solution was composed of 0.1 M dehydrate zinc acetate dissolved in methanol, the substrate temperature was fixed at 300 °C and flow rate of 10 ml/h, the obtained ZnO film have a thickness of 200 nm. The *I–V* characteristic of the obtained heterostructure was recorded using a curve tracer 370 Sony Tetronix.

3. Results and discussion

In Fig. 1 we have reported the prepared films thickness variation as a function of flow rate. In figure inset, we have drawn the variation of the deposition rate, the later is estimated from the ratio of film thickness on the deposition time fixed at 20 min. As can be seen, bellow 20 ml/h the deposition rate is almost constant and equal to 200 nm/min, while above this critical value the deposition rate varies linearly with the flow rate.

The XRD spectra recorded in different films are shown in Fig. 2. In the whole spectra, only two peaks assigned respectively to the planes (111) and (002) assigned to CuO tetragonal structure are present (PDF card #45-0937).

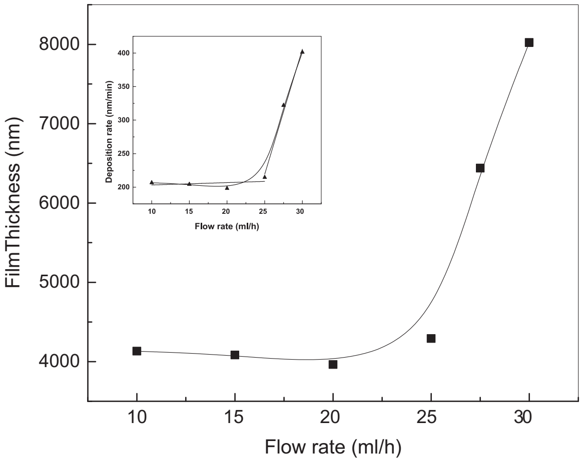

Fig. 1. Variation of film thickness as a function of solution flow rate, inset shows deposition rate dependence on solution flow rate.

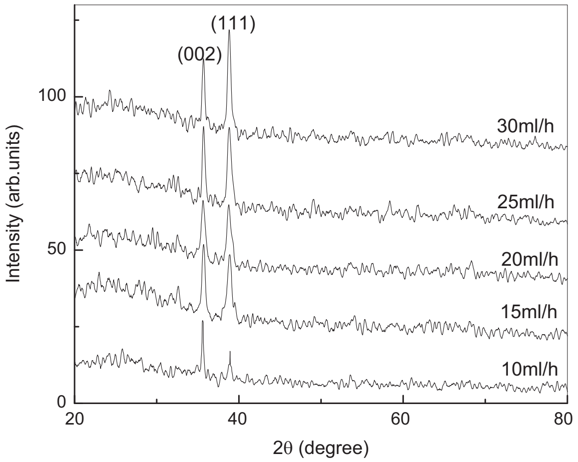

Fig. 2. XRD diffraction pattern of CuO thin films prepared with different solution flow rates.

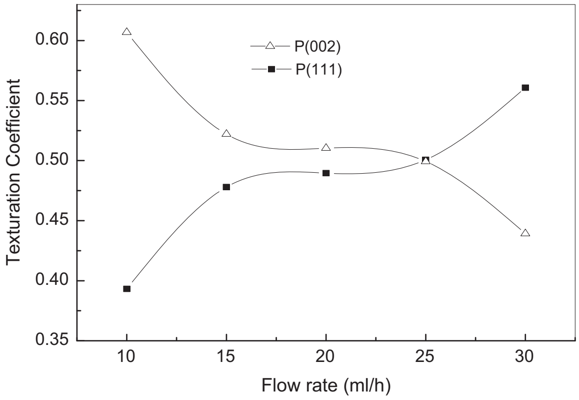

Fig. 3. Variation of the texturation coefficient of the direction (002) and (111) as a function of the solution flow rate.

No peaks related to Cu_2O phase are seen. Dominant CuO phase has been also reported in different studies [31,32] where (002) preferential orientation is observed, while Kose et al. [33] have observed the (111) preferential orientation. However, in our case, an inversion in the preferential orientation with varying the flow rate is seen, as drawn in Fig. 3 showing the variation of the preferential orientation expressed by the texturation coefficient $T(hkl)$ of each direction (hkl) defined as [34]:

$$T(hkl) = \frac{I(hkl)}{I_0(hkl)}\left[\frac{1}{n}\sum_{i=1}^{n}\frac{I(hkl)}{I_0(hkl)}\right]^{-1} \tag{1}$$

where $I(hkl)$ is the measured intensity of the plane (hkl) and I_0 (hkl) the standard intensity of the plane (hkl) taken from PDF card data, n is the reflection number.

From Fig. 3 we deduce that CuO film starts with preferential orientation (002) at low flow rate to become along the direction (111) above 25 ml/h. We speculate that the change in the growth direction may originate from the variation in the growth rate. At low growth rate the plane (002) is formed; while at faster growth rate the plane (111) is formed indicating that the latter plane requires less formation energy than the plane (002). This is consistent with the commonly observed (111) preferential orientation observed in CuO films formed with conditions involving low energy such as sol–gel or low substrate temperatures [35–38].

The films crystallite size and internal lattice strain have estimated from Hall–Williamson equation [39] expressed as:

$$\beta \cos\theta/\lambda = 1/D + \varepsilon \sin\theta/\lambda \tag{2}$$

where β is the FWHM (full width at half-maximum) of diffraction peaks, θ is the Bragg angle, λ is the wavelength of the used X rays, D is the crystallite size and ε is the internal strain. D and ε are estimated from the last square fit of $\beta\cos(\theta)/\lambda$ versus $\sin(\theta)/\lambda$ of different peaks. The intercept of the equation plot with the y axis yields to the crystallite size, while the strain is equal to the slope of the plot. The positive slope confirms the tensile strain nature in the prepared films [40].

The variations of the crystallite size together with the film strain are reported in Fig. 4. The obtained films have a polycrystalline nanostructure, the obtained crystallite size are ranged from 60 to 10 nm. As seen, the crystallite size is reduced with increasing the flow rate. Indeed at low flow rate the deposition rate is low; thereafter the film formation process is slow yielding to larger crystallites formation. On the other hand an increase in the flow rate causes the rise of internal strain in the formed crystallites. Above 25 ml/h flow rate we noticed a strain relaxation and an increase in the crystallite size, this can be due to the change in growth direction at this flow rate as suggested from Fig. 3.

Fig. 5 shows the Raman spectra of the as-prepared CuO thin films with different flow rates. The Raman spectra are composed with three main phonon modes (Ag and 2Bg) located at 297, 334 and 608 cm^{-1}. These peaks are largely reported in the literature [41–43]. This confirms the presence of a single phase CuO with a monoclinic structure as deduced from XRD analysis. The position of the intense peak Ag is shifted with the flow rate as seen in inset Fig. 5. The variation of peak position correlates with the strain

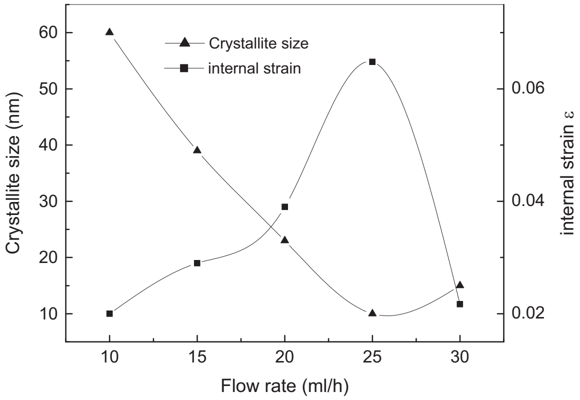

Fig. 4. Crystallite size and internal stress in grain as a function of flow rate.

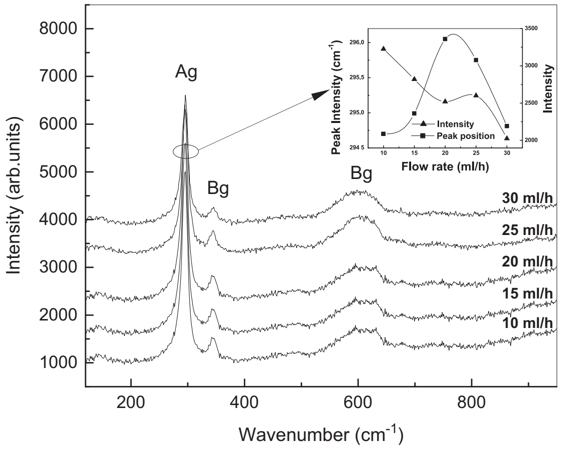

Fig. 5. Micro-Raman spectra of CuO deposited with various flow rates. Inset figure shows the variation of the Ag peak position and width at half-maximum.

variation in the crystallite. This confirms that the peak shift is due to the strain in the crystallite. The Ag peak intensity (inset Fig. 5) is reduced with increasing flow rate indicating the reduction in crystalline quality of film as suggested from the variation of the crystallite size with the deposition flow rate (Fig. 4).

The transmittance spectra in UV–visible region of the prepared CuO films are shown in Fig. 6. The films deposited with low flow rates exhibit higher transparency due to their low thickness. It can be seen that when the flow rate increases the transmittance decreases until 20 ml/h, and increases again with further flow rate increase. It is well argued that the deposition rate may alter the nucleation step, at low deposition rate the nuclei size is larger than in rapid growth rate one [44]. Moreover, larger nuclei yields to a rougher film surface. Thereafter, the film prepared at 20 ml/h have a rougher film surface due to its lower deposition rate (Fig. 1). The surface roughness causes the scattering of incident light [45], this explains then the low transmittance measured in the film prepared at 20 ml/h.

Films optical band gaps are estimated, as shown in Fig. 7, from the plot $(\alpha h\nu)^2$ as a function of photon energy $(h\nu)$, according to Tauc formula for direct band gap semiconductors [46]:

$$(\alpha h\nu)^2 = B\ (E_g - h\nu) \tag{3}$$

where α is a absorption coefficient, B is a constant, h is Planck constant, E_g is the energy band gap and ν is incident photon frequency.

Due to the disorder in film network, localized states appears near the bands edges which causes band tails formation. These band tail states are responsible for the photon absorption in the low energies range. In this range the absorption coefficient is given by [47]:

$$\alpha(h\nu) = \alpha_0 \exp(h\nu/E_{00}) \tag{4}$$

where α_0 is the pre-exponential factor, $h\nu$ the photon energy and E_{00} is the band tail width or disorder energy commonly called Urbach tail [48]. E_{00} can be estimated from the inverse slope of the linear plot of ln(α) versus $h\nu$.

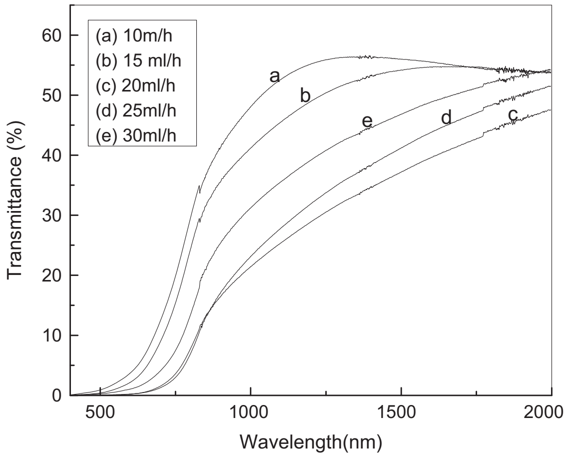

Fig. 6. UV–visible transmittance spectrum of CuO thin films deposited using different flow rates.

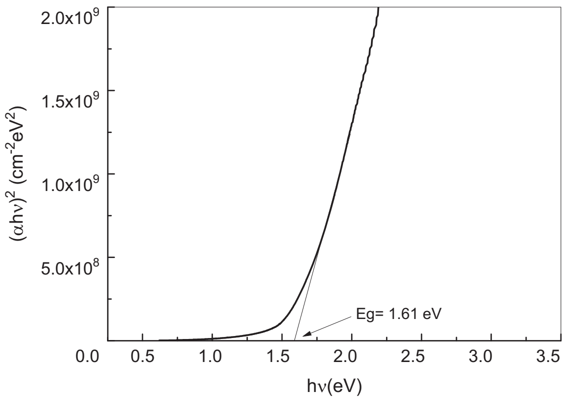

Fig. 7. Typical variation of the quantity $(\alpha h\nu)^2$ as a function of photon energy, for the sample prepared at 10 ml/h used for the determination of the optical gap.

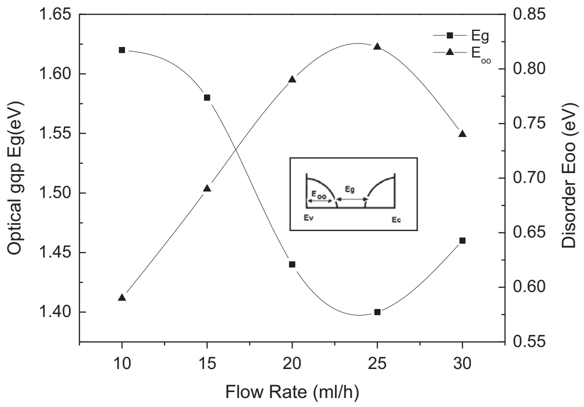

Fig. 8. Variation of the optical band gap and disorder in film network as a function of the flow rate. Inset figure is a schematic drawn of energy band diagram.

The variations of the calculated band gap and band tail width E_{00} with flow rate are reported together in the same graph (Fig. 8). The optical gap is ranged from 1.4 to 1.6 eV, this is in the same order than the reported values in the literature [28,29]. However, film prepared at flow rate of 25 ml/h have an optical band gap close to 1.4 eV required for solar cells since it matches well with solar spectrum. At low deposition rate the incoming species on surface substrate have enough time to find a favorable site and to form a more organized material. In contrary, higher deposition rate case leads to much disordered network due to the fast film formation. Thus, the observed enhancement of the network disorder with increasing the flow rate (Fig. 8) can be explained in terms of deposition rate variation. An increase in the band tail width is followed by the reduction in the optical band gap (as depicted in inset Fig. 8). This suggests that the variation of the optical gap is governed by the disorder in the film network.

The films electrical conductivity was characterized by mean of Hall Effect measurements in order to determine the dark conductivity, free carriers concentration and mobility. In Fig. 9 we have reported the electrical

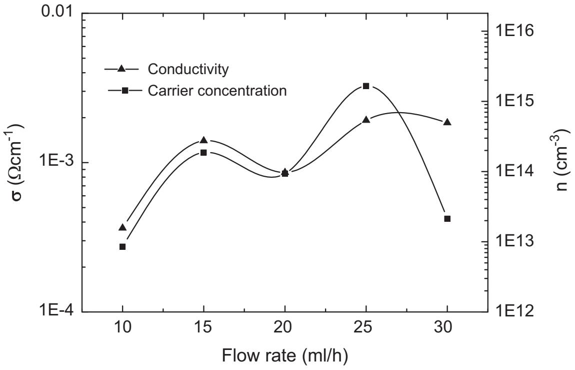

Fig. 9. Dependence of the CuO film conductivity and free carrier concentration upon the flow rate.

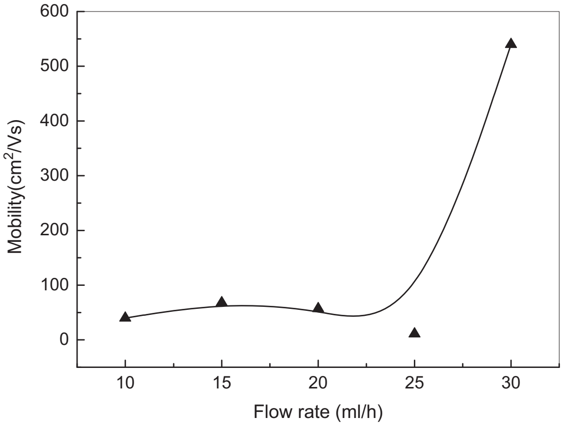

Fig. 10. Variation of the carrier mobility versus the solution flow rate.

conductivity variation together with the free carriers concentration as a function of solution flow rate. Fig. 10 shows the variation of the carrier mobility. As can be seen, the electrical conductivity follows faithfully the trend of the carriers concentration. Indeed, the electrical conductivity in semiconductors is proportional to the product of the free carrier concentration n and their mobility μ ($\sigma = q\mu n$). The carriers concentration varies by three decades while the mobility variation is less than one decade (see Figs. 9 and 10). This indicates clearly that the conductivity is rather controlled by the free carrier concentration than by their mobility.

The whole prepared films have p type conductivity according to Hall constant sign. With increasing flow rate above 20 ml/h, the conductivity is enhanced by one decade due to the increase in the free carriers concentration. As mentioned above, increasing the flow rate causes the formation of disorder in film network (Fig. 8). This disorder yields to the appearance of defects such as cation vacancy or oxygen in interstitial sites. These defects act as doping impurities in film network [49], causing an increase in free carriers concentration and consequently the conductivity.

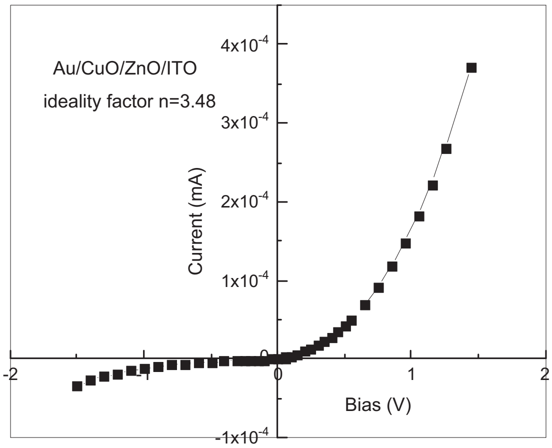

Fig. 11. Typical current–voltage characteristic of a realized ZnO/CuO heterojunction.

The prepared CuO films have been used as partner to a wide band gap semiconductor such as ZnO to produce ZnO/CuO heterojunction structure. This structure has found applications as thin film solar cell for photovoltaic solar energy conversion and as gas sensors [50–53]. The *I–V* characteristic of the prepared heterojunction n-ZnO/p-CuO is shown in Fig. 11. The realized hetrostructure present a good rectifying behavior with low leakage current (~12 μA) and ideality factor of 3.4. The realized structure may found application as gas sensor or thin film solar cell. They are under investigation.

The required flow rate to achieve better solar cell efficiency is the larger flow rate, since under this condition, the obtained films are thicker with large conductivity and mobility. These characteristics may enhance the light absorption due to the thickness, reduce the series resistance due to low material resistivity and increase the photocurrent due to the large carriers mobility.

4. Conclusion

In present work, CuO thin films have been synthesized using spray pyrolysis technique. The influence of solution flow rate on films properties has been investigated. The obtained results indicate that CuO films properties are sensitive to the flow rate. The deposition rate is almost constant for a flow rate below 20 ml/h, while above this value the deposition rate varies linearly with the solution flow. The structural analysis reveals that, in the whole investigated flow rate range, films are mainly composed only with CuO mono phase with a tetragonal structure. The crystallite size is reduced with increasing the flow rate. Raman spectroscopy confirms the films composition with CuO single phase. The films optical gap varies in the range of 1.4–1.6 eV which is suitable for solar cells fabrication. Films are p type, their conductivity and free carrier concentration are increased with increasing the flow rate. The prepared n-ZnO/p-CuO heterojunction exhibits a good rectifying behavior suggesting its application as solar cells or gas sensor. Finally, the ideal condition for better solar cell efficiency is increasing the flow rate.

References

[1] S.J. Appleyard, Phys. Educ. 41 (5) (2006) 409.
[2] V.R. Katti, A.K. Debnath, K.P. Muthe, Manmeet Kaur, A.K. Dua, S.C. Gadkari, S.K. Gupta, V.C. Sahni, Sens. Actuators B 96 (2003) 245–252.
[3] S. Aygun, D. Cann, Sens. Actuators B 106 (2005) 837–842.
[4] I. Singh, R.K. Bedi, Appl. Surf. Sci. 257 (2011) 7592.
[5] T. Ito, H. Yamaguchi, K. Okabe, J. Mater. Sci. 3 (1998) 3555.
[6] R. Prasad, J. Therm. Anal. Calorim. 85 (2006) 279.
[7] M. Cyrot, D. Pavuna, Introduction to Superconductivity and High-Tc Materials, World Scientific Publishing Co. Pvt. Ltd, USA, 1992, 170 (in).
[8] X.P. Gao, J.L. Bao, G.L. Pan, H.Y. Zhu, P.X. Huang, F. Wu, D.Y. Song, J. Phys. Chem. B 108 (2004) 5547.
[9] J. Morales, L. Sanchez, F. Martın, J.R. Ramos-Barrado, M. Sanchez, Thin Solid Films 474 (2005) 133.
[10] R.V. Kumar, Y. Diamant, A. Gedanken, Chem. Mater. 12 (2000) 2301.
[11] A. Chowdhuri, V. Gupta, K. Sreenivas, R. Kumar, S. Mozumdar, P. K. Patanjali, Appl. Phys. Lett. 84 (2004) 1180.
[12] H. Cao, S.L. Suib, J. Am. Chem. Soc. 116 (1994) 5334.
[13] Y.S. Gong, C. Lee, C.K. Yang, J. Appl. Phys. 77 (1995) 5422.
[14] E.R. Kari, K.S. Brown, C. Choi, Chem. Commun. (2006) 3311.
[15] N. Serin, T. Serin, S. Horzum, Y. Celik, Semicond. Sci. Technol. 20 (2005) 398.
[16] T. Maruyama, Jpn. J. Appl. Phys. 37 (1998) 4099.
[17] K. Santra, C.K. Sarkar, M.K. Mukherjee, B. Ghosh, Thin Solid Films 213 (1992) 226.
[18] S. Kose, E. Ketenci, V. Bilgin, F. Atay, I. Akyuz, Curr. Appl. Phys. 12 (2012) 890.
[19] J. Morales, L. Sanchez, F. Martın, J.R. Ramos-Barrado, Miguel Sanchez, Electrochim. Acta 49 (2004) 4589.
[20] V.F. Drobny, D.L. Pulfrey, Thin Solid Films 61 (1979) 89.
[21] A. Mosbah, M.S. Aida, J. Alloys Compd.s 515 (2012) 149.
[22] F. Ynineb, A. Hafdallah, M.S. Aida, N. Attaf, J. Bougdira, H. Rinnert, S. Rahman, Mater. Sci. Semicond. Process. 16 (2013) 2021.
[23] M. Messaoudi, M.S. Aida, N. Attaf, T. Bezzi, J. Bougdirab, G. Medjahdi, Mater.Sci Semicond. Process. 17 (2014) 38.
[24] A. Hafdallah, F. Yanineb, M.S. Aida,and, N. Attaf, J. Alloys Compd. 509 (2011) 7267.
[25] A.S. Kumar, K. Perumal, P. Thiruunavukkarsu, Optoelctron. Adv. Mater. l4 (2010) 831.
[26] I. Singha, R.K. Bedib, Appl. Surf. Sci. 257 (2011) 7592.
[27] Y.S. Chaudharya, A. Agrawala, R. Shrivastava, V.R. Satsangib, S. Dassa, Int. J. Hydrog. Energy 29 (2004) 131.
[28] F. Atay, V. Bilgin, I. Akyuz, S. Kose, J. Optoelectron. Adv. Mater. 9 (11) (2007) 3604.
[29] S. Kose, E. Ketenci, V. Bilgin, F. Atay, I. Akyuz, Curr. Appl. Phys. 12 (2012) 890.
[30] M.S. Aida, L. Baghriche, N. Zebbar, N. Attaf, J. Nanoeng. Nanosyst. 223 (2010) 25.
[31] J.H. Lee, B.W. Yeo, B.O. Park, Thin Solid Films 457 (2004) 333.
[32] C. Luyo, I. Fabregas, L. Reyes, J.L. Solis, J. Rodriguez, W. Estrada, R. J. Candal, Thin Solid Films 516 (2007) 25.
[33] S. Kose, F. Atay, V. Bilgin, I. Akyuz, Mater. Chem. Phys. 111 (2009) 351.
[34] C.S. Barret, T.B. Massalski, Structure of Metals, Pergamon Press, Oxford, 1980 (in).
[35] Y.-S. Kim, I.-S. Hwang, S.-J. Kim, C.-Y. Lee, J.-H. Lee, Sens. Actuators B 135 (2008) 298.
[36] V. Dhanasekaran, T. Mahalingam, J. Alloys Compd. 539 (2012) 50.
[37] L. De Los Santos Valladares, D. Hurtado Salinas, A. Bustamante Dominguez, D. Acosta Najarro, S.I. Khondaker, T. Mitrelias, C.H. W. Barnes, J. Albino Aguiar, Y. Majima, Thin Solid Films 520 (2012) 6368.
[38] T. Okun, R. Motoyoshi, K. Fujimoto, T. Akiyama, B. Jeyadevan, J. Cuya, J. Phys. Chem. Solids 72 (2011) 1206.
[39] N.S. Ramgir, Y.K. Hwang, I.S. Mulla, J. Chan, Solid. State Sci. 8 (2006) 162.
[40] I. Singh, G. Kaur, R.K. Bedi, Appl. Surf. Sci. 257 (2011) 9546.
[41] D.P. Volanti, D. Keyson, L.S. Cavalcante, A.Z. Sim~oes, M.R. Joya, E. Longo, J.A. Varela, P.S. Pizani, A.G. Souza, J. Alloys Compd. 459 (2008) 537.
[42] H. Fan, B. Zou, Y. Liu, S. Xie, Nanotechnology 17 (2006) 1099.
[43] T. Yu, C.-H. Sow, A. Gantimahapatruni, F.-C. Cheong, Y. Zhu, K.-C. Chin, X. Xu, C.-T. Lim, Z. Shen, J.T.-L. Thong, A.T.-S. Wee, Nanotechnology 16 (2005) 1238.
[44] H. Moualkia, S. Hariech, M.S. Aida, N. Attaf, E.L. Laifa, J. Phys. D: Appl. Phys. 42 (2009) 135404.
[45] S. Schröder, A. Duparré, L. Coriand, A. Tünnermann, D.H. Penalver, J.E. Harvey, Opt. Express 19 (2011) 9820.
[46] J.J. Tauc, Amorphous and Liquid Semiconductors, Plenum, London, 1974 (in).
[47] F. Urbach, Phys. Rev. 92 (1953) 1324.
[48] I. Singh, R.K. Bedi, Appl. Surf. Sci. 257 (2011) 7592.
[49] G. Uozumi, M. Miyayama, H. Yanagida, J. Mater. Sci. 32 (1997) 2991.
[50] J.D. Choi, G.M. Choi, Sens. Actuators B: Chem. 69 (2000) 120.
[51] D.H. Yoon, J.H. Yu, G.M. Choi, Sens. Actuators B: Chem. 46 (1998) 15.
[52] K.K. Baek, H.L. Tuller, Solid State Ion. 75 (1995) 26.
[53] S.J. Jung, H. Yanagida, Sens. Actuators B: Chem. 37 (1996) 55.

World Academy of Science, Engineering and Technology
International Journal of Mathematical, Computational, Physical, Electrical and Computer Engineering Vol:9, No:10, 2015

International Science Index, Physical and Mathematical Sciences Vol:9, No:10, 2015 waset.org/Publication/10002779

CuO Thin Films Deposition by Spray Pyrolysis: Influence of Precursor Solution Properties

M. Lamri Zeggar, F. Bourfaa, A. Adjimi, F. Boutbakh, M. S. Aida, N. Attaf

Abstract**—**CuO thin films were deposited by spray ultrasonic pyrolysis with different precursor solution. Two staring solution slats were used namely: copper acetate and copper chloride. The influence of these solutions on CuO thin films proprieties of is instigated. The X rays diffraction (XDR) analysis indicated that the films deposed with copper acetate are amorphous however the films elaborated with copper chloride have monoclinic structure. UV- Visible transmission spectra showed a strong absorbance of the deposited CuO thin films in the visible region. Electrical characterization has shown that CuO thin films prepared with copper acetate have a higher electrical conductivity.

Keywords**—**Thin films, cuprous oxide, spray pyrolysis, precursor solution.

I. INTRODUCTION

METAL OXIDE thin films used in various technological application are predominantly governed by their properties. Among these, cuprous oxide (CuO) thin films have been intensely studied as a promoting materiel for many industrial applications.

CuO has a monoclinic crystal structure and important p-type semiconductor with an optical band gap ranged from 1,2 to 1,6 eV and a high absorption coefficient [1]. CuO thin films were utilized in different applications such as: gas sensor for detection of CO and CO_2 [2], absorber layers for solar cells with theoretical predicted efficiency of 20% [3], lithium battery [4] and material for the magnetic storage [5]. Several techniques have been employed to prepare CuO thin films for example: sol-gel [6], electrode position [7], chemical vapor deposition [8], thermal oxidation [9] and reactive sputtering [10]. Among these techniques CuO thin films have been grow typically by spray pyrolysis on diverse type of substrates. It is a simple and easy technique for deposition of various metal oxide thin films. Two major interests in this method are the operating at atmospheric pressure and the deposition on a large surface. Investigations of deposition parameters influence on CuO thin films properties have been intensively carried. Parameters such as: substrates temperature [11], substrate nature [12] and doping [13]. However fewer studies have been devoted to the influence of precursor solution on the proprieties of CuO thin films.

In the present paper we address a comprehensive study of the influence of the solution nature and properties on the characteristics of CuO thin films deposited by spray pyrolysis technique.

II. EXPERIMENTAL

CuO thin films were deposited by spray ultrasonic pyrolysis on clean glass substrates using 0,05M of two aqueous solution of copper chloride ($CuCl_2.2H_2O$) and copper acetate ($C_4H_6O_4Cu.2H_2O$).To prepare 40 ml of the precursor solution the required quantity of salt is dissolved in double distilled water. The substrate temperature was kept at 300°C and the deposition time was fixed for 30 min.

Films structural properties were determined by XRD using PhilipsX'Pert system with CuKα radiation (λCu=0.154056nm). The diffract meter reflections were taken at room temperature and the 2θ value were varied in the range 20–80°. Films morphology was analyzed using scanning electron microscope Jeol5400SEM microscope. The optical transmission in the UV–visible range (200–2400nm) measurements was performed using ShimadzuUV-3101PC spectrophotometer. Films thicknesses were estimated from fitting optical transmission data. Films electrical characterization was performed using Hall Effect measurement system at room temperature (27°C), to determine electrical conductivity.

III. RESULTS AND DISCUSSION

A. Deposition Rate

In Table I, we have reported the film thickness and the deposition rate with different precursor solutions used. The deposition rate is estimated from the ratio of the thickness of the layer on the deposition time. As can be seen the deposition rate of CuO thin films deposited with copper chloride is almost three times greater than the deposited rate of the films obtained with copper acetate.

TABLE I
THICKNESS AND DEPOSITION RATE WITH DIFFERENT PRECURSOR SOLUTION

Precursor	Thickness (μm)	Deposition rate (nm/min)
Copper chloride	2.8	192
Copper acetate	1	67.3

The difference in thickness originates from the difference in the precursor properties that may alter the films growth mechanism. The formation of the films is produced by the pyrolytic reaction on the surface of substrate. When using copper chloride the reaction on surface is spontaneous.

M. LamriZeggar is with the Department of Physics, Laboratory of Thin Films and Interface, University Constantine 1, Algeria (e-mail: meryemlamri@gmial.com).

M. S. Aida is with the Faculty of Science, Department of Physics, Laboratory of Thin Films and Interface, UniversityConstantine1, Algeria (e-mail:aida_salah2@yahoo.fr).

However, when using copper acetate as starting solution the pyrolytic reaction is slowly. In fact, the decomposition of copper acetate in water leads to the formation of compound copper hydroxide $Cu(OH)_2$.Therefore, Copper ions (Cu^{+2}) are trapped by the hydroxide, the decomposition of this compound release requires else intermediate reactions which delays the formation of CuO phase in the case of copper acetate. On contrary to the solution prepared with copper chloride the copper ions are free which leads dialectally to the growth of CuO thin films.

B. Structural Proprieties

Fig. 1 shows XRD spectra of CuO thin films deposited with the two studied salts. As can be seen, the films deposited with copper chloride solution are polycrystalline in nature. Two most prominent peaks can be clearly located at 2θvalue 35.5° and 39.1° corresponding to atomic planes (111) and (200), respectively of CuO phase. This indicated that the obtained CuO films have a monoclinic structure with the preferential orientation normal to the (200) direction. However the films deposited with copper acetate are amorphous in nature, since no peaks corresponding to monoclinic CuO planes were observed in the XRD pattern (Fig. 1 (b)).

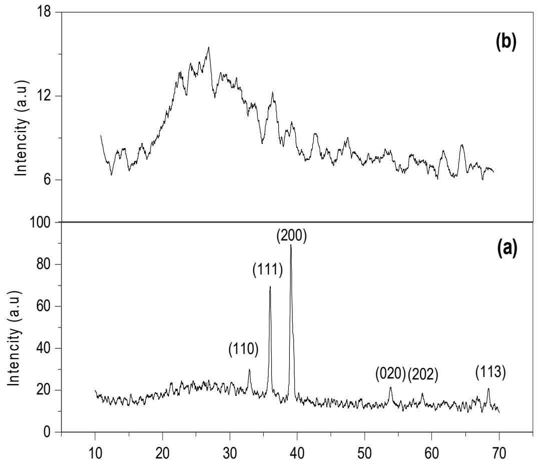

Fig. 1 XRD spectra of CuO thin films deposited at substrate temperature equal to 300°C with different solutions: (a) Copper chloride and (b) Copper acetate

Fig. 2 shows the Raman spectra of the as-prepared CuO thin films with different precursor solution. The Raman spectra are composed with three main phonon modes (Ag and 2Bg) located at 295,343 and 605 cm^{-1}. These peaks are largely reported in the literature [14]–[16]. This confirms the presence of a single phase CuO for all deposited films.

Fig. 3 shows typical SEM images of films deposited with the tow studied precurs or solutions. As can be seen, the film morphology depends strongly on the nature of the used precursor. The films elaborated with copper acetate are characterized by a rough, granular surface, consisting of crystallites distributed randomly with the presence of a needle structures. While films prepared with copper chloride salt gave a densely packed structure with uniformly distributed grains.

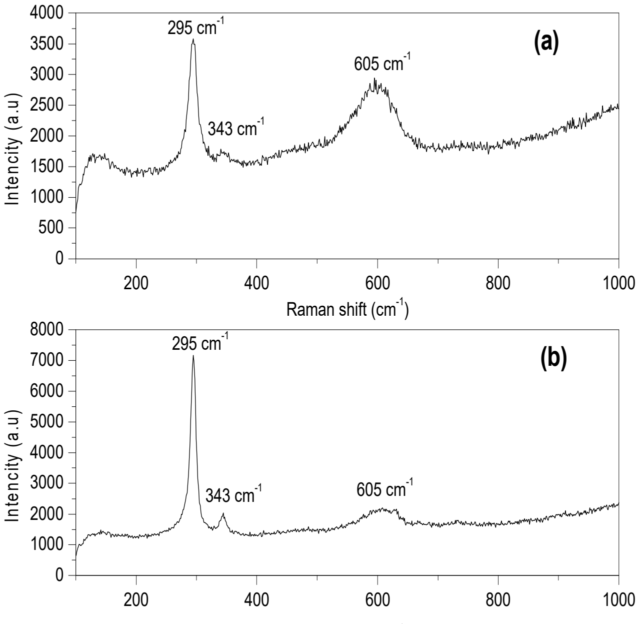

Fig. 2 Micro-Raman spectra of CuO deposited with different solutions: (a) Copper acetate and (b) Copper chloride

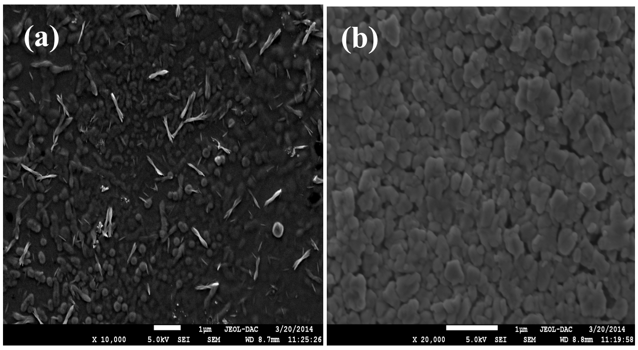

Fig. 3 SEM images of CuO thin films deposited at substrate temperature equal to 300°C with different solutions: (a) Copper acetate and (b) Copper chloride

C. Optical Proprieties

The transmittance spectra in UV–visible region of the prepared CuO films are shown in Fig. 4. As deposited CuO thin films exhibit a strong absorption in visible region. Films deposited with copper chloride have low transparency than films prepared with acetate due to the difference in thickness of the deposited films.

The optical band gaps of films have been estimated, as shown in Fig. 5, from the plot of their absorption coefficient as a function of photon energy and using Tauc formula for direct band gap semiconductors [17]:

$$(\alpha h\upsilon)^2 = B\,(E_g\text{-}h\upsilon) \qquad (1)$$

where α is a absorption coefficient, B is a constant, h is Planck constant, E_g is the energy band gap and $\nu$is incident photon frequency.

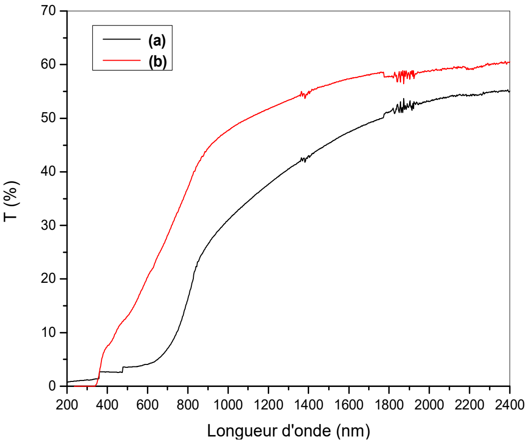

Fig. 4 UV-visible transmittance spectrum of CuO thin films deposited at 300 °C using different salts: (a) Copper chloride and (b) Copper acetate

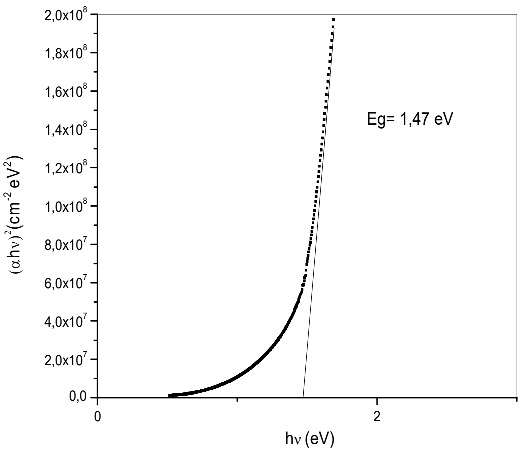

Fig. 5 Typical variation of the quantity $(\alpha h\nu)^2$ as a function of photon energy, for the sample prepare with copper chloride used for the determination of the optical gap

The obtained values of optical band gap and band tail width are reported in Table II. Films optical band gap are found equal to 1.47 and 1.30 eV for films prepared with copper chloride and copper acetate respectively which is in good agreement with CuO band gap values reported by [18]. These values are required for absorber layer in solar cells since it matches well with solar spectrum.

Due to the disorder in film network, localized states appear near the bands edges which cause band tails formation. These band tail states are responsible for the photon absorption in the low energies range. In this range the absorption coefficient is given by [19]:

$$\alpha\,(h\nu) = \alpha_0 \exp\,(h\nu/E_{00}) \qquad (2)$$

where α_0 is the pre-exponential factor, hν the photon energy and E_{00} is the band tail width or disorder energy commonly called Urbach tail. E_{00} can be estimated from the inverse slope of the linear plot of ln(α) versus hν.

The values of the band tail width E_{00} with various precursor solutions are reported in Table II. As can be seen value of the band tail width for the films prepared with copper acetate is more important is due to the presence of the amorphous phase in these films. This confirms the presence of amorphous phase as deduced from XRD analysis. The variation of the band tail and the optical band gap are opposite. This suggests that the variation of the optical gap is governed by the disorder in the film network.

TABLE II
OPTICAL BAND GAP AND BAND TAIL WIDTH WITH DIFFERENT PRECURSOR SOLUTIONS

Precursor	E00 (eV)	Eg (eV)
Copper chloride	0.40	1.47
Copper acetate	0.75	1.30

D. Electrical Proprieties

The films electrical conductivity was characterized by mean of Hall Effect measurements in order to determine the dark conductivity, free carriers concentration and mobility. In Table III we have reported the electrical conductivity and free carriers concentration of the deposited CuO thin films. As can be seen, the electrical conductivity follows faithfully the trend of the carriers' concentration. This indicates clearly that the conductivity is rather controlled by the free carrier concentration. The whole prepared films have p type conductivity according to Hall constant sign. The free carriers concentration in film prepared with copper chloride is three decades lower than in film prepared with the copper acetate indicating that using copper chloride as precursor yields to a film with low density of defects such as copper vacancies or oxygen in interstice sites since the latter are a source of free carriers.

TABLE III
ELECTRICAL CONDUCTIVITY AND FREE CARRIERS CONCENTRATION WITH DIFFERENT PRECURSOR SOLUTION

Precursor	σ (Ω.cm^{-1})	Free carriers concentration (cm^{-3})
Copper chloride	3.46×10^{-3}	7.73×10^{17}
Copper acetate	1.46×10^{-4}	9.37×10^{13}

IV. CONCLUSION

In present work, CuO thin films have been synthesized using spray pyrolysis technique. The influence nature of precursor solution on films properties has been investigated. The obtained results indicate that CuO films properties are sensitive to staring solution slats. The films deposited with copper chloride are crystalline with monoclinic structure. While films deposited with copper acetate are composed with micros-crystallites embedded in an amorphous phase. SEM image reveals that films elaborated with copper acetate are characterized by the presence of a needle structures. All CuO thin films have direct band gaps and strong absorption in visible region this property is suitable for photovoltaic applications.

REFERENCES

[1] F. Marabelli, G. B. Parravicini, F. Salghetti-Drioli, Phys. Rev. B52 (1995) 1433–1436.

[2] A. Chowdhuri, V. Gupta, K. Sreenivas, R. Kumar, S. Mozumdar, P. K. Patanjali, Appl. Phys. Lett. 84 (2004) 1180–1182.

[3] K. Han, M. Tao, Sol. Energy Mater. Sol. Cells 93 (2009) 153.

[4] X. P. Gao, J. L. Bao, G. L. Pan, H. Y. Zhu, P. X. Huang, F. Wu, D. Y. Song, J. Phys. Chem. B 108 (2004) 5547–5551.

[5] R. V. Kumar, Y. Diamant, A. Gedanken, Chem. Mater. 12 (2000) 2301–2305.

[6] A. Y. Oral, E. Mensur, M. H. Aslan, E. Basaran,MaterChemPhys, 83(1), 140 (2004).

[7] E. R. Kari, K. S. Brown, Choi, Electrochemical synthesis and characterization of transparent nanocrystalline Cu2O films and their conversion to CuO films, Chem. Commun. (2006) 3311–3313.

[8] T. Maruyama, Copper oxide thin films prepared from copper dipivaloylmethanate and oxygen by chemical vapor deposition, Jpn. J. Appl. Phys. 37(1998) 4099–4102.

[9] J. H. Benjamin, K. Nikolai, L. Ganhua, L. I. - Khan, C. Junhong, Z. Xin, Transport, analyte detection and optoelectronic response of p-type CuO nanowires, J. Phys. Chem. C 114 (2010) 2440–2447.

[10] V. F. Drobny, D. L. Pulfrey, Properties of reactively-sputtered copper oxide thinfilms, Thin Soild Films 61 (1979) 89–98.

[11] D. Gopalakrishna, K. Vijayalakshmi, C. Ravidhas Effect of pyrolytic temperature on the properties of nano-structured Cuo optimized for ethanol sensing applications, J Mater Sci: Mater Electron (2012).

[12] V. Dhanasekaran, T. Mahalingam, Physical properties evaluation of various substrates coated cupric oxide thinfilms by dip method, Journal of Alloys and Compounds 539 (2012) 50–56.

[13] S. Kose, E. Ketenci, V. Bilgin, F. Atay, I. Akyuz, Some physical properties of In doped copper oxide films produced by ultrasonicspray pyrolysis, Current Applied Physics 12 (2012) 890-895.

[14] D. P. Volanti, D. Keyson, L.S. Cavalcante, A.Z. Sim~oes, M.R. Joya, E. Longo, J. A. Varela, P. S. Pizani, A. G. Souza, J. Alloys Compd. 459 (2008) 537.

[15] H. Fan, B. Zou, Y. Liu, S. Xie, Nanotechnology 17 (2006) 1099.

[16] T. Yu, C.-H. Sow, A. Gantimahapatruni, F.-C. Cheong, Y. Zhu, K.-C. Chin, X. Xu, C.-T. Lim, Z. Shen, J.T.-L. Thong, A.T.-S. Wee, Nanotechnology 16 (2005) 1238.

[17] J. J. Tauc, Amorphous and Liquid Semiconductors, Plenum, London, 1974.

[18] L. Chabane, N. Zebbar, M. Lamri Zeggar, M. S. Aida, M. Kechouane a, M. Trari, Effects of CuO film thickness on electrical properties of CuO/ZnO and CuO/ZnS hetero-junctions Materials Science in Semiconductor Processing 40 (2015) 840–847.

[19] F. Urbach, Phys. Rev. 92 (1953) 1324.

International Science Index, Physical and Mathematical Sciences Vol:9, No:10, 2015 waset.org/Publication/10002779

Copper oxide thin films for ethanol sensing

Article · March 2016

DOI: 10.1088/1757-899X/108/1/012004

Meryem Lamri zeggar
University of Constantine 1

M.s. Aida
University of Constantine 1

Copper oxide thin films for ethanol sensing

2016 IOP Conf. Ser.: Mater. Sci. Eng. 108 012004

(http://iopscience.iop.org/1757-899X/108/1/012004)

Copper oxide thin films for ethanol sensing

M Lamri Zeggar[1], F Bourfaa[1], A Adjimi[1], M S Aida[1] and N Attaf[1]

[1]Laboratory of thin films and interfaces, Faculty of science, University Constantine 1, Algeria

meryemlamri@gmail.com

Abstract. The present is a study of a new active layer for ethanol (C2H5OH) vapour sensing devices based on copper oxide (CuO). CuO films were prepared by spray ultrasonic pyrolysis at a substrate temperature of 350 °C. Films microstructure was examined by X-ray diffraction and atomic force microscopy. Vapour-sensing testing was conducted using static vapour-sensing system, at different operating temperatures in the range of 100°C to 175°C for the vapour concentration of 300 ppm. The results show a high response of 45% at relatively low operating temperatures of 150°C towards ethanol vapour.

1. Introduction

Gas sensors based on semiconducting metal oxides are widely studies for solving applications spanning from the detection of toxic, dangerous and pollutant gas. They are having several advantages such as easy and low cost production, controlled size and simple measure electronics [1, 2].

However the performance of such gas sensors is considerably influenced by the proprieties of sensing materials such as the morphology and structure. Among the used sensing materials, copper oxide have been the subject of interest for the detection of many different gas such as H_2 [3], NO_3, CO and C_5H_2OH [4].CuO is generally p-type semiconductor with bad gap in the rage of 1, 21 to 1, 51 eV [5, 6]. Several researches in the field of gas sensing have been reported, they are based on the association of metal oxide with CuO, and forming of the p-n heterojuction such as CuO/ZnO, CuO/Cu_2O and CuO/SnO_2. These structures have achieved a high sensitivity and selectivity [7–9].CuO films have been deposited by various conventional deposition methods; with include electrodeposition [10]; dip coating [11]; chemical vapor deposition [12] and reactive sputtering [13].Ultrasonic spray pyrolysis technique has been used extensively because it is very attractive method to deposit adherence and stochiometric thin films. The important features of this technique are the low cost and the simplicity of equipments.

In this work, we have synthesized CuO films by ultrasonic spray pyrolysis technique and investigate their ethanol vapor sensing performance.

2. Experimental

2.1. Preparation of CuO thin film

Copper oxide thin film has been prepared on glass substrates by ultrasonic spray pyrolysis. The precursor solution was prepared by dissolving 0.05 M copper chloride ($CuCl_2.2H_2O$) in distilled water. Then, the precursor solution sprayed in fine droplets of 40 µm in diameter, by an ultrasonic generator on heated glass substrate. Film was formed by pyrolytic reaction. During deposition, the substrate temperature is kept at 350°C. The deposition time was fixed 10 min. Films structural properties were determined by XRD using Philips X'Pert system with Cu K_α radiation (λ_{Cu} = 0.154056 nm). The reflections were taken at room temperature and at 2θ value ranged from 20° to 80°. The film surface morphology was characterized by using atomic force microscopy (AFM) was carried out in air at ambient condition (300 K) using Nanosurf easy scan 2.

2.2. *Sensing system for measurement of vapour response*

The vapour-sensing studies were carried out using a static gas chamber to ethanol vapor detection in air ambient. The CuO thin film deposited at 350°C was used as the sensing elements. Two gold interdigitated electrodes were evaporated on the top surface of the sensing layer. A thermocouple is mounted to measure the temperature. The output of the thermocouple is connected to a temperature indicator. Gas concentration inside the system is achieved by injecting a known volume of test vapor.

The electrical response of the sensing layer was investigated under two atmospheres: synthetic air and a mixture of air + vapour ethanol (300 ppm) by registering the variations in resistance with Keithley 617 programmable electrometer as a function of time. The response of the sensor was calculated using the expression given in the literature [14]:

$$Sensitivity = \left| R_v - R_{air} \right| / R_{air} \; x \; 100 \qquad (1)$$

Where R_{air} is the reference resistance in the presence of air and R_v is the measured resistance in the presence of ethanol.

3. Results and discussion

3.2 Structural characterization of CuO thin films

The XRD study was primarily carried to determinate the structure and orientation of deposited thin films CuO. Figure 1 shows the XRD diffraction pattern of the sensitive CuO thin film. The presence of intense peaks in the XRD patterns of the film indicates that the CuO film is polycrystalline in nature. Two most prominent peaks can be clearly seen at 2θ value 35.5° and 38.7° corresponding to atomic planes (002) and (111), respectively of CuO phase. No peak corresponding to Cu2O phase of copper oxide has appeared in the XRD pattern thereby indicating the formation of pure CuO films.

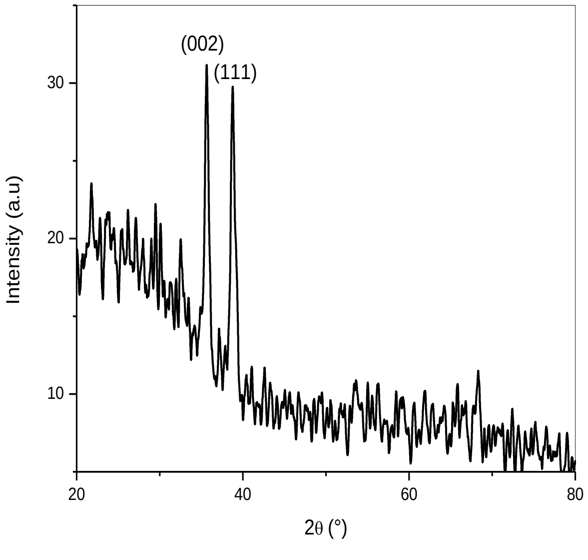

Figure 1. XRD pattern of the sensitive layer CuO thin film.

Atomic force microscopy (AFM) has been proved to be a unique method to analyze surface morphology of a film. Figure 2(a and b) shows typical two dimensional (2-D) and three dimensional (3-D) AFM image of CuO film deposited on glass substrate. The (3-D) image indicate that the surface evolution of the film shows hills and valley like structures, which are uniformly distributed over the entire substrate surface. The 2-D images of the deposits show compact and granular morphology with presence of pores in the surface this is a good argument to increase the sensitivity of the gas sensor. It is recognized that porous materials have been extensively investigated due to high surface area and accordable pore size in the fields of catalysis and gas sensing.

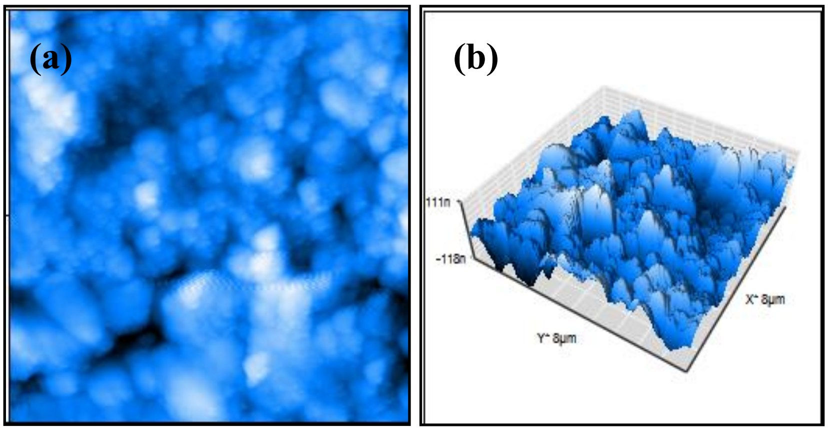

Figure 2. (a) The AFM 2-D image , (b) the AFM 3-D image of the deposited CuO film.

3.3 Ethanol sensing characteristics of CuO thin films

The response of semiconducteur based on sensor is greatly influenced by its operating temperature. In fact, the adsorption of gases is directly related to the temperature at the surface of the sensing layer.
In order to determine the operation temperature for the sensor based on CuO thin film to vapor ethanol, it was exposed to 300 ppm of ethanol at different operation temperature between 100 and 175 °C and the resultant responses are showing in figure 3. A typical operation temperature correspond to maximum response is widely reported in literature. In our case, the evolution of the response of the layer shows that this maximum is located around 150°C.

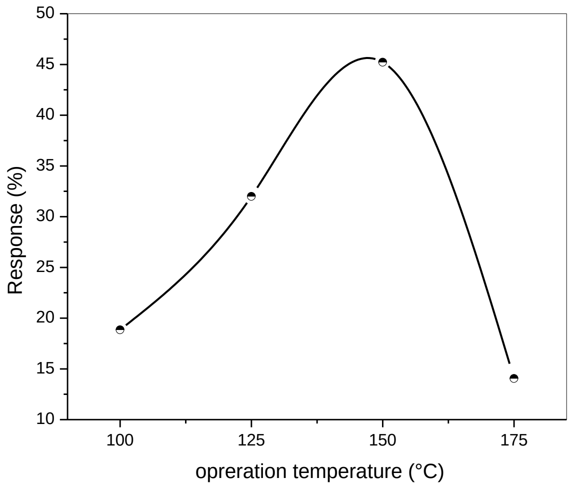

Figure 3. Sensor response curves of the CuO based sensor towards ethanol (300 ppm) at different operating temperatures

Figure 4 shows the resistance transient of CuO layer recorded at the optimum temperature of 150 °C. The decrease in resistance when vapor of ethanol is injected reveals that Rv is lower than Rair. The response is found to be 45% for 300 ppm of ethanol concentration at operation temperature. The CuO based sensor fabricated by Mitesh.al [15] shows a relatively sensor response of 8,3% towards 700 ppm ethanol vapor at operation temperature of 400 °C. It is observed that our thin film CuO based sensor has the lowest operating temperature (150 ◦C) as well as the highest response (45%).The higher response of sensor in this case may be attributed to the large amount of porosity in the material as suggested by Jimenez et al. [16]. The response and recovery time are respectively the duration by which the sensor response reaches to almost 90% of the saturation value and the time to recover its initial value when the vapor is evacuated. The sensing layer exhibits response and recovery times of 2,98 min and 2,11 min respectively. The long response and recovery time observed is probably the result of a complex mechanism of adsorption and desorption of molecules when the layer is exposed to vapor of ethanol. The kinetics of each of this mechanism is strongly influenced and controlled by the morphology and deposition conditions of the film. Modification of these conditions to obtain more porosity and decrease of the layer thickness may be a suitable method to improve the response time.

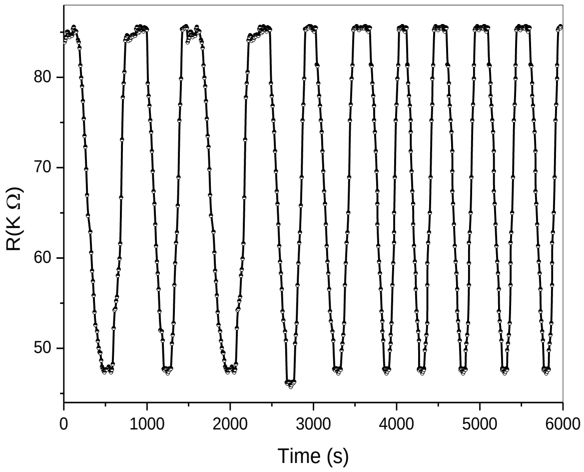

Figure 4. Resistances change vs. time during 300 ppm of ethanol sensing at the operation temperature.

4. Conclusion

A CuO thin film was tested for ethanol vapour sensing. This film was deposited by spray ultrasonic pyrolysis on heated glass substrate. Two gold interdigitated electrodes were used for gas-sensing measurement. The optimal response was obtained at a temperature of 150°C with a value of 45%. These results obtained with a simplified test device are very promising due to the low operating temperature and the high sensitivity of the material. These characteristics are promising for industrial applications, especially in gas and vapour related chemical sensing.

References

[1] Tomchenko, A.A.; Harmer, G.P.; Marquis, B.T.; Allen, J.W. Semiconducting metal oxide sensor array for the selective detection of combustion gases. *Sens. Actuat. B* 2003, *93,* 126-134.
[2] Kanan, S.M.; El-Kadri, O.M.; Abu-Yousef, I.A.; Kanan, M.C. Semiconducting metal oxide based sensors for selective gas pollutant detection. *Sensors* 2009, *9*, 8158-8196.
[3] S.A. Patil, L.A. Patil, D.R. Patil, G.H. Jain, M.S. Wagh, CuOmodified tin titanate thick film resistors as H2gas sensors, Sens. Actuators B: Chem. 123 (2007) 233–239.
[4] P. Samarasekara, N.T.R.N. Kumara, N.U.S. Yapa, J. Phys.: Condens. Matter 18 (2006) 2417
[5] Marabelli F, Parraviciny GB, Drioli FS. Phys Rev B 1995;52:1433.

[6] Ghijsen J, Tjeng LH, Elp JV, Eskes H, Westerink J, Sawatzky GA, Czyzyk MT. Phy Rev B 1988;38:11322.

[7] S.J. Appleyard, Simple photovoltaic cells for exploring solar energy concepts, Phys. Educ. 41 (5) (2006) 409–419.

[8] V.R. Katti, A.K. Debnath, K.P. Muthe, Manmeet Kaur, A.K. Dua, S.C. Gadkari, S.K. Gupta, V.C. Sahni, Mechanism of drifts in H2S sensing properties of SnO2/CuO composite thin film sensors prepared by thermal evaporation, Sens. Actuators B 96 (2003) 245–252.

[9] S. Aygun, D. Cann, Hydrogen sensitivity of doped CuO/ZnO heterocontact sensors, Sens. Actuators B 106 (2005) 837–842.

[10] E.R. Kari, K.S. Brown, Choi, Electrochemical synthesis and characterization of transparent nanocrystalline Cu2O films and their conversion to CuO films, Chem. Commun. (2006) 3311 3313.

[11] N. Serin, T. Serin, S. Horzum, Y. Celik, Annealing effects on the properties of copper oxide thin films prepared by chemical deposition, Semicond. Sci. Technol. 20 (5) (2005) 398.

[12] T. Maruyama, Copper oxide thin films prepared from copper dipivaloylmethanate and oxygen by chemical vapor deposition, Jpn. J. Appl. Phys. 37(1998) 4099–4102.

[13] V.F. Drobny, D.L. Pulfrey, Properties of reactively-sputtered copper oxide thin films, Thin Soild Films 61 (1979) 89–98.

[14] S. Kar, B.N. Pal, S. Chaudhuri, D. Chakravorty, One-dimensional ZnO nanostructure array: synthesis and characterization. J. Phys. Chem. C 110, 4605–4611 (2006).

[15] Mitesh Parmar and K.Rajanna Copper (II) oxide thin film for methanol and ethanol sensing vol. 4, December 2011 710-725.

[16] I. Jimenez, M.A. Centeno, R. Scotti, F. Morazzoni, J. Arbiol, A. Cornet, J.R. Morante, NH3 interaction with chromium-doped WO3 nanocrystalline powders for gas sensing applications, J. Mater. Chem. 14 (2004) 2412–2420.

Investigation of photocalalytic activity of ZnO prepared by spray pyrolis with various precursors

Article · March 2016

DOI: 10.1088/1757-899X/108/1/012049

5 authors, including:

Meryem Lamri zeggar
University of Constantine 1
7 PUBLICATIONS **12** CITATIONS
SEE PROFILE

M.s. Aida
University of Constantine 1
134 PUBLICATIONS **1,123** CITATIONS
SEE PROFILE

Investigation of photocalalytic activity of ZnO prepared by spray pyrolis with various precursors

2016 IOP Conf. Ser.: Mater. Sci. Eng. 108 012049

(http://iopscience.iop.org/1757-899X/108/1/012049)

Investigation of photocalalytic activity of ZnO prepared by spray pyrolis with various precursors

F Bourfaa[1] **, M Lamri Zeggar**[1]**, A Adjimi**[1]**, M S Aida**[1] **and N Attaf**[1]

[1]Laboratory of thin films and interfaces, Faculty of science, University Constantine 1, Algeria

fouzia_bourfaa@yahoo.fr

Abstract. Semiconductor photocatalysts such as ZnO has attracted much attention in recent years due to their various applications for the degradation of organic pollutants in water, air and in dye sensitized photovoltaic solar cell. In the present work, ZnO thin films were prepared by ultrasonic spray pyrolysis by using different precursors namely: acetate, chloride and zinc nitrate in order to investigate their influence on ZnO photocatalytic activity. The films crystalline structure was studied by mean of X-ray diffraction measurements (XRD) and the films surface morphology by Scanning Electron Microscopy (SEM). The films optical properties were studied by mean of UV–visible spectroscopy. The prepared films were tested for the degradation of the red reactive dye largely used in textile industry. As a result, we found that the zinc nitrate is the best precursor to prepare ZnO thin films suitable for a good photocatalytic activity.

1. Introduction

Semiconductor-assisted photocatalysis has recently emerged as an efficient method for conversion of photon energy into chemical energy and environmental purification [1, 2]. Among the semiconducting catalysts, zinc oxide (ZnO) has been extensively studied due to its low cost, non-toxicity, outstanding stability, and high efficiency [3-5]. ZnO is an n-type semiconductor with wide band gap (3.3 eV), large exciton binding energy (60 meV). Illuminated ZnO material with ultraviolet (UV) light can generates electron/hole pairs. These electrons and holes can migrate and initiate redox reactions with water and oxygen, by which they degrade organic molecules adsorbed on the surface of a photocatalyst [6, 7]. It is well known that ZnO thin films morphology controls its properties and subsequently their relevant potential applications. ZnO thin films were mainly used in : biomedical [8], piezoelectricity, biosensors, photocatalysis [9-11], biotechnology [12], light emitting diodes (LED's), laser systems [13] transparent electrodes [14], gas sensors [15,16], solar cells [17] and cosmetic products [18]. Various techniques have been used for ZnO thin films deposition namely: magnetron sputtering [19], reactive evaporation [20], chemical vapor deposition (CVD) [21], pulsed laser deposition (PLD) [22] and spray pyrolysis [23]. Among these methods, spray pyrolysis technique has several advantages, such as, simplicity, safety and vacuum less equipments. It is widely used and succeeded in oxide metallic thin films production [24-26].

In the present paper we studied the influence of the solution nature and properties on the characteristics of ZnO thin films on the photocatalytic activity.

2. Experimental

The ZnO films were grown onto glass substrates; using a Spray Pyrolysis Equipments (HOLMARC). Three different solutions, with 0.1 M molarity were prepared by mixing zinc salts with methanol. The used salts are zinc acetate, zinc nitrate and zinc chloride with 99.9995% of purity. ZnO thin films were deposited with the prepared solutions on well cleaned glass substrates with methanol and distilled water. The prepared solutions are then sprayed on the heated glass substrates by a pneumatic pump with flow rate of 100µl/min. During deposition, the substrate temperature is kept at 350°C. Deposition time for each precursor was 5 min. The crystalline structure was studied by X-ray diffraction measurements (XRD) and the films surface morphology was characterized by means of Scanning Electron Microscope (SEM). The UV–Visible transparence of the films is performed by Shimadzu UV–3101 PC spectrophotometer within the wavelength range of 200–800 nm. The films thickness and refractive index were derived from optical transmission measurement. The films electrical conductivity was carried out using D.C electrical measurements in dark and at room temperature.

In the present work, we have studied the photocatalysis application of ZnO thin films prepared by various precursors for study the degradation of the red reactive dye largely used in textile industry. The used solution was prepared from red reactive 184 powder dissolved in distilled water to obtain a solution with concentration of $4*10^{-6}$ mole/l. ZnO samples were placed inside a beaker containing 250 ml of polluted solution in contact with ZnO layer placed in horizontal position. The ZnO sample is exposed to an UV irradiation with a wavelength of 365nm and 2W power.

3. Results and discussion

3.1 *Films structure*

Figure 1 shows XRD spectra of different films deposited with the three studied salts. As can be seen, the ZnO films prepared from zinc nitrate and zinc chloride were polycrystalline with hexagonal wurtzite structure. While, films prepared with zinc acetate exhibits an amorphous phase due to the absence of any relevant peak. The XRD diffraction pattern of both films deposited using nitrate and zinc chloride are composed with several peaks assigned to (101), (002), (101), (110) planes as shown in figure1. We noticed that when we using a chloride as a precursor, diffraction peak, assigned to the plane (002) became the preferential orientation indicating that the film have the Wutrzite hexagonal and the growth is achieved along the axis c normal to the substrate surface. However in the case of zinc nitrate precursor, the deposited film shows that the plane (101) is the most intense peak. The XRD results are in good agreement with Lehraki et al [27] results, they reported that the ZnO thin films obtained by zinc chloride are polycrystalline and the zinc acetate has an amorphous phase.

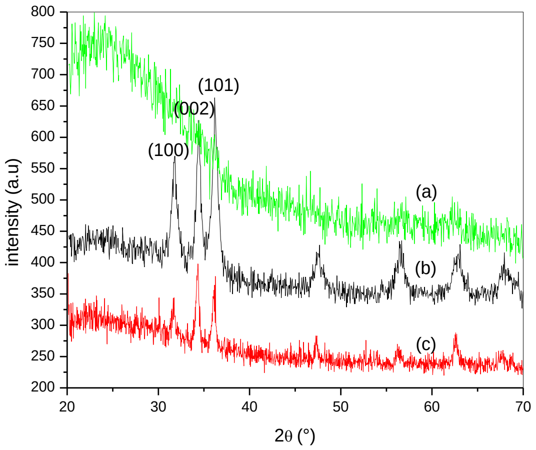

Figure 1. XRD diffraction pattern of ZnO thin films obtained by various precursors: (a) zinc acetate, (b) zinc nitrate and (c) zinc chloride.

Figure 2 shows typical SEM images of ZnO films prepared using the three different precursors. As shown, the films morphology depends strongly on the nature of the used precursor. Film prepared with zinc nitrate as starting solution is porous and exhibits a non continuous network (figure 2.a).While film prepared with zinc chloride exhibits a rough surface morphology and non continuous structure (figure 2.b). However as can be seen in figure 2.c, zinc acetate precursor yields to a dense and continuous structure film structure with a smooth surface. Due to its structure, zinc nitrate films have a larger specific surface then the others films, consequently this precursor will offers larger reactive surface with the environment which is required for gas sensing or for water treatment.

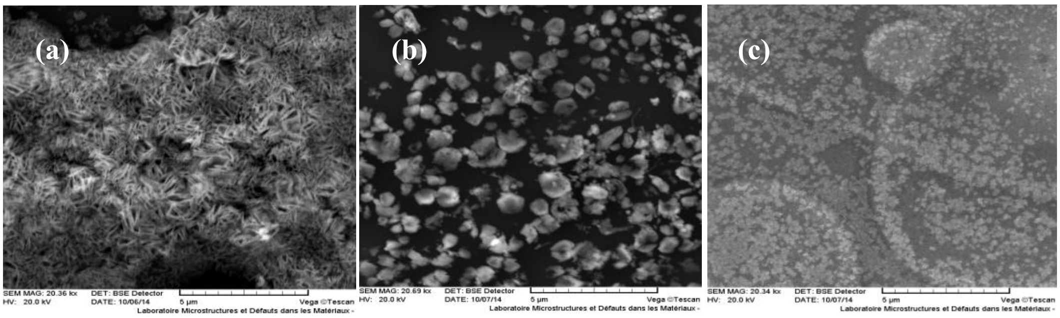

Figure2SEM images of ZnO thin films deposited at substrate temperature equal to 350 °C with different solutions: (a) Zinc nitrate (b) Zinc chloride and (c) Zinc acetate

3.2. Optical properties

In figure 3 we have reported the transmittance spectra of UV-visible range of ZnO films prepared with different precursors. The film deposited with zinc acetate (figure. 3(a)) has the higher transparency of 87% than films deposited with zinc nitride and zinc chloride (curves 3.b and c). This is due to the smooth surface of the former. It is well known that rough surface causes the light scattering resulting in transmittance reduction. This explains the low transmittance measured in films deposited with zinc chloride and nitride despite that they have better crystallinity then the films deposited with zinc acetate. Since these films have rough surfaces as can be seen in SEM images (figure 2).

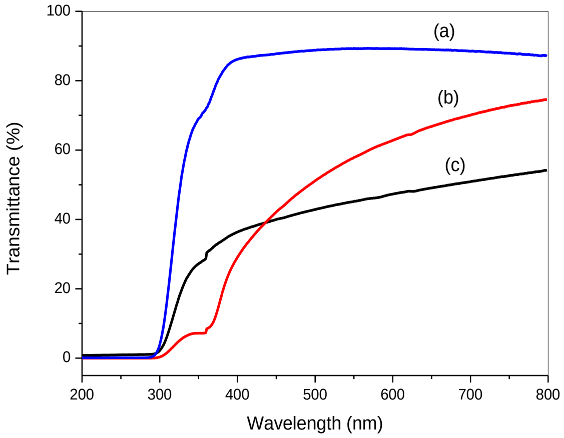

Figure 3. UV-visible transmittance spectrum of ZnO thin films deposited at 350 °C using different salts: (a) Zinc acetate-(b) Zinc nitride-(c) Zinc chloride.

The optical band gaps of films have been estimated from the plot of their absorption coefficient as a function of photon energy and using Tauc formula for direct band gap semiconductors [28]:

$$(\alpha h\upsilon)^2 = B\,(E_g - h\upsilon).$$

Were α is a absorption coefficient, B is a constant, h is Planck constant, E_g is the energy band gap and v is incident photon frequency.

Films optical band gap are found equal to 3.12 and 3.20 eV for films prepared with zinc nitrate and zinc acetate respectively .While the optical gap of film deposited with zinc chloride is close to its value for ZnO bulk material which is 3.27 eV because of the good crystallinity of this film. The films thickness, refractive index and optical band Eg deduced from optical transmittance spectra were reported in Table 1.

Table 1: thickness, band gap, refractive index, degradation rate k and conversion rate of ZnO thin films deposited with different precursors**.**

ZnO precursors	d (nm)	Eg (eV)	n	Rate k (10^{-4})	Conversion rate (%)
Nitrate	209.936	3.12	1.88	18	36
Chloride	202.463	3.25	1.93	6.58	17
Acetate	134.864	3.20	1.69	8.56	20

3.3. Electrical properties:

Figure 4 shows the variation of the electrical conductivity, of ZnO thin films deposited by various precursors, measured in the dark and at room temperature. As can be seen the conductivity of films obtained with zinc nitrate have the slightly larger conductivity value $7.23\text{x}10^{-5}(\Omega\text{cm})^{-1}$. This is due to the fact that film prepared with this precursor is dense and continuous in contrary to others ones.

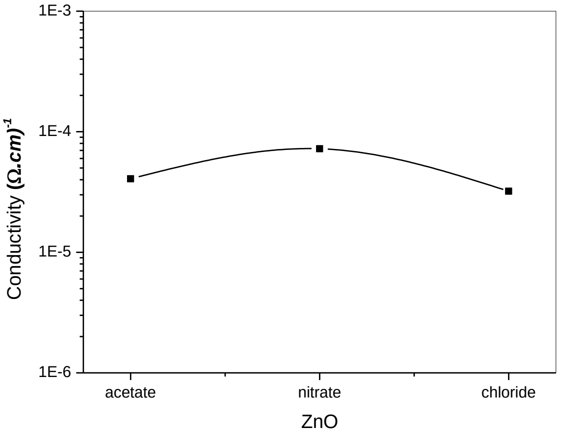

Figure 4. Variation of the conductivity for the three precursors.

3.4. Photocatalytic activity:

We have studied the variation of absorbance spectra of polluted solution after different UV light exposure times. The wavelength region is ranged from 450 to 600 nm; this broad absorption band is a characteristic of the used red dye. The absorption peak intensity is used as signature of the dye degradation. From the variation of this absorption peak with exposure time , we concluded that the photo degradation is more significant when solution is in contact with film prepared using zinc nitrate then the ones prepared with zinc acetate and zinc chloride films.

To have more insight on the photo degradation kinetics and the influence of ZnO precursors, we have monitored the variation of the intensity of the absorption located at 542 nm. We have reported in figure 5 the variation of the ratio $C/C_{0,}$ where C is the peak intensity at time t and C_0 is the peak intensity before light exposure. As can be seen, the photo degradation is more important when using film obtained with zinc nitrate salt, the ratio is reduced with increasing exposure time; it reaches 0.64 after 240 minutes of irradiation. However in the case of zinc acetate and zinc chloride films salt source, the ratio is slightly reduced up to 0.78 and 0.83 after 240 minutes, respectively. As can be seen in figure 6, the photocatalytic decomposition of red pollutant, in contact with the surface of ZnO thin films of the three precursors, follow a pseudo first-order kinetic law, it can be expressed as [31]:

$$-\mathrm{Ln}\,(C/C_0) = kt$$

Where C and C_0 are the reactant concentration at time t and t = 0, respectively and k rate constant (reaction rate constant) [29].

In table I we have reported the calculated value of the rate k for the all ZnO thin films. Zinc nitrate film is characterized by a larger rate k then the other films.

The conversion rate defined as $\tau = (C_0\text{-}C\ (t)/C_0)\ \mathrm{x}100$, is an interesting quantity that can yield information about the pollutant degradation, it represents the relative quantity of removed pollutant from the solution. In figure 6 we have reported the variation of the conversion rate obtained with all ZnO thin films. In the case of zinc nitrate film, 36 % of pollutant is removed after 240 minutes of exposure time, while only less than 22% and 17% are removed when using zinc acetate and zinc chloride films, respectively. The discrepancy in the photocatalysis activity of all thin films of ZnO may found explication in the difference between their microstructure. As deduced from SEM images, zinc nitrate and zinc chloride films are rough and have a porous structure while zinc acetate film is smoother and has a continuous structure. Therefore, the reactive specific surface of the first film is larger than in the others films, thereafter, more reactive surfaces are available for the water than in the other ones (acetate and chloride). The same conclusion has been outlined by Li et al [32] in ZnO/CuO structure, they reported that a material with an open and porous surface exhibit higher degradation efficiency. So, the reactive specific surface is one of the important parameters to controller the photocatalytic activity of ZnO thin films.

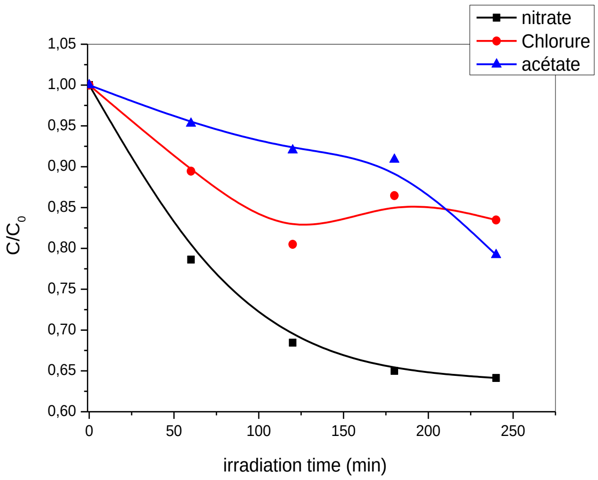

Figure 6. Evolution temporal of the conversion rate of dye red pollutant during its degradation in contact with ZnO thin films deposited by various salts.

4. Conclusion:

In order to investigate the influence of the precursor’s salt nature, we have studied the ZnO thin films deposited with spray pyrolysis by different precursors. The obtained ZnO thin films are polycrystalline when using zinc nitrate and zinc chloride, however using zinc acetate salt leads to an amorphous film microstructure. From this investigation we inferred that the starting salt source nature and morphology of the Zn salt play an important role on the photocatalytic activity. Thin and porous films offer more reactive sites due the large surface to volume ratio and larger charge transfer, thereafter their better photocatalytic activity. According to the obtained films SEM images and to morphologies, we concluded that zinc nitrate source is the best precursor for the preparation of ZnO thin film suitable to the red dye photo degradation.

References:

[1] J. Zhou, N.S. Xu, Z.L. Wang, Adv. Mater. 18 (2006) 2432.
[2] C.Riggio, V.Raffa and A. Cuschieri, Micro & Nano Letters 5(2010)35
[3] M.A. Behnajady, N. Modirshahla and R. Hamzavi, J. hazard.Mater.20 (2006)133.
[4] T.J. Brunner , P Wick , P Manser , P Spohn , RN Grass , L.K.Limbach , A.Bruinink W.J. Stark ,Environ Sci Technol. 15(2006)4374.
[5] Y. Lu, Y. Lin, D. Wang, L. Wang, T. Xie and T. Jiang, J. Phys. D: Appl. Phys. 44 (2011) 315502.
[6] R. Yokoyama, S. Suzuki, K. Shirai, T. Yamauchi, N. Tsubokawa and M. Tsuchimochi, Eur. Polym. J. 42 (2006) 3221.
[7] J. M. Szarko, J. K. Song, B C. W. Lackledge, I. Swart, S. R. Leone, S. Li, Y.Zhao, Chem. Phys. Lett., 404(2005) 171.
[8] T. Ootsuka, Z. Liu, M. Osamura, Y. Fukuzawa, R. Kuroda, Y. Suzuki, N. Otogwa, T. Mise, S. Wang, Y. Hoshino, Y, Nahayama and H. Tanoue, Thin Solid Films, 476(2005)30.
[9] B. Baruwati, D.K. Kumar and S.V. Manorama, Sens. Actuators B 119 (2006) 676.
[10] G.-C. Yi, C. Wang, W.I. Park, Semicond. Sci. Technol. 20 (2005) S22.
[11] Z.S. Wang,C.H. Huang,Y.Y. Huang, Y.J. Hou, P.H. Xie, B.-W. Zhang and H. M. Cheng, Chem. Mater. 13 (2001) 678.
[12] T. Iwasaki, M. Satoh, T. Masuda, T. Fujita and J. Mater. Sci. 35 (2000)4025.
[13] X. Yu, J. Ma, F. Ji, Y. Wang, X. Zhang and H. Ma,Thin Solid Films,483(2005) 296.
[14] J. Ma, F. Ji, D. Zhang, H. Ma and S. Li, Thin Solid Films, 357(1999) 98.
[15] D. A. Lamb and S. J. C. Irvine, Journal Cryst. Growth 273(2004)111.
[16] J. Zou, S. Zhou, C. Xia, Y. Hang, J. Xu, S. Gu, and R. Zhan, J. Cryst. Growth 280(2005)185.
[17] P. Nunes, E. Fortunato, P. Tonello, F. Braz Fernandez, P. Vilarinho and R. Martins, Vacuum, 64(2002)281.
[18] A. Mosbah, M.S.Aida, J. of Alloys and Compds, 515(2012)149.
[19] F.Ynineb, A. Hafdallah, M.S. Aida, N. Attaf, J.Bougdira, H.Rinnert and S.Rahman, Mater. Sci. in Sem. Process. 16 (2013)2021.
[20] M. Messaoudi, M.S. Aida, N. Attaf, T. Bezzi, J. Bougdirab and G. Medjahdi. Mater. Sci in Sem. Process. Volume 17, (2014) 38.
[21] A. Hafdallah, F. Yanineb, M.S. Aida and N. Attaf, J. of Alloys and Compnds, 509 (2011) 7267.
[22] N. Kislov, J. Lahiri, H. Verma, D. Yogi Goswami, E. Stefanakos, and M. Batzill, Langmuir 25 (2009) 3310.
[23] S. Baruah, M. Jaisai, R. Imani1, M. M. Nazhad and J. Dutta, Sci. Technol. Adv. Mater 11 (2010).
[24] H. Zhu, R. Jiang, Y. Fu, Y. Guan , J. Yao, L. X. Guangming Zeng, Desalination 286 (2012) 41.
[25] M. Qamar and M. Muneer, Desalination 249 (2009) 535.
[26] R. Ullah and J. Dutta, Journal of Hazardous Materials 156 (2008) 194.
[27] N. Lehraki, M.S. Aida,, S. Abed, N. Attaf, A. Attaf and M. Poulain Jornal of Current Applied Physics 12(2012)1283-1287.
[28] J.J. Tauc, Amorphous and Liquid Semiconductors, Plenum, London, 1974.
[29] B. X. Li and Y. F.Wang, Super lattice Microstruct. 47(2010) 615.
[30] Q. Xiang, G. Meng, Y. Zhang, J. Xu, P. Xu, Q. Pan and W.Yu, Sens. Actuator B-Chem.143. (2010) 635.

Journal of New Technology and Materials
JNTM
Vol. 04, N°01 (2014)86-88

OEB Univ. Publish. Co.

Copper oxide thin films deposition by spray pyrolysis

M. Lamri Zeggar*, M. S. Aida and N. Attaf

Laboratory of Thin Films and Interfaces Faculty of Science University of Constantine, Algeria,

Received: 30 April 2014, accepted 26 May 2014

Abstract

CuO thin films have been growth on to heated glass substrates by varying substrate temperatures from 280 to 400°C. The effect of the pyrolysis on structural, optical and electrical proprieties of CuO films has been investigated in the present work. Phase analysis was carried out using Micro-Raman scattering. The optical properties were studied by mean of UV–visible and near infrared spectroscopy. The conductivity was measured by the electrical D.C transport. The structural analysis indicates the presence of a single CuO phase with a monoclinic structure. The optical transmittance spectra show a high absorption of all films in the visible region. The electrical characterization indicates a maximal electrical conductivity of $1{,}03 \times 10^{6}$ *(*Ω *.cm)*^{1}*.*

Keywords: Copper oxide, solar cells, Spray pyrolysis.

1. Introduction

In recent years, copper oxide (CuO) thins films have attracted great interest due to their important applications in many technological fields. This is due, firstly, to the low cost, the non-toxicity and the availability of copper in the nature, secondly to the simplicity of the deposition process of its components. Copper oxide is known to have two stable forms, namely CuO and Cu_2O with different properties. CuO is a p-type semiconductor with a monoclinic structure; it has a relatively low band gap of 1,2-1,9 eV [1,2]. Furthermore, Cu_2O materials, in general, is a p-type semiconductor which crystallizes in cubic structure with a large direct band gap of 2 et 2,6 eV [3]. These two phases were mainly used in the fields of electronics and optoelectronics such as: high Tc superconductors [4], lithium batteries [5], for magnetic storage [6], gas sensors [7] and absorbers layers in solar cells [8].Various techniques have been used for CuO thin films deposition namely: sol-gel [9] chemical vapor deposition [10], plasma evaporation [11] and electrodeposition [12].

Among these techniques, spray pyrolysis is a very attractive and versatile technique; it has been largely used to produce adherent, homogenous and stoichiometric films. The main goal of the present work is to produce CuO thin films with good optoelectronic properties by optimizing the substrates temperature while keeping constant the others operating parameters.

2 Experimental

Copper oxide thin films have been prepared on glass substrates by ultrasonic spray pyrolysis. The precursor solution was prepared by dissolving 0.05 M copper chloride ($CuCl_2.2H2O$) in distilled water. Then, the precursor solution sprayed in fine droplets of 40 µm in diameter, by an ultrasonic generator on heated glass substrate. Films were formed by pyrolytic reaction. During deposition, the substrate temperature is kept at 280, 300, 350, 400 °C for four different runs. The deposition time for each run is 20 min.

The films crystalline phases are analyzed by micro-Raman measurements performed at room temperature using the 514.5 nm line of an argon ion laser as the excitation source (Renishow). The UV-Visible transparence of the films is performed by Shimadzu UV-3101 PC spectrophotometer within the wavelength range of 200–1800 nm. The values of films thickness and refractive index were derived from optical transmission measurement. The electrical characterization of the films was carried out using the electrical D.C transport to measure the conductivity in dark and at room temperature.

3 Results and discussion

3.1 The deposition rate and the refractive index

In Figure.1 we have reported the variation of deposition rate and the refractive index of CuO thin films as a function of substrate temperatures. The deposition rate is estimated from the ratio of the layer thickness on the deposition time, fixed at 20 minutes. As can be seen the deposition rate decreases with increasing of substrate temperature, it is maximal

(Vd=275.15nm/min) at substrate temperature equal to 280 ° and minimal (Vd=216.32nm/min) for the sample prepared at 400 ° C. The reduction of deposition rate can be explained by the phenomenon of densification. The rise in substrate temperatures yields to an increases in the formation energy of the material by the pyrolytic reaction on the surface, which influence on the growth kinetics and produces denser film. This result is in good agreement with the increase of the refractive index from 1,53 to 1,65which is a clear indication of films densification.

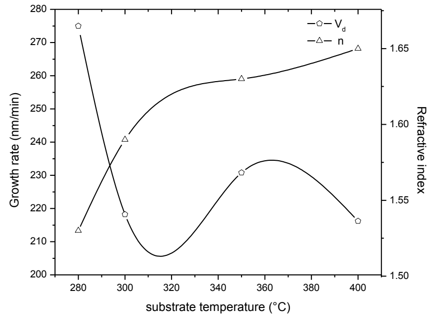

Figure1: Variation of deposition rate and refractive index as a function of substrate temperatures

3.2. Structural properties

Figure.2 shows the Raman spectra of the as-prepared CuO thin films with diverse substrate temperatures. The Raman spectra are composed with three main phonon modes (Ag and 2Bg) located at 297, 334 and 608 cm^{-1} which are assigned to a single phase CuO with a monoclinic structure. These peaks are largely reported in the literature [13-15]. No other secondary phase modes are present as Cu$_2$O [16].

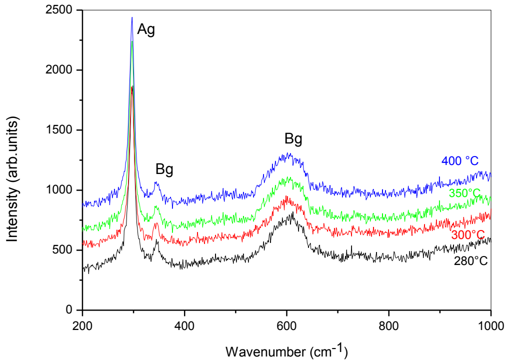

Figure 2: Micro Raman spectra of CuO deposited with various substrate temperatures.

3.3 Optical properties

The transmittance spectra in UV-Visible region of CuO films prepared with different substrate temperatures are shown in figure.3. The measurements were performed in the UV-visible, corresponding to the wavelength range: 200 - 1800 nm. It was determined that all films behaved as transparent materials in the 800-1100 nm wavelength range located in infrared field. On the other hand, in the visible region films transmittance values decreases sharply in the wavelengths range less than 800 nm due to their highly absorbing properties. This wavelength range represents the material fundamental absorption region. Films optical band gap have been estimated, as show in Fig.4 from the plot $(\alpha h\nu)^2$ as a function of photon energy (hν), according to Tauc formula for direct band gap semiconductors [17]:

$(\alpha h\nu)^2 = B\,(Eg-h\nu)$

Where α is a absorption coefficient, B is a constant, h is Planck constant, Eg is the energy band gap and ν is incident photon frequency.

The obtained optical gaps increase with substrate temperature increasing from 1.44 eV to 1.76 eV which is in good agreement with CuO band gap values reported by Gopalakrishna et al. [18]. They found optical band gap values laying between 1.8 eV and 1.2 eV for substrate temperature ranged from 250 to 400 ° C. However, film prepared at 280 °C have an optical band gap close to 1.44 eV , this value is required for solar cells since it matches well with solar spectrum.

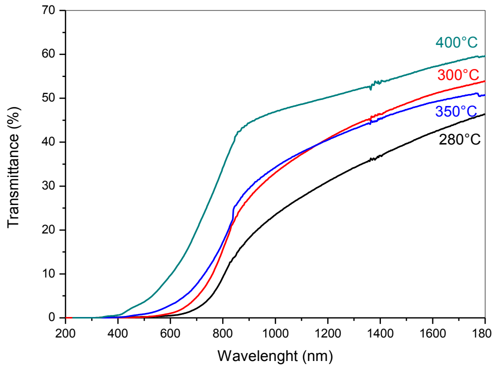

Figure 3: UV-Visible transmittance spectrum of CuO thin films deposited spectra at different substrate temperatures.

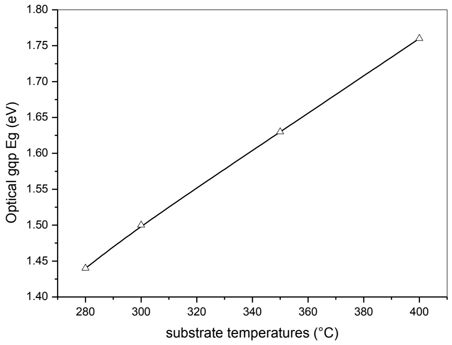

Figure 4: Variation of optical band gap of CuO films with substrate temperature

3.4. The electrical properties

The electrical conductivity variation, measured in the dark and at room temperate, with different deposition temperatures is shown in Figure.5. From this figure we observe that the conductivity increases from 7.11 x 10^{-8} to 1.03 x 10^{-6} $(\Omega.\ Cm)^{-1}$ for substrate deposition temperature increase from 280°C to350 ° C, while at 400 °C the conductivity decreases by one order of magnitude.

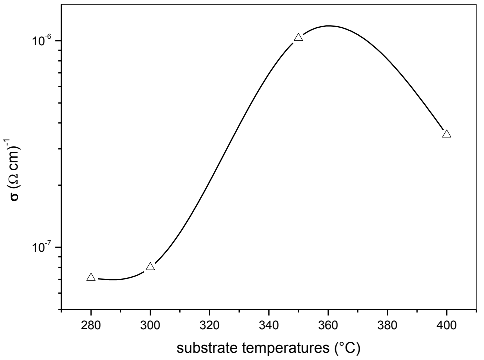

Figure 5: Variation of the conductivity versus the substrate temperatures.

4. Conclusion

CuO thin layers were deposited by ultrasonic spray on glass substrates. The influences of the substrate temperature on structural, optical and electrical properties were studied. The films prepared at different temperatures showed the presence of a single phase CuO with a monoclinic structure. The optical characterization showed a strong absorbance in the visible range with values of optical gap varied from 1.44 to 1.76 eV. All the deposited films exhibit p-type conductivity with a relatively high conductivity. Film deposited at 350°C seems to have suitable optical and electrical properties for efficient thin film solar cell fabrication.

References:

[1] M. Yin, C.-K.Wu, Y. Lou, C. Burda, J.T. Koberstein, Y. Zhu, S. O'Brien, J. Am. Chem. Soc. 127 (2005) 9506.
[2] M.K. Wu, J.R. Ashburn, C.J. Torng, P.H. Hor, R.L. Meng, L. Gao, Z.J. Huang, Y.Q. Wang, and C.W. Chu, Phys. Rev. Lett. 58 (1987) 908.
[3] S. C. Ray, Sol Energy Mater Sol Cellsi, 68, 307 (2001)
[4] X.G. Zheng, C.N. Xu, Y. Tomokiyo, E. Tanaka, H. Yamada and Y. Soejima, "Observation of Charge Stripes in Cupric Oxide", Phys. Rev. Lett. 85, 5170 (2000).
[5] X.P. Gao, J.L. Bao, G.L. Pan, H.Y. Zhu, P.X. Huang, F. Wu, D.Y. Song, J. Phys. Chem. B 108 (2004) 5547–5551.
[6] R.V. Kumar, Y. Diamant, A. Gedanken, Chem. Mater. 12 (2000) 2301–2305.
[7] A. Chowdhuri, V. Gupta, K. Sreenivas, R. Kumar, S. Mozumdar, P.K. Patanjali, Appl. Phys. Lett. 84 (2004) 1180–1182.
[8] K. Han, M. Tao, Sol. Energy Mater. Sol. Cells 93 (2009) 153.
[9] A. Y. Oral, E. Mensur, M. H. Aslan, E. Basaran,Mater Chem Phys, 83(1), 140 (2004).
[10] T. Maruyama, Jpn. J. Appl. Phys. 37(1998) 4099–4102.
[11] K. Santra, C. K. Sarker, M. K. Mukherjee, B. Ghosh, Thin Solid Films, 213, 226 (1992).
[12] E.R. Kari, K.S. Brown, Choi, Chem. Commun. (2006) 3311–3313.
[13] D.P. Volanti , D. Keyson , L.S. Cavalcante , A.Z. Sim˜oes,M.R. Joya , E. Longo, J.A. Varela P.S. Pizani and A.G. Souza, J. of Allo. and Compds.459 (2008) 537
[14] H. Fan, B. Zou, Y. Liu, S. Xie, Nanotechnology 17 (2006) 1099.
[15] T. Yu, C.-H. Sow, A. Gantimahapatruni, F.-C. Cheong, Y. Zhu, K.-C. Chin,
X. Xu, C.-T. Lim, Z. Shen, J.T.-L. Thong, A.T.-S. Wee, Nanotechnology16 (2005) 1238.
[16] K. Reimann, K. Syassen, Phys. Rev. B 39 (1989) 11113.
[17] J.J. Tauc, Amorphous and Liquid Semiconductors, Plenum, London, 1974.
[18] D. Gopalakrishna ,K. Vijayalakshmi, C. Ravidhas. J Mater Sci: Mater Electron DOI 10.1007/s10854-012-0866-7 (2012).

Abstracts

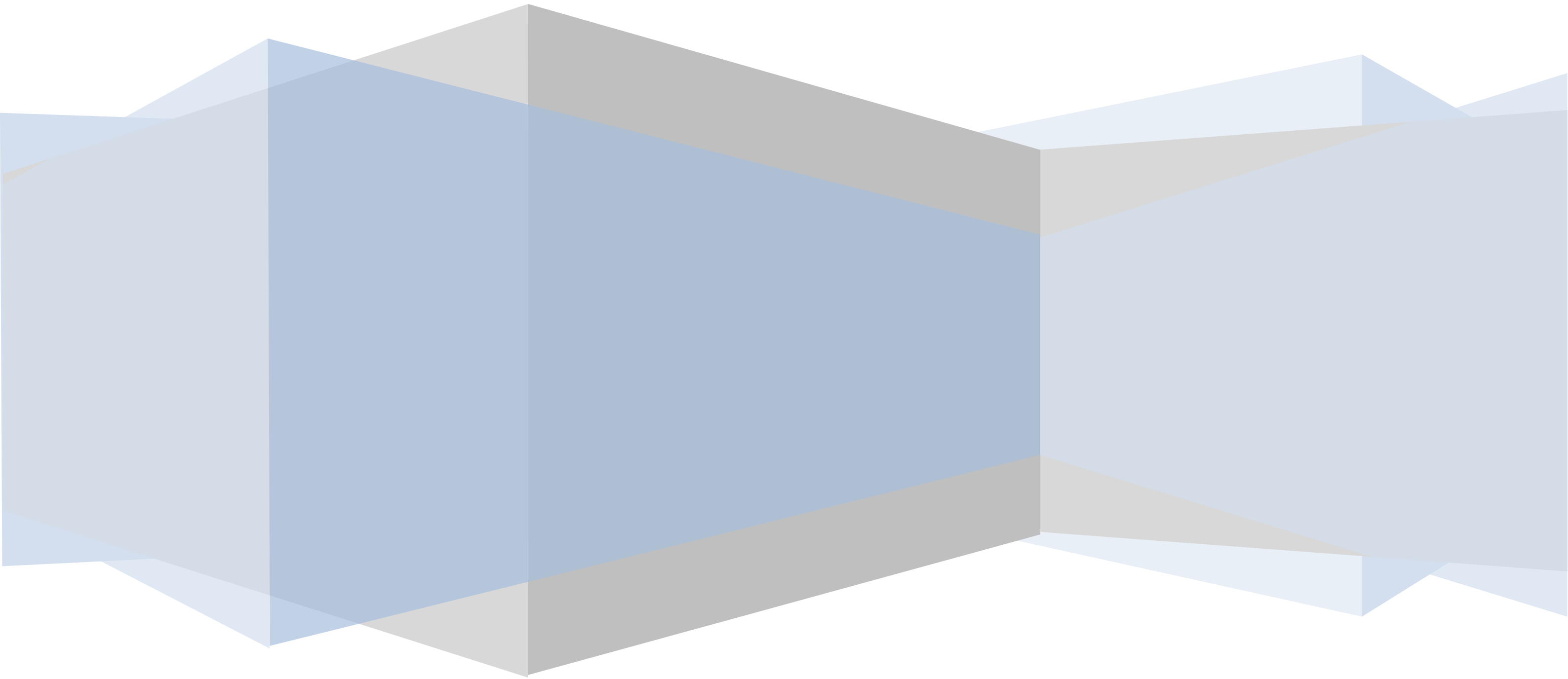

تحضير شرائح الرقيقة CuO لاستعمالها كمجسات للغازات

ملخص

موضوع الرسالة يتناول تحضير و دراسة الشرائح الرقيقة CuO باستعمال تقنية سهلة و بسيطة و التى تتمثل فى تقنية الرش الحرارى (spray pyrolysis SP) . فى الجزء الاول من هذا العمل قمنا بتحضير سلسلة من العينات بتغيير الشروط التجريبية من اجل ايجاد افضل الشروط التى تؤدى الى شرائح ذات خصائص كهروضوئية جيدة حيث يمكن استعمالها كخلايا شمسية او مجسات للغازات. الوسائط التى قمنا بدراستها كانت على التولى : درجة حرارة المسند,تدفق المحلول, تركيز و نوعية الملح الاولى. الدراسة البنيوية وضحت ان التركيب البلورى للشرائح كان ذو تركيبة monoclinique بينما الاتجاه البلورى المفضل يتعلق بشروط التحضير.الدراسة الضوئية و الكهربائية وضحت ان شرائح CuO المحضرة خلال هذا العمل تمتاز بخصائص جيدة والتى تتمثل فى امتصاص عال للضوء و ناقلية كهربائية جيدة مما يرشحها للاستعمال فى الخلايا الشمسية بصفة خاصة و المركبات الكهروضوئية بصفة عامة. دراسة مجسات لغاز الميثانول المصنوعة من شرائح CuO وضحت ان هذه الاخيرة لها حساسية قيمتها %90 عند درجة حرارة 50 ° C , زمن الاستجابة و العودة كانا 2,98 و 2,11 د على التوالى بينما حدود الحساسية وصلت الى 20 ppm . كمجس لغاز الإيتانول فإن حساسيته تقارب 45% عند درجة حرارة الاستعمال 150 ° C بأزمنتي الاستجابة و العودة 2,98 و 2,11 د, أما حدود تحسسه تقدر 24 ppm. فان المجس المصنوع من CuO قد بين حساسية تناهز 9% عند درجة حرارة 06° C و ضغط CO_2 يساوى 5 hPa بأزمنتي الاستجابة و العودة تتغير في المجالين 29 -41 و 30- 35 ثا على التوالي عند تغي ضغط CO_2 من 2- 20 hPa. اجهزة الخلايا الشمسية CuO/ZnO و CuO/ZnS اعطت المردوين % 5.2×10^{-4} and 7×10^{-4} على التوالي.

الكلمات المفتاحية: شرائح رقيقة,CuO,الرش الحرارى,الخلايا الشمسية, مجس الغازات

.

Elaboration des couches minces d’oxyde de cuivre en vue de la réalisation de capteur à gaz

RESUME

L'objectif de ce travail porte sur l'élaboration et la caractérisation des couches minces de CuO par une technique simple et bon marché, en l'occurrence la méthode de dépôt par Spray pyrolyse ultrasonique (SP). Dans la première partie de ce travail nous avons élaboré des séries de films avec différentes conditions de déposition en vue d’optimiser le procédé pour obtenir de films avec de bonnes propriétés optoélectroniques afin d’être appliqués en photovoltaïque ou en détection des gaz. Les paramètres étudiés sont : la température du substrat, le débit de la solution, la molarité et le type de précurseur. La caractérisation structurale des films a révélé que ces derniers ont une structure monoclinique cependant, l’orientation préférentielle est liée au paramètre expérimental varié. Les caractérisations optiques et électriques ont montré que les films CuO déposés par spray jouissent de bonne propriétés optoélectroniques, i. e une assez bonne absorbance dans le visible avec une conductivité élevée. Ceci nous a permis de conclure que les films CuO, élaborés par une technique simple telle que le SP, trouvent des applications potentielles dans la réalisation des cellules solaires en couche minces en particulier et des composants optoélectroniques en général. Les caractéristiques de capteur à gaz basé sur CuO pour la détection de méthanol montrent une forte sensibilité environs, 90 % pour une basse température de fonctionnement égale à 50°C. Un temps de réponse et de retour égale à 2,45 min et 2,02 min respectivement et une limite de détection de 20 ppm. Pour la détection d’éthanol, le capteur de gaz présente une sensibilité d’environs 45 % mesurée a une température de fonctionnement égale à 150 °C. Un temps de réponse et de retour égale à 2,98 min et 2,11 min et une limite de détection de l’ordre de 24 ppm. Le capteur à gaz basé sur CuO montre aussi une relative sensibilité de l’ordre 9 % pour une température d’opération égale à 60 °C mesurée à une pression de CO_2 égale à 5 hPa. Un temps de réponse et de retour varie de 29 jusqu’à 41 s 30 jusqu’à 35 s quand la pression de CO_2 change de 2 jusqu’à 20 hPa, respectivement. Les dispositifs de cellules solaires obtenues pour CuO/ZnO et CuO/ZnS heretostructures ont des faibles rendements égaux à $5{,}2 \times 10^{-4}$ et 7×10^{-4} %, respectivement.

Most clés : couches minces, CuO, spray pyrolyse, cellules solaire, capteur à gaz

ABSTRACT

The present work deals with the deposition of CuO thin films by a simple and cheap technique such as Spray ultrasonic pyrolysis (SP). In the first, a set of CuO thin film was prepared using various deposition conditions in order to optimize the technique and prepare suitable films devoted to the photovoltaic and sensing applications. The studied deposition parameters were the substrate temperature, flow rate, salt nature and concentration. The structural analysis shows that the obtained films are polycrystalline, they exhibit a monoclinic structure. The preferential orientation is strongly related to the experimental parameters studies. From the optical and electrical characterization results, we inferred that the deposited films have suitable optoelectronic properties for the photovoltaic applications since they present a good absorption in the visible range. The fabricated CuO based sensor show a very high sensitivity equivalent to 90% at lower operation temperature equal to 50°C towards 300 ppm of methanol vapor. The sensing layer exhibits response and recovery times of 2,45 min and 2,02 min respectively with limit detection equal to 20 ppm. For ethanol sensing, the CuO based gas sensor show a sensitivity equal to 45% towards 300 ppm concentration of ethanol at operation temperature equal to 150°C. Response and recovery times are 2,98 min and 2,11 min respectively with limit detection at 25 ppm. The fabricated CuO based gas sensor show also a relative gas response equal to 9% at lower operation temperature above 60°C for CO_2 pressure at 5hPa. The response and recovery times are ranged from 29 to 41 s and 30 to 35 s respectively occurring increases in sensitivity from 4.67 to 13.46 % when varying the CO_2 pressure from 2 to 20 hPa. The obtained solar cells devices for CuO/ZnO and CuO/ZnS have low efficiencies equal to 5.2×10^{-4} and 7×10^{-4} %, respectively.

Key Words : *thin films- CuO – spray pyrolysis - solar cells- gas sensor.*